VOLUME 115 NUMBER 2

THE ASTROPHYSICAL JOURNAL

AN INTERNATIONAL REVIEW OF SPECTROSCOPY AND ASTRONOMICAL PHYSICS

MARCH 1952

THE UNIVERSITY OF CHICAGO PRESS
CHICAGO, ILLINOIS, U.S.A.

March 1952 Vol. 115, No. 2

THE ASTROPHYSICAL JOURNAL

AN INTERNATIONAL REVIEW OF SPECTROSCOPY AND ASTRONOMICAL PHYSICS

Published in Collaboration with the American Astronomical Society

---

The Astrophysical Journal is published bimonthly by the University of Chicago at the University of Chicago Press, 5750 Ellis Avenue, Chicago 37, Illinois, during July, September, November, January, March, and May. ¶Two volumes are published per year, one beginning with the January issue and the other beginning with the July issue. The subscription price is $6.00 per volume or $12.00 per year; the price of single copies is $3.00. (Orders for service of less than a volume will be charged at the single copy rate.) ¶Postage is prepaid by the publishers on all orders from the United States and its possessions. No extra charge is made for postage to countries in the Pan American Postal Union. ¶Postage is charged extra as follows: for Canada, 20 cents per volume, 40 cents per year (total $6.20 per volume, $12.40 per year); on single copies 5 cents (total $3.05); for all other countries in the Postal Union, 50 cents per volume, $1.00 per year (total $6.50 per volume, $13.00 per year), on single copies 10 cents (total $3.10). ¶Subscriptions are payable in advance. Please make all remittances payable to The University of Chicago Press, in United States currency or its equivalent by postal or express money orders or bank drafts.

The following is an authorized agent:

For the British Empire, except North America and Australasia: The Cambridge University Press, Bentley House, 200 Euston Road, London, N.W. 1, England. Prices of yearly subscriptions and of single copies may be had on application.

Claims for missing numbers should be made within the month following the regular month of publication. The publishers expect to supply missing numbers free only when losses have been sustained in transit, and when the reserve stock will permit.

Business correspondence should be addressed to The University of Chicago Press, Chicago 37, Illinois.

Communications for the editors and manuscripts should be addressed to: W. W. Morgan, Editor of THE ASTROPHYSICAL JOURNAL, Yerkes Observatory, Williams Bay, Wisconsin.

Line drawings and photographs should be made by the author, and all marginal notes such as co-ordinates, wave lengths, etc., should be included in the cuts. It will not be possible to set up such material in type.

One copy of the corrected galley proof should be returned as soon as possible to the editor, Yerkes Observatory, Williams Bay, Wisconsin. Authors should take notice that the manuscript will not be sent to them with the proof.

The cable address is "Observatory, Williamsbay, Wisconsin."

The articles in this journal are indexed in the *International Index to Periodicals*, New York, N.Y.

Applications for permission to quote from this journal should be addressed to The University of Chicago Press, and will be freely granted.

Microfilms of complete journal volumes are available to regular subscribers only and may be obtained at the end of the year. Orders and inquiries should be addressed to University Microfilms, 313 North First Street, Ann Arbor, Michigan.

Notice to subscribers: If you change your address, please notify us and your local postmaster immediately.

Entered as second-class matter, July 11, 1940, at the Post-Office at Chicago, Ill., under the Act of March 3, 1879.
Acceptance for mailing at special rate of postage provided for in United States Postal Act of October 3, 1917, Section 1103, amended February 28, 1925.

[PRINTED IN U.S.A.]

THE ASTROPHYSICAL JOURNAL

AN INTERNATIONAL REVIEW OF SPECTROSCOPY AND ASTRONOMICAL PHYSICS

VOLUME 115 MARCH 1952 NUMBER 2

PLEIONE: THE SHELL EPISODE

PAUL W. MERRILL
MOUNT WILSON AND PALOMAR OBSERVATORIES
CARNEGIE INSTITUTION OF WASHINGTON
CALIFORNIA INSTITUTE OF TECHNOLOGY
Received October 18, 1951

ABSTRACT

The shell episode in the spectroscopic history of Pleione began in 1939. Numerous narrow dark lines of hydrogen and of metals reached their maximum intensity in 1945 or 1946, after which they became weaker until, in 1951, they were nearly gone. A negative progression in the displacements of successive Balmer lines appeared about 1946 and became very pronounced by 1951. The negative displacements of the higher Balmer lines were shared in part by the metallic lines. Many data concerning the displacements of various lines are recorded.

The shell was probably formed by atoms which moved outward from the photosphere. At first the motion was so slow that the observed radial velocity of the shell was the same as that of the star as a whole. Gradually the acceleration increased, and the outward velocity of the upper levels became appreciable. Eventually the supply of atoms failed, and the shell blew away.

The Pleione shell episode illustrates several typical characteristics of abnormally extensive atmospheres surrounding early-type stars.

Bright hydrogen lines were discovered in the spectrum of Pleione[1] at the Harvard Observatory in December, 1888. From then until 1903 they were seen or photographed by various observers on numerous occasions. In 1905, however, they were absent on spectrograms taken by E. B. Frost at the Yerkes Observatory. The bright lines were not observed again until October, 1938, when their reappearance was independently discovered by Orren Mohler at the Cook Observatory and D. B. McLaughlin at the Observatory of the University of Michigan. A beautiful shell spectrum soon developed, which persisted for several years but in 1948 began to weaken and by April, 1951, was nearly gone. Valuable descriptions of the shell spectrum have been published by Struve and Swings,[2,3] Jesse L. Greenstein,[4] Kiess, Krogdahl, Eidelman, and Hall,[5] and Anne B. Underhill.[6]

Spectrograms obtained at Mount Wilson since the beginning of the shell episode are listed in three groups: Table 1, one-prism plates, dispersion 35 A/mm at $H\gamma$; Table 2,

[1] 28 Tauri, HD 23862; 1900 R.A. 3^h43^m3; Decl. $+23°15'$; mag. 5.2.
[2] *Ap. J.*, **93**, 446, 1941.
[3] *Ap. J.*, **97**, 426, 1943.
[4] *Ap. J.*, **93**, 453, 1941.
[5] *Pub. A.A.S.*, **10**, 227, 1946.
[6] *Ap. J.*, **110**, 166, 1949.

coudé plates in the photographic region, 10 A/mm; Table 3, coudé plates in the visual region, 20 A/mm. An additional set of 17 high-dispersion spectrograms, 3 A/mm, taken largely by W. S. Adams in the years 1943–1946, is not included in the present discussion, although Mr. Adams kindly made them available for comparison. These plates will be of especial importance for microphotometer studies of the line profiles.

The spectral region most thoroughly covered in the present discussion extends from about λ 3400 to *Hβ*, λ 4860 (Tables 1 and 2). On several plates the spectrum in the

TABLE 1

ONE-PRISM SPECTROGRAMS OF PLEIONE

PLATE	DATE	RADIAL VELOCITY			
		Hydrogen		Metals	
		Km/Sec	No. Lines	Km/Sec	No. Lines
γ 21565	1938 Nov. 30	+ 7	9	(+2)	8
γ 21633	1939 Jan. 10	(+13)	2	(+4)	5
C 7425	Dec. 21	+10	3	(+7)	4
C 7626	1940 Nov. 19	+ 7	6	+6	10
γ 23199	24	+ 8	4	+7	12
C 7654*	1941 Jan. 11	+ 7	18	+8	6
		+ 6	8	+9	7
		+ 8	6	+9	6
γ 23897	Nov. 27	+ 8	4	+8	28
γ 24737†	1942 Nov. 30	(− 2)	26	(−1)	13
γ 27290	1945 Dec. 15	+ 2	6	−1	25

* Three exposures.

† Strong exposure; comparison imperfect.

ultraviolet is usable to λ 3300, and on one or two it extends slightly below λ 3200. A number of plates (Table 3) show the "visual" region from *Hβ* to *Hα*; and one plate covers the infrared to λ 8800.

BRIGHT HYDROGEN LINES

Emission on either side of the dark core is regularly strong at *Hα*, weak at *Hβ*, and absent at *Hγ* and following lines. No radical change in intensity occurred throughout the whole shell episode. Except in 1951, the pattern was nearly symmetrical, although small changes in the structure were observable. Typical profiles are shown in Figure 1. In 1951, when the dark cores were weak, an asymmetry developed either in the emission borders or in the absorption wings or both, the longward portion of the emission appearing relatively strong.

DARK SHELL LINES

The shell spectrum with its numerous narrow dark lines continued to develop for several years after the discovery in October, 1938, of the reappearance of the bright hydrogen lines. The general appearance of the shell spectrum is well shown in the photographs reproduced by Struve and Swings.[3] These observers also gave an excellent list of lines and identifications from λ 3307 to λ 4675.

The shell lines reached maximum intensity in 1945 or 1946, after which they became weaker until, by March, 1951, they were nearly gone. Figure 2, based on eye estimates, shows the general course of the intensities. Emission, except in the *Hα* and *Hβ* lines, is

TABLE 2

COUDÉ SPECTROGRAMS OF PLEIONE: PHOTOGRAPHIC REGION

PLATE	DATE	RADIAL VELOCITY (KM/SEC)				No. MET. LINES
		*H*5	*H*15	*H*25	M II	
2651	1941 Nov. 3	+ 9.5	+ 8.0	+ 6.5	+ 8.0	35
2695	1942 Jan. 2	+ 8.0	+ 7.5	+ 9.2	+ 9.9	23
2719	29	+ 9.0	+ 8.4	+ 8.0	+ 8.5	77
2728	Mar. 1	+ 7.0	+ 8.0	+ 8.0	+ 9.0	33
2737	3	+ 9.6	+ 8.0	+ 9.4	+ 8.0	21
2934	Dec. 26	.....	.....	.....	+ 7.2	7
2955	1943 Feb. 24	+ 8.8	+ 7.0	+ 7.5	+ 9.3	59
2957	25	+ 9.2	+ 8.5	+ 8.4	+ 8.8	161
2969	Mar. 23	+10.8	+ 9.0	+ 8.0	+ 8.8	60
3129	July 22	+ 5.0	+ 3.5	+ 2.0	+ 4.5	58
3221	Oct. 6	+10.0	+ 8.0	+ 8.0	+ 7.7	88
3284	Nov. 13	+10.0	+ 8.0	+ 9.5	+ 9.0	77
3314	Dec. 12	+10.0	+ 8.5	+ 8.0	+ 8.2	81
3539	1944 Aug. 4	+ 6.3	+ 6.0	+ 5.0	+ 5.9	95
4381	1946 Aug. 19	+ 6.8	0.0	− 2.3	+ 1.9	60
4382	19	+ 6.0	+ 1.3	− 2.6	+ 2.1	65
4577	1947 Feb. 5	− 7.0	− 6.2	− 8.4	− 4.6	75
4639	Apr. 6	+ 3.0	− 0.5	− 2.6	+ 1.7	51
4815	Aug. 26	+ 1.5	− 5.0	−12.0	− 2.6	51
4916	Oct. 6	+ 4.5	− 2.2	− 5.5	− 2.1	58
4934	25	+ 4.3	− 0.6	− 5.2	+ 0.8	89
4980	Nov. 29	+ 3.4	0.0	− 3.6	+ 2.2	79
5043	1948 Jan. 3	+ 4.8	+ 1.8	− 1.0	+ 3.3	68
5277	Aug. 16	+ 3.4	0.0	− 3.5	+ 3.3	33
5487	Dec. 11	− 1.6	− 6.6	−12.8	− 5.1	35
5523	1949 Feb. 5	+ 2.8	− 1.2	− 8.0	− 2.2	28
5810	Aug. 3	+ 5.5	− 6.0	−14.0	− 6.3	34
5815	4	+ 7.0	− 5.0	−15.0	− 7.7	53
5926	Sept. 10	+ 4.5	− 4.0	−15.6	− 3.2	60
5986	Oct. 9	+ 5.0	− 2.4	−12.3	− 4.6	56
6029	Nov. 13	+ 3.2	− 3.0	−13.4	+ 1.1	31
6084	1950 Jan. 4	− 5.0	−11.8	−21.0	− 8.4	31
6153	Feb. 21	− 1.0	−12.0	−25.5	− 7.3	11
6158	22	− 2.5	−10.8	−26.5	− 8.5	20
6159	22	− 2.2	−11.0	−24.2	− 8.8	9
6431	Aug. 4	0.0	−10.5	−25.8	− 9.4	11
6432	4	+ 0.4	−13.0	−28.8	− 8.7	21
6447	7	− 4.7	−16.5	−39.8	−11.3	17
6692	Nov. 27	+ 1.2	−12.0	−29.0	− 5.5	7
6693	27	+ 2.8	−14.0	−35.0	− 6.1	7
6697	28	+ 2.0	−18.0	−34.5	− 4.6	10
6698	28	0.0	−16.0	−20.4	− 7.0	14
6699	28	+ 3.5	−15.6	−27.2	− 5.8	11
6881	1951 Feb. 24	+ 2.0	−16.8	−33.2	− 1.9	8
6882	24	0.0	−19.5	−28.0	− 6.6	11
6957	Mar. 27	+ 6	−29	(−51)	.....	.....
6968	27	.....	.....	.....	− 6	2
7217	July 31	+ 4.0	(−22)	.....	(+ 2)	1
7227	Aug. 2	+ 4.0	(−22)	.....	(0)	4

inconspicuous. Traces of emission borders are sometimes visible, however, on either side of several lines of *Fe* II, especially those of longer wave lengths. Superposed on the general rise and fall in the intensity of the shell spectrum were a few rapid changes in line widths. Also certain differential effects between lines of various elements occurred. These appear to correspond to the differences noted by Kiess, Krogdahl, Bidelman, and Hall[5] near the beginning of the shell episode. To discuss them adequately would require numerous microphotometer tracings and careful intercomparison. The present paper is limited largely to data obtained by micrometer measurements of displacements. Of about

TABLE 3

COUDÉ SPECTROGRAMS OF PLEIONE: VISUAL REGION

PLATE	DATE	RADIAL VELOCITY (KM/SEC)			NO. MET. LINES
		*H*5*	*H*α	Metals	
1927	1939 Mar. 5	+9	+ 8	.....	.....
2113	Aug. 30	+9	+10	+14	2
2651	1941 Nov. 3	+8	+13	+10	18
2695	1942 Jan. 2	+8	+12	+12	12
2934	Dec. 26	+8	+14	+ 6	2
3181	1943 Sept. 7	+8	+13	+10	5
3995	1945 Sept. 26	+5	+15	+ 5	9
4814	1947 Aug. 26	+2	+22	(− 9)	19
5276	1948 Aug. 16	+2	+12	− 4	21
5493	Dec. 12	+2	+11	− 9	14
5811	1949 Aug. 3	+5	+18	(− 5)	2

* Interpolated from measures of plates in Table 2.

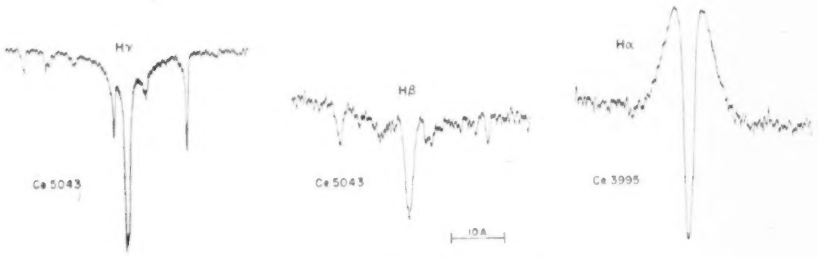

FIG. 1.—Typical profiles of $H\gamma$, $H\beta$, and $H\alpha$

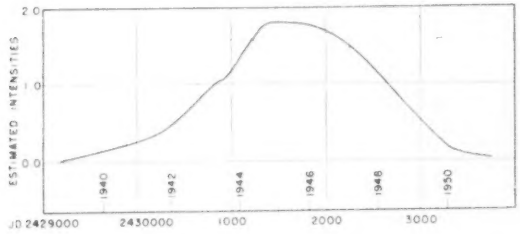

FIG. 2.—Intensities of shell lines

80 plate measurements, some of them long, approximately equal numbers were made by Miss Cora G. Burwell, Miss Sylvia Burd, and P. W. Merrill.

HYDROGEN LINES

On many plates separate Balmer lines can be distinguished as far toward the limit of the series as *H*35. On a number of plates *H*40 is visible; the greatest number is *H*42. Suppression of metallic lines by the Balmer continuum was marked in 1941 but seemed to become less as the shell spectrum grew stronger. This may have been because the hydrogen absorption was more nearly confined to the narrow cores, the overlapping wings and the continuous spectrum beyond the limit of the series actually becoming less potent. In 1951 the dark cores became much weaker and the remaining structure of the lines decidedly unsymmetrical. At *Hβ* the emission on the longward side of the line was relatively strong, and in the ultraviolet, where all emission is weak and the cores not so well marked, the shortward dark wing appeared stronger than the longward.

Before 1945 all the hydrogen lines had nearly the same displacement, the amount of which corresponded closely to the radial velocity of Pleione measured before the shell episode. From 1946 on, the displacements of successive Balmer lines exhibited an increasing negative progression which in 1951 became very pronounced. Sample measurements of individual plates are plotted in Figure 3. During the interval when the shell spectrum

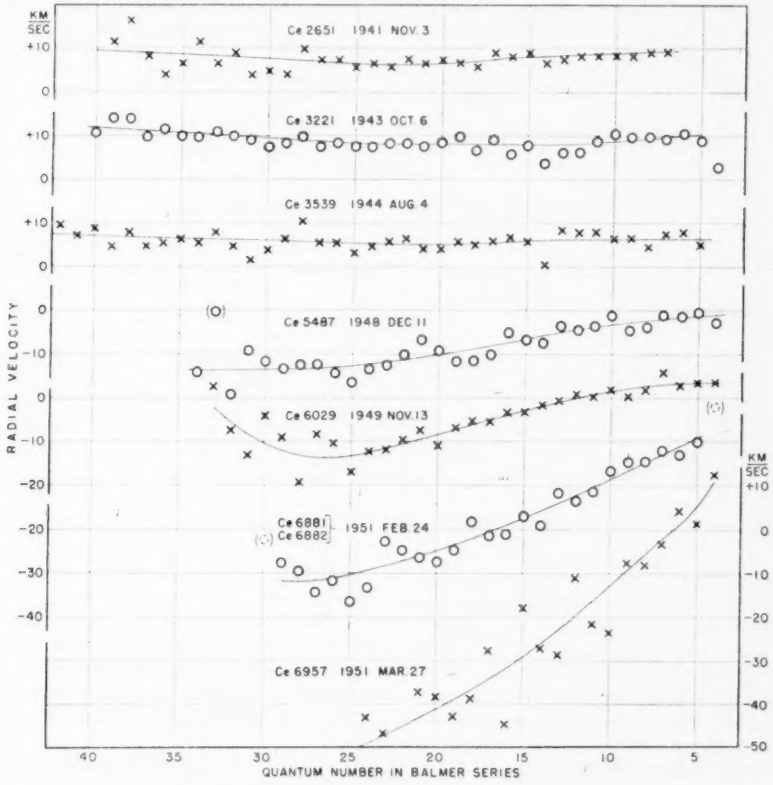

FIG. 3.—Progression in velocities from successive Balmer lines. Individual plates

was strong and the lines sharp, the probable error of measurement on a single plate of one of the Balmer lines *H*5–*H*27 was about ±1.2 km/sec (±0.015 A); toward the limit of the series, from *H*29 on, it was ±2.3 km/sec (0.03 A). During the same interval the probable error of measurement of an average metallic line was ±1.4 km/sec (±0.018 A). At least two of the Balmer lines have systematic residuals differing appreciably from zero, caused by blending with metallic lines. These lines are: *H*14 λ 3721.940, mean residual −0.02 A, blending line *Ti* II (13) λ 3721.632; *H*28 λ 3664.679, mean residual +0.03 A, blending line *Cr* II (156) λ 3664.95. The residuals indicate that *Ti* II λ 3721

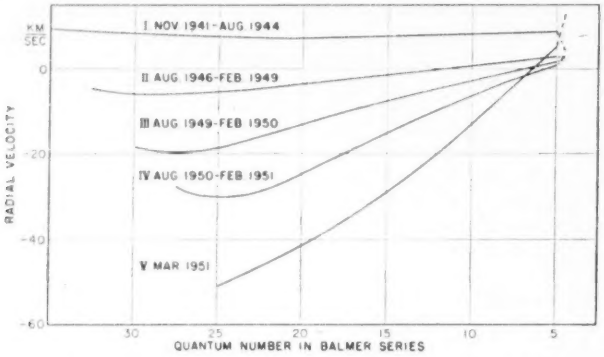

FIG. 4.—Progression in velocities from successive Balmer lines. Mean curves

TABLE 4

MEAN VELOCITIES DERIVED FROM VARIOUS LINES
(Km/Sec)

GROUP	COUDÉ PLATES	INTERVAL	MEAN JD 243	MEAN VELOCITIES					
				*H*25	*H*15	*H*5	*Hβ*	*Hα*	M II
I	2651–3539*	1941, Nov.—1944, Aug.	0804	+ 7.5	+ 7.6	+8.7	+ 4.2	+12.2*	+8.0
II	4381–5523	1946, Aug.—1949, Feb.	2502	− 5.6	− 1.6	+2.6	+ 2.4	+15.2	−0.1
III	5810–6159	1949, Aug.—1950, Feb.	3234	−18.6	− 7.3	+1.3	+ 2.7	+18.4	−6.2
IV	6431–6882	1950, Aug.—1951, Feb.	3600	−30.1	−15.2	+0.6	+ 3.2	.....	−6.7
V	6957–6958	1951, March	3733	(−51)	(−29)	(+6)	(+11)	.....	(−6)
VI	7217–7227	1951, July–Aug.	3861	.....	(−22)	+4	(+ 9)	.....	(0)

* The *Hα* velocity included Ce 1927, taken in March, 1939; Ce 2113, taken in August, 1939; and Ce 3995, taken in September, 1945.

is one-ninth as intense as *H*14, and that *Cr* II λ 3664 is one-eighth as intense as *H*28. The *He* λ 3970.074 line has a mean residual of +0.015 A; the cause is unknown.

Mean progression-curves for successive intervals of time are displayed in Figure 4. Data concerning the groups which serve as the basis for Figure 4 are collected in Table 4. The longward lines of the Balmer series retain nearly the same velocities year after year. To a first approximation, successive progression-curves, as they turn downward, pivot about *Hβ*. The values from *Hα* (Tables 3 and 4) are somewhat higher, probably because of the influence of the strong emission borders.

The increasing Balmer progression observed toward the end of the shell episode (Fig. 5) is doubtless related to the structure of the lines. When the progression became extreme

in 1951, the core at $H\beta$ remained sufficiently strong not to be appreciably affected by the relatively weak background structure, but toward the limit of the series, as the cores become weaker, an increasing asymmetry seems to accompany the measured displacement. In the lines near $H11$ this asymmetry is clearly seen; the shortward dark wing appears stronger than the longward wing. This might be ascribed to weak or incipient emission on the longward side of the core from atoms falling back toward the photosphere, but this interpretation is decidedly uncertain.

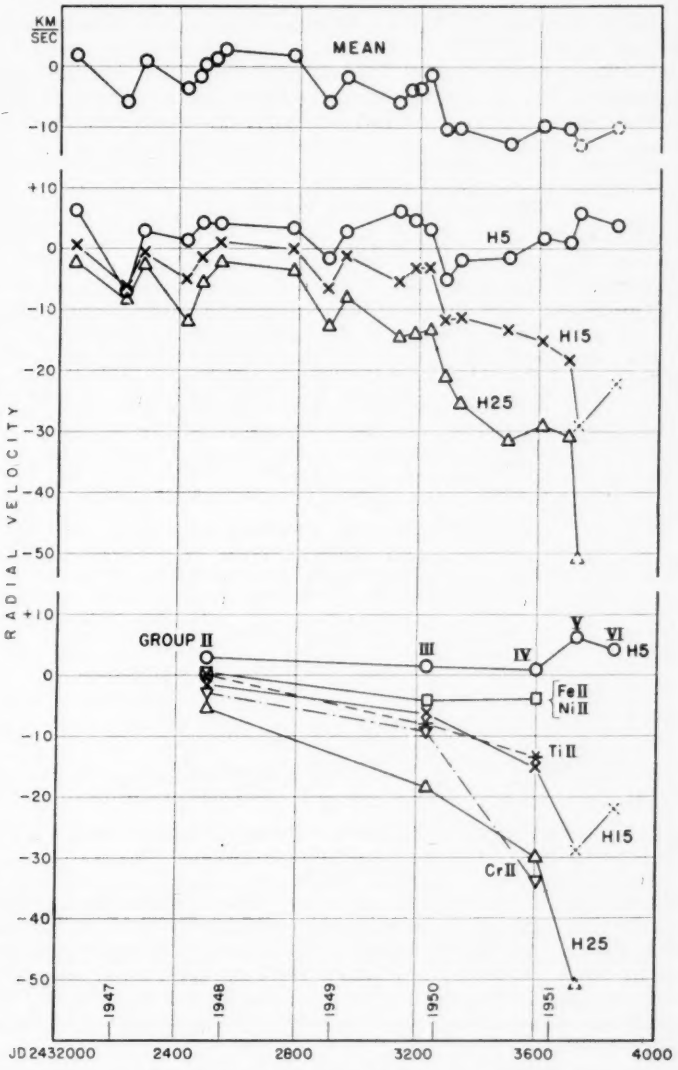

FIG. 5.—Velocity-curves derived from various lines

METALLIC LINES

Lines of *Ca* II, *Ti* II, *Fe* II, and *Ni* II were measured on nearly all the spectrograms. When the shell spectrum was especially strong, lines of *Mg* I, *Fe* I, *Sc* II, *V* II, and *Mn* II were usually included. The mean radial velocities and the number of lines on which they depend are recorded in Tables 1, 2, and 3. Except toward the end of the shell episode, displacements derived from the various neutral and ionized atoms agreed well (Table 5).

On most of the plates of the red region (Table 3) the D lines of sodium are strong and narrow, as they frequently are in shell spectra. Their intensities probably followed the course indicated for other lines in Figure 2. Their velocities agreed with those derived from other metallic lines. One of the coudé plates Ce 3181, taken on September 7, 1943, shows the region from λ 5700 to λ 8800. The longward portion does not differ radically from that reproduced by W. A. Hiltner[7] from a negative taken on September 12, 1946. Lines of *O* I are very strong. The measured velocities in Table 6 agree with those derived at about the same time from lines in other parts of the spectrum.

TABLE 5

VELOCITY RESIDUALS FOR VARIOUS LINES

Group	Mean JD 243	Adopted Rad. Vel. M II	Mean Residuals (Km/Sec)									
			*H*5	*H*15	*H*25	*Mg* I	*Fe* I	*Ca* II	*Sc* II	*Ti* II	*Cr* II	*Fe* II	*Ni* II
I	0804	+8.0	+ 0.7	− 0.4	− 0.5	+1.9	+0.6	+0.9	+2.1	−0.1	− 2.0	+0.2	+1.7
II	2502	−0.1	+ 2.7	− 1.5	− 5.5	−3.0	−3.0	+2.7	+0.3	0.0	− 3.0	−0.2	+2.0
III	3234	−6.2	+ 7.5	− 1.2	−12.4	(+1.5)	...	+1.0	...	−2.1	− 3.1	+1.5	+2.6
IV	3600	−6.7	+ 7.3	− 8.5	−23.4	...	...	−3.5	...	−7.1	−27.2	+2.0	+3.8
V	3733	(−6)	(+12)	(−23)	(−45)	.....	...	...	...	...	.....	.....	.....

TABLE 6

VELOCITIES FROM LINES IN THE INFRARED
PLATE Ce 3181

Element	Lines	Radial Velocity (Km/Sec)
H	P 11–P 26	+4
O I	λλ 7772, 4, 5; λ 8446	+5
K I	λ 7699	+9
Ca II	λλ 8498, 8542, 8662	+7
Fe II	λλ 7462, 7711	+5
Mean	.....	+5

DISCUSSION

From 1938 through 1943, all the lines on a given plate, including those of hydrogen and of several metals, yielded practically the same radial velocity. Moreover, only two plates, Ce 3129 and γ 24737, departed markedly from the mean value. The mean value derived from the coudé plates was +8.2 km/sec or, excluding Ce 3129, +8.5 km/sec; that derived from the low-dispersion plates was +6.3 km/sec or, excluding γ 24737, +7.5 km/sec. These values correspond closely to the velocity of the star as a whole determined before the shell outburst.

The complicated behavior of the velocities throughout the shell episode is shown in

[7] *Ap. J.*, **105**, 212, 1947.

Tables 1 to 6 and in Figures 3, 4, and 5. Interpolated mean values are in reasonable agreement with the low-dispersion measurements of Struve and Swings[3] and with the high-dispersion measurements of Miss Underhill[6] and of W. S. Adams.[5]

Superposed on the slow downward trend of velocities are several minima, but these do not seem to recur with a strict period. The low value yielded by the one-prism spectrogram γ 24737, JD 2430694, falls near the minimum of the section of the curve determined by Struve and Swings.

Toward the end of the shell episode, the measured velocities from various lines became divergent (see Fig. 5). The displacements of *Ti* II lines agreed with those of *H*15; displacements of *Fe* II and *Ni* II lines were algebraically greater; those of *Cr* II lines algebraically less. If increasing negative displacements (outward motions in the stellar atmosphere) correspond to increasing effective heights of absorbing zones above the photosphere, then the order of height is as follows: *H*5; *Ni* II, *Fe* II; *H*15, *Ti* II; *Cr* II; *H*25.

Although the nature of the forces that caused the formation and the dissipation of the shell about Pleione is obscure, the general kinematical history of the shell is revealed by the spectroscopic measurements. After a long period of stability, some relatively minor circumstance caused a very slight but persistent acceleration of gaseous atoms outward from the photosphere and the normal reversing layer. The first result was the formation of an emitting gaseous envelope. When sufficient atoms had accumulated at higher levels, an absorbing shell was detected. At first, the outward motions were too small to be measured; in other words, the radial velocity of the shell was, within errors of observation, the same as that of the star as a whole. Gradually the acceleration increased, and the outward velocity of the upper levels became appreciable. For a while the spectrum showed only slow changes, as a nearly steady stream of atoms passed through the spectroscopically active zone. Eventually, however, the supply of atoms failed, and the shell blew away. Possibly some of the atoms returned, exhibiting a preponderance of emission as they approached the photosphere. Their positive velocities (with respect to the observer) may conceivably account for the unsymmetrical structure of the lines in the final stages. To explore this general interpretation further, detailed studies of the line profiles at successive stages are desirable.

The recent episode in the spectroscopic career of Pleione illustrates several typical characteristics of gaseous shells surrounding early-type stars:

1. Shell spectra exhibit hydrogen emission, at least at *Hα*.
2. Lines of ionized metals predominate, although lines of neutral metals may be present in low intensity.
3. Shells are seldom stabilized.
4. Changes are relatively slow, being measured for the most part in months or years rather than in days or weeks.
5. In a changing shell spectrum, a progression in the displacements of successive Balmer lines frequently appears.

The recent spectroscopic behavior of Pleione brings up questions of long standing concerning the atmospheres of Be stars. What are the circumstances that produce shells? Why do shells occur in certain stars and not in other apparently similar stars? Why are they unstable? Why do very quick changes rarely occur?

Is the effective level of formation of the dark hydrogen lines near the limit of the Balmer series higher than that for lines of greater wave length? I hope to discuss this interesting question in future papers.

I am indebted to Miss Cora G. Burwell and Miss Sylvia Burd for assistance in measuring the numerous spectrograms and to Miss Louise Lowen for assistance in preparing the tables and figures.

[5] Unpublished.

TWO F-TYPE STARS WITH EXPANDING HYDROGEN ATMOSPHERES

PAUL W. MERRILL
MOUNT WILSON AND PALOMAR OBSERVATORIES
CARNEGIE INSTITUTION OF WASHINGTON
CALIFORNIA INSTITUTE OF TECHNOLOGY
Received November 17, 1951

ABSTRACT

Two stars, MWC 490 and HD 59771, studied because of the discovery of a bright *Hα* line, were found to be spectroscopic binaries with large ranges in radial velocity. In the spectra of both stars displaced dark lines indicate a cloud of hydrogen expanding rapidly above a quiescent F-type reversing layer. These systems have much in common with that of *υ* Sagittarii.

In most stars the thin outer layers in which the observable absorption lines are formed are at rest with respect to the underlying photosphere and the body of the star. In certain stars, however, a rapid outflow of gaseous atoms can be detected by means of dark lines having large shortward displacements. Hydrogen, the lightest and most abundant of all the elements, is most frequently found to be moving outward, but other atoms are sometimes observed to have similar motions.

The most spectacular examples of the phenomenon are found in the outbursts of novae, in which the outward velocities exceed the velocity of escape and the shell expands indefinitely into interstellar space. In P Cygni and other early-type stars a slower expansion has been observed to continue for many years. In these stars a succession of outward-moving atoms passes through a zone which retains a nearly fixed position at a moderate distance above the photosphere. Data concerning stars of this kind are compiled in a most useful monograph recently published by C. S. Beals.[1]

The phenomenon is not so common in later-type stars, although on the sun eruptive prominences exhibit rapid outward motions involving very small portions of the atmosphere. In long-period variables the shortward displacements of bright lines indicate a relatively slow outward motion of the gases emitting the bright lines.

The present article describes two unusual stars (Table 1) in which hydrogen atoms are rising rapidly above a quiescent F-type reversing layer.

MWC 490

A bright *Hα* line was discovered[2] in the spectrum of the tenth-magnitude star MWC 490[3] on an objective-prism photograph taken by W. C. Miller with the 10-inch telescope on Mount Wilson on November 30, 1940. Nine slit spectrograms, listed in Table 2, have been obtained since then. Additional data are afforded by the Victoria observations in 1946, concerning which Dr. Beals has been kind enough to send me data more detailed than those published.[1]

Hydrogen emission lines of moderate width and intensity are present on all spectrograms. The velocity ranges approximately from 0 to +25 km/sec. Dark lines of hydrogen with large shortward displacements are present on all plates in varying intensity. They were stronger in 1945 than in 1942 or 1948, and stronger in 1951 than in 1950. The lines are rather wide but are frequently separated from the corresponding bright lines by a shoulder of continuous spectrum. This fact indicates that both bright and dark lines cannot be due to a single expanding shell, as in the standard explanation of nova-like line profiles. In some of the dark lines there appear to be two components, but the

[1] "The Spectra of the P Cygni Stars," *Pub. Dom. Ap. Obs., Victoria*, **9**, 1, 1951.

[2] P. W. Merrill, *Pub. A.S.P.*, **55**, 40, 1943.

[3] P. W. Merrill and C. G. Burwell, *Mt. W. Contr.*, No. 682; *Ap. J.*, **98**, 153, 1943.

velocities recorded in Table 2 correspond to the center of the whole line. The mean velocity from all measurements on the Mount Wilson and Palomar plates is −550 km/sec. This remarkably large velocity has continued without much change for at least nine years. The means from individual plates, Table 2, are not of high accuracy, although, on a given plate, values from various lines, *Hε* to *Hβ*, usually agree fairly well.

The displaced dark line of *He* I, λ 4471, is clearly subject to changes in intensity. It was present on the low-dispersion plates of Table 2, and Beals remarks that it was "a conspicuous feature of the spectrum" in 1946; but it was weak or absent on the coudé plates of 1950 and 1951. Its negative displacement appears to be somewhat less than that of the hydrogen dark lines.

Nearly all the Mount Wilson and Palomar plates show narrow metallic lines, the num-

TABLE 1

TWO STARS WITH EXPANDING HYDROGEN ATMOSPHERES

MWC	HD	BD	1900 R.A.	1900 Decl.	Mag.	Harv. Spect.
490	242257	+33° 997	5^h11^m2	+33° 56′	10.3	G0
	59771	−17°2010	7 26.4	−18 2	9.1	G0

TABLE 2

SPECTROGRAMS OF MWC 490

Plate	Date	Observer*	Disp. at *Hγ* (A/mm)	Radial Velocity (km/sec)			
				H	Metals	No. Met. Lines	*Ca* II
γ 24670	1942 Nov. 13	A. H. Joy	120	(−580)	.....	.....	.....
γ 24742	Dec. 1	P. W. Merrill	80	−584	−26	7	0
γ 24746	Dec. 2	P. W. Merrill	80	(−527)	−31	9	+5
γ 27182	1945 Nov. 9	W. C. Miller	80	−515	(−20)	2	+7
γ 27274	Dec. 9	W. C. Miller	35	−536	+14	15	−3
γ 29292	1948 Jan. 24	W. C. Miller	80	−531	.....	.....	+7
Pc 22	1950 Nov. 16	I. S. Bowen O. C. Wilson	9	−584	+27.4	40	+5.9
Pc 25	Nov. 17	I. S. Bowen O. C. Wilson	9	(−573)	+23.2	42	+4.2
Pc 198	1951 Oct. 18	I. S. Bowen	9	−539	−31.3	30	(+1)

* I am grateful to Messrs. Joy, Miller, Bowen, and Wilson for making their plates available for this study.

ber increasing with the dispersion. On the plates with dispersion 80 A/mm, only a very few lines can be seen with certainty. On the best plate, Pc 25, scores are visible, but they appear rather weak as if slightly veiled by overlying continuous spectrum; their relative intensities resemble those of π Sagittarii, type cF0. On γ 27274 the lines have the same veiled appearance; their relative intensities are comparable to those of α Leporis, type cF0. Measures show a range in radial velocity of nearly 60 km/sec, indicating that the object is a binary.

The strong H and K lines of *Ca* II are probably interstellar. Their displacements do not follow those of the other metallic lines but are probably constant within errors of measurement. The weighted mean velocity +4.6 km/sec, residual velocity −3.8 km/sec, corresponds to a distance of 2480 parsecs for a star in this position. From the intensity of the interstellar line λ 4430, Beals obtained a distance of 2080 parsecs. Without cor-

rection for space absorption, the larger distance corresponds to an absolute photographic magnitude of −1.7.

HD 59771

A bright *Hα* line was discovered[4] in the spectrum of HD 59771 on an objective-prism photograph taken with the 10-inch telescope on Mount Wilson on December 16, 1939. Four slit spectrograms, listed in Table 3, have been obtained since then. The discovery photograph and the last two slit spectrograms were taken by W. C. Miller, to whom I am indebted for much assistance in observing.

Numerous metallic lines resemble those of 25 Monocerotis, type gF5. The lines are not quite so well defined as in *α* Persei, type cF5. The measures reveal large differences

TABLE 3

SLIT SPECTROGRAMS OF HD 59771

Plate	Date	Disp. at $H\gamma$ (A/mm)	Radial Velocity (km/sec)				
			$H\delta$	$H\gamma$	$H\beta$	Metals	No. Met. Lines
γ 23274	1941 Jan. 15	80	−116	−139	−242	+10	16
γ 24739	1942 Nov. 30	35	(+ 40)*	(+ 25)*	−215	+97	26
γ 27362†	1946 Jan. 14	35	.....	.....	.....	.....	.....
γ 30334	1948 Dec. 18	70	− 88	−106	.....	−19	4

* There may be weak components at $H\delta$ and $H\gamma$ having a velocity of about −140 km/sec.

† Underexposed.

in radial velocity at various times, but they are too few to give any indication of period. On the first slit spectrogram the dark hydrogen lines are abnormally wide and intense, with large negative displacements. The $H\beta$ line has weak emission on the longward edge. On the second plate the dark components are much weaker and, except for $H\beta$ (which is strongly affected by the emission), have much smaller displacements. On the last plate the intensities and displacements are intermediate. The data are too meager to bring out any connection between the behavior of the hydrogen lines and that of the F-type spectrum.

DISCUSSION

Both these objects are spectroscopic binaries in which one component resembles a giant or supergiant F-type star. Both have bright hydrogen lines about in their normal positions with greatly displaced dark components indicating large outward velocities; the intensities of the displaced components are subject to large variations. These systems have much in common with that of *υ* Sagittarii.[5]

A kinematical interpretation could be based on a close double star with components revolving within a tenuous cloud of mildly luminous hydrogen whose outer absorbing portions are rapidly expanding. The dynamical explanation might be similar to that developed by O. Struve[6] and G. P. Kuiper[7] for *β* Lyrae. An alternative hypothesis would envisage a local cloud about the F-type star sent up from large areas of the surface after the manner of an eruptive prominence on the sun.

It would be desirable to obtain more knowledge concerning these interesting binaries. Systematic series of spectrograms with dispersion about 10 A/mm would be valuable.

[4] P. W. Merrill, *Pub. A.S.P.*, **54**, 155, 1942.

[5] W. P. Bidelman, *Ap. J.*, **109**, 544, 1949; J. L. Greenstein, *Ap. J.*, **111**, 20, 1950.

[6] *Ap. J.*, **93**, 104, 1941.

[7] *Ap. J.*, **93**, 133, 1941.

RADIAL VELOCITIES OF 360 STARS

RALPH E. WILSON AND ALFRED H. JOY
MOUNT WILSON AND PALOMAR OBSERVATORIES
CARNEGIE INSTITUTION OF WASHINGTON
CALIFORNIA INSTITUTE OF TECHNOLOGY
Received October 22, 1951

ABSTRACT

Herein are presented radial velocities and spectral classifications of 360 stars, determined from observations with the 60-inch and 100-inch reflectors of the Mount Wilson Observatory.

Early in 1950 the authors published[1] radial velocities and spectral classifications of 2111 stars which had been observed at the Mount Wilson Observatory. In the introduction to that paper we stated that some work remained to be done in the early hours of right ascension, the region of the sky covered during our poorest observing season. This work was completed during the winter of 1950–1951, and a number of additional plates were secured of stars with spectra containing poor lines. Most of these stars were on the earlier programs, no results having been published because the characteristics of the spectra and the quality of the plates were such that the measures of velocity displacements were very uncertain. The probable errors of the velocities in this list are, therefore, unavoidably large. A number of stars are published now, only because there appears to be no immediate prospect that additional spectrograms will be secured, and we wish now to complete the publication of the Mount Wilson routine observations of radial velocities.

Most of the velocities are based upon plates taken with dispersions of 38 or 75 A/mm at $H\gamma$. The 1950–1951 plates were taken by R. E. Wilson and W. C. Miller. They were measured by Mary F. Coffeen, Barbara P. Olsen, and R. E. Wilson. The classifications of spectra were made by A. H. Joy.

The tables present the results in the same form as before.

[1] *Ap. J.*, **111**, 221–261, 1950.

TABLE I

RADIAL VELOCITIES OF 360 STARS

STAR	H.D.	1950 R.A.	1950 Decl.	Vis. Mag.	P.M.	Spec.	Vel.	P.E.	No. Pl.	Others
		h m	° ′		″		km	km		
A 308	---	0 02.0	+41 49	9.2	---	dFo	- 36.	var	4•	
SW Scl	151	03.7	-33 06	var	0.014	gM4e	+ 34.	3.9	2	
G 175	598	07.9	+28 23	8.1	.008	gM4	- 13.1	1.6	3	- 7.4 D
G 326	1255	14.2	+09 58	6.8	.018	gM2	+ 11.7	1.4	3	
75° 7	1359	15.5	+76 00	7.1	.029	B9n	0	3.2	4	- 5.0 D
G 453	1831	0 20.3	+38 29	7.0	.007	gM4	- 22.7	1.3	3	
B 66	1952	21.4	+43 59	6.6	.014	sgA7n	- 4.	var	4•	
A 439A	2814	29.2	+36 41	8.1	.043	dG2	- 20.2	1.5	3	
A 582A	3891	39.5	+71 06	8.0	.030	A1	- 15.	var	5•	
A 582B	----	39.5	+71 06	8.2	---	A1	- 11.	var	4•	
43° 187	4134	0 41.5	+46 08	7.5	.089	dF2	+ 9.	var	4•	
G 906	4266	42.9	+56 30	7.6	.050	gF1	- 25.6	2.5	4	
44° 162	4364	43.7	+45 09	7.8	.031	dA5n	+ 9.5	2.1	4	
62° 175	5551	55.2	+63 27	7.7	.007	B1	- 51.	3.3	3•	-51.5 D
G 1176	5735	56.3	-19 54	7.3	.047	gM2	+ 30.	var	4•	
G 1184	5256	0 56.8	+87 03	8.9	.324	dG4	+ 15.1	0.8	3	
A 902A	----	1 03.2	+13 03	9.1	---	sgF9	+ 21.8	2.7	4	
G 1321	6414	03.4	+70 40	6.6	.087	A4n	- 6.	3.4	4•	
G 1399	6833	06.8	+54 28	7.1	.053	dG5	-238.2	1.9	2	-250. V
β And	6860	06.9	+35 21	2.4	.211	gMo	+ 3.2	1.6	4	+ 0.1 M
G 1480	7351	1 11.3	+28 16	6.6	.090	gM2	- 1.8	0.7	2	+ 5.8 D
55° 290	7861	16.3	+56 03	8.9	.025	gM6	+ 5.0	2.3	4	
B 301	8003	17.7	+64 24	6.3	.060	Aon	- 11.	5.3	4	- 19. V
76° 42	8364	22.1	+77 25	8.0	---	dF8	- 11.0	2.0	3	
A 1148A	8803	24.3	+03 17	6.4	.029	B8n	+ 15.5	2.3	4	
A 1148B	----	1 24.3	+03 17	9.0	---	dFo	+ 14.	3.4	4	
G 1811	9030	27.4	+65 50	6.2	.085	A2	+ 7.	var	4•	+ 10. V
G 1886	9500	31.0	+35 21	7.3	.044	gM3	+ 2.0	1.7	2	+ 1. L
63° 224	10304	39.2	+63 39	7.7	.056	gG8	- 8.8	1.5	4	
G 2090	10465	40.1	+48 16	7.0	.018	cM2	- 69.1	0.7	3	
22° 297	11038	1 45.7	-22 28	9.0	.182	dF7	+ 9.	4.1	5	
22° 299	11074	46.1	-22 28	8.3	.118	dG5	- 1.6	1.6	3	
G 2368	11961	55.2	+30 54	7.2	.048	gM5	- 44.3	2.4	3	- 46. L
G 2382	12051	56.2	+32 58	7.1	.433	dG7	- 36.4	1.1	3	
G 2403	12204	57.1	-14 07	7.1	.027	gM3	+ 29.4	2.1	3	
G 2456	12479	1 59.9	+13 14	6.3	.017	gM2	- 9.1	0.6	2	- 4.7 D
γ And	12533	2 00.8	+42 05	2.3	.068	gK3	- 9.1	0.5	3	- 11.7 M
CC 144	12873	03.3	-24 37	9.5	.44	dK1	+ 46.	3.4	2	
CC 145	12889	03.3	-24 37	9.2	.47	dKo	+ 24.2	1.9	2	
G 2524	12872	03.6	+08 01	6.7	.033	gM2	- 27.6	1.3	2	- 24.0 D
56° 444	----	2 08.6	+56 41	9.2	.003	B3	- 18.4	2.0	3	
56° 445	13370	09.0	+57 04	9.4	.014	B3	- 32.	var	4•	
G 2723	14001	13.4	-18 28	8.3	.192	dK4	+ 5.8	0.4	3	
G 2762	14146	15.0	+23 47	6.8	.015	gM1	+ 27.6	1.0	3	
56° 567	14434	18.3	+56 41	8.5	.009	B2n	- 20.	3.5	3	
70° 182	15472	2 28.9	+70 43	8.0	---	B4ne	- 25.	var	5•	- 62. D
G 3040	14955	29.3	+84 51	8.6	.094	dG3	- 48.	var	4•	
G 3048	15755	29.8	+34 19	5.9	.068	gK1	- 1.	3.1	4	- 2.7 S
B 562	15342	30.0	+81 26	8.5	.027	gK5	- 23.	var	4•	
29° 444	16245	34.2	+30 12	7.4	.031	Aon	+ 10.	4.5	4	+ 4.9 D
41° 508	----	2 37.6	+42 03	9.2	.320	dKo	+ 25.3	0.4	3	
G 3339	17382	45.2	+26 52	8.2	.296	dKo	+ 6.2	1.3	4	
G 3509	18142	52.7	+30 50	7.2	.019	gM3	- 21.6	0.5	2	- 25. L
A 22188	----	52.7	+26 40	9.7	---	dMo	+ 26.8	2.1	3	
29° 502	18328	54.6	+29 31	8.9	.049	dGo	- 6.	var	3•	
29° 503	----	2 54.8	+29 28	9.2	.206	dG9	+ 23.2	0.9	5	
G 3621	18760	58.3	-03 05	6.3	.021	gM1	+ 81.6	2.1	4	
α Cet	18884	59.7	+03 54	2.8	.075	gM2	- 26.2	0.2	2	- 25.7 M
G 3722	19382	3 04.3	-13 31	8.0	.067	dF2	- 3.5	2.9	4	
G 3734	19467	04.9	-13 57	7.2	.261	dG5	+ 12.8	1.5	4	

TABLE I (Cont'd)

STAR	H.D.	1950 R.A.	1950 Decl.	Vis. Mag.	P.M.	Spec.	Vel.	P.E.	No. Pl.	Others
		h m	° '		"		km	km		
A 2373AB	19620	3 07.0	+05 01	8.6	0.078	dGo	+ 35.4	1.2	3	
G 3806	19836	08.8	-04 00	6.3	.035	gM1	+ 24.3	0.5	3	
G 3808	19534	08.8	+74 03	7.2	.023	gM2	+ 13.8	1.2	2	+ 12. L
36° 651	19784	09.1	+36 47	8.8	.005	Ao	+ 7.4	1.3	3	
G 3983	20729	17.4	-24 18	6.0	.021	gM2	+ 15.4	2.1	4	
A 2499A	20873	3 19.9	+29 38	8.5	.038	A4	+ 11.	var	4•	
A 2499B	-----	19.9	+29 38	8.5	.041	A6	+ 19.	var	4•	
α Per	20902	20.7	+49 41	1.9	.035	cF4	- 3.0	1.0	3	- 2.4 M
41° 714	22193	32.8	+42 11	8.4	---	dG5	+ 54.2	0.9	3	
G 4465	-----	41.4	+32 00	8.4	.009	B8n	+ 25.	var	4•	
23° 520	23479	3 43.3	+24 02	8.2	.050	dA6n	+ 5.	4.1	3	- 6. Md
B 867	23629	44.4	+23 58	8.1	.052	Aon	+ 4.	4.8	4	+ 6. Md
23° 529	23643	44.5	+23 32	8.1	.033	A3n	+ 8.9	2.1	3	+ 8. Md
B 864	23475	44.9	+65 22	4.7	.008	gM1	- 3.1	1.5	7	- 3.2 L
A 2926B	-----	58.0	+23 04	7.8	.023	B9n	+ 10.	6.5	4	
G 4856	24894	4 00.2	+79 29	8.4	.206	dF8	+ 44.8	2.5	4•	
11° 571	25978	04.4	+12 08	7.4	.055	Aon	+ 22.	var	5•	
29° 700	27514	18.6	+30 05	8.8	.032	gG6	- 25.0	1.7	3	
χ Tau	27638	19.5	+25 31	5.4	.030	Aon	+ 26.3	2.6	4	+ 11. L
29° 706	27787	21.3	+30 01	9.0	.037	A1n	- 24.	3.7	4	
G 5449	28479	4 26.4	-19 34	6.1	.090	gK1	+ 26.7	2.5	4•	
Anon.	-----	29.6	+36 05	10.8	---	gG8	+ 34.1	2.3	3•	
G 5617	29248	33.8	-03 27	4.1	.001	B2	+ 15.	var	5•	+ 15.4vM
19° 762	-----	39.8	+20 08	9.6	.092	Ao	- 5.	4.7	4r	
44° 1013	29882	41.0	+44 41	7.8	.044	dA6n	+ 23.4	2.4	3	
A 3417A	30101	4 42.1	+05 12	8.9	.159	dG7	- 18.4	0.5	2	
A 3417B	-----	42.1	+05 12	8.9	---	dK1	- 19.2	0.1	2	
G 5827	30165	44.6	+61 25	7.7	.019	gM5	+ 53.8	1.2	3	
41° 1002	31085	51.3	+41 41	8.0	.029	dF5	- 4.5	1.0	3	
A 3514A	31208	51.6	+07 18	7.9	.323	dK2	+ 46.4	1.6	3	
A 3514B	-----	4 51.6	+07 17	8.2	.300	dK1	+ 40.6	1.9	3	
42° 1180	-----	5 05.2	+42 30	9.2	.051	gM6	+ 5.	var	4•	
38° 1040	33061	06.0	+38 57	8.6	.048	B8	- 12.	var	5•	
G 6316	33340	07.2	+08 07	7.1	.128	dF5	- 64.	var	4•	
A 3835A	-----	12.6	+29 25	9.0	.052	dG3	- 65.9	1.6	4	
G 6425	34180	5 12.8	-01 28	6.1	.058	dF2	+ 13.2	3.0	4	
14° 1080	34309	13.7	-14 34	7.7	.047	B9	+ 46.	var	4•	
A 3866B	-----	14.6	+20 05	9.5	---	dK2	- 35.5	1.2	2	
G 6483	34454	15.2	+13 22	7.9	.022	gM5	+ 10.3	1.8	3	
G 6511	34721	16.6	-18 11	5.9	.387	dGo	+34.9	1.7	4•	+ 48.v Md
15° 790	34811	5 17.9	+15 35	7.7	.021	dA5n	+ 29.	var	4•	
14° 1105	35042	19.1	-14 36	7.2	.038	B6	+ 21.	4.1	4	
G 6622	35171	20.7	+17 17	8.2	.270	dK5	+ 37.9	1.6	3	
B 1294	35296	21.5	+17 20	5.1	.249	dF8	+ 33.9	2.3	3	+ 37.0 M
G 6747	35991	25.5	-21 25	6.1	.040	gG7	+ 34.4	0.5	3	
G 6779	36134	5 26.9	-03 29	6.1	.046	gG8	+ 23.6	2.0	4	
G 6869	36065	30.4	+74 17	7.0	.120	dF2	- 18.	3.3	4	
A 4193B	-----	33.0	-05 56	7.3	---	B8	+ 23.2	2.9	2	
5° 1325	-----	33.1	-05 18	9.1	.015	B8n	+ 48.	var	3	+ 36.8 V
1° 1001	37674	37.7	-01 29	8.4	.010	B5n	+ 15.	var	4•	
2° 1345	37903	5 39.2	-02 17	8.6	.017	B3n	+ 10.	5.	3	+ 5.9 L
43° 1332	-----	39.8	+43 27	8.8	.024	gM1	+ 15.	var	4•	
2° 1350	38087	40.5	-02 20	8.6	.005	B3n	+ 33.	4.1	4	
B 1447	39070	47.3	-14 30	5.6	.052	gG6	- 1.8	2.0	4	
24° 1036	249499	54.2	+25 00	9.3	.063	dK4	+ 3.	var	4•	
G 7515	40301	5 55.2	-06 06	7.6	.011	gM2	+ 40.9	1.7	3	
G 7589	40635	57.6	-00 30	7.7	.022	B9n	+ 31.	var	4•	
G 7617	38847	58.9	+85 00	8.8	.177	dG2	- 70.2	2.5	4	
A 4629B	-----	6 00.3	+27 39	9.3	---	dA7n	+ 27.	var	4	
G 7824	42049	06.5	+22 12	6.0	.020	gK4	+ 6.9	2.3	3	+ 10.3 D

TABLE I (Cont'd)

STAR	H.D.	1950 R.A.	1950 Decl.	Vis. Mag.	P.M.	Spec.	Vel.	P.E.	No. Pl.	Others
		h m	° ′		″		km	km		
G 7844	42216	6 07.5	+23 01	6.7	0.007	B9n	- 5.	var	4•	
B 1542	42443	07.7	-22 46	5.7	.106	dF6	+ 21.7	1.9	4	
B 1541	42398	08.5	+24 26	5.9	.057	gKo	+ 22.	var	4•	
G 7888	42471	09.1	+32 42	6.0	.008	gM1	- 48.0	2.3	2	- 51.4 D
CC 380	-----	13.0	+47 05	9.2	.53	dG6	+ 27.3	0.1	2	
G 8065	43745	6 15.0	-22 42	6.0	.280	dGo	- 3.4	1.9	4	
B 1586	43760	15.2	-10 42	6.7	.008	gF2	+ 26.2	1.9	3	
G 8238	43680	21.1	+79 41	8.4	.157	gKo	+ 3.2	1.8	4	
B 1612	44780	21.6	+25 05	6.6	.012	gG9	+ 6.	var	4•	+ 9.v D
G 8438	45783	27.7	+32 50	8.1	.031	gM2	+ 48.5	1.3	3	
G 8456	46114	6 28.5	-17 53	7.7	.274	dG4	+ 0.8	0.9	3	
30° 1256	46158	29.9	+30 21	8.0	.038	A2n	- 9.	var	4•	
B 1557	42855	30.2	+86 44	6.6	.107	gG8	+ 26.8	1.1	3	+ 24.8 V
B 1658	46318	31.8	+56 26	6.5	.066	dFon	+ 1.7	2.3	3	
B 1679	46781	33.1	+16 50	6.7	.037	dF8	+ 27.8	0.7	2	+ 30.5 V
B 1691	-----	6 34.2	-18 37	7.9	.044	dA8	+ 33.8	2.8	4	
44° 1501	46981	34.8	+44 21	7.8	.046	gF1	- 19.3	2.8	4	
G 9042	50420	51.6	+43 58	6.0	.018	gFo	- 7.1	2.5	3	- 8.5 V
B 1778	50635	51.8	+13 15	4.7	.117	dA8n	+ 27.	3.5	4	+ 21.0 L
+0° 1717	51220	54.0	+00 10	7.7	.042	dG5	+ 47.7	1.8	4	
1° 1473	51473	6 54.9	-01 18	8.7	.022	Ao	+ 9.	var	6•	
A 5752AB	53299	7 01.8	-02 58	8.6	.055	dG6	+ 7.	var	4•	
10° 1848	53367	02.1	-10 23	7.0	.040	B1ne	+ 24.	4.7	7•	+ 11.1 V
8° 1734	53667	03.2	-08 39	7.8	.018	Bde	+ 40.	6.	4	+ 36. L
G 9366	53532	03.3	+22 46	8.1	.119	dG6	+ 39.4	1.6	3	
G 9385	53766	7 04.2	+24 15	6.9	.040	gM1	- 11.7	0.7	3	
A 5864A	54649	08.6	+55 53	7.7	.046	gK1	+ 11.	var	3•	
B 1848	55057	08.8	-00 13	5.4	.034	dA8n	+ 23.	3.3	4	+ 36. L
4° 1862	55684	11.3	-05 04	7.5	.012	•	+ 3.	var	4•	
14° 1628	56714	15.8	+14 27	7.7	.015	B9	+ 31.	var	4•	
G 9720	56196	7 15.9	+65 32	9.4	.321	dGo	+ 35.9	0.5	3	
14° 1843	57435	18.3	-14 47	9.1	.022	gK3	+129.1	2.2	3	
B 1923	57749	20.0	-05 53	5.8	.013	gF2	+ 10.9	1.5	3	
B 1936	58367	22.9	+09 23	5.1	.015	gG5	- 12.4	1.2	2	- 7.6 M
G 9923	58526	23.4	-05 40	6.1	.030	cG2	+ 13.6	1.7	3	
27° 1387	58578	7 24.2	+27 24	8.2	.028	A2	- 0.7	2.3	4	
B 1951	58954	24.9	-17 46	5.7	.014	dA5n	- 29.7	0.9	3	
G 9963	58640	25.0	+48 01	6.9	.102	gM4	+ 26.0	0.9	3	
G 10022	59381	27.0	-10 13	6.0	.031	gK5	- 6.8	0.4	3	
G 10091	59201	29.8	+73 23	8.4	.354	dK2	- 24.	var	4•	
B 1985	60414	7 31.5	-14 25	5.1	.015	gM3ep	+ 40.0	1.4	5	+ 20.v M
G 10136	60336	32.0	+24 23	7.9	.025	gM2	+ 25.4	0.9	3	
B 2002	-----	35.8	+05 11	8.5	.006	gM2	+ 1.	var	4•	
G 10280	61295	36.7	+32 08	6.1	.052	gF3	+ 25.9	0.8	3	+ 25.v DS
G 10298	61856	37.3	-01 24	9.7	.282	dG2	+ 44.8	1.0	3	
G 10566	63696	7 47.4	-13 58	6.6	.049	dM1	+ 33.8	2.7	4•	
B 2066	63697	47.4	-17 06	5.5	.130	gK3	+ 44.5	1.6	4	
G 10619	63889	49.0	+19 27	6.1	.064	gK1	+ 37.9	0.7	2	+ 40.7 D
B 2073	64077	49.3	-12 41	6.5	.013	dF2	+ 20.9	2.7	4	
B 2082	64238	50.0	-14 43	5.7	.014	cF3	+ 16.7	1.5	3	
B 2083	64235	7 50.3	-05 18	5.8	.036	gF5	- 2.3	0.4	3	
G 10671	64351	51.3	+21 14	7.0	.015	gM1	+ 9.6	1.1	3	
B 2092	64685	52.8	+09 00	5.8	.091	dF4	+ 24.8	0.4	2	+ 19.8 V
B 2104	65345	55.8	+02 22	5.4	.187	gG6	+ 44.0	1.0	2	+ 46.8 M
G 10788	65275	56.2	+34 49	7.7	.015	gM2	- 24.3	1.7	3	
G 10911	66175	8 00.4	+36 29	6.8	.037	gM5	- 0.5	1.0	3	
G 10924	65871	00.8	+68 32	7.6	.306	dF7	- 5.1	2.1	3	
G 11079	67743	07.2	+17 10	7.4	.019	gM2	+ 22.6	1.5	4	
G 11137	68168	09.0	+16 41	7.2	.293	dG2	+ 8.0	0.7	3	
G 11165	68461	10.2	+16 40	6.1	.026	gG3	- 18.4	0.6	2	- 20.v DS

TABLE I (Cont'd)

STAR	H.D.	1950 R.A.	1950 Decl.	Vis. Mag.	P.M.	Spec.	Vel.	P.E.	No. Pl.	Others
		h m	° ′		″		km	km		
G 11200	-----	8 11.7	+27 19	8.1	0.004	gMo	+ 27.5	0.7	3	
14° 2460	69772	15.7	-14 49	8.0	.052	B9n	+ 27.	4.1	4	
74° 360	69659	19.1	+74 36	8.6	.016	gK3	+ 1.2	2.1	4	
G 11480	70937	22.1	-04 33	6.0	.056	dF4	- 35.	var	4•	
A 6800B	-----	23.0	-23 53	9.0	.032	gK3	+ 19.		1	
G 11906	73844	8 37.6	-17 07	7.0	.160	gM5	+ 31.6	1.1	3	
B 2261	71986	38.6	+85 14	7.4	.140	dF5	+ 0.3	2.2	4	
G 11958	74011	39.4	+34 22	7.4	.267	dF7	+ 44.4	1.7	4	
B 2339	74521	42.0	+10 16	5.6	.027	A4p	+ 24.1	2.2	4	+ 24.6 YV
B 2353	74873	44.2	+12 17	5.7	.090	Ao	+ 25.1	2.1	3	+ 21.0 D
CC 490	-----	8 46.2	+36 41	10.0	.56	dM1	+ 1.2	0.0	2	
-0° 2087	76082	51.4	-00 25	8.4	.017	gK1	+ 58.7	1.9	4	
A 7114B	-----	55.8	+48 14	10.8	---	dM1	+ 15.		1	
B 2423	77309	9 00.4	+54 29	5.7	.005	A2n	+ 6.	3??	4•	- 8.9 D
G 12566	77985	03.5	+17 19	7.6	.070	gG7	- 4.2	1.9	4	
G 12569	78011	9 03.6	+15 29	8.0	.023	gM4	+ 20.2	2.0	4	
B 2415	76990	05.3	+84 23	6.3	.030	dF2	- 20.9	1.7	3•	+ 1. V
G 12691	79097	09.4	-06 46	8.0	.007	gM2	+ 7.2	1.8	3	
G 12882	80567	18.0	+00 24	6.8	.026	gM4	+ 3.1	1.7	4	
81° 295	80113	19.9	+80 45	8.8	---	gG8	- 27.0	2.2	2	
G 12950	81109	9 21.0	-20 49	7.1	.014	gM3	+ 17.	var	3•	+ 17. L
A 7352A	81212	21.8	+06 34	7.5	.182	dF5	+ 44.6	0.9	2	
A 7352B	-----	21.8	+06 34	7.6	---	dF7	+ 40.6	2.0	2	
20° 2334	82372	29.2	+20 16	8.3	.015	dA9	+ 7.8	1.2	3	
G 13148	82428	29.2	-10 20	6.1	.027	gA8	- 18.	var	4•	
48° 1780	82287	9 29.3	+48 23	7.9	.033	dA8n	- 14.	3.1	5	
G 13305	83205	35.4	+58 46	7.5	.031	gM2	+ 20.0	1.8	3	
B 2595	83618	37.3	-00 55	4.1	.083	gK3	+ 25.5	2.2	3	+ 23.0 M
33° 1895	83630	37.8	+33 13	7.8	.040	dA8	+ 24.0	1.7	4	
G 13430	84165	42.1	+65 51	7.2	.031	gM1	- 37.0	1.8	2	- 32. L
G 13572	85461	9 49.2	-11 06	6.8	.040	gM2	+ 13.0	1.4	3	
B 2657	85859	51.9	-25 42	5.0	.195	gK3	+ 54.0	1.1	3	+ 50.5 M
G 13659	85676	53.1	+54 29	6.8	.046	gM2	- 31.1	1.1	3	
B 2688	87427	10 02.0	-24 03	5.8	.099	dA8n	+ 3.6	2.8	4	
G 13908	87806	05.0	+01 10	7.0	.021	gM2	- 29.2	0.9	3	
G 13910	87870	10 05.2	-22 15	7.3	.018	gM4	+ 31.0	2.8	2	
G 13912	87855	05.3	-07 23	6.9	.047	gM2	+ 32.5	1.8	3	
51° 1577	87852	05.9	+51 05	7.6	.016	A2	- 11.3	3.5	4	
G 13936	87955	06.3	+38 41	8.0	.041	gM2	- 31.5	1.3	3	
B 2712	88372	08.8	-07 04	6.1	.012	Aon	+ 22.	var	5•	- 6. V
G 13998	88419	10 08.9	-18 43	7.0	.095	gM3	+ 37.3	2.2	3	
G 14060	88806	11.8	-23 34	6.7	.022	gM2	- 5.7	1.5	3	
G 14118	89053	14.3	+41 43	6.9	.091	gM2	- 32.1	2.0	4	
G 14284	90068	21.5	+34 26	7.3	.035	gM4	+ 3.3	2.3	2	+ 1.4 L
G 14286	-----	21.5	+41 15	8.8	.013	gK4	+ 28.5	2.2	4	
A 7894B	-----	10 39.8	+51 04	9.4	---	dG6	- 2.6	0.2	3	
G 14977	94190	51.3	+77 21	7.0	.027	gM2	- 89.5	1.1	3	
G 15322	96572	11 06.3	+78 03	7.4	.046	gM1	- 25.4	0.8	3	
G 15690	99363	23.4	-13 29	7.0	.055	gM2	+ 6.1	1.6	4	
G 15826	100214	29.6	+56 22	8.0	.265	dF7	+ 12.8	1.3	3	
A 8202A	100287	11 29.8	-28 59	5.8	.141	dF6	+ 3.8	1.8	2	
A 8202B	100286	29.8	-28 59	5.9	.132	dF7	+ 9.3	1.1	3	
G 15933	100933	34.6	+62 28	7.5	.023	gM3	- 27.0	2.0	3	
A 8250C	------	36.1	+45 23	9.0	.014	gG5	- 39.9	1.7	4	
B 3120	103483	52.5	+46 45	6.5	.001	A2	- 5.	var	5•	-10. DV
A 8495A	106784	12 14.2	+39 52	7.2	.021	A2	+ 4.2	3.0	4	
A 8495B	------	14.2	+39 52	10.0	---	dG5	+ 7.2	1.7	3	
B 3202	107070	16.1	-00 31	5.9	.034	A3n	- 19.	7.	4	-13. V
15° 3450	107149	16.7	-16 00	7.8	.021	gM1	+ 14.2	2.1	4	
A 8531B	------	20.0	+05 35	9.0	---	dK5	+ 6.4	2.5	4	

TABLE I (Cont'd)

STAR	H.D.	1950 R.A.	1950 Decl.	Vis. Mag.	P.M.	Spec.	Vel.	P.E.	No. Pl.	Others
		h m	° ′		″		km	km		
A 8576B	------	12 28.0	+03 47	9.6	.---	dF5	0	3.2	3	
A 8585A	109005	29.0	-10 46	7.5	0.051	A4	- 14.	var	4•	
A 8585B	------	29.0	-10 48	8.3	---	dF1	- 1.	3.1	4	
G 17115	109282	31.0	+24 43	7.4	.021	gM3	- 10.4	1.1	4	
G 17345	110932	42.9	+14 39	6.8	.045	B9	+ 4.	var	3•	+ 4. V
α CVn	112413	12 53.7	+38 35	2.9	.238	A1	- 1.0	0.8	2	- 3.5 M
B 3405	112149	13 06.7	-22 51	5.1	.051	gK1	- 22.3	2.0	4	- 18.4 M
G 17903	------	10.8	-18 34	7.3	.033	A2	- 27.	var	4•	
G 17906	------	10.8	+37 38	9.6	.034	gK4	- 41.	var	4•	
G 17912	114975	11.3	+37 09	6.7	.028	gM2	+ 1.8	2.3	4	
A 8871A	116206	13 19.4	+18 02	8.1	.043	dF2	- 24.0	1.4	3	
A 8871B	------	19.4	+18 02	10.3	---	dG2	- 21.8	1.9	3	
G 18102	116275	20.1	-12 56	7.7	.038	A2	- 22.	var	4•	
B 3480	116842	23.2	+55 15	4.0	.121	A1n	- 5.2	0.5	3	- 2.0 M
A 9053B	------	52.4	-07 49	7.7	---	dG1	- 19.9	1.8	4	
9° 2842	122769	14 01.2	+08 44	7.8	.037	dF5	- 4.0	2.2	3	
G 19058	123710	04.5	+74 49	8.3	.165	dG2	+ 6.3	1.5	3	
G 19059	123408	04.5	+35 01	7.1	.015	gK0	- 2.9	1.3	3	
G 19175	124304	10.5	-13 38	7.2	.054	gM4	- 44.4	0.8	2	- 46. L
A 9188B	-----	13.8	+06 19	10.0	---	dG0	- 25.	var	4•	
G 19505	126944	14 25.6	+33 10	8.4	.027	dF0	- 6.	var	4•	
A 9273B	------	25.6	-02 00	9.7	---	dK0	- 8.	var	4•	
A 9405B	------	47.9	+51 35	9.9	---	dG7	- 29.	3.4	3	
G 20396	134807	15 07.6	+65 59	6.8	.034	gM4	- 26.2	1.7	4	
A 9527B	------	08.0	+39 10	10.1	---	dK4	- 5.	var	4•	
B 3868	134967	15 10.5	-19 28	6.0	.067	Aon	+ 1.	var	4•	
B 3909	136562	17.9	+50 24	7.4	.012	A2	- 11.	var	3•	- 11. v V
G 21065	140227	37.5	+69 27	5.9	.069	gMo	- 32.2	2.7	4	- 25.2 D
A 9778B	------	43.9	+15 35	9.2	---	dK3	+ 2.8	2.5	4	
A 9799B	------	47.4	+25 37	10.1	---	dG8	- 32.6	1.3	4	
B 4033	142096	15 50.4	-20 01	5.1	.034	B3n	- 12.	5.	4	0 M
29° 2739	142796	53.4	+29 41	7.7	.021	A1	- 14.4	1.1	4	
G 21411	142804	54.3	-15 53	6.8	.039	gM1	- 10.0	1.9	4	
B 4115	145482	16 09.2	-27 48	4.7	.036	B3	+ 10.	9.	3	+ 9. L
A 10005A	147103	17.6	-20 00	7.7	.020	Ao	+ 18.	5.3	4	
A 10005B	147104	16 17.6	-20 00	8.0	.061	Ao	+ 2.	5.3	5	
24°12684	147889	22.4	-24 21	8.0	.025	B3	- 3.	6.	5	
A 10049A	147933	22.6	-23 20	5.2	.026	B5n	- 6.	6.	5•	- 13. M
A 10049C	147932	22.6	-23 18	7.1	.038	B9n	- 19.	3.2	4	
A 10072A	148515	26.1	-08 01	6.6	.100	dF3	- 0.5	0.7	3	
A 10072B	------	16 26.1	-08 01	9.0	---	dK1	- 2.	3.7	3	
G 22342	149881	34.7	+14 35	6.6	.009	B2	- 8.	3.0	2•	+ 18. v M
Anon.	------	34.8	+31 13	10.	---	dA7	- 24.9	2.5	4•	
B 7740B	------	42.6	+06 11	9.0	---	dK5	- 4.	var	4•	
B 4338	154204	17 01.8	-20 26	6.2	.031	B9n	- 11.2	2.9	4	
G 23358	156890	17 15.5	+60 46	6.7	.031	gA9n	- 22.0	1.3	6	
G 23364	156652	15.6	+28 58	7.1	.001	gM2	- 37.4	1.8	4	
G 23606	157857	23.5	-10 57	7.4	.024	07	----	---	7•	+ 58.6 VL
B 4432	158460	25.0	+60 05	5.7	.025	A2	- 5.	5.2	5•	+ 12.7 V
G 24016	160869	39.9	-04 50	6.8	.021	gM2	+ 39.7	1.3	3	
G 24380	163296	17 53.3	-21 27	6.6	.035	A2e	- 3.	3.2	6	
B 4543	164212	56.4	+43 25	6.9	.015	Aon	- 5.	var	5•	- 41.3 V
B 4560	164794	18 00.8	-24 22	5.9	.003	05	+ 4.4	1.9	7•	+ 15.3 V
B 4636	168720	18.2	+21 56	5.0	.060	gMo	- 37.9	2.4	3•	- 32.0 L
B 4640	168812	18.5	+28 58	6.5	.010	Ao	- 7.	4.1	4	
17° 5155	168673	18 18.8	-17 18	9.4	.006	Ao	- 38.	6.	4	
G 25064	168814	19.4	-14 25	7.3	.045	cA2	- 15.	4.5	4•	
A 11292B	------	19.9	+11 24	10.4	---	gM2	- 48.	var	3•	
G 25133	169454	22.4	-14 00	6.8	.009	cBoe	---	---	4•	- 25. L
A 11326A	169457	22.4	-16 32	9.8	---	dF3	- 28.0	2.3	3	

TABLE I (Cont'd)

STAR	H.D.	1950 R.A.	1950 Decl.	Vis. Mag.	P.M.	Spec.	Vel.	P.E.	No. Pl.	Others
		h m	° ′		″		km	km		
A 11326B	------	18 22.4	-16 32	10.8	---	dF8	- 16.2	0.8	2	
65° 1277	------	31.8	+65 20	8.7	0.02	dFo	- 19.	6.	5	
B 4712	171802	34.1	+09 05	5.4	.128	dF2	- 23.4	0.6	2	- 21.6 L
8° 4675	172488	38.1	-08 46	7.9	.032	Bp	+ 50.	6.	3	
G 25649	173740	42.2	+59 33	9.7	2.268	dM4	+ 3.	4.1	5r	- 4. Md
A11711BC	------	18 46.7	+16 12	10.0	---	A4	+ 22.	4.3	3	
A 11910B	------	57.1	+40 37	9.5	---	A4	- 3.	var	3•	
G 26095	176582	57.5	+39 09	6.2	0.009	B7n	- 12.	3.7	6	- 18.2 V
G 26099	176269	57.7	-37 08	6.8	.023	B9n	+ 10.	var	4•	
G 26100	176270	57.7	-37 08	6.6	.042	B9	- 27.	var	4•	
G 26107	176541	18 57.9	+22 45	6.4	.029	gM3	- 49.5	0.5	2	- 52.5 D
G 26153	176825	59.3	+08 40	8.9	.022	gG5	- 19.4	1.7	4	
G 26171	176915	59.8	+08 41	9.1	.010	gG2	- 13.3	1.4	2	
G 26173	176916	59.8	+08 41	8.3	.004	gG8	- 20.9	2.2	4	
A 12040B	------	19 04.2	+30 22	9.7	---	dG7	- 48.	---	1	
B 4881	179323	19 10.1	-26 00	5.9	.012	cKo	+ 1.4	0.3	2	
A 12197B	------	12.1	+39 04	8.5	---	Ao	- 25.0	1.1	3	
B 4954	182645	23.3	-15 09	5.7	.021	B8	- 7.	3.8	4	
G 26960	183986	29.0	+36 07	6.0	.014	Ao	+ 8.0	2.5	4	
B 4992	184171	29.9	+34 21	4.8	.003	B5	- 26.	6.	2	- 21.8 M
A 12864C	------	19 42.6	+10 39	9.5	---	B4n	- 14.	var	4•	
32° 3634	188876	54.1	+32 56	7.2	.015	B8	- 17.	4.0	4	- 19. D
B 5117	189253	55.4	+50 46	6.3	.007	A1	- 18.1	2.2	3	- 21. V
A 13196B	------	56.6	+33 08	8.2	---	dF3	- 19.	---	1	
G 27730	189690	58.0	+29 47	7.3	.010	Aon	- 36.	7.	5	
A 13312A	190429	20 01.6	+35 53	7.2	.016	O5n	- 12.	---	1•	- 13. V
A 13312B	------	01.6	+35 53	7.8	---	O9n	- 22.	---	1•	- 22. V
A 13429A	191566	07.3	+35 20	7.7	.005	B2	- 10.	---	2•	- 45. V
A 13429B	------	07.3	+35 20	8.7	---	B2	- 1.	---	1•	- 29. V
39° 4082	192281	10.8	+40 07	7.5	.004	O5n	- 59.	---	1•	- 60. V
A 13545A	------	20 11.6	+49 02	7.8	.022	Ao	- 22.7	3.0	4	
A 13545B	------	11.6	+49 02	10.2	---	agG8	- 27.4	1.9	4	
16° 4200	------	12.1	+16 36	9.8	.035	gG8	- 28.4	2.7	4•	
B 5249	195050	25.7	+38 17	5.4	.076	A1n	+ 2.	4.9	4	0 v M
B 5269	195710	29.3	+49 03	6.5	.006	Aon	+ 5.	var	4•	+ 5. V
A 14054A	196310	20 34.2	-12 55	8.0	.034	dF1	- 32.0	2.4	4	
A 14054B	------	34.2	-12 55	9.0	.051	dF5	- 20.0	0.7	2	
14° 4389	197040	38.3	+14 21	7.7	.027	A2n	- 36.	var	4•	
α Cyg	197345	39.7	+45 06	1.3	.003	cA2e	- 3.8	0.9	10	- 4.6vM
B 5345	198134	45.2	+34 11	5.2	.043	gK3	- 23.7	0.5	2	- 22.5 L
B 5499	203836	21 09.3	+86 50	7.4	.085	A4n	+ 1.	3.8	4	- 3.6 D
G 29673	202128	11.1	+15 47	6.2	.044	A3n	- 34.	9.	4	- 28.1 VS
A 14847B	------	16.9	-26 34	9.0	---	dG6	+ 3.	4.9	2	
B 5626	208008	50.9	-10 33	6.5	.006	B9	- 11.2	1.7	4	
G 30749	208971	56.1	+65 54	7.0	.019	gM2	+ 11.	var	3•	
G 30855	209691	22 01.5	+65 49	6.8	.024	B8	- 40.	3.3	4	
B 5751	211554	14.6	+56 58	6.0	.042	gG4	- 9.1	1.1	5	- 8.3 V
B 5818	213798	29.5	+78 34	5.5	.016	A1n	+ 14.	4.1	3	- 6. M
B 5876	215664	43.9	+44 17	5.8	.140	dA8n	- 8.6	0.6	4	- 12.8 D
B 5954	218356	23 04.7	+25 12	5.0	.031	cKo	- 25.9	1.6	4	- 26.7 L
A 16661A	219813	23 16.0	+46 59	7.7	---	B9	- 16.2	1.2	3	
A 16661B	------	16.0	+46 59	10.1	---	Ao	- 24.	6.	3	
60° 2552	------	18.5	+60 55	8.0	.024	B1n	- 35.7	2.6	3•	+ 2. V
G 32631	220876	24.8	-13 12	7.5	.033	gM3	- 18.3	2.0	4	
32° 4649	220951	25.3	+32 43	7.4	.040	dA6n	- 9.8	2.9	4	
G 32697	221327	23 28.6	+18 30	7.4	.019	A3	- 3.0	0.9	4	
G 33135	223835	50.5	+41 04	7.2	.017	gM2	- 5.0	1.4	4	- 12. L
G 33217	224364	54.8	+60 45	7.0	.009	gM2	- 76.3	1.4	3	
75° 904	224917	59.2	+76 07	9.0	.024	gK3	- 6.0	3.0	4	
G 33336	224980	59.7	+60 25	7.0	.017	gM2	- 24.0	0.4	3	

NOTES

STAR	R.A. h m	
A 30B	0 02.0	-8, -54, -27, -57
75° 7	15.5	Broad lines
B 66	21.4	+4, +10, -16, -12
A 582A	39.5	-23, -4, -28, -23, +3
A 582B	39.5	-29, -19, +7, -2
45° 187	41.5	Two spectra
62° 175	55.2	IS -17.6
G 1176	56.3	+29, +44, +23, +21
A 902A	1 03.4	Velocity is probably variable: -18, +7, -7, -7
G 1811	27.4	+22, +12, -18, +13
56° 445	2 09.0	-66, -10, -46, -7
70° 182	28.9	-21, -43, -40, -1, -19
G 3040	29.3	-35, -48, -46, -62
B 562	30.0	-33, -21, -27, -11
29° 502	54.6	-6, +5, -17
A 2499A	3 19.9	-9, 0, +2, +50
A 2499B	19.9	+5, +64, -6, +13
G 4465	41.4	+42, +20, +80, -43
G 4856	4 00.2	Velocity is probably variable: +45, +42, +55, +37
11° 571	04.4	+7, +53, -2, +29
G 5449	26.4	Velocity is probably variable: +27, +21, +37, +21
Anon.	29.6	Plates taken for Luyten's pm. star, which was probably misidentified
G 5617	33.8	+13, +16, +26, +21, -1; IS +10. ± 3.0
42° 1180	5 05.2	+8, 0, +17, -5
38° 1040	06.0	-6, +5, +6, -36, -29
G 6316	07.2	-58, -67, -55, -77
14° 1080	13.7	Two spectra
G 6511	16.6	+28, +35, +39, +38
15° 790	17.9	+27, -2, +28, +63: poor lines
5° 1325	33.1	+40, +67, +39
1° 1001	37.7	+20, +18, +38, -13
43° 1332	39.8	+11, +20, +29, 0
24° 1036	54.2	+20, +4, -6, -4
G 7589	57.6	+41, +14, +44, +18
A 4629B	6 00.3	+51, +8, +60, -11
G 7844	07.5	+6, -28, +13, -13
B 1541	08.5	+32, +6, +11, +43
B 1612	21.6	+22, -2, -18, +20
30° 1256	29.9	Two spectra
1° 1473	54.9	Two spectra
A 5752AB	7 01.8	-2, -4, +17, +18
10° 1848	02.1	IS +26.0 ±0.1 3
A 5854A	08.6	+21, +12, 0
4° 1862	11.3	Sp Ao + gKo: +22, -27, +8, -13
14° 1628	15.8	+23, +59, +34, +10
G 10091	29.8	-12, -32, -31, -23
B 2002	35.8	-18, +10, -5, +18
G 10566	47.4	Velocity is probably variable: +24, +30, +39, +42
G 11480	8 22.1	-44, -23, -24, -48

STAR	R.A.	
	h m	
B 2423	9 00.4	Velocity is probably variable: +9, +9, -10, +15
B 2415	05.3	Large difference, V-W; velocity probably variable
G 12950	21.0	+11, +11, +30
G 13148	29.2	-27, -17, -27, -1
B 2712	10 08.8	+57, 0, +23, +26
B 3120	11 52.5	Two spectra
A 8585A	12 29.0	-19, -40, +6, -4
G 17345	42.9	-11, +2, +22
G 17903	13 10.8	-34, -20, -43, -8
G 17906	10.8	-41, -27, -45, -51
G 18102	20.1	+1, -29, -24, -34
A 9188B	14 13.8	-26, -37, -20, -17
G 19505	25.6	Two spectra
A 9273B	25.6	-8, +6, -18, -12
A 9527B	15 08.0	+9, -2, -5, -22
B 3868	10.5	+3, -6, +26, -18
B 3909	17.9	-24, -21, +12
A 10049A	16 22.6	IS -7.9 $\pm$0.3 2
G 22342	34.7	IS -17.5 $\pm$1.7 5
Anon.	34.8	In field of C2217
B 7740B	42.6	-2, -8, +12, -26; comp. to B 4257
G 23606	17 23.5	IS -8.9 $\pm$0.9
B 4432	25.0	Velocity is probably variable; +15, -7, -2, -25, -21
B 4543	56.4	0, -4, -39, +21, -4
B 4560	18 00.8	IS -13.7 $\pm$ 1.5 4
B 4636	18.2	Velocity is probably variable
G 25064	19.4	Velocity is probably variable; -12, -36, -6, -8
A 11292B	19.9	-36, -50, -59
G 25133	22.4	IS -5.4 $\pm$ 0.9
A 11910B	57.1	+35, -7, -37; two spectra
G 26099	57.7	-14, +8, +20, +28
G 26100	57.7	-47, +22, -52, -33
A 12864C	19 42.6	Two spectra
A 13312A	20 01.6	IS -8.2 $\pm$ 0.9 13
A 13312B	01.6	IS -7.8 $\pm$ 1.2 7
A 13429A	07.3	IS -7.6 $\pm$ 0.2 2
A 13429B	07.3	IS -12.2 $\pm$ 2.2 3
39° 4082	10.8	IS -12.2 $\pm$ 1.6 2
16° 4200	12.1	In field of R Sge
B 5269	29.3	-22, +8, +16, +19
14° 4389	38.2	-4, -44, -40, -56
G 30749	21 56.1	+10, +1, +21
60° 2552	23 18.5	In NGC 7635; large difference, V-W; velocity is probably variable

ASYMMETRY IN THE LINE PROFILES OF ETA AQUILAE

A. VAN HOOF AND R. DEURINCK*
Astronomical Institute, University of Louvain, Louvain, Belgium
Received September 27, 1950

ABSTRACT

The faintest absorption lines visible on Mount Wilson coudé spectrograms taken by W. S. Adams of the cepheid variable η Aquilae show asymmetric profiles entirely consistent with the theoretical profiles derived for the spectral lines of a pulsating star. For sufficiently large velocities the observed profiles lend themselves to a determination of the coefficient of limb darkening. The micro- and macro-turbulences have been followed throughout the star's period. The ratio of observed radial velocity to velocity along the star's radius depends on the line strength. An interpretation is given of the small differences found between the radial-velocity-curves derived from *Fe* I and from *Fe* II, respectively.

INTRODUCTION

In his book *The Pulsation Theory of Variable Stars*,[1] S. Rosseland mentions two semi-empirical tests of the pulsation theory: (1) Baade's criterion, the consistency of the computed variation of the stellar radius—as derived from the observed changes in light and color—with the same variation deduced from the observed radial-velocity-curve, and (2) Schwarzschild's criterion, the consistency between the computed light-curve—as derived from the radial velocities—and the directly observed one. Both criteria give considerable support to the belief that the pulsation hypothesis is correct in its broad outlines.

It is clear, however, that a more direct and more convincing proof for the reality of radial pulsations in the atmospheres of cepheids would be available if the asymmetry could be detected which these pulsations inevitably introduce into the profiles of the spectral lines and if the observed profiles could be shown to be in keeping, throughout the cycle, with the requirements of the pulsation theory. Many astronomers have looked for this asymmetry but have not been able to detect it, probably because of the insufficient dispersion used. Recently Dr. Adams has discovered an asymmetry of many lines in the spectrum of η Aquilae at minimum phase; whether this asymmetry agreed with that to be expected because of the pulsation was, however, not investigated.

The theoretical profile of an absorption line under the effect of an outward or inward motion of a stellar atmosphere was first established by H. Shapley and S. B. Nicholson.[2] Later, contributions to the same problem were published by J. A. Carroll,[3] O. C. Wilson,[4] and A. B. Underhill.[5]

A point of special merit in the investigation by Shapley and Nicholson is that it shows, in a more striking manner than the others do, the influence of the amount of limb darkening on the expected distorted profile. This influence seemed important enough to the senior author to make an attempt to derive the coefficient of limb darkening of the disk of a cepheid from the observed line profiles. As is well known, the amount of limb darkening has been determined, up to now, only for the components of eclipsing binaries. The new possibility gave stimulus to the search for the asymmetry in the shape of the absorption lines—already important enough from its providing a crucial test for the pulsation hypothesis.

* Chargé de recherches of the Fonds National de la Recherche Scientifique.

[1] Oxford: Clarendon Press, 1949.

[2] *Proc. Nat. Acad. Sci.*, **5**, 417, 1919.

[3] *M.N.*, **88**, 548, 1928.

[4] *Ap. J.*, **82**, 233, 1935.

[5] *Ap. J.*, **106**, 128, 1947.

Dr. I. S. Bowen, Dr. M. Schwarzschild, and Dr. W. S. Adams took enough interest in the attempt to provide the necessary material in the form of microphotometer tracings of coudé spectrograms of η Aquilae which had already been utilized by Schwarzschild and Adams, in collaboration with B. Schwarzschild,[6] for an investigation of the pulsations in the star's atmosphere.

Full particulars concerning this material are given in the paper just referred to; we can restrict ourselves to the repetition here of the main data: dispersion 2.9 A/mm; spectral range λλ 4370–4650; enlargement 40×; the number, date, and phase of individual plates are listed in Table 1. The phases have been computed by M. and B.

TABLE 1

PLATES OF η AQUILAE

Plate No.	Date	Phase	Plate No.	Date	Phase
2333	June 16, 1940	0.013	2587	July 6, 1941	0.651
2394	Aug. 20, 1940	.037	2054	June 28, 1939	.671
2335	June 17, 1940	.145	2592	Aug. 4, 1941	.686
2425	Oct. 11, 1940	.280	2375	July 13, 1940	.755
2070	Aug. 1, 1939	.398	2594	Aug. 5, 1941	.820
2428	Oct. 12, 1940	.418	2397	Sept. 9, 1940	.824
2431	Oct. 13, 1940	.556	2391	Aug. 19, 1940	.898
2373	July 12, 1940	.632	2035	June 1, 1939	.923
2422	Sept. 22, 1940	.638	2401	Sept. 10, 1940	.961
2802	June 1, 1942	0.643	2607	Sept. 4, 1941	0.985

Schwarzschild and W. S. Adams with Gliese's ephemeris:

$$\text{Phase} = \frac{\text{JD} - 2{,}414{,}827.30}{7.176678},$$

which was carefully checked by them.

THEORY

I. THE COMPUTED PROFILES OF FAINT LINES

We confine ourselves to the assumption that the intensity of the absorption line that comes from an element of the stellar disk, where the normal to the surface makes the angle θ with the direction to the observer, follows the same law as that admitted for the integrated light,

$$I_\theta = I_0 (1 - u + u \cos \theta),$$

or, in Unsöld's notation and for the wave length λ,

$$I_{\lambda\theta} = \frac{I_{\lambda 0} (1 + \beta \cos \theta)}{1 + \beta}.$$

Let the surface have a velocity of expansion v; then the corresponding radial velocity V of the surface element considered will be

$$V = - v \cos \theta,$$

which causes a Doppler shift,

$$\Delta\lambda = - \lambda \frac{v}{c} \cos \theta.$$

[6] *Ap. J.*, **108**, 207, 1948.

The light emitted in the direction of the observer by the annular element of width $d\theta$ will be proportional to

$$dI_\lambda = I_{\lambda\theta} \cos\theta \sin\theta d\theta .$$

Putting

$$\cos\theta = -\frac{\Delta\lambda}{\lambda}\frac{c}{v} = x ,$$

we have

$$dI_\lambda = -I_{\lambda\theta} x\, dx = -I_{\lambda 0}\frac{1+\beta x}{1+\beta}\, x\, dx ;$$

hence the intensity distribution in a line, originally of width zero, becomes

$$-\frac{dI_\lambda}{dx} = I_{\lambda 0}\frac{(1+\beta x)\, x}{1+\beta} \qquad \text{or} \qquad W(x) = \frac{(1+\beta x)\, x}{\frac{1}{2}+\beta/3} \tag{1}$$

if we arrange to make

$$\int_0^1 W(x)\, dx = 1$$

(we have, of course, $W(x) = 0$ outside the interval $x = 0$ to $x = 1$).

Formula (1), equivalent to that of Shapley and Nicholson, gives the way in which each spectral line, originally of wave length λ and of width zero, is spread out by the effect of a velocity of expansion or contraction.

Let us now consider a faint line, which for $v = 0$ has the Gaussian profile $A(\lambda) \approx e^{-[\Delta\lambda/(\Delta\lambda)_N]^2}$. As soon as an expansion or contraction develops, this can be written in the form

$$A(x) = \sqrt{\frac{C}{\pi}}\, e^{-Cx^2} .$$

But for $v \neq 0$ the line will, according to the above, suffer a distortion and assume the form[7]

$$S(x) = \sqrt{\frac{C}{\pi}} \int_{x-1}^{x} e^{-C\xi^2} \frac{[1+\beta(x-\xi)](x-\xi)}{\frac{1}{2}+\beta/3}\, d\xi , \tag{2}$$

or, after integration,

$$S(x) = \frac{1}{1+2\beta/3}\left\{\left(\beta x^2 + x + \frac{\beta}{2C}\right)[\Theta(x\sqrt{C}) - \Theta([x-1]\sqrt{C})] + \frac{(\beta x+1)\, e^{-Cx^2} - (\beta x+1+\beta)\, e^{-C(x-1)^2}}{\sqrt{(\pi C)}}\right\} . \tag{3}$$

For the U-hypothesis ($\beta = 0$), this reduces to

$$S_U(x) = x[\Theta(x\sqrt{C}) - \Theta([x-1]\sqrt{C})] + \frac{e^{-Cx^2} - e^{-C(x-1)^2}}{\sqrt{(\pi C)}} , \tag{4}$$

while for the D-hypothesis ($\beta = \infty$), we get

$$S_D(x) = \frac{3}{2}\left\{\left(x^2 + \frac{1}{2C}\right)[\Theta(x\sqrt{C}) - \Theta([x-1]\sqrt{C})] + \frac{x\, e^{-Cx^2} - (x+1)\, e^{-C(x-1)^2}}{\sqrt{(\pi C)}}\right\} . \tag{5}$$

[7] A somewhat more compact form is:

$$S(x) = \sqrt{\frac{C}{\pi}} \int_0^1 \frac{(1+\beta\xi)\,\xi}{\frac{1}{2}+\beta/3}\, e^{-C(x-\xi)^2} d\xi .$$

For the intermediate case $\beta = \frac{3}{2}$ (equivalent to $u = 0.6$), we obtain

$$S_{\beta=3/2}(x) = \tfrac{1}{2}[S_U(x) + S_D(x)]. \tag{6}$$

Figure 1 illustrates the S_U and S_D profiles for $C = 25$, $C = 9$, and $C = 4$. The W_U and W_D profiles have been added for comparison. The figure shows clearly how much the asymmetry is reduced by the effect of the natural dispersion of the undistorted line. In fact, the asymmetry will almost certainly escape detection for values of $C < 6$, which

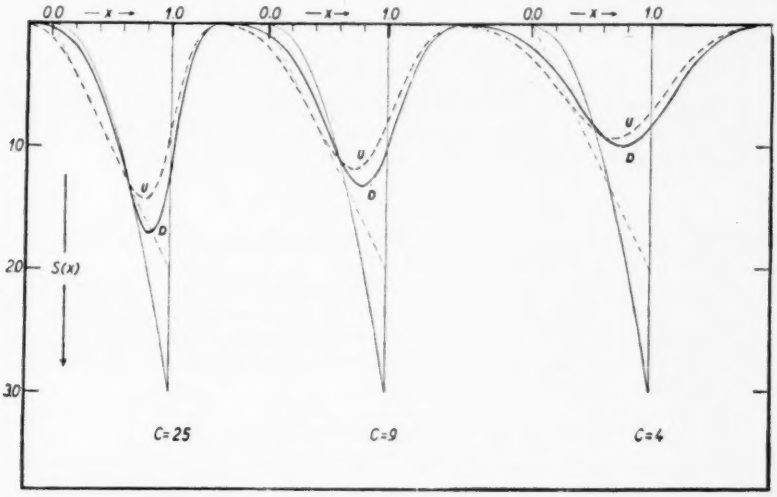

FIG. 1.—The S_U and S_D profiles for $C = 25$, $C = 9$, and $C = 4$. The W_U and W_D profiles are shown for comparison.

means, for values of the velocity giving Doppler shifts $(\Delta\lambda)_D$ less than 2.5 times the dispersion $(\Delta\lambda)_N$ of the undisturbed line.

We have indeed

$$C = \frac{1}{(\Delta x)_N^2};$$

hence, from the relation between our $\Delta\lambda$ and x scales,

$$\frac{(\Delta\lambda)_N}{\lambda} = \frac{v}{c}(\Delta x)_N = \frac{v}{c}\frac{1}{\sqrt{C}}$$

or

$$\frac{(\Delta\lambda)_N}{(\Delta\lambda)_D} = \frac{1}{\sqrt{C}},$$

which proves the foregoing statement.

Since moderate Doppler shifts are the rule among cepheids, we conclude that the pulsation asymmetry will be revealed only by very narrow lines—lines that, in fact, can be perceived only on spectrograms of the highest dispersion. It is readily understood, then, why so many searches for asymmetry in the observed profiles were doomed to remain unsuccessful.

It may also be noticed that the superposition of the Gaussian profile upon the simpler $W(x)$ profile leaves unaltered the position of the optical center of gravity of the line, the general expression of which is, therefore,

$$\bar{x} = \int_0^1 x W(x)\, dx = \frac{2\,(1+\frac{3}{4}\beta)}{3\,(1+\frac{2}{3}\beta)}, \tag{7}$$

with

$$\bar{x} = 0.667 \quad \text{for} \quad \beta = 0 \ (L\text{-hyp.}),$$

$$\bar{x} = 0.708 \quad \text{for} \quad \beta = \tfrac{3}{2} \ (u = 0.6),$$

$$\bar{x} = 0.750 \quad \text{for} \quad \beta = \infty \ (D\text{-hyp.}).$$

If the setting can be made on this optical center when a spectrogram is measured, we will, of course, have the following relation between the observed radial velocity V_ρ, the mean radial velocity V_0, and the actual velocity v along the star's radius,

$$V_\rho - V_0 = -\bar{x}\, v .$$

In numerical applications it is general practice to adopt for $\bar{x}$ the value $\frac{17}{24} = 0.708$, corresponding to the hypothesis $\beta = \frac{3}{2}$.

From a glance at the computed $S(x)$ profiles in Figure 1, it looks rather improbable that the settings will be made in that way, and it seems much more plausible to believe that the settings are actually made on, or at least very near, the abscissa of maximum line depth, in which case the reduction factor $\bar{x}$ must be changed. We pay further attention to this important point in Section VIII.

II. COMPUTED PROFILES OF HIGH-LEVEL LINES

Let us now examine the profile of an absorption line that originates at high level above the stellar photosphere. Let R denote the radius of the line-generating layer, r that of the stellar photosphere, θ_1 the angle between the direction of the observer and the normal to an element of the layer, θ_2 the corresponding angle for the photospheric element that serves as background (see Fig. 2).

We shall first consider the case of an infinitely narrow line of wave length λ, the intensity of which we suppose to be distributed over the disk according to the law

$$I_{\lambda\theta_1} = I_{\lambda 0}\,\frac{1+\beta\cos\theta_2}{1+\beta}.$$

With an outward motion of velocity v, we get the expressions

$$V = -\,v\cos\theta_1$$

for the radial velocity;

$$\Delta\lambda = -\,\frac{\lambda}{c}\,v\cos\theta_1$$

for the corresponding Doppler displacement; and

$$d I_\lambda = I_{\lambda\theta_1}\cos\theta_1 \sin\theta_1 d\theta_1 = \frac{I\lambda_0\,(1+\beta\cos\theta_2)\cos\theta_1\sin\theta_1 d\theta_1}{1+\beta}$$

for the intensity of the line, coming from an annular element.

But, because

$$R\sin\theta_1 = r\sin\theta_2 ,$$

the latter expression can be written

$$\frac{dI_\lambda}{\sin\theta_1 d\theta_1} = \frac{I\lambda_0(1+\beta\sqrt{[1-(R/r)^2\sin^2\theta_1]})\cos\theta_1}{1+\beta}.$$

Putting

$$\cos\theta_1 = x \qquad \text{and} \qquad -\sin\theta_1 d\theta_1 = dx,$$

this becomes

$$-\frac{dI_\lambda}{dx} = \frac{I\lambda_0(1+\beta\sqrt{[1-(R/r)^2(1-x^2)]})x}{1+\beta}.$$

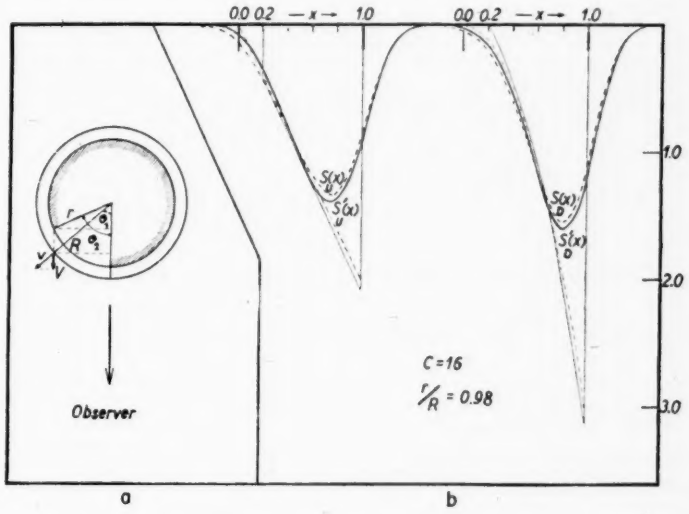

FIG. 2.—*a*, Diagram of origination of absorption line at high level. *b*, S'_U and S'_D profiles computed for $C = 16$ and $r/R = 0.98$. The corresponding S_U and S_D profiles are shown for comparison.

We arrange to make

$$\int_{\sqrt{[1-(r/R)^2]}}^{1} \frac{I\lambda_0(1+\beta\sqrt{[1-(R/r)^2(1-x^2)]})x}{1+\beta}\,dx = 1,$$

and thus obtain, for the pulsation profile of the originally narrow line,

$$W'(x) = \frac{(1+\beta\sqrt{[1-(R/r)^2(1-x^2)]})x}{(r/R)^2(\frac{1}{2}+\beta/3)}. \tag{8}$$

The quantity x can vary in this expression only between the limits $\sqrt{[1-(r/R)^2]}$ and 1, so that the optical center of gravity of the line will have, as abscissa,

$$\bar{x} = \int_{\sqrt{[1-(r/R)^2]}}^{1} xW'(x)\,dx, \tag{9}$$

which gives

$$\bar{x} = 0.689 \quad \text{for} \quad \beta = 0 \quad \text{and} \quad \frac{r}{R} = 0.98,$$

$$\bar{x} = 0.727 \quad \text{for} \quad \beta = \tfrac{3}{2} \quad \text{and} \quad \frac{r}{R} = 0.98,$$

$$\bar{x} = 0.764 \quad \text{for} \quad \beta = \infty \quad \text{and} \quad \frac{r}{R} = 0.98.$$

The value of $\bar{x}$ remains unaltered when we superpose on the simple $W'(x)$ profile the Gaussian profile

$$A(x) = \sqrt{\frac{C}{\pi}}\, e^{-Cx^2}$$

of a faint normal line.

The expansion profile of such a line can thus be written

$$S'(x) = \frac{\sqrt{C}}{\sqrt{\pi}\,(r/R)^2\left(\frac{1}{2} + \beta/3\right)} \int_{\sqrt{[1-(r/R)^2]}}^{1} \times \left(1 + \beta\sqrt{\left[1 - \left(\frac{R}{r}\right)^2 (1-\xi^2)\right]}\right) \xi\, e^{-C(x-\xi)^2} d\xi\,. \tag{10}$$

For $\beta = 0$ (U-hypothesis), the integral has an analytic solution

$$S'_U(x) = \left(\frac{R}{2}\right)^2 x \left[\Theta\left(x - \sqrt{\left[1 - \left(\frac{r}{R}\right)^2\right]}\right) - \Theta\left([x-1]\sqrt{C}\right)\right] + \frac{e^{-C(x-\sqrt{[1-(r/R)^2]})^2} - e^{-C(x-1)^2}}{\sqrt{(\pi C)}}. \tag{11}$$

For $\beta = \infty$ (D-hypothesis), the integration is to be performed numerically and for $\beta = \frac{3}{2}$ (or $u = 0.6$), we have again

$$S'_{\beta=3/2}(x) = \tfrac{1}{2}\left[S'_U(x) + S'_D(x)\right]. \tag{12}$$

Figure 3 illustrates an S'_U and an S'_D profile, both computed for $C = 16$ and $r/R = 0.98$. The corresponding S_U and S_D profiles have been added for comparison. As could be foreseen from the outset, the S' profiles are somewhat less asymmetric than the S profiles for equal amounts of limb darkening.

III. PULSATION PROFILES FOR LINES WITH VARIABLE DISPERSION FROM CENTER TO LIMB

We can imagine the absorption line produced by an element of a stellar disk to have a normal profile with a dispersion that varies with the distance of the element from the center of the disk. The effect might be caused by a difference between the turbulent motions parallel to the surface and normal to it. If we assume the dispersion to vary with the angle θ like the radius of an ellipsoid of revolution with its minor axis in the direction of the star's radius, this profile can be written

$$A''(x) = \frac{e^{-x^2/[a^2(1-\epsilon^2\xi^2)]}}{a\sqrt{[\pi(1-\epsilon^2\xi^2)]}},$$

where $\xi = \cos\theta$.

Superposing this upon the $W(x)$ profile, we get the resulting expansion profile,

$$S''(x) = \frac{1}{a\sqrt{\pi}\,(\frac{1}{2}+\beta/3)} \int_0^1 \frac{(1+\beta\xi)\,\xi\, e^{-(x-\xi)^2/[a^2(1-\epsilon^2\xi^2)]}}{\sqrt{(1-\epsilon^2\xi^2)}}\, d\xi\,. \tag{13}$$

The profile has the slope of an $S(x)$ profile of dispersion $a\sqrt{(1-\epsilon^2)}$ in the wing that corresponds to the center and that of an $S(x)$ profile with dispersion a in the wing that corresponds to the limb.

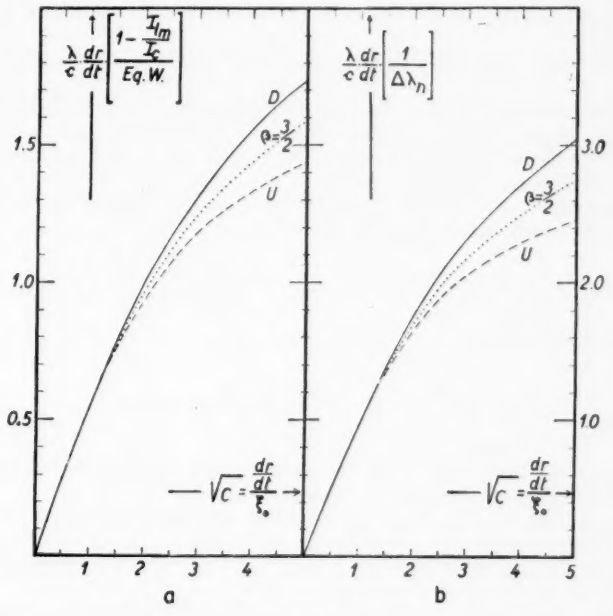

FIG. 3.—*a*, The function $[S(x)]_{max}$ for values of 0, $\frac{3}{2}$, and ∞ of β. *b*, The function $1/(\Delta x)_n$ for values of 0, $\frac{3}{2}$, and ∞ of β.

The effect of a center-to-limb variation on a line originating at high level will obviously be to change the already computed $S'(x)$ profile into

$$S'''(x) = \frac{1}{(r/R)^2 a\sqrt{\pi}\,(\frac{1}{2}+\beta/3)} \int_{\sqrt{[1-(r/R)^2]}}^1 \times \frac{(1+\beta\sqrt{[1-(R/r)^2(1-\xi^2)]})\,\xi\, e^{-(x-\xi)^2/[a^2(1-\epsilon^2\xi^2)]}}{\sqrt{(1-\epsilon^2\xi^2)}}\, d\xi\,. \tag{14}$$

It will, of course, be necessary to replace ξ^2 by $(1-\xi^2)$ in the expression for $A(x)$ (and corresponding S'' and S'''), if the dispersion ellipsoid has its major axis in the direction of the star's radius.

IV. COMPARISON OF THE COMPUTED WITH THE OBSERVED PROFILES

From the foregoing sections we conclude that if the Doppler shifts observed for the spectral lines of a cepheid variable are really due to pulsations in the star's atmosphere,

these lines must have one or another of the computed profiles $S(x)$, $S'(x)$, $S''(x)$, or $S'''(x)$—at least as far as the so-called "Doppler lines" are concerned, i.e., lines with a Gaussian profile for $v = 0$.

We shall confine ourselves to the further treatment of the $S(x)$ profiles alone, as they appear to be the most probable.

The investigation can now be carried through as follows:

a) Compute theoretical profiles for various sets (β, C).

b) Multiply their abscissas by the factor $\lambda v/c$ to reduce them to the scale of the observed profiles, and their ordinates by the reciprocal, in order to keep the area of the curve unchanged.

c) Compare these "adapted" theoretical profiles with the "normalized" observed ones.

If consistent coincidences can be found at all phases, they will provide a crucial proof of the pulsation hypothesis and, besides, inform us about the amount of limb darkening (through the mediation of β) and about the magnitude of the turbulent velocities (through the mediation of C [see Sec. VI]).

The computational work involved can be substantially reduced by taking into account that both the theoretical line depth,

$$[S(x)]_{\max} = [S(\Delta\lambda)]_{\max} \frac{\lambda v}{c} = \frac{1 - I_{l\max}/I_{\text{cont}}}{\text{Equiv. width}} \frac{\lambda v}{c},$$

and the natural half-width,

$$(\Delta x)_n = \frac{x''_{(S=1/2S\max)} - x'_{(S=1/2S\max)}}{2} = (\Delta\lambda)_n \frac{c}{\lambda v},$$

are functions of C. The functions $[S(x)]_{\max}$ and $1/(\Delta x)_n$ are represented in Figure 4, *a* and *b*, respectively, for the values of 0, $\frac{3}{2}$, and ∞ of β.[8]

With the aid of these graphs, the following trial-and-error procedure can be used:

a) From measurements on an observed profile compute $S(x)_{\max}$ and $1/(\Delta x)_n$.

b) Introduce $S(x)_{\max}$ as ordinate in Figure 4, *a;* read off the corresponding abscissa $\sqrt{C}$ of the graph for the β value on trial.

c) Introduce this $\sqrt{C}$ as abscissa in Figure 4, *b;* read off the corresponding ordinate of the graph for the same β value. This ordinate should be equal to the above-computed $1/(\Delta x)_n$.

d) Once a satisfactory set of (β, C) is found, check it by computing the entire corresponding $S(x)$ profile and comparing it with the observed profile. The degree of fit will decide whether the set is to be retained or improved.

As was stated in Section I, the investigation is only worth while for large values of C, i.e., for large velocities and narrow lines; for small C's the asymmetry becomes unnoticeable, and β has no longer any perceptible bearing on the line profile.

THE APPLICATION TO η AQUILAE

V. THE ANALYSIS OF THE OBSERVED PROFILES OF THE FAINTEST LINES

Attention was first paid to the *Fe* I lines lying on the Doppler asymptote of the curve of growth. Those that could be picked out as free from blends are listed in Table 2.

These lines have a Gaussian profile for $v = 0$, thus making their comparison possible with our computed profiles; moreover, these lines are the best suited to show the expected asymmetry because of their narrowness, and their observed profiles can at each phase be

[8] In all the figures v has been replaced by dr/dt.

averaged to a single one, a procedure that saves labor and reduces the influence of errors of measurement.

At the phases with the largest values of v a well-marked asymmetry revealed itself at first glance and made a closer investigation most promising. The densities were measured at intervals of 1 mm (corresponding to 0.07 A). They were transformed into intensities with the aid of the calibration-curves that Schwarzschild had established by means of a tube photometer. For the radial velocities, Adams' values were adopted throughout. A large-scale plot was then made of each normalized profile and read off at intervals of 0.05 A.

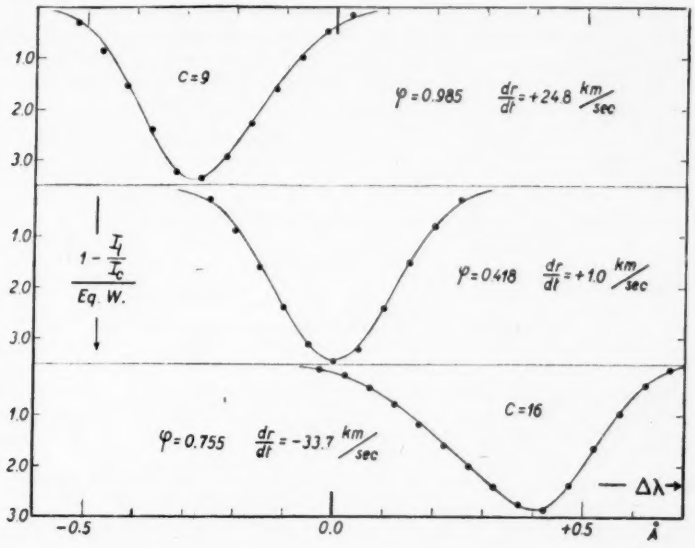

FIG. 4.—Observed (*dots*) and computed $S(\Delta\lambda)$ (*solid line*) profiles for $\beta = \frac{3}{2}$ ($u = 0.6$)

TABLE 2

EQUIVALENT WIDTH OF LINES

PHASE	v (KM/SEC)	EQUIVALENT WIDTH (A)							ξ_0 (KM/SEC)	ξ_μ (KM/SEC)	ξ_M (KM/SEC)	ξ_T (KM/SEC)
		Fe I 4376.68	*Fe* I 4392.59	*Fe* I 4439.88	*Fe* I 4445.48	*Fe* I 4551.71	*Fe* I 4572.87	*Fe* I 4587.13				
0.013	+24.6	0.040	.....	.....	.....	.....	.....	.....	8.1	4.0	5.8	7.1
.145	+17.1	.039	.....	.....	.....	.....	.....	.....	8.5	4.1	6.4	7.6
.280	+ 7.5	.045	.....	.....	.....	.....	.....	.....	9.3	4.3	7.3	8.5
.398	+ 1.4	.057	.....	.....	.....	.....	.....	.....	9.8	4.6	8.1	9.3
.418	+ 1.0	.062	0.037	.....	0.055	0.040	0.030	.....	11.0	4.7	9.1	10.4
.755	−33.7	.077	.....	.....	0.071	.....	0.044	.....	8.4	5.8	4.9	7.5
.824	−23.8	.....	0.036	.....	.....	.....	.....	.....	7.8	5.5	4.6	6.9
.898	+ 8.0	.040	.....	.....	.....	.....	.....	0.048	9.0	5.2	6.3	8.2
0.985	+24.8	0.047	.....	0.046	.....	.....	.....	0.049	8.3	4.3	6.0	7.4

At first, trials were made to fit the observations by some theoretical high-level profile. The analysis showed that the observed profiles were definitely broader, near the base, than were the $S'(x)$ profiles computed for the same line depth and velocity and for levels down to 2 per cent of the radius of the photosphere ($r/R = 0.98$). The conclusion is therefore justified that the observations do not show any perceptible level effect.

A second series of trials concerned the $S''(x)$ profiles. Again we had to conclude that the observed profiles do not yield any indication that a substantial center-to-limb variation, of the kind suggested in Section III, is present in the absorption lines examined. The introduction of material values for ϵ in formula (13) always led to computed profiles that were unmistakably of a different form from the observed ones; in particular, we always found $x_{S''_{\max}} \neq x_{\text{obs. max}}$ for the same line depth and appropriate velocity.

The $S'''(x)$ profiles computed for significant values of ϵ and of r/R were even more unsatisfactory. The simple $S(x)$ profiles, finally, used in the manner explained in the preceding section, readily led to an almost perfect agreement with the observations. For $\beta = \frac{3}{2}$ ($u = 0.6$), we found the close correspondence illustrated in Figure 5.

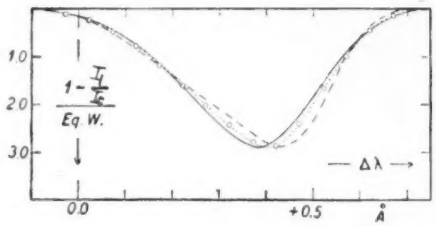

FIG. 5.—Observed profile at $\phi = 0^p755$ (*circles*); theoretical profiles for $\beta = 0$, $C = 30$, $\bar{x} = 0.667$, $dr/dt = -35.8$ km/sec (*dashed line*); $\beta = \frac{3}{2}$, $C = 16$, $\bar{x} = 0.708$, $dr/dt = -33.7$ km/sec (*dotted line*); $\beta = \infty$, $C = 10$, $\bar{x} = 0.750$, $dr/dt = -31.8$ km/sec (*full line*).

For the largest velocity involved, $v = -33.7$ km/sec at phase 0.755, no other set of (β, C) values succeeded in giving so close a fit; for the smaller velocity of expansion $v = +24.8$ km/sec at phase 0.985, on the contrary, several sets (with β ranging from $\frac{3}{2}$ to ∞), did nearly as well.

Outside the phase intervals around maximum velocity of contraction or expansion, the asymmetry of the observed profiles gets so small (in keeping with theory) that an analysis of their shape is no longer worth while, but their depths and widths were further used for the determination of C in the way explained above, in order to find out the variation of turbulence with phase.

Our general conclusion from the investigation is therefore that the analyzed profiles fully check the prediction of the pulsation theory and that, with the resolving power used, velocities along the star's radius above 30 km/sec allow a determination of the amount of limb darkening.

It may be noticed that η Aquilae, because of its moderate maximum velocity of expansion, does not permit the determination of whether the limb darkening is different at maximum and at minimum light. Among the brighter cepheids, X Cygni, with extreme values of $+45$ and -45 km/sec for its velocity, will serve that purpose much better.

It should be emphasized, however, that in future investigations of β it will be necessary to have the comparison spectrum registered on the same sheets as the star's spectrum, in order that the origin of the abscissas may be accurately fixed for each profile. Figure 6 illustrates the importance of this requirement. It contains, besides the observed profile at 0.755, theoretical $S(x)$ profiles corresponding to different values of β, with adequate values of v, so chosen that they have the same depth as the observed line. As

they stand, no hesitation is possible about which is to be adopted. But when the observed profile is allowed to move along the axis of abscissa—and this will always be the case when the origin of $\Delta\lambda$ is unknown—the $(\beta = \infty)$-curve can give about as good a fit as does the $(\beta = \frac{3}{2})$-curve. All values $\frac{3}{2} \leqslant \beta < \infty$ then become possible.

The figure also gives some idea about the precision with which the amount of limb darkening can be deduced, if the zero point of $\Delta\lambda$ is known. Had this requirement been fulfilled, our material would have been able to yield the coefficient of limb darkening u with an error of just 0.1, as was proved by a computation in which the errors of the measured ordinates were considered to be $\frac{1}{4}$ mm.

VI. THE DETERMINATION OF TURBULENCES

Let us consider a phase to which corresponds a velocity v along the star's radius, and let $\xi_0 = v/\sqrt{C}$, the dispersion, expressed in km/sec, of the basic Gaussian absorption line (it can be derived from the observed distorted profile with the aid of Fig. 4, *a* and *b*, in the manner already explained); ξ_a = the dispersion of the apparatus function (assumed Gaussian) (according to L. Spitzer, Jr., $\xi_a = 3.5$ km/sec);[9] $\xi_{th} = \sqrt{[2RT/\mu]}$, the thermal velocity, which can be considered to remain constant throughout the period; and $\xi_g = (1/R_e)X$, the vertical shift necessary to bring the empirical curve of growth upon

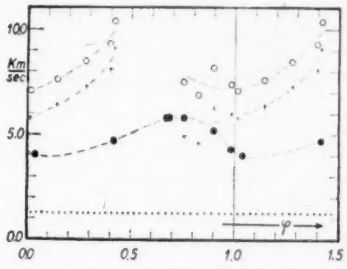

FIG. 6.—Turbulent velocities as a function of phase. *Dots*, ξ_u; *full circles*, ξ_μ; *crosses*, ξ_M; *open circles*, ξ_T

the theoretical. The empirical curve of growth was formed by plotting the equivalent widths of twenty selected *Fe* I lines against the corresponding values of log x_0; the latter were derived from C. W. Allen's[10] solar equivalent widths with the aid of K. O. Wright's[11] empirical curve of growth for the sun. For R_e we adopted the intermediate value 0.85.

With ξ_a and ξ_{th} known from the outset and ξ_0 and ξ_g easily found from the observations, the computation of the turbulences becomes an easy matter. We have

$$\xi_\mu = \sqrt{(\xi_g^2 - \xi_{th}^2)} \text{ for the micro-turbulence ,}$$

$$\xi_M = \sqrt{(\xi_0^2 - \xi_a^2 - \xi_{th}^2 - \xi_\mu^2)} \text{ for the macro-turbulence ,}$$

$$\xi_T = \sqrt{(\xi_\mu^2 + \xi_M^2)} \text{ for the total turbulence .}$$

Table 2 lists and Figure 7 illustrates graphically the results arrived at.

VII. THE OBSERVED PROFILES OF RADIAL-VELOCITY LINES

A good many *Fe* I lines lying on the horizontal branch of the curve of growth presented —rather unexpectedly—an almost Gaussian profile at the phases with $v = 0$; conse-

[9] *Ap. J.*, **90**, 498, 1939.

[10] *Mem. Comm. Sol. Obs., Mt. Stromlo*, **1**, No. 5, Part 2, 14, 1934.

[11] *Ap. J.*, **99**, 249, 1944.

quently, we examined their profiles at the phases with large radial velocity in the same manner as was done for the faintest lines, in order to find out whether they confirmed our former conclusions or not.

Averaging being no longer allowed, each line had to be compared separately with the theoretical profiles. Our results can be summarized as follows:

a) At phase 0.985, corresponding to maximum velocity of expansion, $v = +24.8$ km/sec, all the contours gave an excellent fit with the $S(x)$ profiles computed for the hypothesis $\beta = \frac{3}{2}$. Theoretical profiles corresponding to larger β's and appropriate velocities did practically as well.

b) At phase 0.671, corresponding to an equal velocity of contraction, $v = -24.7$ km/sec, the observed contours proved to be the perfect mirror images of the foregoing.

c) At phase 0.755, corresponding to maximum velocity of contraction, $v = -33.7$

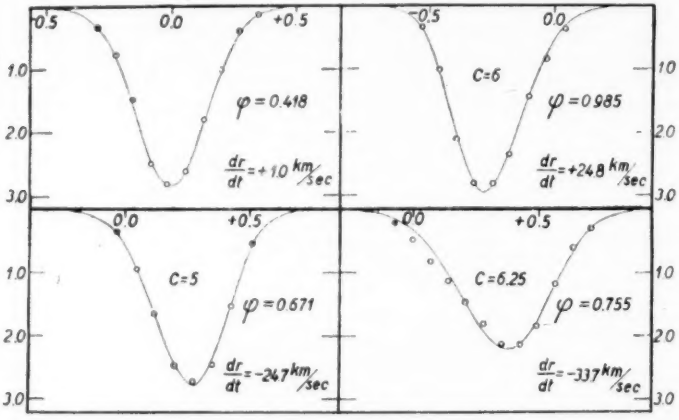

FIG. 7.—Profile of *Fe* I 4602.00 (*open circles*). Computed $S(\Delta\lambda)$ profiles for $\beta = \frac{3}{2}$ and for the values of C and dr/dt shown in the figure (*full line*).

km/sec, the observed profiles showed a larger asymmetry than could be accounted for by a limb darkening $\beta = \frac{3}{2}$ and the proposed velocity. The (perhaps not unjustified[12]) increase of the adopted velocity by some 10 per cent and the simultaneous change of β from $\frac{3}{2}$ into ∞ considerably improved the fit, but left the computed red wings still somewhat weaker than the observed. The discrepancy, therefore, cannot be ascribed entirely to errors in the adopted velocity but is perhaps mainly due to the fact that the basic profile went over from a nearly Gaussian into a more typical Voigt contour. Further investigations are, however, necessary to throw more light on this point. Figure 8 shows the behavior of *Fe* I 4602.00, which was typical for the lines here considered.

As a whole the results from the present sections can certainly be said to strengthen the conclusion reached from the consideration of the more trustworthy fainter lines: the observed profiles can be accounted for by the existence of radial pulsations in the stellar atmosphere.

[12] The coudé plate corresponding to this critical phase could not be measured by Adams because of poor quality of the comparison spectrum. M. Schwarzschild and his collaborators therefore adopted Jacobsen's values of the radial velocity around this phase, but it is easy to see from their curve (*Ap. J.*, **108**, 208, 1948) that Adams' measurements show a tendency to give, for comparable phases, slightly larger velocities. A small increase of the adopted velocity by about 4 km/sec is therefore not impossible.

VIII. THE RATIO OF VELOCITY ALONG THE STAR'S RADIUS TO OBSERVED RADIAL VELOCITY

It is evident from the profiles represented that their very small amount of asymmetry will pass unnoticed on the spectrograms themselves and, consequently, that in the course of radial-velocity measurements the settings will be made at, or at least very near, the point of maximum depth and not at the optical center of gravity of the line. But this circumstance has its bearing upon the factor by which the measured radial velocity must be multiplied in order to be transformed into velocity of contraction or expansion. If, for instance, the very faint lines shown in Figure 5 could be used for radial-velocity measurements, this factor should be about $\frac{3}{4}$ instead of $\frac{24}{17}$, as generally considered. With actual

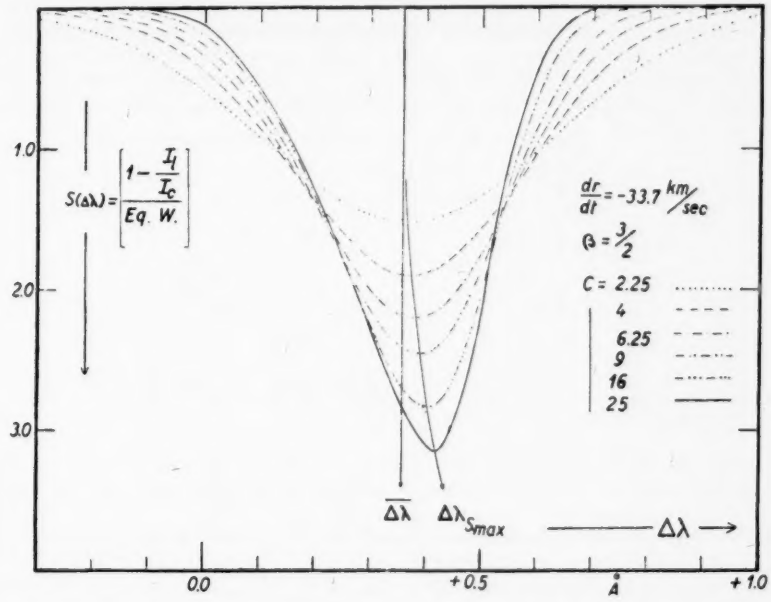

FIG. 8.—$S(\Delta\lambda)$ profiles corresponding to the values of dr/dt and C shown. During radial-velocity measurements, settings on the narrower of these profiles will not be made at $\overline{\Delta\lambda}$ but probably very near their $\Delta\lambda S_{max}$; consequently, the ratio of observed radial velocity to velocity along the stellar radius will be larger than 17/24 for narrow lines.

radial-velocity lines the difference is certainly less, but here also the ratio v/V seems different from what was thought hitherto. Figure 9 makes clear that this ratio will be a function of the line width—more exactly, of the parameter $\sqrt{C} = v/\xi_0$.

This correlation between line width and v/V ratio is responsible, to a certain extent, for the discrepant Doppler shifts derived from different lines of the same cepheid at the same phase and should certainly be considered also when a correct interpretation is sought for the discrepant center-of-mass velocities that correspond to different lines or line groups—a phenomenon that so many cepheids show.

IX. THE DIFFERENCES IN THE RADIAL VELOCITIES DERIVED FROM *Fe* I AND FROM *Fe* II LINES

We have tried to find out whether the effect presented in the preceding section was able to account in full for the slight differences between the extremely accurate radial

velocities which Adams derived from the neutral and from the ionized iron lines, respectively, and which were considered by M. and B. Schwarzschild and himself as insignificant. This judgment then led to the conclusion that the two kinds of lines originated at the same height in the stellar atmosphere.[6]

There exists between the average radial velocities of the two groups of lines a difference of 0.43 km/sec in the sense

$$\bar{V}\,(\text{neutral}) - \bar{V}\,(\text{ionized}) = -0.43 \text{ km/sec},$$

hence a difference between the center-of-mass velocities of $-0.43 \times 24/17 = 0.61$ km/sec.

Table 4 of the article just referred to shows the individual values of the difference in radial velocity between the two groups at the various phases. In our opinion these values need to be corrected for a difference in average line width between the two groups. We computed, therefore, with the aid of Table 3 of the paper just quoted, mean line depths

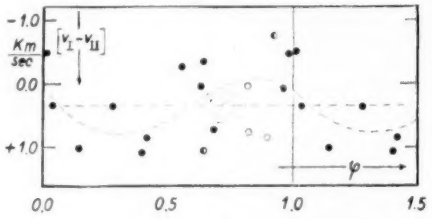

FIG. 9.—Differences in velocity between neutral and ionized *Fe* lines as a function of phase. *Closed circles*, full-weight observations; *half-filled circles*, half-weight observations, few lines measured; *open circles*, low-weight observations, poor settings.

for each group at the various phases, and from them the expression $(1 - I_{l\max}/I_{\text{cont}})$. The results, however, are not yet directly comparable, owing to the fact that Schwarzschild and his collaborators did not measure the maximum line depth, but the one below which the intensity stays for an interval of 0.03 A. This procedure, of course, cuts down the depths of the narrower lines somewhat more than those of the broader ones. The corresponding correction to the already computed $(1 - I_{l\max}/I_{\text{cont}})$ is easily found to be $0.015(1 - I_{l\max}/I_{\text{cont}})^2$/ equiv. width. After corrected values $(1 - I_{l\max}/I_{\text{cont}})_{\text{corr}}$/equiv. width had been found, they were compared with sets of $S(\Delta\lambda)$ profiles corresponding to the various velocities involved, in order to find the appropriate v/V ratio for each group and therefrom the actual v. Table 3 gives the details of this investigation, and Figure 9 shows the results.

It is seen that the average difference $\bar{v}$ (neutral) $-$ $\bar{v}$ (ionized) has shrunk and that, when the three "poor" results at phases 0.820, 0.824, and 0.898 are omitted, a phase effect cannot be denied. This phase effect can be interpreted as denoting a small phase lag between the two radial-velocity-curves (the *Fe* I-curve coming behind), together, perhaps, with an extremely small excess of the amplitude from the *Fe* I lines over that from the *Fe* II lines; such excess will reduce the difference concerned toward the phases of maximum velocity—either of expansion or of contraction—and increase it for a while after the time of these maxima. This is about what can be seen from the corrected points. The accidental spread in the latter renders a quantitative determination of the run in phase and amplitude rather hazardous, and the values of $\Delta\phi = 0.01$ (Period) and $\Delta A = 0.3$ km/sec we propose should be considered as simple guesses.

Against the objection that the strongly negative differences at phases 0.824 and 0.898 are in contradiction with our assumed phase lag, we can argue that these large deviations

are mainly due to two or three strongly deviating lines, that Adams himself qualifies all his settings on these plates as "poor," and, finally, that the particularly strong red wing, already mentioned in Section VII, of the *Fe* I lines at the phases with large velocity of contraction may well have become apparent on the plates themselves and have influenced the settings on these lines, reducing the resulting radial velocity. For all these reasons we believe that these discordant values provide no proof against the phase effect revealed by the more reliable results from the other phases. It remains questionable, however, whether the successive large negative differences can be reconciled with the large positive values that are necessary at these phases if the average [$\bar{v}$ (neutral) − $\bar{v}$ (ionized)] should be zero. This looks rather improbable, and the safest conclusion is perhaps that the improved differences reveal (*a*) a difference of about 0.3 km/sec between

TABLE 3

INTENSITIES OF *Fe* LINES

Plate No.	Phase*	Line Depth		$(1-[I_{l\,max}/I_{cont}])_{Schwarzschild}$		Equivalent Width		$0.015(1-[I_{l\,max}/I_{cont}])^2$/Equiv. Width		$(1-[I_{l\,max}/I_{cont}])_{corr}$	
		Fe I	*Fe* II	*Fe* I	*Fe* II	*Fe* I	*Fe* II	*Fe* I	*Fe* II	*Fe* I	*Fe* II
2333...	0.013	0.210	0.346	0.383	0.549	0.13	0.23	0.017	0.021	0.400	0.570
2394...	.037	.247	.393	.434	.595	.16	.24	.018	.022	.452	.617
2335...	.145	.254	.369	.443	.572	.16	.22	.018	.022	.461	.594
2373...	.632	.390	.390	.593	.593	.29	.25	.018	.021	.611	.613
2802...	.643	.383	.391	.586	.594	.29	.25	.018	.021	.604	.615
2587...	.651	.345	.356	.548	.559	.25	.25	.018	.019	.566	.578
2592...	.686	.306	.279	.506	.474	.21	.21	.018	.016	.524	.490
2594...	.820	.266	.343	.458	.546	.25	.30	.013	.015	.471	.561
2397...	.824	.252	.328	.440	.530	.26	.35	.011	.012	.451	.542
2401...	.961	.178	.341	.336	.544	.16	.25	.011	.018	.347	.562
2607...	0.985	0.223	0.368	0.402	0.571	0.18	0.28	0.013	0.017	0.415	0.588

* Obviously, only phases with sufficiently large radial velocities are considered here; the other phases had their representative points in Fig. 9 directly derived from Schwarzschild and Adams' Table 4.

Plate No.	Phase*	$(1-[I_{l\,max}/I_{cont}])_{corr}$/Equiv. Width		$-V/v$		V† (Km/Sec)		v (Km/Sec)		$v_{Fe\,I}-v_{Fe\,II}$
		Fe I	*Fe* II	*Fe* I	*Fe* II	*Fe* I	*Fe* II	*Fe* I	*Fe* II	
2333.....	0.013	3.08	2.48	0.751	0.724	−18.19	−17.91	+24.22	+24.74	−0.52
2394.....	.037	2.82	2.57	.737	.727	−18.05	−17.56	+24.49	+24.15	+0.34
2335.....	.145	2.88	2.70	.740	.731	−14.11	−13.20	+19.07	+18.06	+1.01
2373.....	.632	2.11	2.45	.717	.724	+13.69	+13.85	−19.09	−19.13	+0.04
2802.....	.643	2.08	2.46	.717	.724	+16.21	+16.11	−22.61	−22.25	−0.36
2587.....	.651	2.26	2.31	.718	.721	+15.73	+16.55	−21.91	−22.95	+1.04
2592.....	.686	2.50	2.33	.727	.721	+20.22	+20.56	−27.81	−28.52	+0.71
2594.....	.820	1.88	1.87	.713	.713	+17.96	+17.98	−25.19	−25.22	+0.03
2397.....	.824	1.73	1.55	.711	.710	+16.68	+17.19	−23.46	−24.21	+0.75
2401.....	.961	2.17	2.25	.718	.718	−16.93	−16.88	+23.58	+23.51	+0.07
2607.....	0.985	2.31	2.10	0.721	0.717	−18.59	−18.82	+25.78	+26.25	−0.47

† Planimeter measurements gave for the center-of-mass velocity corresponding to Schwarzschild and Adams' "average" velocities: −14.62 km/sec; the inspection of our $-V/v$ values showed, on the other hand, that the *Fe* I velocities will differ by about −0.1 km/sec, on the average, from the *Fe* II velocities, so we adopted −14.67 km/sec for the center-of-mass velocity corresponding to the *Fe* I lines and −14.57 km/sec for that corresponding to the *Fe* II lines.

the averages, in the sense

$$\bar{v}\,(Fe\ \text{I}) - \bar{v}\,(Fe\ \text{II}) = -0.3\ \text{km/sec},$$

upon which is superimposed (*b*) a phase effect with a semi-amplitude of about the same value.

Both features give evidence that the neutral iron lines are formed at a somewhat higher level than are the lines of the ionized element. It is well known indeed that "high-level" lines show, besides a phase lag in the radial-velocity-curve, an average velocity of approach relative to "low-level" lines.[13]

The latter phenomenon might well constitute the observational evidence of Pannekoek's viewpoint[14] that an outward flow of matter is going on in cepheids.

The phase effect also lends itself to some interesting conclusions. First of all, a glance at Figure 9 reveals that the star layer between the representative levels of the *Fe* I and of the *Fe* II lines is in expansion for about the first six-tenths of the period and is being compressed for the further four-tenths. Maximum expansion of the layer thus occurs practically at minimum brightness, maximum compression almost coincides with maximum brightness. Not the degree of contraction of the star as a whole but the degree of contraction of the photosphere will be decisive for the brightness.

Second, the phase effect provides a means of deriving an approximate value of the difference in altitude between the representative *Fe* I and *Fe* II levels. Adopting, for Figure 9, 0.3 km/sec for the semi-amplitude of the $v(Fe\ \text{I}) - v(Fe\ \text{II})$ difference, we find, by integration, about 50,000 km for the excess of the semi-amplitude of the pulsation at the *Fe* I level over that at the *Fe* II level. If we further adopt 8/1 for the ratio of the extreme values for the density of the layer between these levels, from Schwarzschild's Figure 2, we readily find $\pm 65{,}000$ km for the average difference in altitude.

The amount may seem excessive and calls for a check. We have tried to derive one from the consideration of the various velocities at phase 0.45. Here $v = 0$, and the difference in level arising from our interpretation of Figure 9 is about 80,000 km, to which will correspond, with the adopted value of $0.01P$ for the phase lag, a velocity of propagation of the pulsation wave through the layer of $80{,}000/6{,}000 = 13$ km/sec, as compared with $11\sqrt{2} = 8$ km/sec given by the turbulence, which is 11 km/sec at this phase. The agreement is rather good but cannot be said to be convincing, in view of the uncertainty in the adopted $\Delta\phi$ and of the large scatter of the points in both our Figure 9 and in Schwarzschild's density diagram. We are aware that the differences between the two radial-velocity-curves considered are very near the limit of detectability and that the numerical results of this section may be largely in error; we hope, however, to have shown that valuable information can be expected from the intercomparison of radial-velocity-curves derived from different chemical elements and showing in a more conspicuous manner the differences here analyzed.

As a final remark we may mention that the layers in which the *Fe* I and *Fe* II lines develop are almost certainly overlapping one another and that their respective thicknesses may reach several times their difference in average level. This implies that the progressive variation of phase and amplitude with level must manifest itself within each layer itself. The effect will, of course, be to broaden the lines; part of the observed "turbulence" must be ascribed to this.

Acknowledgments are due to Dr. I. S. Bowen, Dr. M. Schwarzschild, and Dr. W. S. Adams for having put at our disposal the most valuable material on which this investigation is based, and to Dr. M. Minnaert for many valuable suggestions.

[13] See, e.g., J. A. Aldrich, *Pub. Obs. U. Michigan*, Vol. **4**, No. 5, 1932.

[14] *Report of the Zeeman Congress* (Amsterdam, 1946).

A STUDY OF THE STRUCTURE OF THE λ 7054 BAND OF *TiO* IN THE SPECTRUM OF BETA PEGASI*

JOHN G. PHILLIPS
Berkeley Astronomical Department, University of California
Received September 26, 1951

ABSTRACT

It is shown that it is possible, from theoretical considerations, to compute a profile of the λ 7054 band of *TiO* which agrees, within the accuracy of the photometry, with the profile obtained from a tracing of a high-dispersion spectrogram of β Pegasi. The dispersion on the spectrogram is 5.8 A/mm. The numerical values of the parameters in the theoretical expressions which lead to agreement are the following: $T = 3000°$ K; Doppler width = 0.1 A; damping constant = 0.1 A; $R_e = 0.73$; $K = 0.0477$, in which K is a constant, combining such quantities as the total number of molecules in the $v'' = 0$ vibrational level, the partition function, etc. While these numerical values do result in good agreement with observation, it is found that the profile is not sensitively a function of certain of them. This fact, together with the approximate nature of the theoretical expressions that are used, makes it necessary to consider the study as a preliminary one.

A. INTRODUCTION

Three general methods are available for determining the temperature of molecules in a spectroscopic source from the relative intensities of features in the corresponding band spectra: (*a*) The first involves the integrated relative intensities in emission or absorption of two or more band systems. The initial electronic states of the systems must be different, the relative transition probabilities of the electronic transitions must be known, and the integrations must be carried out over all bands belonging to each system. This method does not have much application to astronomical problems, since the observed spectra of few molecules can satisfy the requirements. (*b*) The second method, requiring the measurement of the relative integrated intensities of individual bands within a given system and a knowledge of the relative transition probabilities of the bands, is the most convenient to use when only low-dispersion spectrograms are available. Recently this method was applied by McKellar and Buscombe[1] to the determination of the temperatures of three R-type stars from the Swan-band intensities. (*c*) The third method derives a temperature from the relative intensities of the rotational lines of an individual band. It is applicable whenever the rotational fine structure of a band is resolved or the profile of the band can be observed. An advantage of the method is the fact that relative transition probabilities have been computed for a variety of types of transition and have been widely verified in the laboratory. It has been applied to molecular bands in the sun by numerous investigators;[2] by Meinel to the *OH* emission bands in the night sky;[3] and to band profiles in cometary spectra by Swings and Nicolet,[4] McKellar,[5] Hunaerts,[6] and others. However, up to the present time, the only attempt to apply the method of rota-

* This article is based upon material obtained by the author as guest investigator at the Mount Wilson and Palomar Observatories.

[1] *Pub. Dom. Ap. Obs. Victoria*, **7**, 361, 1948.

[2] See, e.g., R. T. Birge, *Ap. J.*, **55**, 273, 1922; R. S. Richardson, *Pub. A.S.P.*, **44**, 250, 1932; *Ap. J.*, **73**, 216, 1931; M. G. Adam, *M.N.*, **98**, 544, 1938; F. E. Roach, *Ap. J.*, **89**, 99, 1939; L. Blitzer, *Ap. J.*, **91**, 421, 1940; J. Hunaerts, *Ann. d'ap.*, **10**, 237, 1947.

[3] *Ap. J.*, **112**, 120, 1950.

[4] *Ap. J.*, **88**, 173, 1938.

[5] *Ap. J.*, **98**, 1, 1943; *Rev. Mod. Phys.*, **14**, 179, 1942.

[6] *Ann. Obs. r. Belgique*, Ser. 3, Vol. **5**, No. 1, 1950.

tional-line intensities to a stellar spectrum has been made by McKellar and Buscombe[4] on a *CH* band in R stars. Blending with atomic lines was found to be too serious for conclusive results to be obtained.

It should be pointed out that only in cases of thermodynamic equilibrium will the three methods yield the same temperature. Therefore, until the presence of thermodynamic equilibrium is definitely established, the resulting temperatures should be called, respectively, "electronic," "vibrational," and "rotational" temperatures.

During a recent investigation of the spectrum of the *TiO* molecule in the laboratory, it was found that certain sections of the γ-system ($A^3\Delta - X^3\Pi$) showed a comparatively simple structure. One of these sections is to be found between two of the three subheads of the (0–0) band, at λ 7054 and λ 7088, respectively. The arrangement of the rotational lines in this wave-length region is shown by the leading lines in Figure 1. The lengths of the leading lines correspond to the computed relative intensities for a temperature of 3000° K.

On high-dispersion spectrograms of M-type stars most of these rotational lines are clearly resolved. Figure 1 presents the intensity profile of this section of the spectrum of β Pegasi. Intensities are plotted relative to the intensity at the λ 7054 head. The profile was derived from a tracing of a plate taken with the coudé spectrograph of the 100-inch telescope at Mount Wilson. Table 1 lists the pertinent data on the plate.

It is seen in Figure 1 that each absorption feature in the stellar profile coincides with a line in the laboratory spectrum. Also included are the locations of a few atomic lines listed by Dorothy N. Davis[7] in the spectrum of this star. In general, the effects of these atomic lines are negligible. Thus the fact that the region is so free of complicating atomic absorptions and also that the spectrum is relatively simple makes it an attractive region for testing the method of rotational-line intensities in determining the rotational temperature of the *TiO* molecules in β Pegasi. Another reason why the region is a convenient one for study is that the $\Delta v = 0$ sequence of the γ-system is comparatively isolated in the *TiO* spectrum, so that it is possible that the true continuum is reached immediately to the violet of the sequence at λ 7054. For this reason it has been assumed, in deriving the relative intensities in Figure 1, that the true continuum is actually reached at this point and also that the intensity of the continuum does not change in the interval from λ 7054 to λ 7088. Both these assumptions can be checked and, if necessary, modified as the analysis of the profile proceeds.

In order to derive a temperature from the relative intensities of rotational lines in a band, it is, of course, necessary that the rotational analysis of the band be available. Such an analysis of the γ-system had not been carried out in earlier investigations of the *TiO* spectrum. Accordingly, as a preliminary step, the analysis was undertaken of the three most intense bands of the system. The results of this analysis have appeared in an earlier publication.[8] For the sake of completeness, the wave lengths in air of the lines in the region of interest are presented in Table 2. The table includes the locations of several lines not observed on the laboratory plates, either because they are too near the origin and hence too weak or because they are unresolved in the head. However, the analysis of the laboratory spectra provides data which make it possible to compute the locations of these additional lines.

The fact that none of the stellar lines are completely unblended means that one cannot use the usual methods for determining the rotational temperature, which require the measurement of the relative absorptions of individual lines. Therefore, an indirect procedure must be followed. From theoretical considerations, synthetic profiles of the band may be computed, and it is assumed that those parameters which lead to a computed profile agreeing with the observed profile also describe the condition of the molecules in the stellar atmosphere.

[7] *Ap. J.*, **106**, 28, 1947.

[8] J. G. Phillips, *Ap. J.*, **114**, 152, 1951.

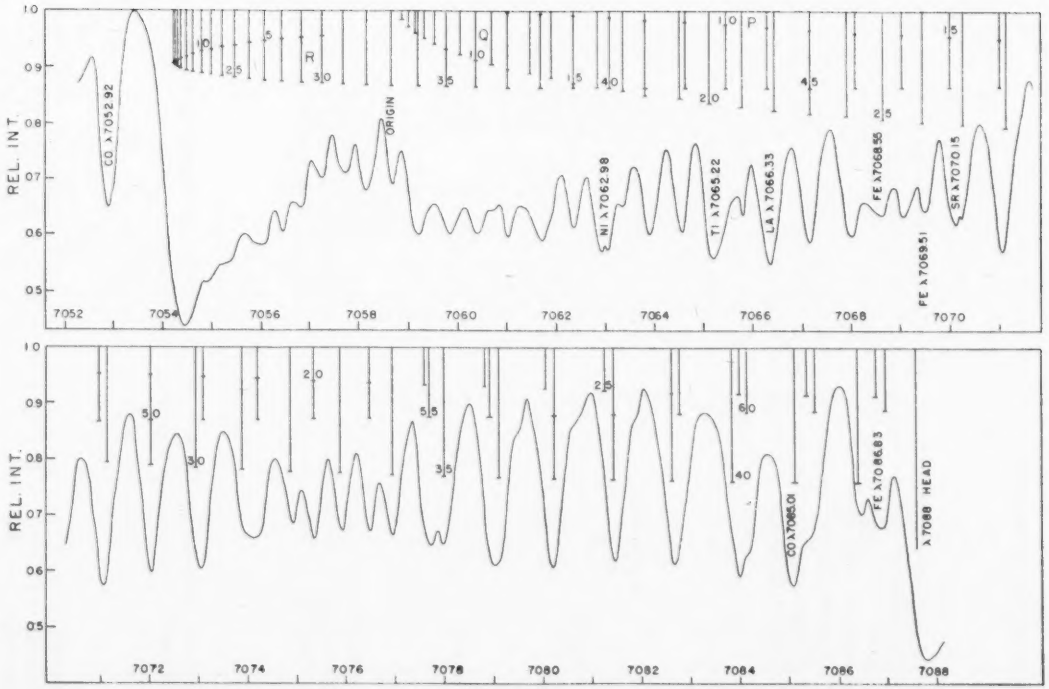

FIG. 1.—Absorption profile in the region λλ 7052–7088 in the spectrum of β Pegasi. The leading lines present the locations of rotational lines of the *TiO* molecule as observed in the laboratory. The relative lengths of the leading lines correspond to the relative intensities of the rotational lines at a temperature of 3000° K.

B. DETERMINATION OF LINE INTENSITIES

In computing the band profile, it has been assumed that the depth at each point in an absorption line, $R_\lambda = (F_{0,\lambda} - F_\lambda)/F_{0,\lambda}$, can be related to the optical thickness, x_λ, of the stellar atmosphere by the equation of Minnaert:

$$\frac{1}{R_\lambda} = \frac{1}{R_C} + \frac{1}{x_\lambda}, \tag{1}$$

in which R_C is a limiting depth for $x_\lambda \gg 1$. The optical thickness can be given as $N_{J''}^{X} \alpha_\lambda$, where $N_{J''}^{X}$ is the number of molecules involved in the absorption in a particular line, with initial quantum number J'' and in the branch $X(X = P, Q, \text{or } R)$, and α_λ is the molecular absorption coefficient.

Since the rotational lines in the band are strong, it is necessary to include in the equation for the absorption coefficient the effects of both Doppler motion and damping. Theoretical considerations lead to the familiar equation:

$$\alpha_\lambda = \frac{\pi^{1/2} e^2 \lambda}{m c} f \sqrt{\frac{A m_0}{2kT}} \left[\frac{a}{\pi} \int_{-\infty}^{+\infty} \frac{e^{-y^2} dy}{(v-y)^2 + a^2} \right],$$

TABLE 1

DATA ON MOUNT WILSON COUDÉ PLATE NO. 2899

Date of exposure	October 31, 1942	Camera	114-inch
Exposure time	302 minutes	Slit-width	0.10 mm
Emulsion	IV-N sensitized	Dispersion	5.8 A/mm

where the terms a, y, and v are defined as

$$a = \frac{\gamma}{\Delta\lambda_D}; \qquad y = \frac{\Delta\lambda}{\Delta\lambda_D}; \qquad v = \frac{\lambda - \lambda_0}{\Delta\lambda_D},$$

γ being the effective natural width in angstrom units; $\Delta\lambda$ the shift in angstroms produced by the component of the velocity of an individual molecule in the line of sight; λ_0 the wave length of the line center; and $\Delta\lambda_D$ the Doppler width, given by the relationship

$$\Delta\lambda_D = \frac{\lambda}{c} \sqrt{\frac{2kT}{A m_0}}.$$

Other terms have the usual significance. In the limiting case of zero damping, the absorption coefficient at the line center becomes α_0, defined by

$$\alpha_0 = \frac{\pi^{1/2} e^2 \lambda}{m c} f \sqrt{\frac{A m_0}{2kT}}.$$

The expression in brackets, which is usually abbreviated as $H(a, v)$ in the literature, has been evaluated by Born[9] and Hjerting[10] for various values of a and v.

If it is assumed that a Boltzmann distribution of the molecules among the various rotational levels prevails, then

$$N_{J''}^{X} f = C S_{J''}^{X} \exp\left[-B'' J'' (J''+1) \frac{hc}{kT} \right],$$

[9] *Optik* (Berlin: J. Springer, 1933), Sec. 93.

[10] *Ap. J.*, **88**, 508, 1938.

TABLE 2

WAVE LENGTHS IN AIR OF THE (0–0) BAND OF THE γ-SYSTEM OF *TiO* BETWEEN λ 7054.2 AND λ 7091.4

a) $^3\Delta_3 - {}^3\Pi_2$ TRANSITION

J	$R(J)$ (λ)	$Q(J)$ (λ)	$P(J)$ (λ)	J	$R(J)$ (λ)	$Q(J)$ (λ)	$P(J)$ (λ)
2	7057.262			34	7059.228	7076.940	
3	56.845	7058.902		35	59.799	78.014	
4	56.464	59.022	7061.045	36	60.393	79.121	
5	56.108	59.172	61.692	37	61.045	80.241	
6	55.786	59.349	62.381	38	61.692	81.438	
7	55.492	59.560	63.112	39	62.381	82.631	
8	55.233	59.799	63.836	40	63.112	83.858	
9	55.004	60.065	64.651	41	63.836	85.120	
10	54.805	60.393	65.465	42	64.651	86.410	
11	54.633	60.701	66.311	43	65.465	87.727	
12	54.490	61.043	67.171	44	66.311	89.084	
13	54.385	61.480	68.093	45	67.171	90.476	
14	54.311	61.915	69.039	46	68.093		
15	54.267	62.381	70.011	47	69.039		
16	54.252	62.863	71.014	48	70.011		
17	54.267	63.389	72.039	49	71.014		
18	54.311	63.836	73.113	50	72.039		
19	54.385	64.518	74.214	51	73.113		
20	54.490	65.135	75.339	52	74.214		
21	54.633	65.772	76.513	53	75.339		
22	54.805	66.449	77.613	54	76.513		
23	55.004	67.171	78.828	55	77.704		
24	55.233	67.892	80.068	56	78.927		
25	55.492	68.659	81.272	57	80.241		
26	55.786	69.453	82.631	58	81.438		
27	56.108	70.280	83.997	59	82.791		
28	56.464	71.144	85.367	60	84.141		
29	56.845	72.039	86.767	61	85.528		
30	57.262	72.952	88.204	62	86.949		
31	57.707	73.900	89.673	63	88.412		
32	58.185	74.885	91.161	64	89.904		
33	58.686	75.900		65	91.400		

b) $^3\Delta_2 - {}^3\Pi_1$ TRANSITION

J	$R(J)$ (λ)	J	$R(J)$ (λ)	J	$R(J)$ (λ)
1	7091.431	12	7087.987	23	7088.037
2	90.973	13	87.846	24	88.218
3	90.545	14	87.736	25	88.429
4	90.148	15	87.655	26	88.669
5	89.781	16	87.600	27	88.935
6	89.439	17	87.575	28	89.232
7	89.127	18	87.580	29	89.562
8	88.842	19	87.615	30	89.904
9	88.585	20	87.675	31	90.304
10	88.359	21	87.766	32	90.727
11	88.158	22	87.886	33	91.161

where the constant C includes the total number of molecules in the $v'' = 0$ vibrational level, as well as the partition function. The intensity factors, $S_{J''}^{X}$, are known from the theoretical work of Hönl and London.[11] They are, for a $^3\Delta - {}^3\Pi$ transition, between states with couplings, between the various molecular angular momenta, corresponding to Hund's case *a*:

$$S_{J''}^{P} = \frac{(J''+\Omega)(J''-\Omega+1)}{J''},$$

$$S_{J''}^{Q} = \frac{(2J''+1)(J''+\Omega)(J''-\Omega+1)}{J''(J''+1)}, \tag{2}$$

$$S_{J''}^{R} = \frac{(J''+\Omega+1)(J''+\Omega)}{(J''+1)}.$$

For an $A^3\Delta_3 - X^3\Pi_2$ subband, $\Omega = 3$, in these equations.

By combining the various relationships, equation (1) may be written in the following form:

$$\frac{1}{R_\lambda} = \frac{1}{R_C} + \frac{1}{\Sigma K S_{J''}^{X} H(a, v) \exp\left[-B''J''(J''+1)hc/kT\right]}, \tag{3}$$

where K is a constant combining a number of constant terms. The summation is extended over all lines making contributions to the absorption at a particular wave length.

There are, therefore, five adjustable parameters to be evaluated: γ, the damping width; $\Delta\lambda_D$, the Doppler width; the temperature, T; R_C; and K. It is also necessary to study the location of the continuum.

While the absorption at any single wave length is, of course, a function of all the parameters, it is found that the profiles or relative intensities of certain features are more sensitive functions of certain of the parameters than of others. Thus it is possible, through the use of the profile presented in Figure 1, to obtain first approximations to the parameters. The first approximations may then be applied to a study of the location of the continuum. After any adjustments required in the location of the continuum have been made, then the parameters may be further adjusted until computed absorptions at various points in the band agree as well as possible with the observed absorption. Each of these steps will be considered in turn.

C. THE FIRST APPROXIMATIONS

a) THE CORRECTION FOR SLIT BROADENING

The true line profile produced by the 1942 form of the coudé spectrograph for monochromatic incident radiation is not known. According to the theory of van Cittert,[12] the theoretical profile of such a line, in the focal plane of the 114-inch camera, with a slit width of 0.10 mm, is a rectangle flanked by short Gaussian wings. The width at half-intensity is 0.32 A in the first order. A good approximation is a rectangular line with this width. However, the actual spectrograph could not have produced a monochromatic image with a rectangular profile as wide as this, since some resolved lines of the band—for instance, $R(27)$ and $R(28)$—are separated by very little more, i.e., 0.35 A. Computation shows that a slit integrating over the theoretical profile would not have resolved these lines. In the observed profile, lines near the λ 7054 head cease to be resolved at about $R(25)$. The separation of $R(24)$ and $R(25)$ is 0.24 A. Accordingly, the approxima-

[11] *Zs. f. Phys.*, **33**, 803, 1925.

[12] *Zs. f. Phys.*, **65**, 547, 1930; see also A. Unsöld, *Physik der Sternatmosphären* (Berlin: J. Springer, 1938), p. 210.

tion is made that the monochromatic image has a rectangular profile with a total width of 0.24 A.

The method of correcting for the slit broadening is to assume temporarily that the observed profile of Figure 1 is the true profile and to apply the slit broadening to it. The differences between the broadened and unbroadened lines are then applied with opposite sign to the true profile. This approximate method of proceeding can be checked by applying the slit broadening to the final true profile and comparing with the observations. At very few wave lengths are the differences (O−C) greater than 1 per cent. The profiles in all figures in this paper, with the exception of Figure 1, are corrected in this way.

According to Greenstein,[13] while scattered light is troublesome in the ultraviolet region of the coudé spectrograph, at the wave lengths employed in this study the effect of scattered light can be neglected.

b) FIRST APPROXIMATIONS TO THE DOPPLER WIDTH AND DAMPING CONSTANT

First approximations to the Doppler width and damping constant may be made by attempting to reproduce theoretically the profiles of the strong, fairly well-resolved lines near the λ 7088 head. The strong line at λ 7081.4 is the most favorable feature for this purpose. It is formed by a blend of $Q(38)$, $R(58)$, and $P(25)$. The last of these lines has its center at λ 7081.3. At the color temperature of the star, 2850° K,[14] the line $Q(38)$ is twice as intense as $R(58)$ and almost four times as intense as $P(25)$. Thus the fact that $P(25)$ has its center displaced 0.1 A to shorter wave lengths may modify the short-wavelength half of the contour of the blend but would have less influence on the long-wavelength half. Thus, to a first approximation, the half of the contour of the blend to long wave lengths, from the center of the blend, can be assumed to have the same shape as an unblended line.

It can be seen in Figure 1 that the wing of the λ 7081.4 line is blended with the wing of the strong feature at λ 7082.6. Since the two strong features have very close to the same central absorption, the assumption is made that, at the intermediate wave length λ 7082.0, half the observed absorption is produced by each of the neighboring lines. The method of van de Hulst and Reesinck[15] is then used to derive the Voigt profile best reproducing the observed profile. Figure 2 presents the observed curve and the Voigt profile. It can be seen that it is necessary to introduce a wide wing on the Voigt profile in order to reproduce the absorption at λ 7082.0, at a distance of 0.6 A from the line center. It should be pointed out that the observed curve in Figure 2 is based upon the location of the continuum assumed in Figure 1. If later study indicates that the continuum requires modification, then the observed curve in Figure 2 would also be modified.

The Voigt curve is used, together with equation (1), to find the effective optical thickness, $N_P^X \cdot a_\lambda$, at various points in the line. Since the limiting depth, R_C, is still unknown, five values are assumed, namely, $R_C = 0.6, 0.7, 0.8, 0.9$, and 1.0, and the reductions are carried out for each value. The optical thickness at various points in the profile may be expressed in terms of the thickness at the line center, resulting in the ratios a_λ / a_c. These ratios are plotted in Figure 3, where the unit of distance from the line center, $\Delta\lambda_{1/2}$, is the distance at which the ratio is $\frac{1}{2}$. It can be seen that varying R_C does not noticeably affect the shapes of these curves. The magnitude of $\Delta\lambda_{1/2}$ will, of course, depend upon R_C. The actual dependence is presented in the first part of Table 3.

The observed relative absorption coefficients in Figure 3 can be compared with profiles obtained from the tabulated values of a_λ / a_0 computed by Hjerting[10] and by Born.[9] For a given damping coefficient, a, the tabulated ratios a_λ / a_0 may be expressed in terms of the ratio at the line center, resulting again in the ratios a_λ / a_c. If the unit of distance

[13] Private communication.

[14] See Russell, Dugan, and Stewart, *Astronomy* (Boston: Ginn & Co., 1938), p. 737.

[15] *Ap. J.*, **106**, 121, 1947.

from the line center is taken to be $v_{1/2}$, which is that value of v for which the relative absorption coefficient is half the central value, then these profiles can be plotted on the same diagram as the observed profiles, i.e., Figure 3. The dependence of $v_{1/2}$ upon a is shown in the second part of Table 3. Since $v_{1/2}$ has the same significance as $\Delta\lambda_{1/2}$, the two sets of data in Table 3 make it possible to find, for each a and R_C, the Doppler

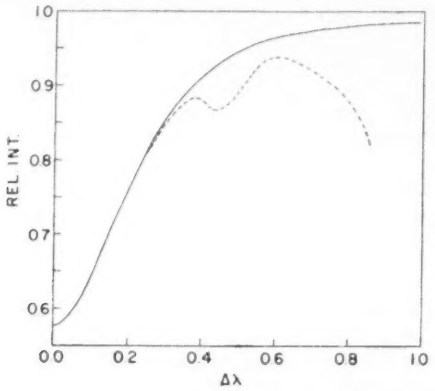

FIG. 2.—*Dotted line:* The long-wave-length half of the absorption profile of the λ 7081.4 line. *Solid line:* The Voigt profile.

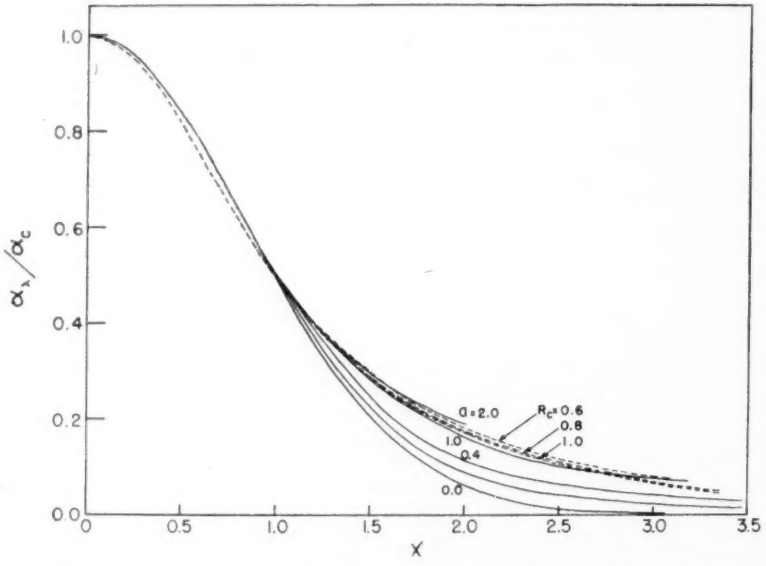

FIG. 3.—Relative absorption coefficients as functions of distance from the line center. Unit of x is the distance from the line center at which absorption coefficient is half the value at the line center. *Solid lines:* Computed on basis of tables of Born and Hjerting, for various values of a. *Dashed lines:* Observed curves from the λ 7081.4 line, for various values of R_C.

width $\Delta\lambda_D$, which would reproduce the observed width of the line. The results are represented in Figure 4, in which $\Delta\lambda_D$ is plotted as a function of R_C, assuming a series of values of a.

In Figure 3 it can be seen that a must be of the order of 1.0, so that the observed absorption-coefficient profile will be followed, even approximately. If $a = 1.0$ is assumed as the first approximation, then, according to Figure 4, the Doppler width varies from 0.09 A for $R_C = 0.6$, to 0.12 A for $R_C = 1.0$. Since R_C is still unknown, the temporary assumption is made that $\Delta\lambda_D = 0.11$ A, its value for $R_C = 0.8$. A later, more accurate, determination of R_C will make it possible to be more specific concerning the value of $\Delta\lambda_D$.

TABLE 3

DISTANCES FROM LINE CENTERS AT WHICH ABSORPTION COEFFICIENT IS HALF THE CENTRAL VALUE

FROM OBSERVED PROFILE OF 7081.4 LINE		FROM TABLES OF BORN AND HJERTING	
R_C	$\Delta\lambda_{1/2}$	a	$v_{1/2}$
0.6	0.129 A	0.0	0.835
0.7	.150	0.2	0.947
0.8	.162	0.4	1.060
0.9	.171	0.5	1.137
1.0	0.176	1.0	1.456
		2.0	2.294

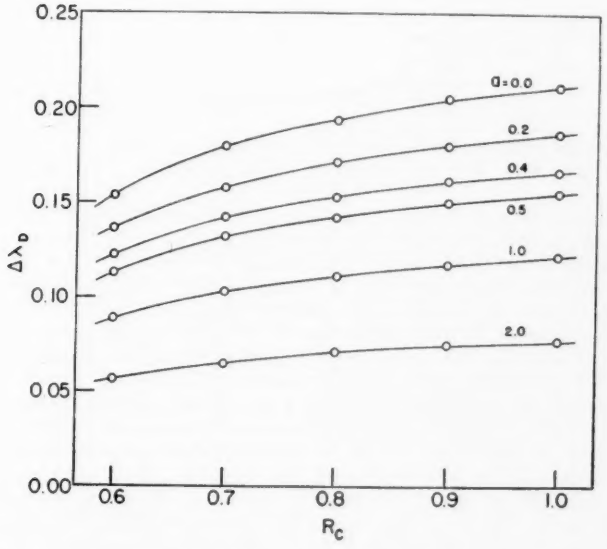

Fig. 4.—The Doppler width, $\Delta\lambda_D$, as a function of R_C, for various values of a

c) THE TEMPERATURE

In the wave-length interval between λ 7074.5 and λ 7077.5, the lines of the Q branch fall between the blended lines of the P and R branches, and, according to the profile in Figure 1, the central intensities of the Q lines are approximately the same as the central intensities of the intervening blends. If one selects for study the $Q(33)$ line at λ 7075.9 and the blend of the $R(54)$ and $P(21)$ lines at λ 7076.5, it is possible to compute the manner in which the relative intensities of the two features change with temperature. To do this, it is necessary merely to compare the terms $\Sigma S_{J''}^{N} H(a, v) \exp -[BJ''(J''+1)hc/kT]$ at the centers of the two lines, using the values of a and $\Delta\lambda_D$ obtained in the previous section. The ratio of the terms obtained for the two lines is presented in Figure 5 as a function of the temperature. According to the figure, the equality of central intensity mentioned above will be achieved at two temperatures, namely, 340° K and

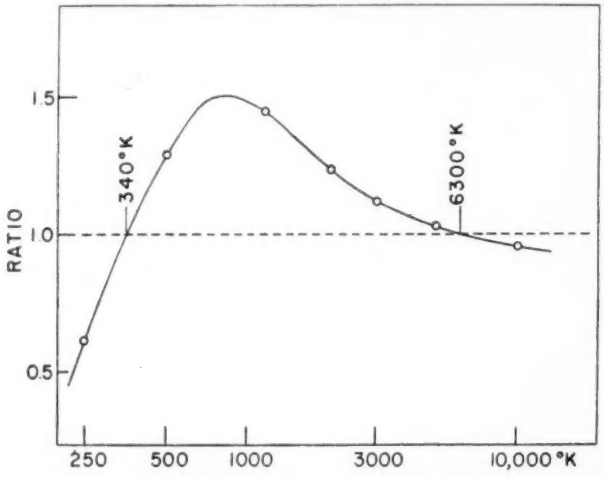

FIG. 5.—The ratio of the optical thickness at the center of the λ 7075.9 [$Q(33)$] line to the optical thickness at the center of the λ 7076.5 line [$R(54) + P(21)$], as a function of the temperature.

6300° K. The reason why there are two possible temperatures is that at low temperatures the $P(21)$ component of the blend becomes as intense as the $Q(33)$ line, whereas at high temperatures the $R(54)$ line becomes predominant.

The low temperature can be eliminated from further consideration, because further test shows that it does not reproduce the relative intensities of features in other spectral regions. On the other hand, a temperature of 6300° K is surprisingly high, in view of the color temperature of the star, namely, 2850° K. The discrepancy arises when it is assumed that the two features in the spectrum have equal intensity. However, this may not be strictly the case. In Figure 1 it can be seen that the resolved features in the interval between λ 7074 and λ 7078 have an unsystematic difference in central intensity of at least 3 per cent, which can be taken as a measure of the accuracy of the photometry. It will be shown later that the temperature may be as low as the color temperature without producing a difference in the absorption in the two lines greater than 3 per cent. Thus all that can be said about the temperature from the relative intensities of the two lines is that it is of the order of 6300° K, but may be as low as, say, 3000° K. Closer approximations can be made by comparing the relative absorptions at widely separated

points in the spectrum, but this requires accurate knowledge of the location of the continuum, so that such closer approximations are deferred until later. Since a temperature of 3000° K is within the accuracy of this initial determination and is also compatible with the color of the star, it has been assumed as the first approximation.

d) THE DETERMINATION OF R_C

According to Figure 1, the strong absorption at the λ 7054 head is produced by a blending of lines which are closely spaced relative to their individual widths. Therefore, the slope of the absorption profile between λ 7054 and about λ 7057 is, to a first approxi-

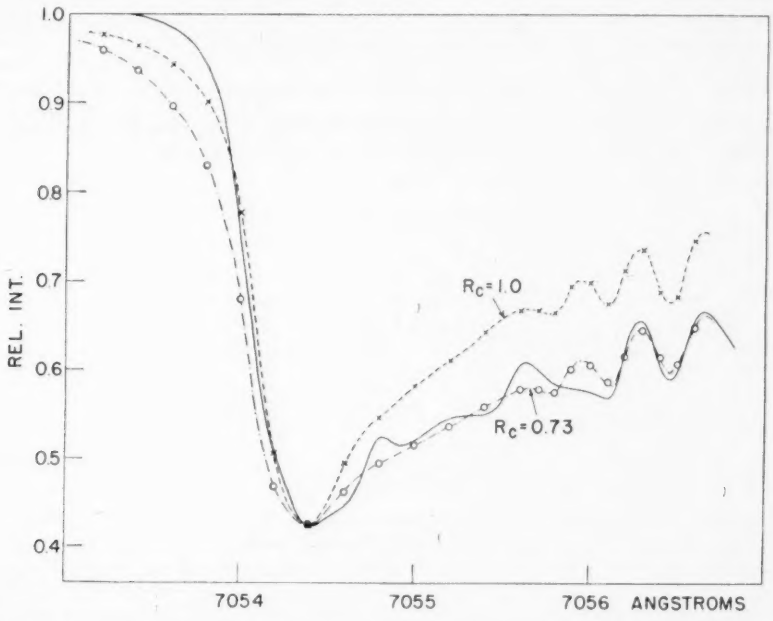

FIG. 6.—Absorption profiles at the λ 7054 head. *Solid line:* Observed profile. *Dashed lines:* Computed profiles, assuming $R_C = 0.73$ and $R_C = 1.0$.

mation, independent of the line profiles. Calculation shows that it is also not strongly a function of the temperature. This is because, at each point in the region between the head and the origin, the absorption is produced by a blend of lines of low and high J value. To a first approximation, therefore, the effect of changing the temperature, i.e., of changing the relative intensities of lines of high J and lines of low J, has little effect in the relative absorptions at various wave lengths in this region. Thus the observed mean slope of the profile between λ 7054 and λ 7057 is predominantly a function of: (1) the increasing separation of the lines; (2) R_C; and (3) the assumed location of the continuum. Figure 6 presents the observed absorption-curve in this interval, after correcting for the slit according to the method described above. The computed profiles for $R_C = 1.0$ and $R_C = 0.73$ are also included in Figure 4. In computing the profiles, the results of the previous sections have been adopted, namely, that $a = 1.0$ and $\Delta\lambda_D = 0.11$ A. A temperature of 3000° K has been assumed. In each case the constant K has been adjusted so that the observed absorption at λ 7054.4 is reproduced. It is obvious that $R_C = 1.0$

gives too steep a slope but that the general slope is reproduced if R_C is assumed to be equal to 0.73.

This value of R_C is somewhat lower than the value assumed above ($R_C = 0.8$) in approximating a and $\Delta\lambda_D$ from the profile of the λ 7081.4 line. According to Figure 4, the effect would be to reduce $\Delta\lambda_D$ to about 0.105 A. Since $\Delta\lambda_D$ is also dependent upon the adopted value of a, which is itself uncertain, the second and third decimal places in this determination of $\Delta\lambda_D$ have no significance. Therefore, the value $\Delta\lambda_D = 0.1$ A has been adopted in later calculations.

It will be noticed in Figure 6 that, while the computed profile for $R_C = 0.73$ reproduces quite well the observed profile to longer wave lengths from the band head, it predicts too much absorption to shorter wave lengths. This discrepancy will be discussed below in connection with the true location of the continuum.

c) ISOTOPES OF TITANIUM AND OXYGEN

Three stable isotopes of oxygen and five stable isotopes of titanium are known to exist. The masses and terrestrial abundance ratios are listed in Table 4.

TABLE 4

ISOTOPES OF OXYGEN AND TITANIUM

Isotope	Per Cent Abundances	Reference*	Isotope	Per Cent Abundances	Reference*
O^{16}	99.76	Smythe, *Phys. Rev.*, **45**, 299, 1934	Ti^{46}	7.95	Nier, *Phys. Rev.*, **53**, 282, 1938
			Ti^{47}	7.75	
O^{17}	0.041	Murphey, *Phys. Rev.*, **59**, 320, 1941	Ti^{48}	73.45	
			Ti^{49}	5.51	
O^{18}	0.20	Smythe, *Phys. Rev.*, **45**, 299, 1934	Ti^{50}	5.34	

* General reference: Glenn T. Seaborg, *Rev. Mod. Phys.*, **16**, 1, 1944.

The spectral region under investigation in this study is part of the (0–0) band. Hence vibrational isotopic shifts would not be large enough to resolve the lines pertaining to the different isotopes. There is thus no possibility of being able to detect any difference between the stellar and the terrestrial isotopic abundance ratios. It is of interest, however, to determine whether the small isotopic shifts which do occur would be sufficient to affect appreciably the profiles of the rotational features, assuming the isotopic abundance ratio to be the same as on the earth. According to Table 4, it is necessary only to consider the various isotopes of titanium, the relative abundances of O^{17} and O^{18} being too low.

In order to compute the isotope shift, it is necessary to take into account the effect that a change in the atomic weight of the titanium atom has on (1) the vibrational energy, (2) the spin splitting, and (3) the rotational energy. If the shifts of lines of the $Ti^{47}O^{16}$ molecule, relative to corresponding lines of the $Ti^{48}O^{16}$ molecule, are taken as examples, it is found (1) that the vibrational splitting produces a shift of all lines of +0.10 A, i.e., to longer wave lengths; (2) that the spin splitting introduces a shift of all lines of −0.18 A; and (3) that the rotational isotopic shift varies linearly, from −0.02 A at λ 7054 to +0.16 A at λ 7088. The combined result is: (*a*) a shift of lines pertaining to the lighter isotope of −0.10 A at λ 7054; (*b*) a zero shift at about λ 7074; and (*c*) a shift of +0.08 A at λ 7088.

The resulting effects on the line profiles, taking all five isotopes of titanium into account, are small relative to the uncertainties introduced by the approximate nature of both the photometry and the stellar model upon which the computed profiles are based.

Hence the effects of isotopes may be neglected at the present preliminary state of the problem. However, when more exact analyses are made, the isotope effects will have to be taken into account, even in the case of the (0–0) bands of this molecule.

D. THE INTENSITY OF THE CONTINUUM

In the first approximation it has been assumed (1) that the continuum has an intensity corresponding to the observed intensity to the violet of the λ 7054 head and (2) that the intensity of the continuum is constant throughout the interval λλ 7054–7088. Both these assumptions can be checked as follows:

1. As is pointed out in the previous section, a discrepancy is found between the computed and the observed profiles in the violet wing of the λ 7054 head. The observed profile shows a maximum intensity at λ 7053.3. It has been assumed that this corresponds to zero absorption. At this same wave length the approximate parameters lead to 5 per cent absorption. In order to make the computed and observed profiles agree, it is found that it would be necessary to assume that the lines near the head have widths corresponding to the parameters $a = 0.06$ and $\Delta\lambda_D = 0.2$ A. There is no obvious way in which this change of parameters could be justified. It is much more probable that the true continuum is not reached at λ 7053.3 and that 5 per cent absorption should be introduced at that wave length. This probability is strengthened somewhat by the presence of a strong atomic line of cobalt at λ 7052.9, which may mask the extremity of the wing at the band head. Accordingly, it seems reasonable to increase the intensity of the true continuum at λ 7053.3 by an amount sufficient to produce 5 per cent absorption at that wave length and to recompute the absorptions in the neighborhood of the λ 7054 head. No appreciable error would be made if it were assumed that the intensity of the continuum is constant over the very short interval from λ 7053.3 to λ 7056.6. It is found that, by adjusting the intensity of the continuum, the minimum intensity of the head is reduced from 42.5 to 40.5 per cent. The slope of the profile from λ 7054.5 to λ 7056.6 is also changed, but by such a slight amount that no change is required in the value of R_C as determined above.

2. The constancy of the intensity of the continuum throughout the band can be checked by comparing the absorptions at the λ 7054 and λ 7088 heads, using the parameters found in the first approximation. In computing the absorption at λ 7088, it is necessary to include contributions from blended lines of high J belonging to the first subband. The intensity factors $S_{J'}^{J''}$ for lines of the second subband ($A^3\Delta_2 - X^3\Pi_1$) can be found from equations (2) with $\Omega = 2$. The result of the computation is that the intensity at the minimum of the λ 7088 head should be 37.5 per cent of that of the continuum at that wave length. In order to reproduce the observed relative intensities at the two heads on the plate, the intensity of the continuum would have to increase by 9.8 per cent in the interval from 7053 A to 7088 A. An increase is actually to be expected, since a black body at a temperature of 3000° K has an intensity maximum at λ 9613; furthermore, an N-type photographic emulsion exhibits a marked sensitivity increase with increasing wave length in this interval, according to the spectral sensitivity-curves published by the Eastman Kodak Company.

A second approximation to the absorption profile can thus be made by adopting these relative intensities of the continuum at the two heads and interpolating linearly for intermediate wave lengths. The stellar absorption curves in Figures 7 and 8 were derived in this way.

E. THE SECOND APPROXIMATIONS

Closer approximations to the parameters can be found by computing absorption profiles based on the numerical values of the parameters found in the first approximations and by comparing the computed profiles with the stellar absorptions based on the improved location of the continuum. Adjustments, if necessary, can then be made to the

parameters, until the differences between the observed and the computed profiles are as small as possible. Since computations covering the entire band would be time-consuming, the computations and comparisons are limited to four sections of the band covering the most important features. They are shown in Figures 7 and 8.

Successive tests indicate that the accuracy of the photometry does not justify any further adjustment in the parameters a, $\Delta\lambda_D$, or R_e. It is possible, however, to be somewhat more specific concerning the temperature. The situation is illustrated in Figure 9. There are, in general, two conditions which must be satisfied by the temperature. The

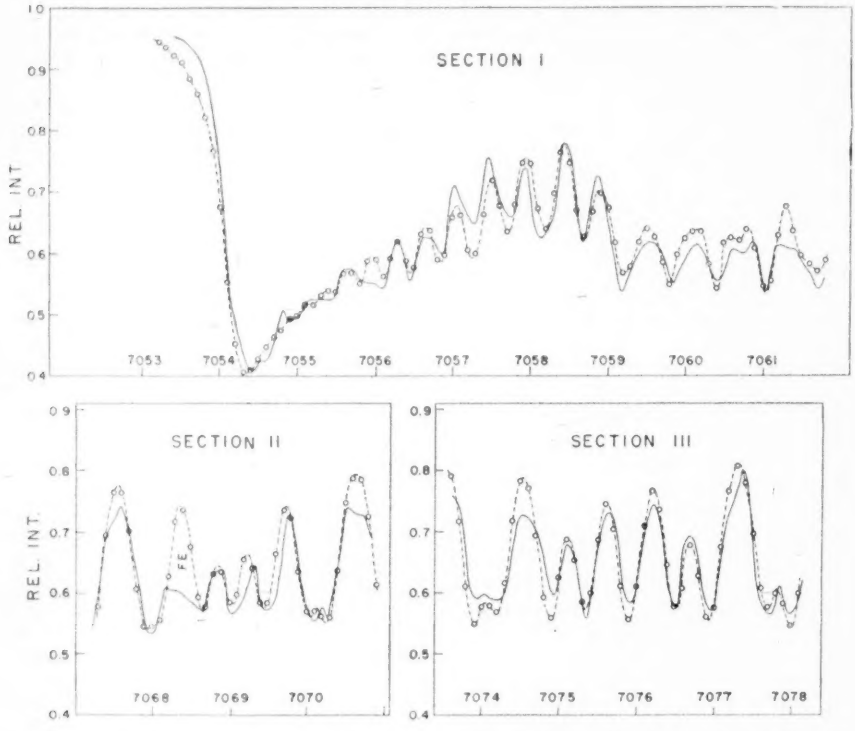

FIG. 7.—Comparison between the observed and computed profiles. *Solid lines:* Observed absorption profile. *Dashed lines:* Computed profile. Open circles are computed points.

first is that the relative intensities of the resolved features in the interval λλ 7074–7078 be reproduced and the second that the average relative intensities at widely separated points in the band be reproduced. The first condition was discussed in connection with the first approximation to the temperature. The resolved lines in this section of the spectrum show an unsystematic variation of intensity about a relative intensity of 58.0 per cent. In Figure 9 the data, resulting in Figure 5, have been used to compute the absorptions at λ 7075.9 [$Q(33)$] and at λ 7076.5 [$R(54)$ plus $P(21)$]. At each temperature the constant K has been adjusted so that the mean of the central intensities of the two lines is 58.0 per cent. As was pointed out earlier, the two lines have equal central intensity at 6300° K. However, it was also pointed out that the observed relative intensities of the lines in this region differ in such an unsystematic fashion that any insistence upon exactly equal intensities at λ 7075.9 and λ 7076.5 has little justification. A difference of as

much as 3 per cent in the intensities at these two wave lengths would be within the apparent accuracy of the photometry.

The effect of the second condition on the temperature may be illustrated by computing the absorption at λ 7055.8. This representative point is near the band head and has an observed relative intensity of 55.5 per cent, which does not differ appreciably from the intensities of the two lines discussed above, so that the effect of an error in R_c is reduced. When the same K-values at each temperature are used, the third curve in Figure 9 results. The observed and computed intensities agree for a temperature of 2600° K, which is much lower than the temperature required to fulfil the first requirement. No single temperature, therefore, leads to agreement with observation at all wave lengths. However, a temperature of 3000° K leads to absorptions, in the case of these

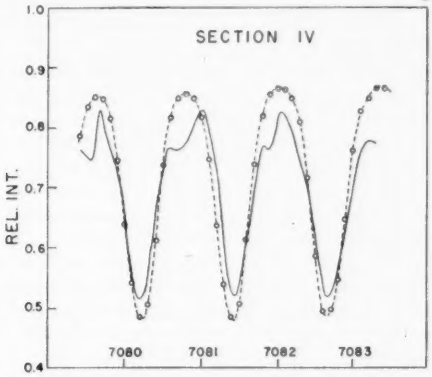

FIG. 8.—Comparison between the observed and computed profiles. *Solid line:* Observed absorption profile. *Dashed line:* Computed profile. Open circles are computed points.

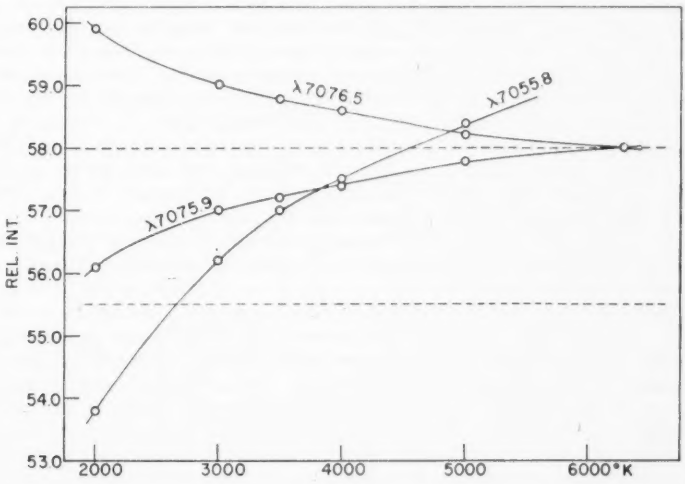

FIG. 9.—Computed relative intensities in per cent units at three different wave lengths as functions of the temperature. Lower dashed line is the observed relative intensity at λ 7055.8 (55.5 per cent). Upper dashed line is the mean observed relative intensity at the centers of features in the interval λλ 7074–7077 (58.0 per cent).

three lines, each of which is approximately 1 per cent in error—well within the accuracy of the photometry.

Similar tests at various points in the band lead to the conclusion that a temperature of 3000° K results in a profile fitting the observations as well as possible. A temperature lower than 2500° K produces systematic errors in the central intensities of lines of the Q branch relative to the central intensities of the blends of lines of the R and P branches, while temperatures above 4000° K lead to profiles which fail to reproduce the observed relative intensities at widely different wave lengths.

It is disappointing that the temperature cannot be determined more accurately than this. The failure results principally from the unfortunate circumstance that, in this particular band, the component lines of the P and R branches coincide exactly.

The parameters that are finally adopted are, accordingly, the following: $T = 3000°$ K, $\Delta\lambda_D = 0.1$ A, $a = 1$, $R_C = 0.73$, and $K = 0.0477$. The corresponding profile is shown in Figures 7 and 8 as a dotted line.

In general, the agreement between the theoretical and the observed profiles is fairly good. It is probable that the agreement could still be improved by further adjustment of the parameters. For instance, the computed absorption between the strong features is too low. This suggests that the numerical value of the parameter a should be increased. However, this introduces a difficulty at the band head, since an increase in a would increase the discrepancy already found between the two profiles. It might be argued that the observed absorption at the band head could be increased, to remove this discrepancy, by increasing the intensity of the continuum still further. This, however, would increase the absorption at all wave lengths. A very great increase in a and in the intensity of the continuum would be required in order to produce the desired agreement, and a is already so large that it is difficult to interpret it in terms of the physical conditions in the stellar atmosphere. The corresponding effective damping constant is 0.1 A, which is very large when compared with the damping constants usually found in the atmospheres of supergiant stars, which are not greatly different from the natural damping constant, i.e., of the order of 10^{-4} A.

There is another possible explanation for the large absorption found between the strong lines. It will be noticed that the profile suggests that each strong line is accompanied by a weaker line 0.4 A to longer wave lengths. These weaker lines are not so prominent in Figure 1, and they are not at all conspicuous on the original tracing, so that they may be spurious, resulting from the attempt to correct for slit-broadening. If, however, further observation shows that they actually exist, the regularity of their spacing almost certainly indicates that they are *TiO* lines, resulting from absorptions by molecules in a region in the atmosphere of the star with a motion in the line of sight relative to the region producing the principal absorptions. Any attempt to improve the agreement between the theoretical and observed profile should be deferred until the presence or absence of these weak lines has been definitely proved.

A Doppler width of 0.1 A is large when compared with the thermal Doppler width of 0.02 A. However, the observed width may be explained by assuming either a turbulent velocity in the stellar atmosphere of 4.3 km/sec or a rotation of the star.

The great uncertainties in the parameters and the approximate nature of the theory upon which they are based make it inadvisable at the present time to interpret them in terms of the physical conditions in the stellar atmosphere. They should rather be regarded as a preliminary set of constants, which, when introduced into equation (3), produce a profile which agrees with observation in the manner shown in Figures 7 and 8. Similar studies of additional *TiO* bands in the spectrum of the star and more exact theoretical discussions will be required before parameters will be found which can be used with confidence in the study of the structure of the stellar atmosphere.

The author is indebted to Dr. Louis Henyey and to Dr. Otto Struve for many valuable suggestions made during the course of this investigation.

HYPERFINE STRUCTURE IN THE SOLAR SPECTRUM

ARTHUR ABT
MOUNT WILSON AND PALOMAR OBSERVATORIES
CARNEGIE INSTITUTION OF WASHINGTON
CALIFORNIA INSTITUTE OF TECHNOLOGY
Received September 28, 1951

ABSTRACT

The hyperfine structure of certain lines can be detected in the solar spectrum as reproduced in the Utrecht atlas; it can contribute appreciably to the width of the lines. The agreement between the predicted and observed half-widths and profiles of lines with hyperfine structure broadening is good. Solar lines with wide hyperfine structure patterns show a wave-length shift toward the weak end of the pattern as compared to the laboratory wave length. Hyperfine broadened lines fall on a different curve of growth, characterized by a larger Doppler velocity and a smaller damping constant. A résumé of the elements most affected by hyperfine broadening is given.

Hyperfine structure (hfs) is a splitting of certain atomic spectral lines due to the effect of nuclear spin on the energy levels of the orbital electrons. The separation and intensities of the components of these lines do not depend on any physical conditions, such as temperature, pressure, or external magnetic field. The total separation of the components of a line is small, usually less than 0.1 A, and the individual components can usually be resolved only with high-resolution laboratory apparatus. The components of a line often form a flag pattern in which the intensities of the components drop off longward or shortward. Relative separations and relative intensities of the components can be predicted from Russell-Saunders or *jj*-coupling, but the total width of the component pattern cannot readily be calculated. For the total widths we must depend on laboratory measurements, of which only a relatively small number is available. For most elements the hfs patterns of only about a dozen lines have been investigated—only enough to determine the nuclear spin of the isotope.

The isotope effect also causes a splitting of some spectral lines, with a total separation of the components of the same order of magnitude as for hfs, and can therefore also be treated here. The lines affected are often different ones. In an isotopic splitting there is one component for each isotope; the relative intensities of the components are proportional to the relative abundances of the isotopes.

We will (1) show that hfs can be detected in the solar spectrum as reproduced, for instance, in the intensity tracings of the Utrecht atlas, (2) investigate the effect of hfs on line widths, (3) list the elements most affected by hfs and isotope effect, (4) show that systematic wave-length differences can occur for hyperfine broadened lines between solar and laboratory sources, and (5) investigate the effect of hfs on curves of growth. That hfs can be detected in the solar spectrum was suggested by E. McMillan,[1] who found that certain lines with wide hfs patterns are also wide in the solar spectrum.

To verify that hfs can be detected and that it does contribute to the width of a solar line, the profile of λ 5516.8 *Mn* I was computed and compared with the observed one. This line is observed to be nearly twice as wide as most lines in the solar spectrum; its hfs pattern as determined in the laboratory[2] is given in Figure 1. First the line-absorption coefficient of each component of the pattern was calculated for a solar turbulent velocity of 1.7 km/sec, a kinetic temperature of 5700°, and a damping constant ten times the

[1] *Phys. Rev.*, **45**, 134, 1934.

[2] R. A. Fisher and E. R. Peck, *Phys. Rev.*, **55**, 270, 1939.

classical value. The line-absorption coefficients of the individual components were added to give the line-absorption coefficient of the whole pattern. Then, to predict the absorption profile of the line, a Milne-Eddington model atmosphere was used; it was assumed that the excitation temperature was 5200° and that the line was formed by pure scattering. Finally, I included the effect of instrumental broadening of the line, using the instrumental profile for the Utrecht atlas as determined by H. C. van de Hulst and J. J. M. Reesinck.[3] The predicted line profile was first replaced by 18 rectangles, each 0.015 A wide. Next each rectangle was replaced by the instrumental profile, and the 18 profiles were added. The final profile is given as the dashed line in Figure 2, along with the observed profile from the Utrecht atlas. The agreement is fairly good, indicating that

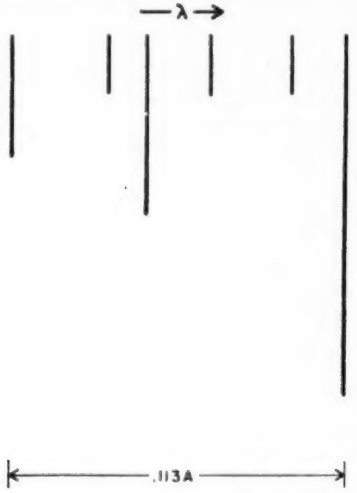

FIG. 1.—The laboratory hyperfine structure pattern of λ 5516.8 *Mn* I. The length of each line represents the intensity of the component.

the abnormal width of λ 5516.8 *Mn* I in the solar spectrum has been explained by the presence of hfs.

Next the predicted and observed half-widths were compared for two dozen unblended solar lines with known wide laboratory hfs patterns. Since most of these hfs patterns are flag patterns in which the last one or two components are too weak to contribute to the width of the total pattern at half-intensity, it was decided to use only three-fourths of the width of the hfs pattern in predicting half-widths. The calculated half-width was predicted by

$$\Delta\lambda = \sqrt{[(\Delta\lambda_D + \tfrac{3}{4}\Delta\lambda_H)^2 + (\Delta\lambda_I)^2]}, \qquad (1)$$

where $\Delta\lambda_D$ is the total Doppler half-width, $\Delta\lambda_H$ is the total width of the hfs pattern, and $\Delta\lambda_I\,(\mathrm{A}) = 8.42 \times 10^{-6}\,\lambda$ is the total half-width of the instrumental profile. The hfs patterns for the *Mn* I, *Co* I, *V* I, and *Cu* I lines used were determined by R. A. Fisher and E. R. Peck,[2] E. Rasmussen,[4] and K. R. More,[5] H. Kopfermann and E. Rasmussen,[6] and H. Schüler and Th. Schmidt,[7] respectively. Table 1 gives the data. In Figure 3, which

[3] *B.A.N.*, **10**, 79, 1946.
[4] *Zs. f. Phys.*, **102**, 229, 1936.
[5] *Phys. Rev.*, **46**, 470, 1934.
[6] *Zs. f. Phys.*, **98**, 624, 1936.
[7] *Zs. f. Phys.*, **100**, 113, 1936.

shows the correlation of predicted and observed half-widths, the horizontal dashed line represents the average width of lines of comparable equivalent width which are not broadened by hfs. All the lines plotted are abnormally broad, and the clustering near the 45° diagonal shows that the observed half-widths of these lines are due, in part, to the presence of hfs. The scatter is attributed to the use of the arbitrary factor $\frac{3}{4}$, a factor which should actually be different for each differently shaped pattern. Note that a line

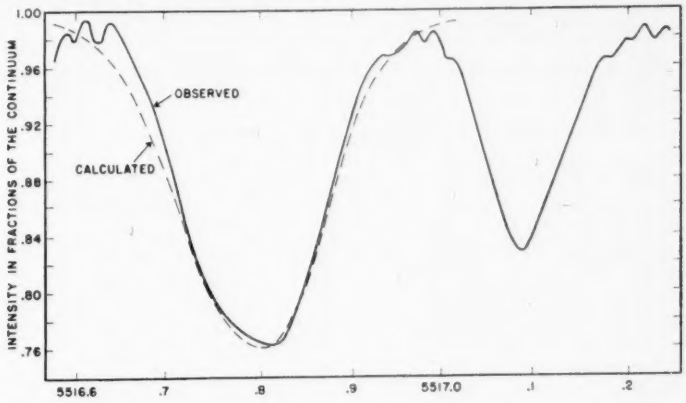

FIG. 2.—The computed and observed profiles for λ 5516.8 *Mn* I. The observed profile on the right is that of an unbroadened *Fe* I line.

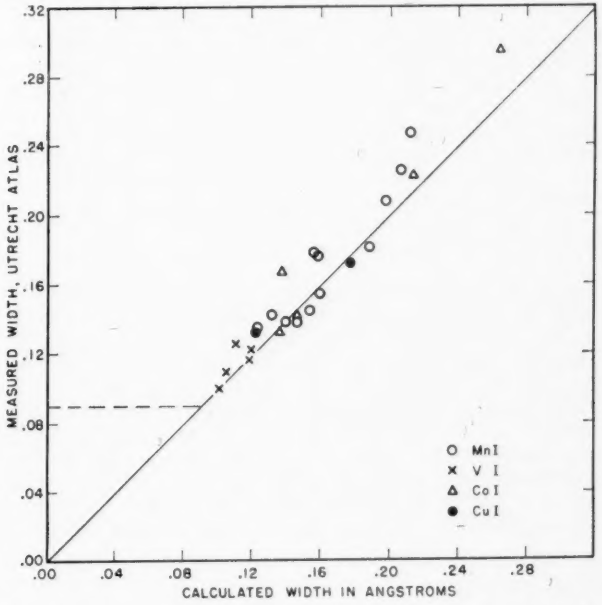

FIG. 3.—The correlation of predicted and measured half-widths for lines with wide hfs patterns

like λ 5516.8 *Mn* I (measured half-width of 0.179 A) would give a solar turbulent velocity of 5.5 km/sec or a temperature of 96,000° if the effect of hyperfine broadening were not considered.

An attempt was made to improve on the profiles and resolution of the Utrecht atlas tracings by taking plates in the third and fourth orders of the Michelson grating in the 150-foot tower spectrograph on Mount Wilson. It was found that the instrumental profile was 0.02 A narrower than for the Utrecht atlas but that no appreciable increase in structural detail was observed in the lines. It was then decided to base this work on Utrecht atlas profiles.

Not all spectral lines are affected by hfs, but only those involving penetrating electron

TABLE 1

PREDICTED AND OBSERVED HALF-WIDTHS

Element	λ (A)	$\Delta\lambda_H$ (A)	Predicted Δλ (A)	Observed Δλ (A)
Mn I	4061.7	0.107	0.133	0.142
	5341.1	.193	.213	.248
	5377.6	.066	.122	.135
	5394.7	.119	.160	.154
	5399.5	.100	.146	.139
	5407.4	.182	.206	.227
	5413.7	.110	.154	.146
	5420.4	.173	.199	.209
	5432.6	.091	.140	.139
	5470.7	.155	.187	.181
	5516.7	.113	.157	.179
	5537.8	.115	.159	.177
V I	4586.4	.054	.103	.105
	4594.1	.076	.119	.117
	4851.5	.059	.110	.127
	4875.5	.043	.100	.100
	4881.5	.071	.120	.122
Co I	4190.7	.110	.136	.133
	4530.9	.116	.146	.143
	4749.7	.102	.138	.168
	6082.4	.181	.214	.222
	6450.2	.242	.263	.295
Cu I	5105.5	.074	.121	.133
	5782.1	0.140	0.178	0.173

orbits of atoms with a large nuclear spin. Some of the lines of *V*, *Mn*, *Co*, *Cu*, and probably of *Sc* and *La* show wide hfs patterns; some lines of *Na* and *Al* have a small, but possibly detectable, amount of hfs broadening. Some of the lines of *Mg*, *Zn*, *Ti*, and *Ni* may have a detectable amount of broadening due to isotope effect; the isotope effect in solar lines of the elements *H* through *B* has been, or is being, studied.[8] Lines of *Si*, *Ca*, *Cr*, and *Fe* should show no hfs or isotope-effect broadening. Data on laboratory measurements of hfs patterns can be obtained from the bibliography by W. F. Meggers.[9]

The suggestion has often been made[10] that the abnormally large widths of *V* and *Mn* lines in the solar spectrum are due to hfs. This is probably true. Unfortunately, the hfs patterns of only 16 *V* and 26 *Mn* lines have been determined. Of these, only 5 *V* and 12 *Mn* lines are unblended in the solar spectrum and are wide enough to show a de-

[8] See, e.g., J. L. Greenstein, *Ap. J.*, **113**, 531, 536, 1951.

[9] *J. Opt. Soc. Amer.*, **36**, 431, 1946.

[10] E.g., Barbara Bell, thesis, Radcliffe College, 1951.

tectable amount of broadening, namely, an hfs pattern width of at least 0.04 A. The abnormal widths of those 17 lines are well explained by the presence of hfs (Fig. 2), but the percentage of all *V* and *Mn* lines that are broadened by hfs is not known.

It was decided to investigate the possibility of a systematic difference in wave length of hyperfine broadened lines between solar and laboratory sources. It was expected that, since saturation would first affect the strong end of the hfs flag patterns, the line profile might be so changed as to shift the center of the line, as measured at half-intensity, in the direction of the weak end of the pattern. This was first tested by computing the laboratory emission-line profile of λ 5516.8 *Mn* I for a temperature of 5500° and the same instrumental profile as for the Utrecht atlas and by comparing it with the computed solar absorption-line profile. A shift of 0.0011 A in the expected direction was found. The size of the shift should depend strongly on the intensity gradient of the components of the flag pattern, on the total width of the pattern, and on the strength and saturation of the absorption line.

A second test is a comparison of the solar and laboratory wave lengths of a number of lines. Of the 24 unblended solar lines with wide hfs patterns listed in Table 1, 9 are listed as double lines[11] in the *Revised Rowland Catalogue* and cannot be used for this purpose. The remaining 15 lines were divided into two groups: those with flag patterns degraded shortward and those degraded longward. These groups should show the solar lines shifted shortward and longward, respectively. For laboratory and solar wave lengths Miss Moore's *Revised Multiplet Table* and the *Revised Rowland Catalogue*, respectively, were used. Before the laboratory and solar wave lengths could be compared, it was necessary to correct for a systematic difference between these two catalogues. Using 55 standard iron lines, it was found that the solar wave lengths are larger by 0.0064 A, with a probable error per line of 0.0032 A. In Table 2 the solar wave lengths have been corrected by this amount. Wave-length differences for individual lines probably are not reliable, but the two average values, both of the expected sign, indicate that the shift is real.

Next the effect of hfs on curves of growth was investigated. Hyperfine-broadened lines, being shallower and broader than normal lines of the same equivalent width, will not show saturation effects so quickly. A predicted curve of growth for λ 5516.8 *Mn* I was constructed by changing the assumed absorption coefficient at the center of the line by known amounts and calculating the corresponding line profiles and equivalent widths. The curve of growth formed in this way was compared with the theoretical curves of growth given by M. H. Wrubel.[12] It was found that the calculated curve could be fitted to the theoretical curve only with a Doppler width and damping factor different from those used in calculating the line-absorption coefficients. For λ 5516.8 *Mn* I the curve of growth can be fitted only to a curve for which the Doppler velocity is 3.69 km/sec and $\log a = -3.6$, while the parameters used in constructing the line profiles were a Doppler velocity of 2.15 km/sec and $\log a = -1.8$. Obviously, the parameters derived from the curve of growth no longer have the meaning of a kinetic velocity and a relative pressure, since we are not dealing with a single sharp line but with a composite, closely spaced, unresolved line. For such a composite line, the line half-width is no longer related simply to the temperature and turbulent velocity. On the basis of this *one* example it is suggested that the Doppler velocity, ξ, necessary to make the curve of growth of a line with a wide hfs pattern fit a theoretical curve is given by

$$\xi^2 = \frac{2RT}{\mu} + \xi_t^2 + \left(\tfrac{1}{2}\Delta\lambda_H \frac{c}{\lambda}\right)^2. \qquad (2)$$

[11] For lines with wide hfs patterns the large frequency of double lines in the sun is evidence of asymmetry and internal structure.

[12] *Ap. J.*, **111**, 157, 1950.

The first two terms on the right are the temperature and turbulent-velocity part of the Doppler velocity; the last term is a correction term which depends on the width, $\Delta\lambda_H$, of the hfs pattern. The factor $\frac{1}{2}$ is approximate, in that it depends on the shape of the hfs pattern of the line. Since experimental f-values are measured from lines on the linear portion of the curve of growth, the resulting f-values of lines with wide hfs patterns should not be affected by this correction. However, an incorrect and larger solar abundance would be deduced for the line with a wide hfs pattern, if the line is put on a normal curve of growth.

TABLE 2

WAVE-LENGTH SHIFTS FOR HYPERFINE BROADENED LINES

ELEMENT	LAB. λ (A)	CORRECTED SOLAR λ (A)	DIFF. (SOLAR − LAB.) (A)
	1. Patterns Degraded Shortward		
Mn I	5341.065	.029	−0.036
	5377.628	.610	− .018
	5399.489	.473	− .016
	5413.687	.681	− .006
Co I	4190.712	.713	+ .001
	4530.949	.951	+ .002
	4749.68	.660	− .02
	6082.431	.427	− .004
Cu I	5105.541	.541	0.000
Mean			−0.011
	2. Patterns Degraded Longward		
Mn I	5432.548	.544	−0.004
V I	4586.364	.374	+ .010
	4594.103	.122	+ .019
	4851.483	.492	+ .009
	4875.462	.488	+ .026
	4881.554	.557	+0.003
Mean			+0.009

The isotope effect in certain atomic lines in the solar spectrum has already been used to determine isotopic abundances.[8] It was hoped that isotopic abundance ratios in certain elements could be determined from lines showing both a wide hfs pattern and an isotopic shift. In such a line each isotope would have a wide, asymmetric pattern, due to hfs. The patterns due to the various isotopes would be shifted with respect to one another by the isotope effect. The large width and asymmetry of the hfs pattern might cause the final profile to be sensitive to the relative abundances of the isotopes. A good test is λ 5782.1 *Cu* I, which has an isotope shift for the two isotopes (terrestrial abundance ratio $Cu^{63}/Cu^{65} = 68/32$) of 0.025 A, and each isotope has an hfs pattern width of 0.115 A. However, computed profiles for various abundance ratios are not sufficiently different to determine the solar abundance ratio. The best way to determine this ratio

would be from wave-length measurements when the absolute wave lengths of the isotopic lines are known from laboratory measurements.

It is a pleasure to express my thanks to Dr. Jesse L. Greenstein for the suggestion of looking for hfs in the solar spectrum and for helpful suggestions. I wish to thank Dr. Seth B. Nicholson for help in obtaining the solar spectrograms.

THE RADIO-FREQUENCY LINE SPECTRUM OF ATOMIC HYDROGEN AND ITS APPLICATIONS IN ASTRONOMY

J. P. WILD
Division of Radiophysics, Commonwealth Scientific and Industrial Research Organization, Australia
Received September 8, 1951

ABSTRACT

Formulae are obtained for the frequencies, transition probabilities, and natural widths of the discrete lines of atomic hydrogen that fall within the radio spectrum. Such lines are due to transitions within either the fine structure or the hyperfine structure of the energy levels.

The conditions necessary for the formation of observable emission and absorption lines are examined. Thence an inquiry is made into which of the hydrogen lines are likely to be observable from astronomical systems. It is found that the sun may give a detectable absorption line at about 10,000 Mc/sec, corresponding to the $2^2S_{1/2}-2^2P_{3/2}$ fine-structure transition, but that other solar lines are not likely to be observable. From the interstellar gas, the emission line already observed (i.e., the 1420 Mc/sec hyperfine-structure line) is probably the only detectable hydrogen line. The importance of this line in the study of the interstellar gas is discussed. Some general conclusions are drawn from the preliminary evidence regarding the motion and kinetic temperature of the regions of un-ionized hydrogen. The ratio data are used to obtain a measure of the product of "galactic thickness" and average hydrogen concentration.

I. INTRODUCTION

The first astronomical observation of a spectral line in the radio-frequency band has recently been announced by Ewen and Purcell[1] and has had independent confirmation by two other groups of workers.[2,3] The observed line is an emission line of frequency 1420 Mc/sec due to the transition between the hyperfine-structure substates in the ground state of atomic hydrogen. It is observed from the general direction of the galaxy. The likelihood that this line is detectable from the galaxy was first pointed out by van de Hulst.[4] In a subsequent discussion, Shklovsky[5] concluded that no atoms other than hydrogen are likely to produce observable lines, although certain molecules could. The possibility of observing radio-frequency lines has also been discussed briefly by Reber and Greenstein[6] and by Saha.[7] The discovery of Ewen and Purcell now arouses new interest in the subject.

The present paper has two objectives. The first is a detailed investigation of the radio-frequency line spectrum of atomic hydrogen. The second is an inquiry into which of these lines are likely to be observable from astronomical systems. Included in this part is a discussion of the 1420 Mc/sec galactic line and its importance to astronomy. The conclusions of the paper are summarized in the final section.

II. THE RADIO-FREQUENCY LINE SPECTRUM OF ATOMIC HYDROGEN

A radio-frequency spectral line originates in transitions between a pair of closely spaced energy states of an atom or molecule. In the case of atomic hydrogen sufficiently close spacing exists (1) between the main levels of high quantum number, (2) between

[1] *Nature*, **168**, 356, 1951.

[2] C. A. Muller and J. H. Oort, *Nature*, **168**, 357–358, 1951.

[3] W. N. Christiansen and J. V. Hindman, reported by J. L. Pawsey, *Nature*, **168**, 358, 1951.

[4] *Nederlandsch. Tijdschr. v. Natuurkunde*, **11**, 201, 1945.

[5] *A.J. U.S.S.R.*, **26**, 10, 1949.

[6] *Observatory*, **67**, 15, 1947.

[7] *Nature*, **158**, 717, 1946.

the fine-structure states of a particular main level, and (3) between the hyperfine-structure substates of a particular fine-structure state. Transitions of the first of these kinds are of no particular interest in the study of discrete lines because they are so numerous that, without the presence of some selective excitation mechanism, they may be regarded merely as contributing toward a continuous spectrum. We have therefore to consider only the fine-structure and hyperfine-structure lines.

a) THE FINE-STRUCTURE LINES

The splitting of each main level (characterized by the principal quantum number n) into a fine structure is ascribed to the combined effect of the spin and relativistic properties of the electron. In describing the fine structure, we shall initially assume Dirac's theory of the hydrogen atom. The effects of known departures from this theory will be discussed later.

An outcome of Dirac's theory is that pairs of states having the same n and j (but different l) quantum numbers coincide. The energy levels are given with sufficient accuracy by

$$W_{nj} = -\frac{Rhc}{n^2} - \frac{Rhc\alpha^2}{n^3}\left(\frac{1}{j+\frac{1}{2}} - \frac{3}{4n}\right), \tag{1}$$

where h is Planck's constant, c the velocity of light, R Rydberg's constant, and α the fine-structure constant. The quantum numbers l and j can assume the following values:

$$l = 0,\ 1,\ 2,\ \ldots,\ n-1\ ;$$

$$j = l \pm \tfrac{1}{2}\ .$$

The selection rules for electric dipole radiation allow transitions to take place when the l and j of the initial and final states differ by $\Delta l = \pm 1$, $\Delta j = 0, \pm 1$. It follows that, apart from degenerate transitions of the type $(n, l, j) - (n, l-1, j)$, allowed transitions between fine-structure states of the same n are of the type

$$(n,\ l,\ j) - (n,\ l-1,\ j-1)\ .$$

The frequency, ν, of the transitions of this type is given, from equation (1), by

$$h\nu = W_{nj} - W_{nj-1} = \frac{Rhc\alpha^2}{n^3}\left(\frac{1}{j-\frac{1}{2}} - \frac{1}{j+\frac{1}{2}}\right),$$

where j may assume the values $\frac{3}{2}, \frac{5}{2}, \ldots, n-\frac{1}{2}$. Numerically,[8]

$$\nu = 1.7510 \times 10^{11} n^{-3} \{(j-\tfrac{1}{2})^{-1} - (j+\tfrac{1}{2})^{-1}\}\ \text{sec}^{-1}\ . \tag{2}$$

The frequencies of the fine-structure lines associated with main levels up to $n = 4$, calculated by equation (2), are given in Table 1.

We shall now calculate the transition probabilities of this series of lines. The Einstein transition probability of spontaneous emission, A_{21}, for a transition between an upper state 2 and a lower state 1, is given by

$$A_{21} = \frac{6.4\pi^4\nu^3}{3hc^3 g_2} S_{21}\ , \tag{3}$$

where $g_2 = 2j + 1$, the statistical weight of state 2, and S_{21} is the "strength" of the line. The strengths of the fine-structure transitions may be calculated by combining four equations given by Condon and Shortley,[9] namely, their equations numbered 7[45], 11[38],

[8] The values of physical constants used throughout this paper are those given by R. T. Birge, *Rev. Mod. Phys.*, **13**, 233, 1941.

[9] *The Theory of Atomic Spectra* (Cambridge: At the University Press, 1935).

$6^2 3$, and $6^2 2$. For transitions of the type $(n, l, j) - (n, l-1, j-1)$ we obtain

$$S_{21} = \frac{9n^2}{16j}(4j^2-1)(n^2-l^2)\,a_0^2 e^2\,, \tag{4a}$$

where a_0 is the radius of the first Bohr orbit and e is the electronic charge. Also, for the degenerate transitions of the type $(n, l, j) - (n, l-1, j)$, we obtain

$$S_{21} = \frac{9n^2}{16j}\frac{2j+1}{j+1}(n^2-l^2)\,a_0^2 e^2\,. \tag{4b}$$

Since S_{21} is expressed in terms of $a_0^2 e^2$, the most convenient numerical form of equation (3) is

$$A_{21} = 7.521\times 10^{-38}\frac{\nu^3}{g_2}\left(\frac{S_{21}}{a_0^2 e^2}\right)\text{sec}^{-1}\,. \tag{5}$$

Transition probabilities of the fine-structure lines associated with levels up to $n = 4$, calculated from equations (5) and (4*a*), are included in Table 1.

TABLE 1

FINE-STRUCTURE LINES FOR $n = 2$, 3, AND 4, ACCORDING TO DIRAC'S THEORY

Designation	Frequency (Mc/Sec)	Transition Probability (Sec^{-1})	Natural Half-width (Mc/Sec)
$2^2P_{3/2}-2^2S_{1/2}$	10,944	8.9×10^{-7}	100
$3^2P_{3/2}-3^2S_{1/2}$	3243	1.4×10^{-7}	30
$3^2D_{3/2}-3^2P_{1/2}$	3243	8.7×10^{-8}	40
$3^2D_{5/2}-3^2P_{3/2}$	1081	3.9×10^{-9}	40
$4^2P_{3/2}-4^2S_{1/2}$	1368	3.5×10^{-8}	13.6
$4^2D_{3/2}-4^2P_{1/2}$	1368	2.8×10^{-8}	17.2
$4^2D_{5/2}-4^2P_{3/2}$	456	1.2×10^{-9}	17.2
$4^2F_{5/2}-4^2D_{3/2}$	456	7.2×10^{-10}	6.6
$4^2F_{7/2}-4^2D_{5/2}$	228	9.6×10^{-11}	6.6

Finally, we calculate the natural widths of these lines. Even in the absence of all extraneous causes of line broadening (e.g., Doppler effect and collisions), a spectral line has a finite "natural" width due to the finite lifetime of the excited state. In optical spectroscopy this natural width is rarely of practical importance because instrumental limitations and other causes of line broadening tend to make it insignificant. However, the natural widths of the radio-frequency fine-structure lines are relatively very large and may be the chief factor in determining the widths of actual lines. The natural shape of a line is given by

$$f(\nu) = \frac{2}{\pi\,\delta\nu}\left\{\frac{1}{1+[2(\nu-\nu_0)/\delta\nu]^2}\right\}, \tag{6}$$

where $f(\nu)d\nu$ denotes the probability that a transition of the type (1, 2) occurs within the frequency interval $(\nu, \nu + d\nu)$, ν_0 is the center frequency of the line, and $\delta\nu$ is the *half-width* of the line (defined as the *total* width between half-maximum points). The half-width is related to the lifetimes τ_1 and τ_2 of the lower and upper levels by

$$\delta\nu = \frac{1}{2\pi}\left(\frac{1}{\tau_1}+\frac{1}{\tau_2}\right).$$

This equation and values of lifetimes tabulated by Condon and Shortley[9] have been used to calculate the half-widths of the fine-structure lines given in Table 1.

b) THE HYPERFINE-STRUCTURE LINES

In the above discussion we have ignored the effects of the nuclear magnetic moment upon the electron. When this is taken into account, each level (nlj) is split into two sublevels. This hyperfine-structure splitting is small but not negligible compared with the fine-structure splitting. Following the first calculations of Fermi, Bethe[10] derived the following expression for the hyperfine-structure energy shifts:

$$W_{\text{hyperfine}} = \frac{h\nu_0}{n^3}\left\{\frac{f(f+1) - i(i+1) - j(j+1)}{j(j+1)(2l+1)}\right\}, \tag{7}$$

where

$$\nu_0 = g(i)\,\alpha^2 cR\,. \tag{8}$$

Here i is the spin of the nucleus, f is the total quantum number given by the sum of the i and j vectors, and $g(i)$ is the Landé factor for the proton. For hydrogen, $i = \frac{1}{2}$ and $f = j \pm \frac{1}{2}$. It follows from equation (7) that the separation between a pair of hyperfine-structure sublevels, $f = j + \frac{1}{2}$ and $f = j - \frac{1}{2}$, is given in frequency units by

$$\nu = \frac{\nu_0}{n^3}\,\frac{2j+1}{j(j+1)(2l+1)}. \tag{9}$$

This equation gives the frequencies of the hyperfine-structure lines. To determine ν_0, we note that, for the ground state, $1^2S_{1/2}$, the separation is

$$\nu_G = \tfrac{8}{3}\nu_0\,. \tag{10}$$

The value of ν_G has been measured directly by Nafe and Nelson[11] and by Nagle, Julian, and Zacharias,[12] using the atomic-beam magnetic resonance method. The value, as given by Nafe and Nelson, is

$$\nu_G = 1420.410 \pm 0.006 \text{ Mc/sec}\,.$$

Hence, by equation (10),

$$\nu_0 = 532.6_5 \text{ Mc/sec}$$

(the value of ν_0 calculated from eq. [8] differs from the above value by less than 0.3 per cent). The frequencies of these lines, calculated from equation (9), for the $n = 1$ and $n = 2$ levels, are given in Table 2.

The transitions occur between states having the same l quantum number and are therefore magnetic dipole transitions. The transition probability, A_{21}, for a transition of the type $(n, l, j, f) - (n, l, j, f - 1)$ is again given in terms of the line strength, S_{21}, by equation (3), but now we must regard the statistical weight of state 2 as

$$g_2 = 2f + 1\,. \tag{11}$$

Of the hyperfine-structure lines, by far the most important in astrophysical applications is that of frequency 1420 Mc/sec associated with the ground state. The first derivation of the strength of this line was made by Shklovsky,[5] who obtained (in our notation)

$$S_{21} = \tfrac{3}{4}\beta^2\,,$$

[10] *Handbuch der Physik*, Vol. **24/1**, chap. iii, pp. 385 ff., 1933.

[11] *Phys. Rev.*, **73**, 718, 1948.

[12] *Phys. Rev.*, **72**, 971, 1947.

where β denotes the Bohr magneton,

$$\beta = \frac{e h}{4\pi m c}.$$

Recently, however, Ewen[13] and Purcell (personal communication)[14] have found the strength of this line to be

$$S_{21} = 3\beta^2 . \tag{12}$$

In Shklovsky's derivation a quantum-mechanical result of Condon and Shortley, originally expressed in terms of the electronic quantum numbers L, S, and J, was used, but with L, S, and J replaced by J, I, and F, respectively. Although this substitution is often permissible, Purcell pointed out that in this instance it was incorrect, since it implied

TABLE 2

HYPERFINE-STRUCTURE LINES FOR $n = 1$ AND 2

Level	Frequency (Mc/Sec)	Transition Probability (Sec^{-1})
$1^2S_{1/2}$	1420.4	2.85×10^{-15}
$2^2S_{1/2}$	177.5	.....
$2^2P_{1/2}$	59.2	.....
$2^2P_{3/2}$	23.7	.....

that the magnetic moment of the nucleus bears the same ratio to the quantum number I as the orbital and spin components of the electronic magnetic moment bear to the quantities L and $2S$. (In fact, the ratios differ by the factor m/M, where m and M denote the mass of the electron and proton, and it follows that, in calculating the line strength, the magnetic moment of the nucleus may be neglected in comparison with that of the electron.) We therefore adopt result (12) and, in conjunction with equations (3) and (11), obtain for the transition probability of the 1420 Mc/sec line,

$$A_{21} = 2.85 \times 10^{-15}\ \text{sec}^{-1} .$$

The natural half-width of this line has the minute value of 5×10^{-16} c/sec ($=A_{21}/2\pi$) and would be quite insignificant in comparison with extraneous causes of line broadening under all conditions encountered in practice.

c) THE EFFECTS OF DEPARTURES FROM DIRAC'S THEORY UPON THE FINE-STRUCTURE LINES

We now consider how the series of fine-structure lines discussed in subsection II*a* must be modified, owing to (1) known departures from Dirac's theory and (2) the hyperfine structure.

The frequency separation of the 2s and 2p states has recently been measured directly by Lamb and Retherford.[15] They found that, whereas the separation of the $2P_{1/2}$ and $2P_{3/2}$ levels was in accordance with the theory, the $2S_{1/2}$ level did not coincide with the

[13] "Radiation from Galactic Hydrogen at 1420 Mc/Sec" (Ph.D. thesis, Harvard University, May, 1951).

[14] Thanks are due to Professor E. M. Purcell for making this result and the ensuing discussion available to the author prior to publication.

[15] *Phys. Rev.*, **79**, 549, 1950, and **81**, 222, 1951.

$2P_{1/2}$ level, as predicted, but lay higher by 1062 ± 5 Mc/sec. The modified level scheme is shown in Figure 1, *b*. The shift of the $2S_{1/2}$ level has been explained by Bethe and others in terms of the interaction of the electron with the quantized electromagnetic field.

The energy shifts due to the hyperfine structure may be calculated from equation (7). The final scheme of the $n = 2$ sublevels is shown in Figure 1, *c*. The $2^2P_{3/2} - 2^2S_{1/2}$ line is seen to consist of three components (the appropriate selection rule is $\Delta f = 0, \pm 1$). The relative intensities of these components may be calculated by the usual sum rules for Russell-Saunders coupling.[9] Figure 2 shows the theoretical profile of this multiplet,

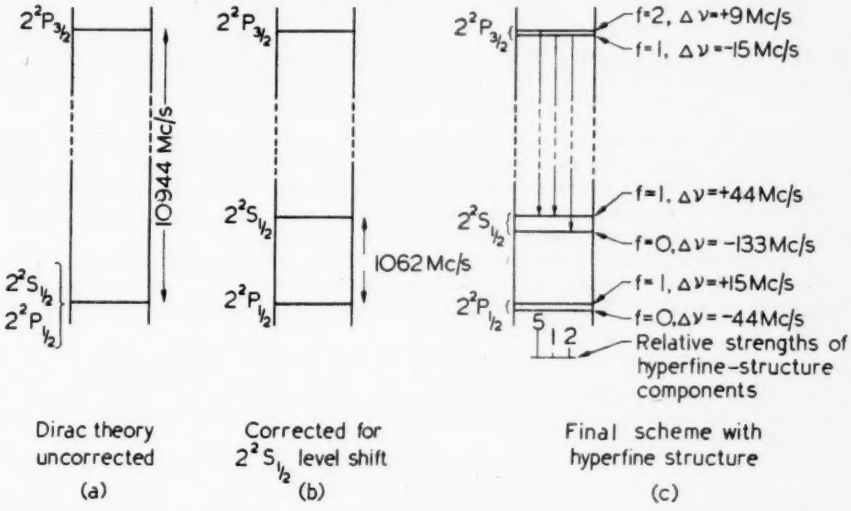

FIG. 1.—The structure of the $n = 2$ level of atomic hydrogen: *a*, the scheme predicted by Dirac's theory; *b*, corrected for the Lamb-Retherford shift; *c*, the final scheme, including the hyperfine-structure splitting. The arrows in *c* show the allowed transitions between the $2^2P_{3/2}$ and $2^2S_{1/2}$ levels. The relative strengths of these components are indicated below the arrows.

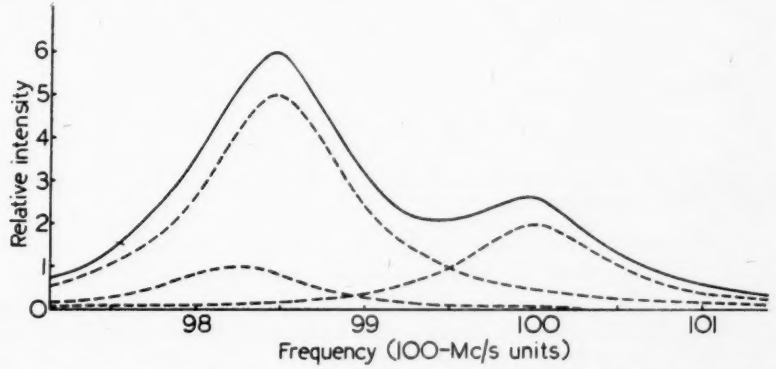

FIG. 2.—The calculated natural profile of the $2^2P_{3/2} - 2^2S_{1/2}$ multiplet. The dotted lines show the three hyperfine-structure components indicated in Figure 1, *c*.

taking account of the natural shape of the components given by equation (6) with $\delta\nu = 100$ Mc/sec (see Table 1).

If the $2P_{3/2} - 2S_{1/2}$ multiplet is regarded as a single line with asymmetrical profile, the frequency of the maximum occurs at

$$\nu_0 = 9847 \pm 5 \text{ Mc/sec},$$

and the "line width," defined by equation (27) as the reciprocal of $f(\nu_0)$, may be calculated to be

$$\Delta\nu = \frac{1}{f(\nu_0)} = 210 \text{ Mc/sec},$$

and the transition probability, using the above value of ν_0, is found to be

$$A_{21} = 6.5 \times 10^{-7} \text{ sec}^{-1}.$$

The removal of the degeneracy between the $2^2S_{1/2}$ and $2^2P_{1/2}$ levels implies that allowed transitions of finite frequency ($\sim$1000 Mc/sec) can occur between them. The strengths of such lines are given by equation (4*b*); they are much less than those of the type $(n, l, j) - (n, l-1, j-1)$ of comparable frequency, because the latter are associated with considerably higher n levels.

These remarks have been confined to the $n = 2$ levels. Similar effects will, of course, arise in the $n = 3$ and higher levels. As a first approximation, however, the results of subsection II*a* may be used to calculate the frequency and transition probability of these lines.

III. THE FORMATION OF EMISSION AND ABSORPTION LINES

In this section we consider the problem of calculating the nature (emission or absorption) and magnitude of a spectral line when the physical conditions affecting its formation are completely specified.

a) THE EQUATION OF TRANSFER

We have first to consider the transfer of radiation along any line of sight passing through some assembly of atoms. Let the volume coefficients of absorption and emission in the frequency element $(\nu, \nu + d\nu)$ at the point in the line of sight at distance s from the observer be $K(\nu)$ and $j(\nu)d\nu$, respectively. Then the specific intensity, $I(\nu)d\nu$, of the radiation at any point is given by the equation of transfer,[16]

$$\frac{dI(\nu)}{ds} = j(\nu) - K(\nu)\, I(\nu).$$

The solution is

$$I(\nu) = \int_0^\infty j(\nu)\, e^{-\int_0^s K(\nu) ds'} ds. \tag{13}$$

Intensities at radio frequencies are often expressed in terms of the equivalent black-body or "brightness" temperature, defined by

$$T = \frac{I(\nu)\, c^2}{2k\nu^2},$$

where k is Boltzmann's constant. This transformation is just the Rayleigh-Jeans formula, which is negligibly different from Planck's exact formula at radio frequencies. Similarly, we can express the emission coefficient in temperature units (degrees per centimeter)

[16] As given here the equation refers to media of unit refractive index. For the general form of the equation applicable at radio frequencies see S. F. Smerd and K. C. Westfold, *Phil. Mag.*, **40**, 831, 1949.

thus,

$$J(\nu) = \frac{j(\nu)\, c^2}{2k\nu^2}.$$

Equation (13) may then be written

$$T = \int_0^\infty J(\nu)\, e^{-\int_0^s K(\nu) ds'} ds. \tag{14}$$

Let us now suppose that some or all of the atoms in view are capable of a transition between some upper state "2" and a lower state "1" corresponding to a line of nominal frequency, ν_0 (the line will, of course, have finite width). It will be assumed that, in the neighborhood of the frequency ν_0, the spectrum of the radiation may be resolved into (1) a continuous uniform "background" (due to a large number of unspecified transitions, no one of which predominates) and (2) the "line" due to the transition (1, 2). This may be stated formally as follows: Let the coefficients $J(\nu)$ and $K(\nu)$ be written as the sum of two terms,

$$J(\nu) = J_a(\nu) + J_b(\nu), \qquad K(\nu) = K_a(\nu) + K_b,$$

where the subscript a denotes the contribution of transitions of the type (1, 2) and b denotes the contribution of all other transitions. Then we assume that in the neighborhood of the line the "background" coefficients J_b and K_b are constant.

In accordance with equation (14), the brightness temperature in the line is

$$T_{ab}(\nu) = \int_0^\infty \{J_a(\nu) + J_b\}\, e^{-\int_0^s \{K_a(\nu) + K_b\} ds'} ds, \tag{15}$$

and that of the background is

$$T_b = \int_0^\infty J_b\, e^{-\int_0^s K_b ds'} ds. \tag{16}$$

The difference between the two will be referred to as the "excess brightness temperature," ΔT:

$$\Delta T = T_{ab} - T_b.$$

Evidently, positive ΔT implies an emission line and negative ΔT an absorption line. It may simply be shown that, if we neglect the very special cases of excitation for which K_a is negative, the excess brightness temperature of an emission line cannot exceed the value

$$(\Delta T)_{\max} = \int_0^\infty J_a(\nu)\, ds. \tag{17}$$

Similarly, the negative excess brightness temperature of an absorption line cannot exceed the value

$$(-\Delta T)_{\max} = T_b(1 - e^{-\tau_a}) \leqslant T_b \tau_a, \tag{18}$$

where

$$\tau_a = \int_0^\infty K_a(\nu)\, ds.$$

b) EVALUATION OF THE COEFFICIENTS OF ABSORPTION AND EMISSION

In terms of the total numbers of atoms per cubic centimeter, n_1 and n_2, in states 1 and 2, the coefficients of absorption and emission for the line radiation are given by[17]

$$K_a(\nu) = \alpha(\nu)\left(n_1 - n_2 \frac{g_1}{g_2}\right), \tag{19}$$

[17] See, e.g., E. A. Milne, *Handbuch der Astrophysik*, Vol. 3, chap. ii, pp. 159 ff., 1930.

$$J_a(\nu) = a(\nu)\frac{g_1}{g_2} n_2 \frac{h\nu}{k}. \tag{20}$$

Here $a(\nu)$ is the atomic absorption coefficient, defined by

$$a(\nu) = \frac{c^2 A_{21}}{8\pi\nu^2}\frac{g_2}{g_1} f(\nu), \tag{21}$$

where $f(\nu)d\nu$ denotes the probability that a transition of type (1, 2) occurs within the frequency range $(\nu, \nu + d\nu)$. The function $f(\nu)$ thus determines the shape and width of the line.

It is often convenient to express the coefficients in terms of the *excitation temperature*, θ_a, defined by

$$\frac{n_2}{n_1} = \frac{g_2}{g_1} e^{-h\nu/k\theta_a}. \tag{22}$$

In general, the excitation temperature expresses merely the relative distribution of atoms between states 1 and 2. In particular circumstances, such as thermodynamic equilibrium, θ_a is identical with the temperature.

When $h\nu \ll k\theta_a$ (which is usual at radio frequencies), equations (19), (20), and (22) give

$$K_a(\nu) = a(\nu) n_1 \frac{h\nu}{k\theta_a} \tag{23}$$

and

$$J_a(\nu) = a(\nu) n_1 \frac{h\nu}{k}. \tag{24}$$

We note that

$$\frac{J_a(\nu)}{K_a(\nu)} = \theta_a. \tag{25}$$

This is Kirchhoff's law and is quite generally valid.

It is shown in the Appendix that, in a uniform medium of thickness l, the excess brightness temperature is given by the following approximation, provided that $K_a l \ll 1$ and $\theta_a \gg T_b$:

$$\Delta T \approx \theta_a (1 - e^{-K_a l}). \tag{26}$$

Finally, we have to consider the "line-shape" function $f(\nu)$. Its value, $f(\nu_0)$, at the center of the line is clearly just the reciprocal of the line width, $\Delta\nu$, when defined by

$$f(\nu_0)\,\Delta\nu = \int_0^\infty f(\nu)\, d\nu = 1. \tag{27}$$

When the line width is determined entirely by the natural width, $f(\nu)$ is given by equation (6). When Doppler broadening predominates, the center of the line is shifted to the frequency $\nu_0' = \nu_0(1 + [\bar{v}/c])$, where $\bar{v}$ is the mean velocity of the atoms along the line of sight. If $n_1(v)dv$ denotes the number of atoms with velocity between v and $v + dv$ and if the velocity dispersion, Δv, is defined by

$$n_1(\bar{v})\,\Delta v = \int_{-\infty}^{\infty} n_1(v)\, dv = n_1,$$

then

$$\Delta\nu = \frac{\nu_0'}{c}\Delta v,$$

and

$$f(\nu_0') = \frac{c}{\nu_0' \Delta v}. \tag{28}$$

When the motion of the atoms is entirely thermal,

$$f(\nu_0) = \frac{1}{\Delta\nu} = \frac{c}{\nu_0}\left(\frac{M}{2\pi k \theta_e}\right)^{1/2}, \tag{29}$$

where M is the atomic mass and θ_e the kinetic temperature.

IV. ASTRONOMICAL APPLICATIONS

Atomic hydrogen is known to be the prevalent constituent of both stars and interstellar gas. Both, therefore, may be sources of radio-frequency hydrogen lines.

Radio-frequency techniques are unsuited to the observation of individual stars, because the angular resolution of practicable aerial systems is extremely low. The only star that can be resolved as a single source is the sun. The aggregate of other stars can occupy only a minute fraction of the solid angle of the aerial beam. The general background continuum of galactic radio radiation is believed to be nonstellar in origin. It follows that, unless lines of great strength can be obtained from the sun (regarded as a typical star), it is unlikely that any lines would be observable in the aggregate radiation of other stars. Apart from the interstellar gas, therefore, the sun is the most likely source of radio-frequency hydrogen lines.

a) THE SUN

When the sun is viewed at radio frequencies, the disk which is seen corresponds not to the photosphere but to some diffuse layer in the solar atmosphere. The height of this absorbing layer above the photosphere is determined by the refractive and adsorptive properties of the solar atmosphere and depends critically on frequency.[18] In general, the lower the frequency, the higher the absorbing layer. It is clear that the only atoms which can contribute to the formation of a spectral line are those which lie above, and to some extent within, the absorbing layer corresponding to the frequency of the line. Let N_1 and N_2 denote the number of atoms in states 1 and 2 contained in a cylinder of 1 cm^2 cross-section between the observer and the absorbing layer corresponding to the frequency, ν_0, of the transition (1, 2). Then it follows from equations (17), (18), (19), and (20) that the maximum possible excess brightness temperature of the line is given by

$$(\Delta T)_{\max} = \alpha(\nu_0)\frac{g_1}{g_2}\frac{h\nu_0}{k}N_2 \qquad \text{for an emission line}, \tag{30}$$

$$(-\Delta T)_{\max} \leqq T_b \alpha(\nu_0)\left(N_1 - N_2\frac{g_1}{g_2}\right) \qquad \text{for an absorption line}. \tag{31}$$

With the use of these equations it may readily be shown that, for all but one of the radio-frequency hydrogen lines, the value of N_2 or $(N_1 - N_2[g_1/g_2])$ required to produce a measurable value of $\Delta T(\sim 10^\circ\,\mathrm{K}$, say) is inconceivably high.

The exception is the fine-structure line $2^2P_{3/2}-2^2S_{1/2}$ (near 10,000 Mc/sec) in absorption. Two circumstances combine to make this line the most favorable for detection. The first is its high frequency: radiation of 10,000 Mc/sec can penetrate quite deeply into the chromosphere, where neutral hydrogen is far more abundant than in the corona. The second is the metastability[19] of the $2^2S_{1/2}$ state; this results in an overpopulation of the

[18] See, e.g., S. F. Smerd, *Australian J. Sci. Res.*, *A*, **3**, 34, 1950.

[19] The metastability of state $2^2S_{1/2}$ is not significantly affected by the allowed transition to the lower state $2^2P_{1/2}$ because the latter transition has a lifetime of some 40 years.

$2^2S_{1/2}$ state (cf. Giovanelli[20])—i.e., a high value of N_1. The atomic absorption coefficient at the center of this line is found, from equation (21) and the numerical values given at the end of subsection II*c*, to be

$$a(\nu_0) = 2.3 \times 10^{-15} \text{ cm}^2 .$$

The average brightness temperature of 10,000 Mc/sec solar radiation over the optical disk is known from observations to be about $2 \times 10^{4\circ}$ K. Taking this value of T_b and neglecting $(g_1/g_2)N_2$ in comparison with N_1, we obtain from equation (31)

$$(-\Delta T)_{\max} \approx 5 \times 10^{-11} N_1 \text{ (in degrees Kelvin, when } N_1 \text{ is measured in cm}^{-2}) .$$

Thus, to obtain an absorption line with an excess brightness temperature of -50° K, we require $N_1 \geqslant 10^{12}$ cm^{-2}. Now in the present case N_1 denotes the number of absorbing atoms in state $2^2S_{1/2}$ contained in a cylinder of 1 cm^2 cross-section between the observer and the absorption layer of the 10,000 Mc/sec background radiation. Most of these atoms will be concentrated into the last thousand kilometers or so near the top of the chromosphere. It may be noted that the value $N_1 = 10^{12}$ cm^{-2} corresponds to a mean concentration of $n_1 = 10^4$ cm^{-3} over a length of 1000 kilometers (about one-tenth the total thickness of the chromosphere). Estimates by Giovanelli[20] of the concentration of atoms in the state $2^2S_{1/2}$ under chromospheric conditions indicate values between about 10 and 10^7 cm^{-3}. Thus with present knowledge it can be concluded only that the line *may* be detectable and that a search for it seems worth while.

The possibility has been considered of clouds of relatively dense, cold matter in the corona, such as prominence material, producing significant line absorption near the center of the solar disk or line emission near the limb. The most likely line was found to be the ground-state hyperfine-structure line (1420 Mc/sec) in emission. For example, a uniform sheet of gas beyond the solar limb of thickness 10^9 cm and kinetic temperature $10^{4\circ}$ K would give a 1420 Mc/sec emission line of excess brightness temperature $\Delta T = 10^\circ$ K (the Doppler width $\Delta\nu = 1.1 \times 10^5$ sec^{-1}) if the total concentration of atoms in the ground state were $n_1 + n_2 \approx 4 \times 10^{11}$ cm^{-3}. (Lower concentrations would suffice for lower kinetic temperatures.) It is generally believed that hydrogen concentrations in prominences are somewhat smaller than this value. Furthermore, the observation of such a line would probably require the use of an aerial of extraordinarily high directivity.

b) INTERSTELLAR GAS

Although it has been known for some years that hydrogen is the principal constituent of the interstellar gas, most of our knowledge on the subject has been derived from the spectroscopic study of other much less abundant elements, notably sodium and calcium. The pioneering observation by Ewen and Purcell[1] of the 1420 Mc/sec hyperfine-structure hydrogen line from the galaxy has initiated what promises to be a powerful new tool for the direct investigation of interstellar hydrogen. The immediate virtues of this new technique arise, first, in the peculiar circumstance that the emission is due to atoms *in the ground state*, and, second, in the relatively high accuracy with which Doppler shifts and line widths may be measured by means of radio techniques.

The interstellar gas is confined mainly to regions near the galactic plane extending to distances of the order of 100 parsecs on either side. The mean density of hydrogen atoms in these regions is generally taken to be about 1 cm^{-3}. The gas distribution is known to be highly irregular, most of the atoms being concentrated in clouds which occupy perhaps 5 per cent of space near the galactic plane.[21] The clouds have random velocities of about 5–10 km/sec (root mean square), though much higher velocities are sometimes observed. The hydrogen in all clouds except those near O and B stars is un-ionized. The kinetic

[20] *Australian J. Sci. Res.*, *A*, **1**, 289, 1948.

[21] B. Strömgren, *Ap. J.*, **108**, 242, 1948.

temperature of the un-ionized clouds has been estimated by Spitzer and Savedoff[22] to be about 60° K. Using these data to make calculations of the kind employed above for the sun, it is found that, even if the clouds are assumed to exist throughout the extent of the galaxy (about 20 kiloparsecs), the possibility of observing any radio-frequency hydrogen line other than that at 1420 Mc/sec is extremely remote. In spite of its low transition probability, the 1420 Mc/sec line gains over all others because of the overwhelming preponderance of neutral interstellar hydrogen in the ground state. Some aspects of this interstellar line and its importance to interstellar studies will now be discussed.

The absorption coefficient of the line, given by equations (21), (23), and (27), is

$$K_a \equiv K_a(\nu_0) = \frac{a(\nu_0)\, n_1 h\nu_0}{k\theta_a} = 8.0 \times 10^{-3} \frac{n}{\Delta\nu\, \theta_a} \text{ parsec}^{-1}, \tag{32}$$

where $n(\approx 4n_1)$ is the total number of ground-state hydrogen atoms per cubic centimeter, θ_a the excitation temperature in ° K, and $\Delta\nu$ the "line width," in the sense of equation (27), in cycles per second. The value of $\Delta\nu$ corresponds to the observed line width only when the line is observed in directions of low optical thickness; otherwise, self-absorption and hence additional broadening occur. The preliminary observations indicate that $\Delta\nu$ is about 60 kc/sec, corresponding to a root-mean-square velocity dispersion of 5 km/sec. The value is in general agreement with the random cloud velocities derived from optical observations.

Let us now suppose that the region of interstellar hydrogen is bounded by two planes, each parallel to and distant d from the galactic plane. For simplicity, we assume the sun to be in the galactic plane, though this assumption is not essential to the main argument. In any direction through the galactic longitude of the galactic center, the line optical thickness will be

$$\tau_a = K_a d \operatorname{cosec} b$$

(where b is galactic latitude), except for very small angles (probably less than 1°) near $b = 0$, where a limit is imposed by the finite extent of the galaxy. Now it is known that the galaxy is optically thin for the general background radiation at frequencies around 1400 Mc/sec. Under this condition the excess brightness temperature of the line is given by the approximation (26),

$$\Delta T \approx \theta_a (1 - e^{-\tau_a}) = \theta_a (1 - e^{-K_a d \operatorname{cosec} b}), \tag{33}$$

provided that θ_a is large compared with the brightness temperature of the general background radiation (about 10° K toward the galactic center at these frequencies). The latter condition will tentatively be assumed to be satisfied. The full curves of Figure 3 show the variation of $\Delta T/\theta_a$ with b, according to equation (33), for various values of $K_a d$. The effect of the finite extent of the galaxy is merely to cut off the tops of the curves near $b = 0$ over a fraction of a degree; the effect should be quite negligible for all but the lowest curve plotted.

Figure 4 shows an experimental plot, obtained by W. N. Christiansen,[23] of the excess aerial temperature through the galactic center. The observations were taken along the line of declination −30°, which passes obliquely across the galactic equator. The width of the aerial beam (about $2\frac{1}{2}$° between half-power points) was narrow in comparison with that of the source, so that the measured (aerial) temperature should give a true measure of brightness temperature. In drawing the curve through the experimental points, it was assumed that the maximum occurred at the galactic equator. The same experimental points are replotted in Figure 3, in which the ordinates have been normalized to the assumed maximum and the abscissas converted into galactic latitudes.

[22] *Ap. J.*, **111**, 593, 1950.

[23] The author is indebted to Mr. Christiansen for making available these observations which are as yet unpublished.

The large angular width of the observed source indicates that the optical thickness near the galactic plane is large, and so the brightness temperature at the maximum is a true measure of the excitation temperature.[24] This deduction was first made by Ewen and Purcell[1] and is contrary to the prediction of Shklovsky[5] that the galaxy should be optically thin through the galactic center. Ewen and Purcell found the absolute value of the temperature (presumably the *aerial* temperature, which would be rather less than the brightness temperature when the width of the aerial beam is comparable with that of the source) to be about 35° K.

It was suggested by Shklovsky[5] that, since the lifetime of the upper level of the transition has an enormous length of the order of 10^7 years, the distribution of atoms in the upper and lower levels is likely to be determined almost entirely by collisions; in this

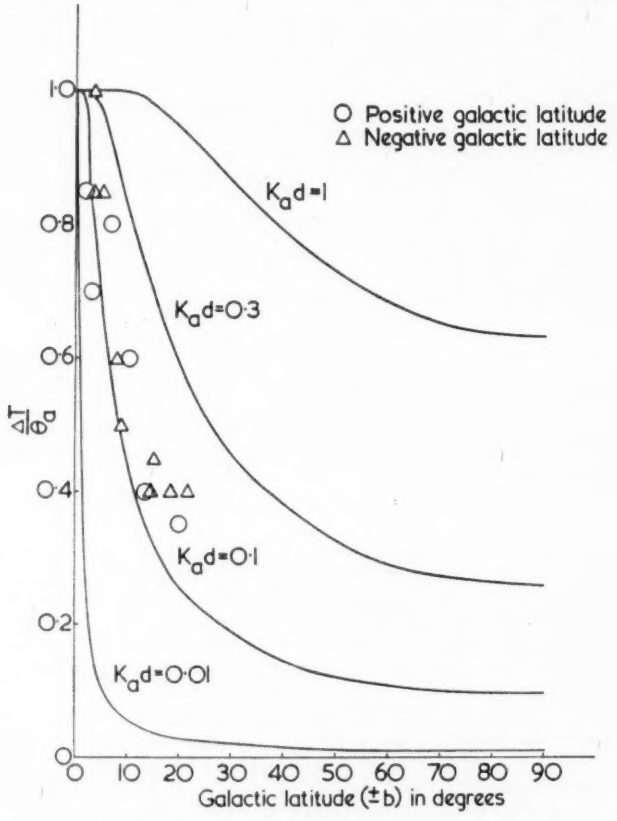

FIG. 3.—The curves show the calculated variation with galactic latitude of the excess brightness temperature (in units of θ_a) of the 1420 Mc/sec hydrogen line along the longitude of the galactic center. Curves corresponding to several values of $K_a d$ are plotted (K_a denotes the line-absorption coefficient in the galactic region of un-ionized hydrogen, and d the distance from the galactic plane to which this region extends). The experimental points correspond to those in Figure 4.

[24] According to the approximate relation (26), $\Delta T \approx \theta_a$ when $\tau_a = \infty$. Precisely, however, the *total* brightness temperature ($\Delta T + T_b$) is equal to θ_a when $\tau_a = \infty$.

case the excitation temperature is just the kinetic temperature of the gas. Ewen and Purcell[1] have suggested that radiative processes may play a significant but minor role and that the kinetic temperature may be rather higher than the excitation temperature. In any case it is not unlikely that the brightness temperature provides us with a direct method of measuring, in order of magnitude at least, the kinetic temperature of the clouds of un-ionized hydrogen. It is noteworthy that the observed value of Ewen and Purcell is in order-of-magnitude agreement with Spitzer and Savedoff's[22] estimate of 60° K.

Returning, now, to Figure 3, we note that the experimental points correspond to a value of $K_a d$ of about 0.15. Hence, substituting $\theta_a = 40°$ K, $\Delta\nu = 6 \times 10^4$ c/sec in equation (32), we obtain

$$K_a d = 3.3 \times 10^{-3} n d = 0.15 ,$$

i.e., $nd = 45$ (n in cm^{-3}, d in parsecs). Muller and Oort[2] consider that, owing to the low random velocities of the atoms producing the emission line, the mean value of d cannot

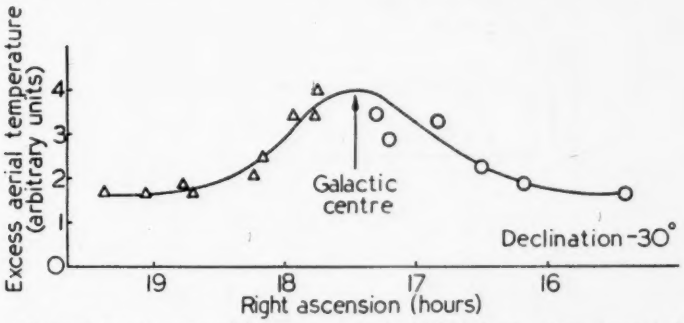

FIG. 4.—The variation of excess aerial temperature in the 1420 Mc/sec hydrogen line with right ascension along declination −30°, observed by W. N. Christiansen (unpublished). Points corresponding to positive and negative galactic latitude are shown by circles and triangles, respectively, to facilitate comparison with Figure 3.

be greater than about 50 parsecs. Taking n to be 1 cm^{-3}, this would give $nd \leq 50$, which is consistent with the above result.

If n is taken to be 1 cm^{-3}, an optical depth of unity is reached in a distance of about 300 parsecs. Hence it seems that, toward the galactic center, the inner regions of the galaxy are not open to observation by this technique. Away from the galactic center, however, the inner regions should be open to investigation, owing to the effect of the differential rotation of the galaxy to introduce systematic variations in velocity along the line of sight. Near the sun the radial velocity varies directly as the distance; its magnitude in the optimum directions (45° away from the galactic center and anticenter) is about 18 km/sec/kiloparsec. In such directions the monochromatic emission and absorption of distant atoms occur at frequencies well displaced from the nominal frequency, and so we should expect to observe considerable line broadening. If it is supposed that the atomic concentration, averaged over large volumes, is the same in the inner regions as locally, then, if Figure 5, *a*, represents the profile (brightness temperature versus frequency) of the line observed toward the galactic center, Figure 5, *b*, shows the kind of profile to be expected from 45° either side of the galactic center (it may be nearly "flat-topped" over several megacycles per second). However, since the more displaced frequencies are received from greater distances and therefore through smaller solid angles, the *observed* profile (i.e., *aerial* temperature versus frequency) will be of the kind

shown in Figure 5, *c;* the rapidity with which the "tail" recedes to the base line increases with the width of the aerial beam.

Experimental confirmation of the increase in line width due to the effects of differential galactic rotation has already been obtained by Muller and Oort,[2] who use their results to make an estimate of galactic rotation. In a particularly elegant demonstration, they show that, when observed at a well-displaced frequency in a direction 30° from that of the galactic center, the source of monochromatic radiation subtends a much smaller angle in galactic latitude than that observed at the nominal frequency. It seems that

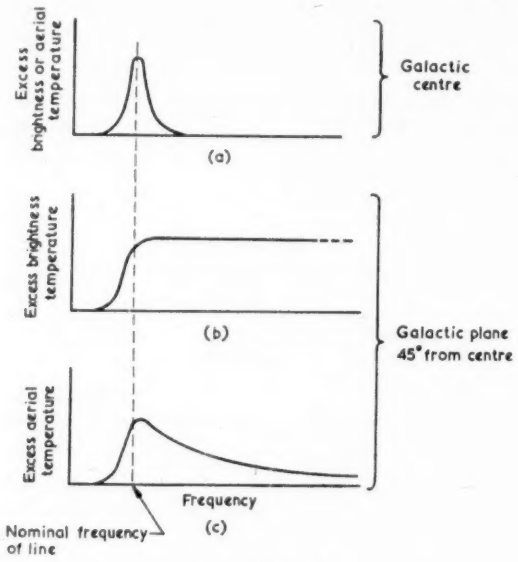

FIG. 5.—Predicted frequency profiles of the 1420 Mc/sec hydrogen line when received from *a* the galactic center and *b*, *c*, 45° away from the galactic center in the galactic plane. The curves are sketched and are intended only to indicate the general shape of profiles to be expected.

sky surveys carried out at displaced frequencies should give useful information on the rotation of the galaxy and the distribution of un-ionized hydrogen in the galactic interior.

V. SUMMARY OF CONCLUSIONS

The discrete radio-frequency lines of atomic hydrogen fall into two main series. The first is associated with transitions in the fine structure of each main level, the second with transitions in the hyperfine structure of each fine-structure level. The highest-frequency line of the fine-structure series is associated with the level $n = 2$ and occurs at about 9850 Mc/sec; the highest frequency of the hyperfine-structure series is associated with the ground level ($n = 1$) and occurs at 1420.4 Mc/sec. The fine-structure lines are due to electric dipole transitions and have much greater transition probabilities than the hyperfine-structure lines which are due to magnetic dipole transitions.

An investigation into the prospects of observing these lines from astronomical systems leads to the conclusion that, apart from the known galactic emission line at 1420 Mc/sec, the only reasonable possibility is the 9850 Mc/sec fine-structure line in absorption from

the sun. There is a slight possibility that the 1420 Mc/sec hyperfine-structure line may be observable in emission from prominences on the solar limb.

The 1420 Mc/sec galactic line must originate mainly in interstellar atoms and provides the only known direct method of investigating interstellar hydrogen in the ground state. Line widths observed so far confirm estimates of random cloud velocities derived from optical observations (about 5 km/sec). Observation of the line is likely to provide a means of measuring the kinetic temperature of the clouds of un-ionized hydrogen; the early measurements indicate temperatures well below 100° K. Observation of the variation of the intensity of the line with galactic latitude allows measurement to be made of the product nd, where n is the large-scale mean atomic concentration and d the average distance from the galactic plane to which the emitting region extends. The early observations indicate a value of $nd = 45$ cm^{-3} parsecs (consistent with the values $n \approx 1$ cm^{-3}, $d \approx 50$ parsecs). At some galactic longitudes the effects of differential galactic rotation make it possible to receive the monochromatic radiation from the inner regions of the galaxy.

Note added November, 1951.—The most recent observations of Christiansen and Hindman (unpublished) indicate that the band width, $\Delta\nu$, of the 1420 Mc/sec interstellar line may be as large as 1.2–1.4×10^5 c/sec, i.e., about twice the value assumed in the text. The latter value would correspond to root-mean-square cloud velocities of about 10 km/sec and would lead to a value of the product nd of about 100 cm^{-3} parsecs.

APPENDIX (SEE EQ. [26])

To show that for a uniform medium (constant K's and J's) of thickness l, the excess brightness temperature is given by the approximation

$$\Delta T \approx \theta_a (1 - e^{-K_a l}) ,$$

provided that $K_b l \ll 1$, $\theta_a \gg T_b$.

When $K_b l \ll 1$, the solutions of the equation of transfer (eqs. [16] and [15]), for a uniform medium are:

$$T_b = J_b l$$

and

$$T_{ab} = \frac{J_a + J_b}{K_a} (1 - e^{-K_a l}) ;$$

so that

$$\Delta T = T_{ab} - T_b = \frac{J_a + (T_b / l)}{K_a} (1 - e^{-K_a l}) - T_b .$$

Writing

$$T_a = \frac{J_a}{K_a} (1 - e^{-K_a l}) = \theta_a (1 - e^{-K_a l}) \tag{34}$$

$$x = \frac{T_a}{\theta_a} , \tag{35}$$

and

$$y = \frac{T_b}{\theta_a} ,$$

where θ_a is given by equation (25), we obtain

$$\Delta T = T_a \left\{ 1 - y \left[\frac{1}{x} + \frac{1}{\log (1 - x)} \right] \right\} .$$

Now the condition that $\theta_a \gg T_b$ implies that θ_a, and therefore K_a, is positive. For positive K_a it follows from equations (34) and (35) that $0 \leqslant x \leqslant 1$. In this range of x the expression in brackets varies between $\frac{1}{2}$ and 1. Hence if $y \ll 1$, $\Delta T \approx T_a$; that is to say, if $\theta_a \gg T_b$, then

$$\Delta T \approx \theta_a (1 - e^{-K_a l}) .$$

THE DISTRIBUTION OF INTERSTELLAR SODIUM. II

LYMAN SPITZER, JR., AND J. B. OKE
Princeton University Observatory
Received August 17, 1951

ABSTRACT

Van Rhijn found no correlation between the equivalent widths of interstellar *Na* and *Ca* lines and either color excess or distance from the nulls of galactic rotation. His analysis is repeated here for the *Na* D lines alone, in an attempt to reconcile his result with previous differing conclusions by Spitzer. The results indicate that a variation of the equivalent widths with galactic longitude, of the sort expected from the radial velocities due to galactic rotation, is present, in agreement with theory. However, the apparent correlation previously found between the equivalent width D and the color excess E_1 for stars with spectroscopic distances of about 1000 parsecs is shown to be due to errors in the distances; according to the mean distance found from stellar radial velocities and the galactic-rotation formula, the unreddened stars are much closer than assumed and have correspondingly weaker interstellar D lines. Whether a correlation between D and E_1 actually exists for stars at the same distance is difficult to tell from this analysis. That some correlation must be present follows from the previously observed and unmistakable correlation between the doublet ratio D_2/D_1 and E_1, which indicates that the larger fraction of the *Na* I atoms are found in the same clouds containing the obscuring grains.

A previous analysis[1] of the interstellar D lines, referred to subsequently as "Paper I," came to the conclusion that two-thirds of the interstellar *Na* I atoms were concentrated in the clouds of grains producing the observed selective extinction. The remaining third of the *Na* I atoms were found to lie outside the so-called "dust clouds," either in an intercloud continuum or in less dense, more transparent clouds. A secondary observational result of this investigation was that the equivalent widths of the interstellar *Na* lines in distant stars showed a variation with galactic longitude in accordance with that expected from galactic rotation, together with random velocities of the clouds.

Both these conclusions are at variance with an analysis published more recently by van Rhijn,[2] which utilizes the same observational data for the D lines that were discussed in Paper I, together with similar data for the interstellar K line. Since van Rhijn was primarily interested in the determination of stellar distances rather than in the distribution of interstellar gas, he did not consider *Na* and *Ca* separately. The present paper applies his analysis to the *Na* D lines in a reconciliation of his approach with the results of Paper I. The interstellar K line is not discussed here. A more detailed analysis of interstellar *Ca*, now in preparation, indicates large differences between the distribution of *Ca* and *Na* in interstellar space; the conclusions reached in Paper I for *Na* are apparently not valid for *Ca*.

The first section is devoted to the effect which the radial velocity produced by galactic rotation has on the equivalent widths of the D lines. The second section considers the variation of the equivalent widths with color excess.

I. VARIATION WITH GALACTIC LONGITUDE

Following van Rhijn,[2] we analyze not the equivalent widths of D1 and D2 directly but rather the distance modulus obtained from these equivalent widths. The procedure is to divide the stars into two groups, one group near the null points of galactic rotation and the other away from the nulls. For each group the mean distance modulus is obtained from the D-line equivalent widths and is compared with the mean distance modulus obtained by spectroscopic means.

[1] L. Spitzer, Jr., *Ap. J.*, **108**, 276, 1948.

[2] *Groningen Pub.*, No. 53, p. 37, 1949.

The observational material was obtained from the following sources. The equivalent widths of D1 and D2 were taken from the list published by Merrill, Sanford, Wilson, and Burwell.[3] Additional equivalent widths were obtained from the list in Paper I. Spectroscopic moduli, corrected for interstellar absorption, were obtained from lists kindly communicated in advance of publication by Miss J. Ramsey[4] and W. W. Morgan. Additional sources were lists published by O'Keefe[5] and Williams.[6] All moduli were reduced to the system of Morgan and Ramsey by comparison of stars common to both. Color excesses were taken from the catalogue by Stebbins, Huffer, and Whitford.[7]

To test the longitude effect, four groups of stars were selected as follows:

Group 1: $E_1 > 0.15$; $|G| > 0.700$; $m_0 - M_{sp} \geq 9.0$; $|b| \leq 5°$;

Group 2: $E_1 > 0.15$; $|G| < 0.500$; $m_0 - M_{sp} \geq 9.0$; $|b| \leq 5°$;

Group 3: $E_1 > 0.15$; $|G| > 0.700$; $m_0 - M_{sp} \geq 11.0$; $|b| \leq 5°$;

Group 4: $E_1 > 0.15$; $|G| < 0.500$; $m_0 - M_{sp} \geq 11.0$; $|b| \leq 5°$.

All stars chosen have photoelectric color excesses E_1 greater than 0.15, and all are within 5° of the galactic plane. Exclusion of less reddened stars helps select those stars with the relatively stronger, more saturated lines, for which the effect of galactic rotation on the equivalent widths should be greatest. The quantity G, which equals $\sin 2(l - l_0) \cos^2 b$, gives the longitude grouping; l_0 was set equal to 330°. Groups 2 and 4 contain stars near the nulls; groups 1 and 3, stars far from the nulls. In the spectroscopic distance modulus, $m_0 - M_{sp}$, M_{sp} is the absolute visual magnitude, while m_0 equals $m - 7E_1$, the apparent visual magnitude corrected for interstellar absorption. Thus groups 3 and 4 contain stars at larger distances.

The equivalent widths of D1 and D2 were corrected for galactic latitude, by means of a formula given by van Rhijn.[8] These corrected values were then used to obtain the distance r of each star, by use of van Rhijn's relation[9] between distance and equivalent width; his longitude correction, however, was not used. From these distances the mean distance modulus $\overline{m_0 - M_i}$ was obtained for each group. Then $\overline{m_0 - M_{sp}}$ was determined and $\overline{M_{sp} - M_i}$ found. These quantities are given in Table 1, along with the

TABLE 1

Group	$\bar{E}_1$	$\overline{\lvert G \rvert}$	$\overline{m_0 - M_{sp}}$	$\overline{m_0 - M_i}$	$\overline{M_{sp} - M_i}$	n
1	0.29	0.922	11.0	11.6	$+0.6 \pm 0.2$	31
2	.26	.286	10.3	10.4	$+ .1 \pm .2$	12
3	.29	.933	11.5	11.8	$+ .3 \pm .2$	18
4	0.21	0.257	11.4	11.1	-0.3 ± 0.4	4

average values of E_1, and $|G|$. In the next-to-last column are listed values of the probable error of the mean $M_{sp} - M_i$ for the n stars in each group; values of n are given in the last column.

The average value of $M_{sp} - M_i$ is affected by a number of possible errors, including inaccuracy in the correction for galactic latitude, zero point of the color excesses, etc. However, these errors should affect different groups in much the same way, and the

[3] *Ap. J.*, **86**, 274, 1937.
[4] *Ap. J.*, **111**, 434, 1950
[5] *Ap. J.*, **94**, 353, 1941.
[6] *Ap. J.*, **83**, 305, 1936.
[7] *Ap. J.*, **91**, 20, 1940.
[8] *Groningen Pub.*, No. 50, p. 9, 1946.
[9] *Ibid.*, p. 21.

difference between groups 1 and 2 seems real. The difference between groups 3 and 4 is of the same magnitude, but the number of stars in group 4 is too few for reliable conclusions. The general trend is that, for stars near the nulls of galactic rotation, the distance moduli obtained from the equivalent widths of the D lines are too small by about 0.5 mag., compared with the corresponding distance moduli for stars at the same spectroscopic distance near the maxima of galactic rotation. In other words, for stars near the nulls and about 1000 parsecs away, the equivalent widths of the D lines are smaller by a factor of about 1.2 than for stars at the same distance but far from the nulls, in agreement with the conclusions of Paper I. This result will presumably not hold for closer stars, for which the radial velocities resulting from galactic rotation are small compared with the random cloud velocities.

Since the probable errors in Table 1 are about half the difference under discussion, the present analysis is by no means conclusive, but it nevertheless provides some confirmation of the longitude variation found in Paper I. It would be surprising theoretically if such a variation did not exist. It is known that the equivalent widths of the saturated D lines depend primarily on the dispersion of radial velocities for the interstellar clouds in the line of sight. This dispersion is between 5 and 10 km/sec for close stars and can scarcely escape being increased by galactic rotation for stars 1000 parsecs or more away, if these are not near the null points for the radial velocity due to galactic rotation. Unless, as suggested by Unsöld,[10] the dispersion in cloud velocities increases with distance in all directions, the resultant variation of equivalent width with galactic longitude should be observable. We conclude that the observations are apparently not inconsistent with the theory presented in Paper I. The differing conclusion by van Rhijn is presumably the result of his including both *Na* and *Ca* lines in his analysis. Since the theory of Paper I is apparently not applicable to *Ca*, it is not surprising that an analysis of both types of interstellar lines together should yield results at variance with the theory.

II. VARIATION WITH COLOR EXCESS

In his discussion of the correlation between the interstellar D lines and color excess, for stars at the same distance, van Rhijn[2] uses radial velocities, both of the stars and of the interstellar lines, as distance criteria, employing the familiar formula for the radial velocity due to galactic rotation. Here we apply his analysis to the D lines alone. Only stellar radial velocities will be used, since one may suspect some correlation between the radial velocities of the D lines and their equivalent widths.

The observational material of the first section was employed here directly. For stars with no recent individual determinations of spectroscopic distance modulus, the values of the distance modulus given by Stebbins, Huffer, and Whitford[7] were employed. The stellar radial velocities required were obtained primarily from the stellar radial-velocity catalogue compiled and published at Lick.[11] A few additional velocities were taken from the Poulkovo publications[12] and from a list by F. J. Neubauer.[13] Vyssotsky's recent value[14] of the solar motion, found to be 15 km/sec toward the apex $\alpha_0 = 265°$, $\delta_0 = +20°.7$, was removed from all the radial velocities. The final residual radial velocity, denoted by ρ, should, on the average, obey the formula for galactic rotation,

$$\rho = K + rAG\,, \tag{1}$$

where K is a small constant term which, according to van Rhijn,[15] has the value $+2.1$; r is the distance of the star from the sun, and A is Oort's constant, taken to be 0.018 km/sec per parsec.

[10] *Zs. f. Phys.*, **125**, 370, 1948.

[11] *Pub. Lick Obs.*, Vol. **18**, 1932.

[12] V. A. Albitzky and G. A. Shajn, *Pub. Obs. Central Poulkovo*, Ser. II, Vol. **43**, 1933.

[13] *Ap. J.*, **97**, 303, 1943.

[14] *A.J.*, **56**, 58, 1951.

[15] *Groningen Pub.*, No. 50, p. 29, 1946.

To test the effect of color excess on the distance-intensity relation, two groups were selected as follows:

Group 1: $E_1 \leq 0.10$; $9.0 \leq m_0 - M_{sp} \leq 11.0$; $|b| < 5°$;

Group 2: $0.20 \leq E_1 \leq 0.30$; $9.0 \leq m_0 - M_{sp} \leq 11.0$; $|b| < 5°$.

As in van Rhijn's work, $m_0 - M_{sp}$ is used for grouping the stars, and errors in this quantity should not invalidate conclusions based on mean values of other quantities for these groups. Two other groups with $m_0 - M_{sp}$ between magnitudes 7 and 9 were considered but were subsequently dropped. In view of the considerable dispersion in stellar velocities, the small distances of the stars, and the relatively few stars in each group, the radial velocities provide no useful measure of distance for these two groups of closer stars.

For each group, the average values $\bar{E}_1$, $\bar{D}$, $\overline{m_0 - M_{sp}}$ and $\overline{m_0 - M_i}$ were computed and are given in Table 2. The average value of $\bar{r}$ was determined for each group by a

TABLE 2

Group	$\bar{E}_1$	$\bar{D}$	$\overline{m_0 - M_{sp}}$	$\overline{m_0 - M_i}$	$\overline{m_0 - M_\rho}$	n
1.....	0.04	0.36	10.0	8.6	8.6±0.5	18
2.....	0.24	0.56	10.0	10.2	10.7±0.3	13

least-squares solution of equation (1). This was converted to an average distance modulus $m_0 - M_\rho$, using the relation

$$\overline{\log r} = \log \bar{r} - 0.046 \qquad (2)$$

given by van Rhijn.[16] The constant in this formula takes account of the dispersion in $\log r$ for stars with a given value of $m_0 - M_{sp}$. A smaller correction, for the finite range of $m_0 - M_{sp}$ present in each group considered, was not applied. Values of the quantity $m_0 - M_\rho$, together with the probable error of this mean for each group, are also given in Table 2. The final column gives the number of stars, n, in each group. Only about two-thirds of the stars in each group have a value of G of $\frac{1}{2}$ or more; most of the remaining one-third of the stars have a low weight in the solution for $m_0 - M_\rho$. The values of $\overline{m_0 - M_{sp}}$, which are given in Table 2 for comparison with the other moduli, are mostly based on mean values of M_{sp} for each spectral type, instead of on the individual spectroscopic absolute magnitudes used in the previous section. Unfortunately, individual absolute magnitudes are not available for most of these distant stars.

If we now compare groups 1 and 2 in Table 2, it appears from the values of $\overline{m_0 - M_\rho}$ that the mean distances of these two groups are different by a factor of nearly 3, with the unreddened stars only about 500 parsecs away, as compared with over 1000 parsecs for the reddened stars. Since the values of $\overline{m_0 - M_i}$ agree well with those of $\overline{m_0 - M_\rho}$, one may conclude that the correlation appearing between E_1 and D for these two groups is largely the result of the correlation of both E_1 and D with distance. In view of the considerable dispersion of stellar radial velocities, the mean value of $m_0 - M_\rho$ is not sufficiently trustworthy to warrant a detailed comparison with $\overline{m_0 - M_i}$. The chief conclusion obtained from the comparison of the two groups is that unreddened stars with distance moduli of about 10.0 are, in reality, fainter stars at closer distances. Hence the low values of D for large r found for unreddened stars in Figure 12 of Paper I must actually be attributed to errors in the spectroscopic distances. Since these distances are

[16] *Ibid.*, p. 17.

largely based on mean absolute magnitudes for each spectral type, instead of on individually determined spectroscopic absolute magnitudes, large errors need occasion no surprise. If there are any unreddened stars in the galactic plane at distances of 1000 parsecs or more, Figure 12 of Paper I indicates that their interstellar D lines must be weaker than the average for that distance; but the present results indicate that such stars, if any, are relatively few.

It would be interesting to test with the present analysis the reality of the correlation found in Paper I between E_1 and the number of *Na* I atoms in the line of sight. Unfortunately, van Rhijn's method cannot be used for the close stars, since the radial velocity due to galactic rotation becomes very small compared with the random stellar velocities.

The chief evidence for the concentration of *Na* I atoms in the same clouds containing interstellar grains is the marked correlation between the doublet ratio D_2/D_1 and the color excess E_1; this correlation is shown in Figures 6–9 of Paper I. Especially for an equivalent width $(D_1 + D_2)/2$ of about 0.40 A, the reddened stars show unmistakably more saturated D lines than do the unreddened stars. Since there is little indication of any distance correlation in these diagrams, this result seems observationally secure and leads directly to the conclusion that a large fraction of the *Na* I atoms must be concentrated in the obscuring clouds responsible for selective extinction. It follows immediately that some correlation between $D_1 + D_2$ and E_1 must be present for stars at the same distance, although saturation of the D lines will weaken this correlation as compared to the correlation between E_1 and the number of *Na* I atoms in the line of sight.

A COMPARISON OF THE COMPONENTS IN INTERSTELLAR SODIUM AND CALCIUM*

PAUL MCRAE ROUTLY AND LYMAN SPITZER, JR.
Princeton University Observatory
Received October 11, 1951

ABSTRACT

Radial velocities and equivalent widths of the interstellar D lines, including a number of faint components, were obtained for some twenty stars from high-dispersion spectrograms taken at the Mount Wilson Observatory. Corresponding measures in *Ca* II were also obtained for four stars.

This material, together with additional measures obtained previously by other investigators, was employed in a comparison between *Na* and *Ca*. For each component $N(Na\,\text{I})$ and $N(Ca\,\text{II})$, the numbers of absorbing *Na* I atoms and *Ca* II ions in the line of sight, were found whenever possible, as were also the values of the Doppler widths $b(Na\,\text{I})$ and $b(Ca\,\text{II})$. For strong components, the data indicate that $b(Ca\,\text{II})$ in kilometers per second is about 1.5 times $b(Na\,\text{I})$, in qualitative agreement with Wilson's analysis; but for weaker lines these Doppler widths are more nearly equal. On the average, a marked decrease occurs in $N(Na\,\text{I})/N(Ca\,\text{II})$ as the residual radial velocity of the component increases in absolute value; in low-velocity clouds *Na* I tends to be more abundant than *Ca* II, while in high-velocity clouds the reverse is true. This result apparently explains why the strong saturated lines of *Na* I and *Ca* II do not lie on the same curve of growth [$b(Ca\,\text{II}) > b(Na\,\text{I})$].

Consideration is given to the possibility that differences of ionization between high-velocity and low-velocity clouds may explain this variation of abundance ratio with cloud velocity. In a rapidly moving cloud the kinetic temperature should be increased, since the intercloud gas in front of the cloud will be compressed and heated. At a temperature somewhere between 5000° and 10,000°, collisional ionization of *Na* I by electrons would reduce the ratio $N(Na\,\text{I})/N(Ca\,\text{II})$ by the observed factor. However, it is uncertain whether the temperature can be so high, and other mechanisms may be important.

I. INTRODUCTION

Indication of the existence of interstellar calcium clouds was first obtained in 1936 by C. S. Beals,[1] who found evidence of complex structure in the interstellar K lines of ϵ and ζ Orionis and ρ Leonis. During the next decade, W. S. Adams much extended the high-dispersion observations of interstellar calcium and showed that, on the average, one star in every two possessed multiple components. In 1943 Adams published a provisional list on the structure of the H and K lines in fifty stars of early type[2] and in 1949 extended the list to three hundred stars.[3] His work includes visual estimates of intensity for the various K-line components, together with accurate determinations of their radial velocities. The following year quantitative measures of equivalent widths of the components of K and H were obtained from Adams' plates by Spitzer, Epstein, and Li Hen.[4]

Owing to greater observational difficulties, the high-dispersion data on *Na* I have not kept pace with those on *Ca* II. Sanford, Merrill, and Wilson[5] showed that the interstellar D lines in ρ Leo and in several stars in Orion were clearly double and that the radial velocities of the components agreed well with the corresponding values obtained from H and K. The existence of interstellar sodium clouds, directly confirmed by this work, had been deduced in 1937 by Merrill and Wilson[6] in an analysis of D-line measure-

* This article is based on observations made by the senior author as guest investigator at the Mount Wilson and Palomar Observatories. The work was supported in part by a contract with the Office of Naval Research.

[1] *M.N.*, **96**, 661, 1936.
[2] *Ap. J.*, **97**, 105, 1943.
[3] *Ibid.*, **109**, 354, 1949.
[4] *Ann. d'Ap.*, **13**, 147, 1950.
[5] *Pub. A.S.P.*, **50**, 58, 1938.
[6] *Ap. J.*, **86**, 44, 1937.

ments by Merrill, Sanford, Wilson, and Burwell.[7] Although the spectrograms were not of sufficiently high dispersion to show faint components, Merrill and Wilson, in order to explain the data, were forced to the view that the interstellar sodium gas was not distributed homogeneously but was concentrated in the form of clouds. More recently, Merrill and Wilson[8] published preliminary equivalent-width measures of strong and faint D-line components in ρ Leo and χ^2 Ori, along with similar data for *Ca* II; in five other stars the weaker components of the D lines could not be seen on the spectrograms.

A number of puzzling differences result from a comparison between the interstellar lines of *Na* I and *Ca* II. Wilson[9] demonstrated one such difference in 1939 by combining the previous analyses of Wilson and Merrill[6] for *Na* I and of Sanford and Wilson[10] for *Ca* II. Wilson used so-called "ratio-curves" of D2/D1 versus D1 and K/H versus H. For the weakest lines the doublet ratio equals 2 but decreases with growing line strength and becomes nearly constant for line strengths exceeding 0.3 A. The surprising feature of these curves, verifying earlier data of Beals, was that the *Ca* II ratio leveled off at a value of approximately 1.58, whereas the *Na* I ratio lay much lower, at 1.20. On fitting these observed ratio-curves by means of theoretical curves of growth, each characterized by a mean velocity parameter or Doppler constant b, Wilson showed that $b(Na\ \text{I}) = 0.12$ A and $b(Ca\ \text{II}) = 0.24$ A, corresponding to mean velocities of 7.5 km/sec for *Na* I and 22 km/sec for *Ca* II. Wilson proposed two alternatives: either a physical mechanism operates which permits the small-scale *Na* I and *Ca* II velocities to differ considerably in the same region of space, with the heavier atoms possessing the higher velocity, or the application of the curve of growth is invalid. Jentzsch and Unsöld[11] have considered the theoretical aspects of this problem further and have shown clearly that the anomalous behavior of the ratio-curves cannot be explained by a uniform difference between the abundance of *Na* I and *Ca* II, by a superposition of velocity distributions common to *Na* I and *Ca* II, or by any combination of both.

Other interesting differences appear between interstellar *Na* I and *Ca* II when faint components are intercompared. Merrill and Wilson[8] found that, while the most intense component of *Na* I is considerably stronger than the corresponding component in *Ca* II, the weaker *Na* I components tend to appear weaker than the corresponding *Ca* II components, if, indeed, they are visible at all. Jentzsch and Unsöld[11] have pointed out that exactly the opposite effect would occur if the ratio of *Na* I to *Ca* II atoms were the same in all interstellar clouds.

The present investigation was undertaken to extend the high-dispersion interstellar observations on *Na* I and to carry out a more thorough comparison than has hitherto been possible with the interstellar *Ca* II data.[3,4] The six sections which follow are concerned with the observational material, measurement of radial velocities, measurement of equivalent widths, interpretation of the observational data, theoretical discussion, and, finally, a summary of the results obtained.

II. OBSERVATIONAL DATA

Observations on interstellar lines in twenty-three stars are presented in this paper. The stars observed are primarily those which showed[3] well-resolved components of H and K. Most of the plates were obtained at the coudé spectrograph of the 100-inch telescope of the Mount Wilson Observatory, chiefly during the summer and fall of 1950, with a few plates obtained in 1947 and 1948. In addition, several plates were kindly taken for this program by Drs. Ira Bowen and O. C. Wilson at the coudé focus of the Hale 200-inch telescope on Mount Palomar. Also included are observations by Merrill and Wilson, who had previously published[8] only the sum of the equivalent widths of

[7] *Ap. J.*, **86**, 274, 1937.
[8] *Pub. A.S.P.*, **59**, 132, 1947.
[9] *Ap. J.*, **90**, 244, 1939.
[10] *Ap. J.*, **90**, 235, 1939.
[11] *Zs. f. Phys.*, **125**, 370, 1948.

D2 and D1 (or of K and H) for each component, but who generously made available the detailed measures from their high-dispersion plates. For six stars, sodium observations were available, but the calcium determinations were of low accuracy or were lacking altogether. In such cases, additional *Ca* II plates were taken by the present authors. Table 1 gives the HD number for all stars observed, together with stellar name, right ascension, and declination for the epoch 1900, galactic longitude and latitude, spectral type, and apparent magnitude. Most of the information was taken from the *Henry Draper Catalogue*.

TABLE 1

STARS OBSERVED FOR INTERSTELLAR LINES

Star HD	Name	R.A. (1900)	Decl. (1900)	l	b	Sp.	m
21278	.....	3^h20^m9	+48°43′	115°	−05°	B5	4.9
24912	ξ Per	3 52.5	+35 30	128	−12	O7	4.0
36822	ϕ^1 Ori	5 29.3	+09 25	163	−11	B0	4.5
36861	λ^1 Ori	5 29.6	+09 52	163	−11	O8	3.7
37043	ι Ori	5 30.5	−05 59	177	−18	O8	2.9
37128	ε Ori	5 31.1	−01 16	173	−16	cB0	1.8
37468	σ Ori	5 33.7	−02 39	174	−16	B0	3.8
37742	ζ Ori	5 35.7	−02 00	174	−15	B0	2.0
38771	κ Ori	5 43.0	−09 42	182	−17	cB0	2.2
41335	.....	5 59.4	−06 42	181	−12	B2e	5.1
42087	3 Gem	6 03.7	+23 08	155	03	B2	5.8
91316	ρ Leo	10 27.5	+09 49	204	54	cB1	3.8
166937	μ Sgr	18 07.8	−21 05	338	−03	cB8e	4.0
167264	15 Sgr	18 09.3	−20 46	338	−03	B0	5.4
169454	.....	18 19.6	−14 02	345	−02	B0e	6.8
175754	.....	18 51.7	−19 17	344	−11	B0p	7.0
184915	κ Aql	19 31.5	−07 15	0	−15	B0	5.0
190429	.....	19 59.8	+35 45	40	02	O	7.8
193322	.....	20 14.6	+40 25	46	02	O8	5.8
199478	.....	20 52.4	+47 02	55	01	cB8e	5.8
212978	.....	22 23.1	+39 19	63	−15	B3	6.1
214680	10 Lac	22 34.8	+38 32	65	−17	O9	4.9
214993	12 Lac	22 37.0	+39 43	66	−17	B1	5.2

The three cameras available at the 100-inch coudé have focal lengths of 114, 73, and 32 inches. In 1947 to 1949 the grating available gave a dispersion for these three cameras of 2.84, 4.49, and 10.3 A/mm, respectively, in the second order, used for the observations of K and H. Observations of the D lines were made in the first order, with correspondingly less dispersion. In 1950 a new grating was available; for K and H, observed in the third order, the dispersion was the same as with the old grating in the second order, but for the D lines, observed in the second order, the dispersion was 4.26, 6.73, and 15.3 A/mm, respectively. For the relatively few bright stars in Table 1, the 114-inch camera was used for both *Na* I and *Ca* II, while for the fainter stars the 73-inch camera was employed almost exclusively. The 32-inch camera was used only for those few faint stars in which the separation of the components was at least 45 km/sec. The four Palomar plates yielding equivalent-width measures were all taken with the 144-inch camera, with a dispersion in the yellow of 3.41 A/mm.

The 103*a*-D Eastman plate was used for *Na* I, and the Eastman IIa-O, usually

baked for several days, for *Ca* II. The exposure times for the *Na* I observations were long, averaging from 3 to 5 hours; those of the *Ca* II observations were considerably shorter, resulting from increased emulsion sensitivity and greater stellar flux in the blue. The long exposure times and the relative coarseness of the plate grain in yellow-sensitive emulsions make it more difficult to observe faint components in *Na* I than in *Ca* II.

III. MEASUREMENT OF RADIAL VELOCITIES

Measurements of the radial velocities were carried out in the standard way. The reliability of each measure was estimated on an arbitrary scale, ranging in decreasing factors of 2 from 2 to $\frac{1}{8}$, and was based upon a general over-all impression of each plate. These numerical weights were used in combining different measures of velocity for a given component. Probable errors corresponding to these weights were calculated from the differences between values obtained from different plates of the same star and are presented in Table 2 for the *Na* measures. Because of the variety of cameras used and

TABLE 2

PROBABLE ERRORS OF SODIUM RADIAL VELOCITIES IN KM/SEC

WEIGHT	SPECTROGRAPHIC CAMERA		
	114-Inch	73-Inch	32-Inch
2	0.8	0.8	3.8
1		1.0	
$\frac{1}{2}$	1.4	.....	3.9
$\frac{1}{4}$	.....	.....	.....
$\frac{1}{8}$	2.5	.....	.....

the lack of sufficient data, it was found necessary to group some of the weights in pairs. The only probable error that could be derived for calcium was 1.3 km/sec, referring to a measure of weight 2 taken with the 32-inch camera. The observational material is rather meager to admit probable error determinations of good quality in all cases. It is felt, however, that the probable errors for the sodium observations of weights 2 and 1, taken with the 114- and 73-inch cameras, are reliable. The approximate correctness of the weighting system is indicated by the fact that the probable errors in Table 2 are about proportional to the inverse square root of the weights.

The agreement between the radial velocity of a component as measured on the *Na* I plates and the corresponding component as measured by Adams[3] in *Ca* II is good. The root-mean-square deviation between the two sets of radial velocities is 2.5 km/sec. In this comparison, Adams' radial velocities have been increased by the constant amount of 1.5 km/sec to account for the fact that Adams used solar wave lengths for H and K, whereas the laboratory values have been adopted in this paper.

Table 3 gives the results of the radial-velocity and equivalent-width measures. Unless otherwise indicated, all the values appearing in the table have been obtained by the present authors. Data on *Ca* II have been included only in those cases where new measures were carried out. Columns 1 and 2 indicate the HD number of the star and the element under consideration. Column 3 denotes the number of plates taken and the cameras used; the notation "3—114″" means that 3 plates were taken with the 114-inch camera. Column 4 gives the order in which the components of the interstellar lines are observed

to occur in *Ca* II. The number 1 is assigned to the most shortward component; the remaining components are then numbered in orderly sequence toward longer wave lengths. In columns 5 and 6 the radial velocities of the D lines and their components (or of the *Ca* II lines) are listed, together with the weight of each determination. In those cases where the radial velocity of blends was measured, the numbers of the two blended components are given in column 4. In the notes at the bottom of Table 3 acknowledgment is made to the work of others, suggestions offered as to the possible existence of com-

TABLE 3

MEASURES OF RADIAL VELOCITIES AND EQUIVALENT WIDTHS

HD No. (1)	El. (2)	Plates (3)	Comp. (4)	R.V. (Km/Sec) (5)	Wt. (6)	D2 or K† (A) (7)	Wt. (8)	D1 or H (A) (9)	Wt. (10)
21278*.....	*Na* I	2—73″	1	+ 1.6	1	0.197	1	0.179	1
			2	.....	.....	< .014	.....	.....	.....
	Ca II	1—73″	1	+ 1.6	½	.061	¼	.040	½
24912, ξ Per....	*Na* I	2—114″	1	+11.8	1	.252	⅜	.198	⅜
			2	.....	.....	< .010	.....	.....	.....
36822*, φ′ Ori...	*Na* I	2—73″	1	.....	.....	< .014	.....	.....	.....
			3	+24.2	1	.29	1	.20	1
36861*, λ′ Ori...	*Na* I	2—114″	1	+ 1.9	⅛	.022	½		
			2	+12.1	⅛	.066	*E*	.204	1
			3	+25.0	4	.207	1		
	Ca II	.....	1	.....	.....	.073	2	.039	2
			2, 3	.....	.....	.094	2	.053	2
37043*, ι Ori....	*Na* I	2—114″	1	+ 4.4	½	.072	2	.057	2
			2	+25.4	¼	.055	2		
37128, ε Ori....	*Na* I	1—114″	1, 2	.....	.....	.091	*E*	.047	*E*
			3	.....	.....	.124	1	.074	1
37468, σ Ori....	*Na* I	1—73″	1	− 2.6	1	.064	*E*	.025	*E*
		1—114″	2	+22.1	2	.183	1	.145	1
37742, ζ Ori....	*Na* I	5—114″	1	− 4.0	6	.060	1	.025	2
			2	+11.9	1	.023	*E*	.018	*E*
			3	+22.8	7	.145	4	.090	3
	Ca II	1—114″	1	.....	.....	.017	1	.011	1
			3	.....	.....	.035	1	.022	1
38771*, κ Ori...	*Na* I	.....	1	− 0.4	.....	.141	4	.094	4
			2, 3	+22.4	.....	.054	*E*	.025	*E*
	Ca II	.....	1	.....	.....	.052	¼	.022	¼
			2, 3	.....	.....	.043	¼	.016	¼
41335.....	*Na* I	1—73″	1	.....	.....	< .006	.....	.....	.....
			2	+19.9	1	.197	1	.102	1
42087, 3 Gem...	*Na* I	2—73″	1	−24.0	¼	.027	½	.010	¼
		1—144″	2, 3	+14.1	3	.542	1	.486	1
91316*, ρ Leo...	*Na* I	.....	1, 2	− 5.8	.....	.124	2	.058	2
			3	+23.1	.....	.043	1	.012	½
	Ca II	.....	1	.....	.....	.075	2	.037	2
			2, 3	.....	.....	.050	1	.017	1
166937, μ Sgr....	*Na* I	2—73″	2	− 6.7	⅜	.202	¼	.164	¼
			4	.....	.....	< .014	.....	.....	.....
167264*, 15 Sgr..	*Na* I	3—73″	1	− 9.4	3	.281	1	.215	1
			2	+ 5.7	2	.032	*E*	.035	*E*
			3	+28.6	2	.041	1	.032	1
169454.....	*Na* I	2—32″	1	− 7.9	1	.680	⅜	.680	⅜
			2	+81.7	1	.152	⅜	.112	⅜
	Ca II	1—32″	1	− 5.8	½	.522	1	.382	½
			2	+83.5	¼	.080	1	.111	*E*
175754*.....	*Na* I	1—32″	1	.....	.....	< .020	.....	.....	.....
			2	− 8.3	½	0.454	2	0.305	2

TABLE 3—*Continued*

HD No. (1)	El. (2)	Plates (3)	Comp. (4)	R.V. (Km/Sec) (5)	Wt. (6)	D2 or K† (A) (7)	Wt. (8)	D1 or H (A) (9)	Wt. (10)
184915*, κ Aql	*Na* I	1—73″	1	−10.8	½	0.29	1	0.22	1
			2			< .020			
190429	*Na* I	3—32″	1			< .008			
		1—144″	2	−33.7	⅛	.090	½	.091	½
			3	− 6.3	⅛	.886	1	.783	1
	Ca II	1—32″	1	−77.7	½	.125	1	.108	¼
			3	−10.1	½	.406	1	.286	¼
193322	*Na* I	2—73″	1			< .022			
			3	−11.7	1	.475	½	.425	½
199478*	*Na* I	2—73″	1, 2	−12.6	3	.535	2	.483	2
		1—144″	3	+22.0	½	.022	½	.021	½
			4	+43.5	2	.081	1	.061	1
212978	*Na* I	1—144″	1			< .008			
			2	−12.2	2	.313	1	.213	1
	Ca II	1—73″	2	−10.9	⅛	.088	2	.064	2
214680*, 10 Lac	*Na* I		1, 2	−31.5		.103	¼		
			3	− 8.5		.237	1	.192	1
	Ca II		1, 2			.055	2	.021	2
			3			.076	2	.042	2
214993, 12 Lac	*Na* I	1—73″	1			< .016			
			2	−10.6	1	0.240	½	0.195	½

NOTES TO TABLE 3

1. Merrill, Sanford, Wilson, and Burwell, *Ap. J.*, **86**, 274, 1937.
2. Merrill and Wilson, elaboration of observations contained in *Pub. A.S.P.*, **59**, 132, 1947.
3. Spitzer, *Ap. J.*, **108**, 274, 1948.

† Equivalent widths preceded by a < sign refer to upper limits described in the next section.

HD 21278 Possible component in *Na* I at 19 km/sec.
HD 36822 Equivalent widths of component 3 in *Na* I by 1.
HD 36861 Equivalent widths of *Ca* II by 2.
HD 37043 Remarkable revetsal observed in this star; stronger component in *Na* I actually the weaker in *Ca* II.
HD 38771 Radial velocities of *Na* I by 2; equivalent widths of *Na* I partly by 2; equivalent widths of *Ca* II by 2.
HD 91316 Radial velocities of *Na* I by 2; equivalent widths of *Na* I and *Ca* II by 2.
HD 167264 Possible component in *Na* I at 56 km/sec.
HD 175754 Possible component in *Na* I at 31 km/sec.
HD 184915 Equivalent widths of component 1 in *Na* I by 3.
HD 199478 Possible component in *Na* I at −47 km/sec.
HD 214680 Radial velocities in *Na* I by 2; equivalent widths of *Na* I and *Ca* II by 2.

ponents in *Na* I not seen in *Ca* II, etc. The remaining columns in Table 3 will be described in the next section dealing with the measurement of the equivalent widths.

IV. MEASUREMENT OF EQUIVALENT WIDTHS

The general technique of measuring equivalent widths has been described many times.[12] Two series of calibration spectra were exposed on either side of the stellar spectrum in the usual way, and calibration-curves of the photographic plates were derived from them. Particular care was taken to assure uniform illumination over the slits producing the calibration spectra; and the stellar and calibration spectra exposure times were made as nearly equal as possible, so as to avoid any complications due to reciprocity failure. Special difficulties were encountered in drawing the profiles of the sodium interstellar components on the tracings because of the coarse plate grain. In handling blends between a weak and a strong component, the procedure outlined by Spitzer, Epstein, and Li Hen was followed.[4]

Each individual measure of equivalent width was assigned a numerical weight of 1, ½,

[12] See, e.g., Williams, *Ap. J.*, **79**, 280, 1934.

or ¼; the letter *E* was reserved to indicate those components which were incompletely resolved from another component. In combining several measures of the same component, the numerical weights were added, but the weight *E* was not; the result of two *E* measures was still taken as *E*. Percentage probable errors, corresponding to these weights, were calculated and are given in Table 4. Because of insufficient data, the probable errors were not broken down for the separate cameras; Spitzer, Epstein, and Li Hen found in their work on *Ca* II that, on the average, the probable errors were independent of the camera focal lengths, since the higher dispersion was used only on the closer stars with weaker interstellar lines. The internal consistency of the weighting system may be checked from the requirement that observations of weight ¼ to ½ should have about 1.6 times the probable error of observations of weight 1. From Table 4 it is evident that the probable errors for weights ½ and ¼ are relatively too high. It was not thought worth while to carry out a revision of the weighting system. A comparison between the values of ½(D2 + D1), as obtained in this present work, and the few corresponding published

TABLE 4

PER CENT PROBABLE ERRORS OF EQUIVALENT-WIDTH MEASURES

Na I		*Ca* II	
Weights	Percentage	Weights	Percentage
1	8.1	1	5.9
½ and ¼	19	½ and ¼	24

values available from Merrill and Wilson and from Spitzer gives a root-mean-square percentage deviation of 16 per cent.

In several stars components were visible in *Ca* II but not in *Na* I. In each case an upper limit on the equivalent width of the corresponding component of D2 was determined in the following way. On the tracing of the spectrogram, the position at which this faint component of D2 would appear, if it existed, was located. A hypothetical absorption line was then drawn in with the same half-width as the instrumental profile and with the greatest depth which could escape certain detection of the component. The equivalent width of this feature, which depends on the graininess of the plate, the width of the spectrum, etc., was then taken as the upper limit for D2. The half-width of the instrumental contour was determined for each camera from the narrow lines in the iron arc. The values found were 7.6 and 12 km/sec for the 114- and 73-inch cameras, respectively, at the 100-inch coudé, and 8.4 km/sec for the 144-inch camera at the 200-inch. For the 32-inch camera a value of 27 km/sec was assumed, on the assumption that for a particular grating the half-width is inversely proportional to the focal length. Justification of this use of the instrumental contour in determining upper limits is indicated by the fact that, on the average, the widths of the faintest components actually observed are of the same order as the widths of the instrumental profiles.

Intensities of the D lines and their components (also a few new measures for K and H) are given in columns 7 and 9 of Table 3, together with their weights. Values in these columns preceded by a < sign designate the upper limits discussed above.

V. INTERPRETATION OF OBSERVATIONAL DATA

The method developed by Strömgren[13] has been used to obtain the number of absorbing atoms per square centimeter in each interstellar cloud, together with the dispersion

[13] *Ap. J.*, **108**, 242, 1948.

in atomic velocities. Table 2 of Strömgren's paper gives the doublet ratios (D2/D1 or K/H) as functions of $\log w^{(\lambda)}/b^{(\lambda)}$ and $\log N/w^{(\lambda)}$, where $w^{(\lambda)}$ represents the equivalent width of D1 or H, N the number of absorbing *Na* I atoms or *Ca* II ions per square centimeter in the line of sight; $b^{(\lambda)}$ is $2^{1/2}$ times the dispersion in atomic radial velocities and is expressed by Strömgren in angstroms. For purely thermal motions, we have

$$b^{(\lambda)} = \frac{\lambda_0}{c}\left(\frac{2kT}{A m_0}\right)^{1/2}, \tag{1}$$

where λ_0 is the wave length of either D1 or H, m_0 is the mass of unit atomic weight, and A is the atomic weight of the atom under consideration. More generally, b would contain a contribution resulting from internal turbulent motions within the cloud.

The values in Strömgren's Table 2 are based on a theoretical curve of growth obtained on the following assumptions: (1) that a single cloud is responsible for the interstellar absorption and (2) that the atoms within the cloud possess a Maxwellian velocity distribution, characterized by the effective velocity parameter b. In an extension of his analysis, Strömgren showed that the ratio $N/w^{(\lambda)}$ was not appreciably affected by the number of clouds which entered into the formation of $w^{(\lambda)}$, although the value of b was strongly affected. If the clouds themselves have a Maxwellian distribution of peculiar velocities, characterized by the Doppler constant b', then, for the case in which the clouds produced partially overlapping absorption lines, the effective b should lie somewhere between b and $(b^2 + b'^2)^{1/2}$. In the extreme case, where N clouds give rise to N nonoverlapping components, the effective b would equal N times the value of b for one cloud.

The values of N and b obtained from the present data by Strömgren's method are given in columns 4–7 of Table 5. The *Na* I doublet ratios, necessary for this method, were derived from Table 3, while the *Ca* II doublet ratios were calculated primarily from the equivalent-width measures of Spitzer, Epstein, and Li Hen.[4] In those cases where new *Ca* II measures were determined (Table 3), averages were taken with the values of Spitzer, Epstein, and Li Hen when such were available. The values of b have been converted from angstrom units to kilometers per second.

Table 5 includes only those lines and components for which good determinations of the N's or b's in both *Na* I and *Ca* II were possible. A few of the observations were omitted immediately on the grounds of low weight; a weight $\frac{1}{2}$ was considered as the lowest accuracy tolerable for any individual equivalent width. Further restrictions were imposed upon the values of the doublet ratios themselves for the calculation of the N's and the b's. No abundances were determined for components having a doublet ratio less than 1.10, while no b's were computed from doublet ratios greater than 1.80.

For an appreciable fraction of the observations used in Table 5, the doublet ratios initially exceeded 2. The lines so involved are all relatively weak. Such measures, showing anomalous values of D2/D1, were corrected by assuming the lines to be completely unsaturated and, therefore, to have doublet ratios equal to 2 exactly. The corrected value D'1 was then obtained by equating 3D'1 to the sum of the measured values of D1 and D2. The resulting changes in the original equivalent widths of D1 and D2 were found to be small in all cases. *Ca* II measures showing anomalous doublet ratios were corrected in the same way. Those abundances in Table 5 derived from equivalent widths altered in the manner described above are followed by dagger signs (†). The assumption of complete unsaturation was also used in one case (HD 36861) to split up a blend and in two other instances to provide values for the equivalent widths of D1 or H where measures of D2 or K only were available. Again the dagger sign was employed to draw attention to the corresponding abundances. Abundances preceded by a $<$ sign are obtained from the upper limits listed in Table 3.

Column 3 of Table 5 gives the residual radial velocities of the components listed in

TABLE 5

ABUNDANCES AND VALUES OF b FOR *Na* I AND *Ca* II

HD No. (1)	Comp. (2)	R.R.V. (Km/Sec) (3)	N(*Na* I) $\times 10^{-11}$ (4)	N(*Ca* II) $\times 10^{-11}$ (5)	b(*Na* I) (Km/Sec) (6)	b(*Ca* II) (Km/Sec) (7)
21278	1	− 2.0	192	10.6	2.34	1.74
	2	+46.4	< 0.62	1.30†	.....	.....
24912	1	+ 4.3	40.4	16.7	4.43	3.63
	2	+19.8	< 0.45	1.86†	.....	.....
36822	1	− 8.9	< 0.62	11.3	.....	.....
	2	+ 1.4	28.2	15.9	6.62	6.35
	3	+10.7	.....	.....	.....	.....
36861	1	− 8.4	0.98†	8.14	.....	.....
	2	+ 1.4 } 10.6	27.9†	11.9	.....	.....
	3	+11.9 }				
37043	1	−10.0	3.12†	2.04†	.....	.....
	2	+12.9	2.32†	10.2	.....	.....
37468	1	−14.3	2.67†	1.67†	.....	.....
	2	+ 9.1	30.2	3.72†	.....	.....
37742	1	−17.4	2.49†	2.96	.....	.....
	3	+ 8.9	10.8	5.65	4.38	1.51
38771	1	−14.9	12.7	3.53	.....	.....
	2	+ 5.4 } 8.7	2.31†	5.77	.....	.....
	3	+18.2 }				
41335	1	−16.9	< 0.27	2.04†	.....	.....
	2	+ 4.6	9.5	8.27	.....	.....
42087	1	−35.7	1.07†	5.30	.....	.....
	2	− 3.6 } 3.0	351	49.0	6.62	12.9
	3	+11.4 }				
166937	4	+39.1	< 0.62	4.65†	.....	.....
167264	1	+ 2.5 } 3.8	54.7	68.4	5.09	5.52
	2	+18.9 }				
	3	+40.6	5.95	11.2	0.713	4.46
169454	2	+94.5	18.1	23.6	3.06	2.26
175754	1	−74.6	< 0.89	8.36	.....	.....
	2	+ 3.3 } 7.3	41.1	56.5	11.2	14.4
	3	+28.0 }				
184915	1	+ 0.9	39.1	16.5	5.60	4.23
	2	+21.3	< 0.89	10.5	.....	.....
190429	1	−65.2	< 0.36	31.6	.....	.....
	3	+ 4.0	392	100	12.2	11.3
193322	1	−26.6	< 0.98	5.39	.....	.....
	2	−10.1				
	3	+ 0.4 } 2.2	256	69.1	6.11	9.07
	4	+10.8 }				
199478	1	− 7.8 } −2.6	349	48.2	6.62	17.8
	2	+ 3.0 }				
	4	+54.6	10.6	9.30	.....	.....
212978	1	−77.9	< 0.36	2.42†	.....	.....
	2	− 4.7	29.4	18.4	7.13	2.94
214680	1	−28.5 } −24.7	4.63†	4.65†	.....	.....
	2	−19.5 }				
	3	− 3.4	45.0	9.18	.....	.....
214993	1	−25.6	< 0.71	6.70†	.....	.....
	2	− 4.0	45.6	18.7	3.97	7.56

column 2. These values were obtained by taking straight arithmetical averages of the *Na* I and corresponding *Ca* II radial velocities[3] and then subtracting the solar motion obtained by Vyssotsky and Janssen:[14] $V = 15$ km/sec, $A = 265°$, and $D = 20°.7$. For interstellar work, the solar motion should be referred to a system of axes rotating around the galactic center with a velocity equal to the mean circular velocity of the solar neighborhood. Since the new solar motion seems to satisfy this requirement better than previous values, it was used in the present paper. No weights were assigned to the residual radial velocities, because Adams did not indicate the accuracy of his individual *Ca* II measures. In some cases the velocities in column 3 refer to blends of two components. Some of these mean values were derived from direct measurement; in others, estimates were obtained from the individual velocities of the two components, averaged with Adams' visual intensities as weights.

Figures 1 and 2 show the results of Table 5 in graphic form. In Figure 1, the values of $N(Na\ \text{I})/N(Ca\ \text{II})$ are plotted against the residual radial velocities of the clouds producing the components. It is difficult to state a probable error for the values of $N(Na\ \text{I})/N(Ca\ \text{II})$, since the error varies from point to point. By altering D2/D1 in one direction by its probable error, K/H in the opposite direction, recomputing $N(Na\ \text{I})$ and $N(Ca\ \text{II})$ through Strömgren's Table 2, and finally taking a grand average, we get the mean probable error as approximately a factor of 2 in either direction. Denoting the residual radial velocity by V, we see that Figure 1 exhibits two distinct features: first, a sharp peak about $V = 0$, with considerable scatter in the vertical co-ordinate, and, second, a pronounced falling-off for increasing values of $|V|$. While the maximum of the peak at $V = 0$ reaches a value of the order of 18, there exist no points having $|V| > 20$ km/sec for which $N(Na\ \text{I})/N(Ca\ \text{II})$ is definitely greater than unity. If we neglect momentarily those points in the vicinity of $V = 0$ for which $N(Na\ \text{I})/N(Ca\ \text{II}) < 1$ and which arise in the main from weak lines, a strong correlation is evident between $N(Na\ \text{I})/N(Ca\ \text{II})$ and the peculiar velocities of the interstellar clouds. For low-velocity clouds *Na* I is more abundant than *Ca* II, while for high-velocity clouds (> 20 km/sec) the reverse is true. That these conclusions result from a real velocity effect and are not due to cloud size is clearly shown by plotting $N(Na\ \text{I})/N(Ca\ \text{II})$ against $N(Na\ \text{I})$ or $N(Ca\ \text{II})$; neither plot indicates any detectable correlation whatever.

Those points lying in the vicinity of $V = 0$ and having $N(Na\ \text{I})/N(Ca\ \text{II}) < 1$ tend to weaken the correlation in Figure 1. The scatter at $V = 0$ is probably even greater than shown, because a considerable number of the low points involved correspond to upper limits on the *Na* I abundance. These low-lying points may have a possible origin in clouds which possess high space velocities but have small radial components. The data were considered too scanty to warrant a statistical analysis.

Figure 2 shows the relationship between $b(Ca\ \text{II})$ and $b(Na\ \text{I})$. Points corresponding to the weaker components considered lie in the lower part of the diagram and are relatively uncertain. One point [$b(Ca\ \text{II}) = 4.5$ km/sec, $b(Na\ \text{I}) = 0.71$ km/sec] lies so far from the straight lines shown that it could not even be plotted in Figure 2. However, except for this one point, all the weaker lines show *b*'s which are somewhat greater for *Na* I than for *Ca* II. Because of the large scatter, it is impossible to decide whether thermal motions [line (*a*) in Fig. 2] or turbulent motions [line (*b*)] prevail inside the interstellar clouds producing these components. One may conclude only that the *b*'s for these weaker lines are about equal.

The stronger lines behave quite differently. These lines, corresponding to points in the upper part of the diagram, are more highly saturated, and the *b*'s are more accurately determined. In this region of Figure 2, $b(Ca\ \text{II})$ is about 1.5 times as great as $b(Na\ \text{I})$, on the average. Evidently the saturated lines of *Na* I and *Ca* II do not lie on the same curve of growth. This result is in qualitative agreement with Wilson's conclusions, deduced from the *Na* I and *Ca* II "ratio-curves." However, Wilson's quantita-

[14] *A.J.*, **58**, 56, 1951.

tive result, that $b(Ca\ II)$ is 22 km/sec and $b(Na\ I)$ is 7.5 km/sec, exaggerates the difference between the b's. These earlier values were found on the assumption that b is the same for lines of all strengths—an assumption which we now know to be invalid.

A plausible explanation of this difference between $b(Na\ I)$ and $b(Ca\ II)$ may be given in terms of the correlation between $N(Na\ I)/N(Ca\ II)$ and V shown in Figure 1. Since the b's represent a mean velocity of the absorbing atoms, they govern the width of the line-absorption coefficient. Let L_ν denote the total line-absorption coefficient, including the effects of all clouds. Evidently, L_ν has a highly complex structure. The central part

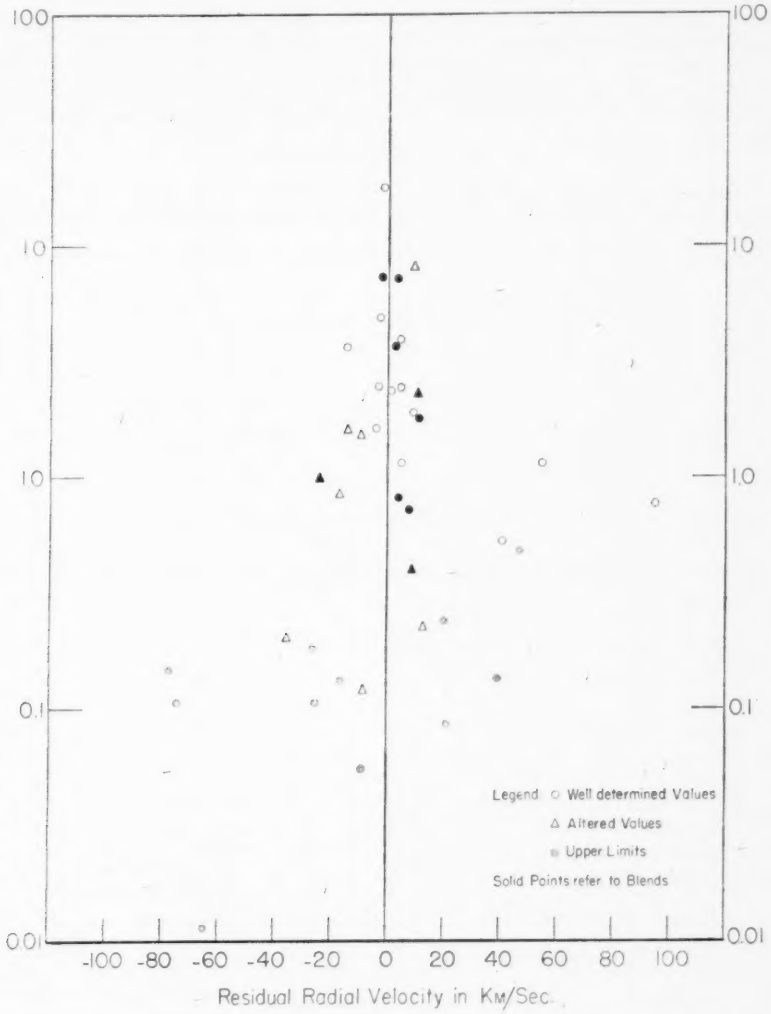

FIG. 1.—Plot of log $N(Na\ I)/N(Ca\ II)$ versus residual radial velocity

of L_ν is due to low-velocity clouds having more *Na* I than *Ca* II (Fig. 1); consequently, the central height of L_ν for *Na* I is greater than for *Ca* II. On the other hand, the wings of L_ν arise from high-velocity clouds, where *Ca* II is more abundant than *Na* I; thus the wings of L_ν for *Ca* II are wider than the wings of L_ν for *Na* I. The final result is a sharply peaked line-absorption coefficient for *Na* I and a lower but broader absorption coefficient for *Ca* II. The effect is illustrated schematically in Figure 3, which shows how $b(Ca\ \text{II})$ for highly saturated lines may exceed $b(Na\ \text{I})$.

It might appear possible to verify the result $b(Ca\ \text{II}) > b(Na\ \text{I})$ by measuring the half-widths of a number of saturated lines directly from the tracings. There are two principal reasons why such an approach is not very feasible. First, the lines involved are all highly saturated, and consequently their half-widths bear only an indirect relationship to the half-widths of their corresponding line-absorption coefficients. Second, most of the *Ca* II and *Na* I plates were taken with different cameras (114- and 73-inch) which possess different instrumental profiles, and corrections for finite resolving power would be required.

VI. THEORETICAL DISCUSSION

It remains to explain the variation of $N(Na\ \text{I})/N(Ca\ \text{II})$ with cloud velocity, shown in Figure 1. The main question is whether this variation represents an intrinsic sys-

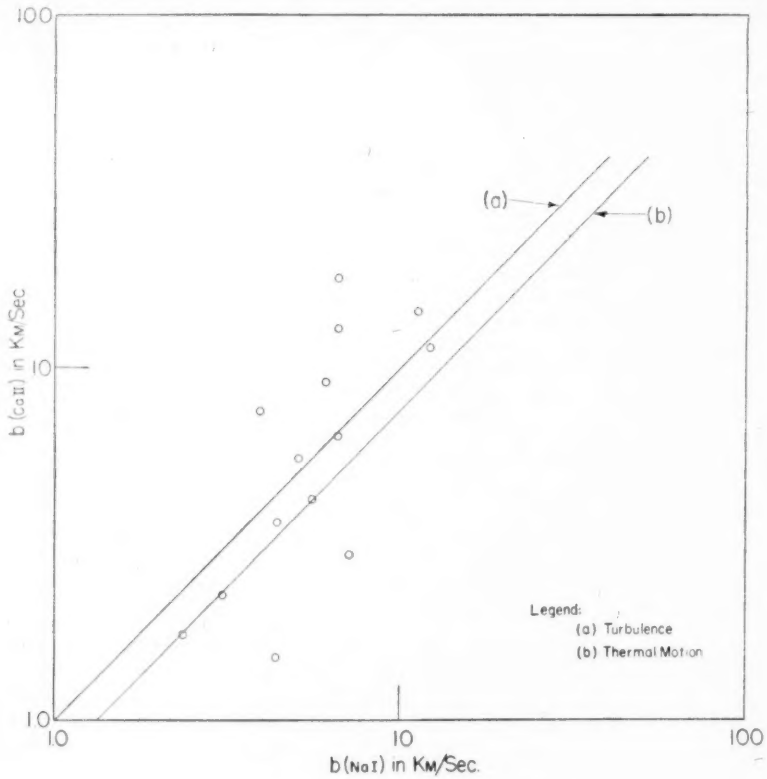

FIG. 2.—Plot of log $b(Ca\ \text{II})$ versus log $b(Na\ \text{I})$

tematic difference in the ratio of sodium vapor to calcium vapor between different clouds or whether it is the result of some mechanism affecting ionization equilibrium which is somehow correlated with cloud velocity.

Since the motion of a high-velocity cloud through an intercloud medium undoubtedly results in some heating effect, it is reasonable to examine those processes dependent upon the kinetic temperature within the cloud. Of these, we shall treat the most obvious, namely, the possibility of ionization of *Na* I by electron collisions; the possible importance of this mechanism in interstellar space does not seem to have been analyzed in previous work. The present discussion consists of two parts: first, a study of the ionization level within a cloud as a function of the internal kinetic temperature and, second, a brief discussion of the actual kinetic temperatures which might be expected inside high-velocity clouds.

Because of the high ionization potentials of *Na* II and *Ca* III (47.06 e.v. and 50.96 e.v., respectively), we assume that sodium is, at most, singly ionized, and calcium doubly

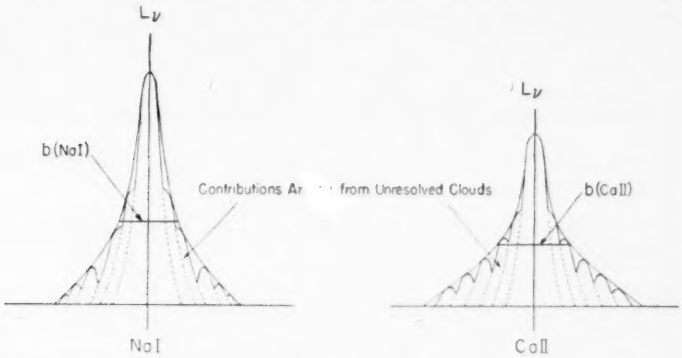

FIG. 3.—Diagram of L_ν for *Na* I and *Ca* II showing how $b(Ca\ \text{II}) > b(Na\ \text{I})$ for saturated lines

ionized. Denoting the particle densities of sodium and calcium nuclei by $n(Na)$ and $n(Ca)$, we may write

$$\begin{aligned} n(Na) &= n(Na\ \text{I}) + n(Na\ \text{II}), \\ n(Ca) &= n(Ca\ \text{I}) + n(Ca\ \text{II}) + n(Ca\ \text{III}). \end{aligned} \tag{2}$$

Under the conditions present in interstellar space, *Na* II and *Ca* III ions will be relatively most abundant. The change in the electron capture cross-sections of *Na* II and *Ca* III produced by a change in electron temperature will then have little effect on the ratio $n(Na\ \text{I})/n(Ca\ \text{II})$, since the two capture cross-sections will change in about the same way with changing temperature, and the ratio $n(Na\ \text{I})/n(Na\ \text{II})$ will change by the same factor as will $n(Ca\ \text{II})/n(Ca\ \text{III})$. Obviously, $N(Na\ \text{I})/N(Ca\ \text{II})$, the ratio of the number of atoms in the line of sight per square centimeter, equals the corresponding ratio of particle densities, used throughout this theoretical section.

The rate of ionization by electron collision will differ markedly for *Na* I and *Ca* II at moderate electron temperatures, in view of the different ionization potentials involved —5.12 and 11.82 volts, respectively. We compute the ionization levels to be expected. In interstellar space recombination in a three-body encounter, with the second electron carrying away the liberated energy, may be neglected; in thermodynamic equilibrium, of course, such recombinations will exactly balance collisional ionizations. For inter-

stellar conditions, the modified ionization equations, including ionization by electron collision, become

$$\frac{n(Na\ \text{II})\,n(e)}{n(Na\ \text{I})} = X_{\text{I}}(T_e) + n(e)\,\Gamma_{Na\ \text{I}}(T_e)\,,$$

$$\frac{n(Ca\ \text{II})\,n(e)}{n(Ca\ \text{I})} = Y_{\text{I}}(T_e) + n(e)\,\Gamma_{Ca\ \text{I}}(T_e)\,, \tag{3}$$

$$\frac{n(Ca\ \text{III})\,n(e)}{n(Ca\ \text{II})} = Y_{\text{II}}(T_e) + n(e)\,\Gamma_{Ca\ \text{II}}(T_e)\,,$$

where T_e denotes the electron temperature and $n(e)$ is the particle density of electrons. The quantities $X_{\text{I}}(T_e)$, $Y_{\text{I}}(T_e)$, and $Y_{\text{II}}(T_e)$ are the functions occurring in the normal ionization equations without electron collisions. These functions have been tabulated in Table 6 of Strömgren's paper[13] for the three electron temperatures 100°, 1000°, and 10,000°. To obtain better coverage, we have interpolated the values to 5000° and extrapolated to 100,000°. The functions $\Gamma_{Na\ \text{I}}(T_e)$, $\Gamma_{Ca\ \text{I}}(T_e)$, and $\Gamma_{Ca\ \text{II}}(T_e)$ in equations (3) express the influence of electron collisions in ionizing *Na* I, *Ca* I, and *Ca* II; these quantities are evaluated below. From equations (2) and (3), $n(Na\ \text{II})$, $n(Ca\ \text{I})$, and $n(Ca\ \text{III})$ may be eliminated, and we obtain the following expression for the ratio $n(Na\ \text{I})/n(Ca\ \text{II})$:

$$\frac{n(Na\ \text{I})}{n(Ca\ \text{II})} = \frac{n(Na)}{n(Ca)}\left\{\frac{1 + [\,Y_{\text{I}}/n(e) + \Gamma_{Ca\ \text{I}}\,]^{-1} + Y_{\text{II}}/n(e) + \Gamma_{Ca\ \text{II}}}{1 + X_{\text{I}}/n(e) + \Gamma_{Na\ \text{I}}}\right\}. \tag{4}$$

In general, the collision term $\Gamma(T_e)$ may be written as the following integral over v, the electron velocity,

$$\Gamma(T_e) = \frac{\displaystyle\int_{v_0}^{\infty} vP(v)\,\sigma_i(v)\,dv}{\displaystyle\sum_{n=1}^{\infty}\int_0^{\infty} v\sigma_{nc}(v)\,P(v)\,dv}, \tag{5}$$

where v_0 is the minimum velocity required for collisional ionization, $\sigma_i(v)$ the cross-section for the process, and $P(v)$ the Maxwellian velocity-distribution function. The numerator of $\Gamma(T_e)$ gives the actual number of ionizations of *Na* I (or *Ca* I, *Ca* II) by electron collisions, while the denominator expresses the total number of recombinations in all levels of the ion. The quantity σ_{nc} in the denominator is the cross-section for electron capture in the nth quantum level of the ion under consideration. To a sufficient degree of accuracy, the denominator of $\Gamma(T_e)$ may be set equal to the expression derived by Spitzer[15] (eqs. [31] and [32]), namely,

$$\sum_{n=1}^{\infty}\int_0^{\infty} v\sigma_{nc}(v)\,P(v)\,dv = \overline{v\sigma_i(v)} = 2.1\left(\frac{2kT_e}{\pi m}\right)^{1/2}\beta\phi_k(\beta)\,, \tag{6}$$

where m is the electron mass, A equals 2.11×10^{-22} cm^2, and β equals $158{,}000\ Z^2/T_e$, Z being the charge on the ion. The functions $\phi_k(\beta)$ are tabulated in Table 3 of Spitzer's paper;[15] in the present instance k is 3 for *Na* II, *Ca* II, and *Ca* III.

The greatest uncertainty in the application of equation (4) is lack of precise information on the value of σ_i, the collisional ionization coefficient. Here we have set σ_i equal to the geometrical cross-section πa^2. This assumption may be in error by an order of magnitude. However, the computed ionization levels vary so rapidly with temperature that indicative results are obtainable with a quite uncertain cross-section.

[15] *Ap. J.*, **107**, 6, 1948.

With the assumption that σ_i equals πa^2 and with the use of equation (6), we find that equation (5) becomes

$$\Gamma(T_e) = \frac{\pi a^2 (1 + m v_0^2 / 2kT_e)}{A \beta \phi_k(\beta)} \exp\left(-\frac{m v_0^2}{2kT_e}\right). \tag{7}$$

From equations (4) and (7), the variation of $n(Na\ \text{I})/n(Ca\ \text{II})$ may be obtained in units of the nuclear ratio $n(Na)/n(Ca)$ for a range of T_e and for various assumed values of the free electron abundance $n(e)$. The results of the computations are given in Table 6. The cutoff and noncutoff cases refer to the radiation in the Lyman continuum below 911 A. For an *H* I region, in which practically all the hydrogen is neutral, the Lyman radiation will not be transmitted, and we have an example of cutoff. The noncutoff case would pertain to an *H* II region, where there is no neutral hydrogen to interfere with the Lyman radiation from neighboring early-type stars. The atomic radius has been set equal to 1.9×10^{-8} cm.

From Table 6 it is seen that the value of the ratio $n(Na\ \text{I})/n(Ca\ \text{II})$ is reduced by approximately a factor of 100 in going from a kinetic temperature of 100° to 10,000°, with

TABLE 6

VARIATION OF $n(Na\ \text{I})/n(Ca\ \text{II})$ FOR VARIOUS T_e AND $n(e)$ IN UNITS OF $n(Na)/n(Ca)$
(Including Ionization by Collision)

TYPE OF RADIATION FIELD	$T = 100{,}000°$ $n(e)$ 10/Cc	$T = 10{,}000°$ $n(e)$ 10/Cc	$T = 5000°$ $n(e)$		$T = 1000°$ $n(e)$			$T = 100°$ $n(e)$	
			10/Cc	1/Cc	10/Cc	1/Cc	10^{-2}/Cc	10^{-2}/Cc	10^{-3}/Cc
Cutoff	0.080	3.1×10^{-4}	0.070	0.068	0.58	0.17	0.075	0.096	0.091
Noncutoff	0.080	3.4×10^{-4}	0.076	0.10	0.61	0.23	0.14	0.18	0.17

the major part of the drop occurring between 5000° and 10,000°. This effect is due entirely to the collisional ionization of *Na* I by electrons. Collisional ionization of *Ca* II is negligible at 10,000° but sets in at higher temperatures until, at 100,000°, as much *Ca* II is ionized by electron collisions as *Na* I. At this high temperature (100,000°) the abundance ratio $n(Na\ \text{I})/n(Ca\ \text{II})$ is practically restored to the same value which it has at 100°. From the results given in Table 6 it is clear that the kinetic temperature inside a high-velocity cloud must be at least 5000° and probably higher before collisional ionization of *Na* I by electrons will become sufficiently effective to reproduce the variation of $N(Na\ \text{I})/N(Ca\ \text{II})$ shown in Figure 1.

Finally, we consider what kinetic temperature may reasonably be expected in a rapidly moving cloud. If one assumes that a rarefied intercloud medium is present, collisions of these atoms with the cloud would provide some heating effect. The precise temperature resulting is difficult even to estimate, since the physical conditions are complicated, probably involving such phenomena as shock waves, turbulence, radiation losses, and heat conduction.

To obtain a lower limit for the temperature in this situation, computations were made for a simplified model in which, at some instant of time, a cloud is assumed to collide with a more rarefied cloud or intercloud medium. Shock waves are produced, one going into the cloud, the other proceeding into the intercloud medium. If conditions are assumed to vary along one direction only, the phenomena become one-dimensional and have been analyzed by Burgers,[16] who gives formulae for the temperatures behind the two

[16] *Proc. Amsterdam Acad. Sci.*, **49**, 589, 1946.

shock waves. For densities of 10 and 0.1 atoms/cc in the cloud and in the intercloud medium, respectively, Burgers' equations give temperatures of 2000° and 200,000° inside and outside the cloud, provided that the relative velocity is set equal to 80 km/sec. At 40 km/sec, however, these temperatures decrease to 500° and 50,000°.

Since the mean free path of an interstellar *H* atom, for the conditions of interest, is a small fraction of a parsec, much less than the diameter of a cloud, it is evident that shock waves will develop. However, this model represents only a transitory state, lasting about a million years. The shock waves will move away from the cloud, and in the steady state a stationary, curved shock wave will probably be present in front of the cloud. Moreover, atomic conduction and turbulent convection will transport heat from the very hot intercloud medium behind the shock wave into the cooler cloud. Even if the geometry of the actual situation were known, which it is not, the computation of the temperature inside the cloud, taking into account the radiation of energy at the increased temperature, would be a difficult task. It is therefore uncertain whether the flow of heat from the high-temperature intercloud medium into the denser cloud may heat up the cloud sufficiently so that collisional ionization may operate to lower the abundance of *Na* I.

If differences of ionization cannot explain the observed correlation shown in Figure 1, other mechanisms must be considered. One possibility is that *Na* and *Ca* atoms (or ions) adhere to, or evaporate from, grains at different relative rates for low- and high-velocity clouds. It is difficult to understand why the evaporation process should favor *Ca* over *Na* or vice versa. In regard to adhesion, it is true that the less massive *Na* atoms would probably undergo more collisions with grains than would *Ca;* but the velocity of the *Na* atoms exceeds that of the *Ca* atoms by a factor of only $(A_{Ca}/A_{Na})^{1/2}$, that is, 1.32, and would be quite ineffectual in bringing about the observed differences in the relative abundances of *Na* I and *Ca* II. If high-velocity clouds contained fewer grains, this hypothesis would seem attractive, but the data in this paper give no indication as to whether the grains are actually concentrated in the low-velocity clouds.

Another effect which demands consideration is the possibility that the radiation field varies from cloud to cloud in virtue of the different distances between the clouds and the O and B stars which lie behind them. It is not clear why this mechanism should be correlated with the cloud velocities; there is no evident reason for supposing that the high-velocity clouds lie systematically closer to the O and B stars or vice versa. But variations in the radiation field must certainly be operative to some degree and can be invoked to explain part of the large scatter in Figure 1 about $V = 0$. The variations to be expected in $N(Na\ \text{I})/N(Ca\ \text{II})$ because of this effect were not calculated, as there is yet no method available for determining the distance between a cloud producing a given interstellar line and the O or B star lying behind it. On the other hand, it has already been pointed out that some of the low-lying points in Figure 1 having $V \sim 0$ probably correspond to clouds possessing high space velocities but with small radial-velocity components.

VII. CONCLUSIONS

The results of the present work may be briefly summarized as follows:

1. In many individual interstellar clouds both sodium and calcium are present.

2. The radial velocities of the *Na* I components agree with the velocities of the corresponding *Ca* II features, in accord with conclusion 1.

3. A velocity effect exists, such that *Na* I tends to be more abundant than *Ca* II in low-velocity clouds, while in high-velocity clouds the reverse is true.

4. For saturated lines, H and K do not lie on the same curve of growth as the D lines, thus verifying the earlier conclusion of Wilson's that $b(Ca\ \text{II}) > b(Na\ \text{I})$; a plausible explanation of this result can be given if use is made of the observed correlation between cloud velocity and the abundance ratio of *Na* I to *Ca* II.

5. If the temperature of the high-velocity clouds is higher than some critical value,

which lies somewhere between 5000° and 10,000°, collisional ionization of *Na* I by electrons can explain the relatively low abundance of *Na* I in these clouds. However, it is uncertain whether the temperature in such a cloud is actually raised so high by contact with the intercloud medium, and other mechanisms may be involved.

THE X- AND Y-FUNCTIONS FOR ISOTROPIC SCATTERING. I

S. CHANDRASEKHAR AND DONNA ELBERT
Yerkes Observatory, University of Chicago
AND
ANN FRANKLIN
Watson Scientific Computing Laboratory, Columbia University
Received November 7, 1951

ABSTRACT

In this paper X- and Y-functions which occur in the solution of transfer problems in atmospheres of finite optical thicknesses and scattering radiation isotropically with an albedo $\varpi_0 \leqslant 1$ for single scattering are tabulated.

The values of the albedo, ϖ_0, and optical thickness, τ, for which solutions are tabulated are: $\varpi_0 = 1$, 0.95, 0.9, 0.8, 0.5, and $\tau = 0.05$, 0.10, 0.15, 0.20, 0.25, 0.5, and 1.

1. *Introduction.*—In a series of papers published in this *Journal* during the years 1944–1949, it was shown how exact solutions for many of the standard problems in the theory of radiative transfer in plane-parallel atmospheres can be expressed in terms of certain H- or X- and Y-functions. The H-functions occur in the solution of problems in semi-infinite atmospheres, while the X- and Y-functions occur in the corresponding problems in atmospheres of finite optical thicknesses. This theory has since been systematically presented in S. Chandrasekhar's *Radiative Transfer* (Oxford: Clarendon Press, 1950).[1] This book also includes tables of H-functions suitable for several problems in the theory of stellar and planetary atmospheres. But so far no similar tables of the X- and Y-functions have been available.

Now the X- and Y-functions are defined as solutions of the pair of integral equations,

$$X(\mu) = 1 + \mu \int_0^1 \frac{\Psi(\mu')}{\mu + \mu'} [X(\mu) X(\mu') - Y(\mu) Y(\mu')] d\mu' \tag{1}$$

and

$$Y(\mu) = e^{-\tau/\mu} + \mu \int_0^1 \frac{\Psi(\mu')}{\mu - \mu'} [Y(\mu) X(\mu') - X(\mu) Y(\mu')] d\mu' , \tag{2}$$

where τ denotes the optical thickness of the atmosphere and the "characteristic function" $\Psi(\mu)$ is, generally, an even polynomial in μ, satisfying the condition

$$\int_0^1 \Psi(\mu)\, d\mu \leqslant \tfrac{1}{2} . \tag{3}$$

In this paper we present tables of the X- and Y-functions for the case

$$\Psi(\mu) = \varpi_0 = \text{Constant} \qquad (\varpi_0 \leqslant 1) . \tag{4}$$

These functions occur in problems involving isotropic scattering, with an albedo, ϖ_0, for single scattering.

2. *The manner of solving for the X- and Y-functions. The tables of the solutions.*—The solutions for the cases $\varpi_0 = 1$, 0.95, 0.9, 0.8, and 0.5 and $\tau = 0.05$, 0.10, 0.15, 0.20, 0.25, 0.5, and 1 have been found by a direct process of iteration applied to the governing integral equations. The iterations were started with the solutions in the corrected second

[1] We shall hereafter refer to this book as "*R.T.*"

approximation as described in *R.T.*, chapter viii, § 60 (see particularly eqs. [117], [118], and [124]). The corrected second approximations were computed at the Yerkes Observatory for values of μ in the interval (0, 1) at steps of 0.01. The iterations were carried out at the Watson Scientific Computing Laboratory with IBM pluggable sequence relay calculators. In view of the factor $(\mu - \mu')^{-1}$ in the equation for Y, the values of the functions for the "even" values of the argument ($\mu = 0.02, 0.04, \ldots, 1.00$) were used for evaluating by numerical integration on the calculators the iterates for the "odd" values of the argument ($\mu = 0.01, 0.03, \ldots, 0.99$). Also it was found more convenient to iterate not for the functions X and Y themselves but for the functions

$$F(\mu) = \Psi(\mu)\, X(\mu) \qquad \text{and} \qquad G(\mu) = \Psi(\mu)\, Y(\mu). \tag{5}$$

These functions satisfy the equations

$$F(\mu) = \Psi(\mu) + \mu \int_0^1 \frac{d\mu'}{\mu + \mu'} [F(\mu) F(\mu') - G(\mu) G(\mu')] \tag{6}$$

and

$$G(\mu) = \Psi(\mu)\, e^{-\tau/\mu} + \mu \int_0^1 \frac{d\mu'}{\mu - \mu'} [G(\mu) F(\mu') - F(\mu) G(\mu')]. \tag{7}$$

For $\tau < 0.25$ it was found that no more than three iterations were needed for satisfactory convergence; however, for $\tau = 0.5$ and 1 (particularly for $\varpi_0 = 0.95$ and 1) as many as six or seven iterations were necessary. And, even so, the iterated functions showed a certain raggedness between 0.9 and 1; in part this can be traced to the relative "flatness" of the functions in this interval, which makes the integrand in equations (6) and (7) sensitive to rounding errors. The solutions have therefore been "smoothed" by plotting the deviations from the corrected second approximations. Table 1 presents these smoothed solutions.

The smoothed values of the differences,

$$\delta = \text{Tabulated solution} - \text{corrected second approximation}, \tag{8}$$

are also listed. These differences may be used to interpolate for the "exact" solution for other values of τ and ϖ_0.

An idea of the over-all accuracy reached in the final tabulated solutions may be obtained by seeing how well the relation (*R.T.*, p. 187, eq. [27])

$$\alpha_0 = \frac{2}{\varpi_0} [1 - (1 - \varpi_0 + \tfrac{1}{4}\varpi_0^2 \beta_0^2)^{1/2}] \tag{9}$$

between the moments

$$\alpha_0 = \int_0^1 X(\mu)\, d\mu \qquad \text{and} \qquad \beta_0 = \int_0^1 Y(\mu)\, d\mu \tag{10}$$

is satisfied. This comparison is made in Tables 1*a* and 1*b* in the paper following this one (p. 269). It would appear from this comparison that for $\tau \leqslant 0.25$ the tabulated solutions are probably trustworthy to one part in 10,000, while for $\tau = 0.5$ and 1 the solutions for the larger values of the albedo are probably to be trusted to only one part in a thousand.

In presenting these first tables of the *X*- and *Y*-functions, S. Chandrasekhar would particularly wish to place on record his indebtedness to Dr. Wallace Eckert and the staff of the Watson Scientific Computing Laboratory for their generous co-operation in carrying out to completion this project. Without their participation the iterations of the *X*- and *Y*-functions to obtain the true solutions would have been impossible.

TABLE 1

THE ITERATED X AND Y FUNCTIONS AND THEIR DEVIATIONS

FROM THE CORRECTED SECOND APPROXIMATIONS

μ	$\tau = 0.05$; $\varpi_1 = 1.00$				$\tau = 0.05$; $\varpi_1 = 0.95$				$\tau = 0.05$; $\varpi_1 = 0.90$			
	X	δ	Y	δ	X	δ	Y	δ	X	δ	Y	δ
0	1.00000	0	0	0	1.00000	0	0	0	1.00000	0	0	0
0.01	1.02487	+2	0.02202	-6	1.02357	+ 6	0.02118	- 4	1.02230	+11	0.02030	- 7
0.02	1.04099	+3	0.11254	-7	1.03885	+12	0.11082	- 8	1.03667	+15	0.10912	-10
0.03	1.05173	+4	0.25090	-5	1.04900	+13	0.22849	-12	1.04622	+15	0.22621	- 9
0.04	1.05911	+5	0.33694	-4	1.05595	+12	0.33406	-12	1.05277	+14	0.33134	- 7
0.05	1.06442	+5	0.42455	-3	1.06094	+10	0.42155	- 9	1.05748	+13	0.41827	- 6
0.06	1.06841	+6	0.49605	-1	1.06468	+ 8	0.49259	- 7	1.06100	+11	0.48924	- 5
0.07	1.07150	+6	0.55474	-1	1.06759	+ 7	0.55109	- 5	1.06374	+10	0.54754	- 3
0.08	1.07396	+6	0.60347	-1	1.06990	+ 6	0.59966	- 4	1.06590	+ 8	0.59595	- 2
0.09	1.07597	+6	0.64443	-1	1.07179	+ 5	0.64051	- 2	1.06768	+ 7	0.63666	- 1
0.10	1.07763	+6	0.67927	-1	1.07336	+ 5	0.67526	0	1.06914	+ 5	0.67128	0
0.11	1.07903	+5	0.70924	0	1.07468	+ 4	0.70513	+ 1	1.07038	+ 4	0.70106	+ 1
0.12	1.08023	+5	0.73524	0	1.07581	+ 4	0.73105	+ 1	1.07145	+ 4	0.72690	+ 1
0.13	1.08127	+5	0.75801	0	1.07679	+ 4	0.75375	+ 1	1.07237	+ 4	0.74953	+ 1
0.14	1.08218	+5	0.77811	0	1.07765	+ 4	0.77379	+ 1	1.07318	+ 4	0.76950	+ 1
0.15	1.08298	+5	0.79597	0	1.07840	+ 4	0.79160	+ 1	1.07389	+ 4	0.78726	+ 1
0.16	1.08368	+5	0.81195	0	1.07907	+ 4	0.80753	+ 1	1.07452	+ 4	0.80314	+ 1
0.17	1.08432	+5	0.82632	0	1.07967	+ 4	0.82185	+ 1	1.07508	+ 4	0.81742	+ 1
0.18	1.08488	+5	0.83932	0	1.08020	+ 4	0.83481	+ 1	1.07558	+ 4	0.83034	+ 1
0.19	1.08540	+5	0.85112	0	1.08069	+ 4	0.84658	+ 1	1.07604	+ 4	0.84207	+ 1
0.20	1.08586	+5	0.86189	0	1.08113	+ 4	0.85732	+ 1	1.07645	+ 4	0.85278	+ 1
0.21	1.08629	+5	0.87177	+1	1.08153	+ 4	0.86715	+ 1	1.07683	+ 4	0.86259	+ 1
0.22	1.08668	+5	0.88084	+1	1.08190	+ 4	0.87620	+ 1	1.07718	+ 4	0.87160	+ 1
0.23	1.08703	+5	0.88920	+1	1.08223	+ 4	0.88454	+ 1	1.07750	+ 4	0.87992	+ 1
0.24	1.08736	+5	0.89694	+1	1.08254	+ 4	0.89226	+ 1	1.07779	+ 4	0.88762	+ 1
0.25	1.08767	+5	0.90413	+1	1.08283	+ 4	0.89942	+ 1	1.07806	+ 4	0.89476	+ 1
0.26	1.08795	+5	0.91081	+1	1.08310	+ 4	0.90608	+ 1	1.07831	+ 4	0.90140	+ 1
0.27	1.08822	+5	0.91704	+1	1.08335	+ 4	0.91229	+ 1	1.07854	+ 4	0.90760	+ 1
0.28	1.08846	+5	0.92287	+1	1.08358	+ 4	0.91810	+ 1	1.07876	+ 4	0.91339	+ 1
0.29	1.08869	+5	0.92833	+1	1.08379	+ 4	0.92355	+ 1	1.07897	+ 4	0.91882	+ 1
0.30	1.08890	+5	0.93345	+1	1.08400	+ 4	0.92866	+ 1	1.07916	+ 4	0.92391	+ 1
0.31	1.08910	+4	0.93828	+2	1.08419	+ 4	0.93346	+ 1	1.07934	+ 4	0.92870	+ 1
0.32	1.08929	+4	0.94282	+2	1.08437	+ 4	0.93799	+ 1	1.07950	+ 4	0.93322	+ 1
0.33	1.08946	+4	0.94711	+2	1.08454	+ 4	0.94227	+ 1	1.07966	+ 4	0.93748	+ 1
0.34	1.08963	+4	0.95117	+2	1.08469	+ 4	0.94631	+ 1	1.07981	+ 4	0.94151	+ 1
0.35	1.08979	+4	0.95500	+2	1.08485	+ 4	0.95014	+ 1	1.07996	+ 4	0.94533	+ 1
0.36	1.08994	+4	0.95864	+2	1.08499	+ 4	0.95377	+ 1	1.08009	+ 4	0.94895	+ 1
0.37	1.09009	+4	0.96210	+2	1.08512	+ 4	0.95721	+ 1	1.08022	+ 4	0.95239	+ 1
0.38	1.09022	+4	0.96539	+2	1.08525	+ 4	0.96049	+ 1	1.08034	+ 4	0.95565	+ 1
0.39	1.09035	+4	0.96852	+2	1.08537	+ 4	0.96361	+ 1	1.08045	+ 4	0.95876	+ 1
0.40	1.09048	+4	0.97150	+2	1.08549	+ 4	0.96658	+ 1	1.08056	+ 4	0.96173	+ 1
0.41	1.09059	+4	0.97434	+2	1.08560	+ 4	0.96942	+ 1	1.08067	+ 4	0.96456	+ 1
0.42	1.09071	+4	0.97706	+2	1.08571	+ 4	0.97213	+ 1	1.08077	+ 4	0.96726	+ 1
0.43	1.09081	+4	0.97966	+2	1.08581	+ 4	0.97472	+ 1	1.08086	+ 4	0.96984	+ 1
0.44	1.09092	+4	0.98214	+2	1.08590	+ 4	0.97720	+ 1	1.08095	+ 4	0.97232	+ 1
0.45	1.09101	+4	0.98453	+2	1.08600	+ 4	0.97958	+ 1	1.08104	+ 4	0.97468	+ 1
0.46	1.09111	+4	0.98681	+2	1.08608	+ 4	0.98185	+ 1	1.08112	+ 4	0.97696	+ 1
0.47	1.09120	+4	0.98900	+2	1.08617	+ 4	0.98404	+ 1	1.08120	+ 4	0.97914	+ 1
0.48	1.09128	+4	0.99111	+2	1.08625	+ 4	0.98614	+ 1	1.08128	+ 4	0.98123	+ 1
0.49	1.09137	+4	0.99315	+2	1.08633	+ 4	0.98816	+ 1	1.08135	+ 4	0.98324	+ 1
0.50	1.09145	+4	0.99508	+2	1.08640	+ 4	0.99010	+ 1	1.08142	+ 4	0.98518	+ 1

TABLE 1-Continued

μ	$\tau = 0.05$; $\varpi_\lambda = 1.00$				$\tau = 0.05$; $\varpi_\lambda = 0.95$				$\tau = 0.05$; $\varpi_\lambda = 0.90$			
	X	δ	Y	δ	X	δ	Y	δ	X	δ	Y	δ
0.51	1.09152	+4	0.99695	+2	1.08647	+ 3	0.99197	+ 1	1.08149	+ 4	0.98704	+ 1
0.52	1.09160	+4	0.99876	+2	1.08654	+ 3	0.99377	+ 1	1.08156	+ 4	0.98884	+ 1
0.53	1.09167	+4	1.00050	+2	1.08660	+ 3	0.99550	+ 1	1.08162	+ 4	0.99057	+ 1
0.54	1.09174	+4	1.00218	+2	1.08667	+ 3	0.99718	+ 1	1.08168	+ 4	0.99224	+ 1
0.55	1.09180	+4	1.00380	+2	1.08673	+ 3	0.99880	+ 1	1.08174	+ 4	0.99385	+ 1
0.56	1.09187	+4	1.00536	+2	1.08679	+ 3	1.00036	+ 1	1.08180	+ 4	0.99540	+ 1
0.57	1.09193	+4	1.00688	+2	1.08685	+ 3	1.00186	+ 1	1.08185	+ 4	0.99691	+ 1
0.58	1.09199	+4	1.00834	+2	1.08690	+ 3	1.00332	+ 1	1.08190	+ 4	0.99836	+ 1
0.59	1.09205	+4	1.00975	+2	1.08696	+ 3	1.00474	+ 1	1.08195	+ 4	0.99977	+ 1
0.60	1.09210	+4	1.01112	+2	1.08701	+ 3	1.00610	+ 1	1.08200	+ 4	1.00113	+ 1
0.61	1.09216	+4	1.01245	+2	1.08706	+ 3	1.00742	+ 1	1.08205	+ 4	1.00245	+ 1
0.62	1.09221	+4	1.01374	+2	1.08711	+ 3	1.00871	+ 1	1.08210	+ 4	1.00373	+ 1
0.63	1.09226	+4	1.01498	+2	1.08716	+ 3	1.00995	+ 1	1.08214	+ 4	1.00497	+ 1
0.64	1.09231	+4	1.01619	+2	1.08720	+ 3	1.01116	+ 1	1.08219	+ 4	1.00617	+ 1
0.65	1.09236	+4	1.01737	+2	1.08725	+ 3	1.01233	+ 1	1.08223	+ 4	1.00734	+ 1
0.66	1.09240	+4	1.01851	+2	1.08729	+ 3	1.01346	+ 1	1.08227	+ 4	1.00847	+ 1
0.67	1.09245	+4	1.01961	+2	1.08734	+ 3	1.01457	+ 1	1.08231	+ 4	1.00957	+ 1
0.68	1.09249	+4	1.02069	+2	1.08738	+ 3	1.01564	+ 1	1.08235	+ 4	1.01064	+ 1
0.69	1.09253	+4	1.02173	+2	1.08742	+ 3	1.01668	+ 1	1.08239	+ 4	1.01168	+ 1
0.70	1.09257	+4	1.02275	+2	1.08746	+ 3	1.01769	+ 1	1.08242	+ 4	1.01269	+ 1
0.71	1.09261	+4	1.02374	+2	1.08749	+ 3	1.01868	+ 1	1.08246	+ 4	1.01367	+ 1
0.72	1.09265	+4	1.02470	+2	1.08753	+ 3	1.01964	+ 1	1.08249	+ 4	1.01463	+ 1
0.73	1.09269	+4	1.02564	+2	1.08757	+ 3	1.02057	+ 1	1.08253	+ 4	1.01556	+ 1
0.74	1.09273	+4	1.02655	+2	1.08760	+ 3	1.02148	+ 1	1.08256	+ 4	1.01647	+ 1
0.75	1.09276	+4	1.02744	+2	1.08763	+ 3	1.02237	+ 1	1.08259	+ 4	1.01735	+ 1
0.76	1.09280	+4	1.02830	+2	1.08767	+ 3	1.02323	+ 1	1.08262	+ 4	1.01822	+ 1
0.77	1.09283	+4	1.02915	+2	1.08770	+ 3	1.02407	+ 1	1.08265	+ 4	1.01906	+ 1
0.78	1.09287	+4	1.02997	+2	1.08773	+ 3	1.02490	+ 1	1.08268	+ 4	1.01987	+ 1
0.79	1.09290	+4	1.03077	+2	1.08776	+ 3	1.02569	+ 1	1.08271	+ 4	1.02067	+ 1
0.80	1.09293	+4	1.03155	+2	1.08779	+ 3	1.02648	+ 1	1.08274	+ 4	1.02145	+ 1
0.81	1.09296	+4	1.03232	+2	1.08782	+ 3	1.02724	+ 1	1.08277	+ 4	1.02221	+ 1
0.82	1.09299	+4	1.03307	+2	1.08785	+ 3	1.02798	+ 1	1.08279	+ 4	1.02295	+ 1
0.83	1.09302	+4	1.03380	+2	1.08788	+ 3	1.02871	+ 1	1.08282	+ 4	1.02368	+ 1
0.84	1.09305	+4	1.03451	+2	1.08790	+ 3	1.02942	+ 1	1.08284	+ 4	1.02439	+ 1
0.85	1.09308	+4	1.03520	+2	1.08793	+ 3	1.03012	+ 1	1.08287	+ 4	1.02508	+ 1
0.86	1.09311	+4	1.03588	+2	1.08796	+ 3	1.03079	+ 1	1.08289	+ 4	1.02576	+ 1
0.87	1.09313	+4	1.03655	+2	1.08798	+ 3	1.03146	+ 1	1.08292	+ 4	1.02642	+ 1
0.88	1.09316	+4	1.03720	+2	1.08801	+ 3	1.03211	+ 1	1.08294	+ 4	1.02707	+ 1
0.89	1.09319	+4	1.03784	+2	1.08803	+ 3	1.03274	+ 1	1.08296	+ 4	1.02770	+ 1
0.90	1.09321	+4	1.03846	+2	1.08805	+ 3	1.03336	+ 1	1.08299	+ 4	1.02832	+ 1
0.91	1.09324	+4	1.03907	+2	1.08808	+ 3	1.03397	+ 1	1.08301	+ 4	1.02892	+ 1
0.92	1.09326	+4	1.03966	+2	1.08810	+ 3	1.03456	+ 1	1.08303	+ 4	1.02952	+ 1
0.93	1.09328	+4	1.04025	+2	1.08812	+ 3	1.03515	+ 1	1.08305	+ 4	1.03010	+ 1
0.94	1.09331	+4	1.04082	+2	1.08814	+ 3	1.03572	+ 1	1.08307	+ 4	1.03067	+ 1
0.95	1.09333	+4	1.04138	+2	1.08816	+ 3	1.03628	+ 1	1.08309	+ 4	1.03122	+ 1
0.96	1.09335	+4	1.04193	+2	1.08819	+ 3	1.03682	+ 1	1.08311	+ 4	1.03177	+ 1
0.97	1.09337	+4	1.04246	+2	1.08821	+ 3	1.03736	+ 1	1.08313	+ 4	1.03230	+ 1
0.98	1.09340	+4	1.04299	+2	1.08823	+ 3	1.03789	+ 1	1.08315	+ 4	1.03283	+ 1
0.99	1.09342	+4	1.04351	+2	1.08825	+ 3	1.03840	+ 1	1.08317	+ 4	1.03334	+ 1
1.00	1.09344	+4	1.04401	+2	1.08826	+ 3	1.03890	+ 1	1.08318	+ 4	1.03384	+ 1

TABLE 1-Continued

μ	$\tau = 0.05$; $\varpi_0 = 0.80$				$\tau = 0.05$; $\varpi_0 = 0.50$				$\tau = 0.10$; $\varpi_0 = 1.00$			
	X	δ	Y	δ	X	δ	Y	δ	X	δ	Y	δ
0	1.00000	0	0	0	1.00000	0	0	0	1.00000	0	0	0
0.01	1.01968	+7	0.01869	0	1.01195	+1	0.01393	+1	1.02583	+ 7	0.01208	-27
0.02	1.03224	+7	0.10591	0	1.01959	+1	0.09646	+1	1.04468	+15	0.03215	-39
0.03	1.04062	+6	0.22175	0	1.02644	+1	0.20878	+1	1.06013	+20	0.07469	-44
0.04	1.04688	+5	0.32596	0	1.02814	+1	0.31035	+1	1.07268	+23	0.13355	-45
0.05	1.05051	+4	0.41222	0	1.03064	+1	0.39469	+1	1.08286	+26	0.19764	-43
0.06	1.05361	+3	0.48268	+1	1.03252	+1	0.46367	+1	1.09117	+27	0.26045	-40
0.07	1.05602	+3	0.54056	+1	1.03397	+1	0.52040	+1	1.09804	+27	0.31915	-37
0.08	1.05794	+3	0.58864	+1	1.03513	+1	0.56755	+1	1.10380	+27	0.37279	-34
0.09	1.05951	+3	0.62907	+1	1.03608	+1	0.60722	+1	1.10868	+26	0.42132	-32
0.10	1.06081	+3	0.66347	+1	1.03687	+1	0.64099	+1	1.11286	+25	0.46509	-30
0.11	1.06191	+3	0.69305	+1	1.03753	+1	0.67003	+1	1.11648	+24	0.50456	-27
0.12	1.06285	+3	0.71873	+1	1.03809	+1	0.69524	+1	1.11964	+23	0.54018	-26
0.13	1.06366	+3	0.74122	+1	1.03858	+1	0.71784	+1	1.12243	+23	0.57243	-24
0.14	1.06437	+3	0.76107	+1	1.03901	+1	0.73884	+1	1.12490	+22	0.60171	-23
0.15	1.06499	+3	0.77872	+1	1.03938	+1	0.75818	+1	1.12710	+21	0.62836	-22
0.16	1.06554	+3	0.79450	+1	1.03972	+1	0.76969	+1	1.12908	+20	0.65273	-20
0.17	1.06604	+3	0.80870	+1	1.04002	+1	0.78364	+1	1.13087	+19	0.67506	-19
0.18	1.06648	+3	0.82154	+1	1.04028	+1	0.79626	+1	1.13249	+18	0.69558	-18
0.19	1.06688	+3	0.83321	+1	1.04052	+1	0.80772	+1	1.13396	+17	0.71450	-17
0.20	1.06725	+3	0.84385	+1	1.04074	+1	0.81819	+1	1.13532	+17	0.73199	-17
0.21	1.06758	+3	0.85360	+1	1.04094	+1	0.82777	+1	1.13656	+16	0.74821	-16
0.22	1.06788	+3	0.86257	+1	1.04113	+1	0.83658	+1	1.13771	+16	0.76327	-16
0.23	1.06816	+3	0.87083	+1	1.04130	+1	0.84471	+1	1.13876	+15	0.77731	-15
0.24	1.06842	+3	0.87848	+1	1.04145	+1	0.85223	+1	1.13975	+15	0.79042	-15
0.25	1.06865	+3	0.88558	+1	1.04159	+1	0.85921	+1	1.14066	+14	0.80268	-15
0.26	1.06887	+3	0.89219	+1	1.04173	+1	0.86570	+1	1.14150	+13	0.81418	-14
0.27	1.06908	+3	0.89835	+1	1.04185	+1	0.87176	+1	1.14230	+13	0.82496	-14
0.28	1.06927	+3	0.90411	+1	1.04197	+1	0.87743	+1	1.14304	+12	0.83514	-14
0.29	1.06945	+3	0.90950	+1	1.04207	+1	0.88273	+1	1.14374	+12	0.84472	-14
0.30	1.06962	+3	0.91457	+1	1.04217	+1	0.88771	+1	1.14440	+12	0.85376	-14
0.31	1.06978	+3	0.91934	+1	1.04227	+1	0.89240	+1	1.14501	+11	0.86232	-13
0.32	1.06992	+3	0.92383	+1	1.04236	+1	0.89682	+1	1.14560	+11	0.87042	-13
0.33	1.07006	+3	0.92807	+1	1.04244	+1	0.90098	+1	1.14615	+11	0.87810	-13
0.34	1.07019	+3	0.93207	+1	1.04252	+1	0.90493	+1	1.14668	+11	0.88540	-12
0.35	1.07032	+3	0.93587	+1	1.04260	+1	0.90866	+1	1.14717	+11	0.89234	-12
0.36	1.07044	+3	0.93947	+1	1.04267	+1	0.91220	+1	1.14763	+ 9	0.89895	-11
0.37	1.07055	+3	0.94288	+1	1.04274	+1	0.91556	+1	1.14807	+ 9	0.90524	-11
0.38	1.07065	+3	0.94613	+1	1.04280	+1	0.91875	+1	1.14850	+ 9	0.91125	-11
0.39	1.07076	+3	0.94923	+1	1.04286	+1	0.92179	+1	1.14891	+ 9	0.91698	-11
0.40	1.07085	+3	0.95217	+1	1.04292	+1	0.92469	+1	1.14930	+ 9	0.92246	-11
0.41	1.07094	+3	0.95499	+1	1.04297	+1	0.92746	+1	1.14967	+ 9	0.92773	- 9
0.42	1.07103	+3	0.95767	+1	1.04303	+1	0.93010	+1	1.15002	+ 9	0.93275	- 9
0.43	1.07111	+3	0.96024	+1	1.04308	+1	0.93263	+1	1.15036	+ 9	0.93757	- 9
0.44	1.07119	+3	0.96270	+1	1.04312	+1	0.93505	+1	1.15069	+ 9	0.94220	- 9
0.45	1.07127	+3	0.96505	+1	1.04317	+1	0.93736	+1	1.15100	+ 9	0.94664	- 9
0.46	1.07134	+3	0.96731	+1	1.04321	+1	0.93959	+1	1.15129	+ 8	0.95090	- 9
0.47	1.07141	+3	0.96948	+1	1.04326	+1	0.94172	+1	1.15157	+ 8	0.95501	- 9
0.48	1.07148	+3	0.97156	+1	1.04330	+1	0.94376	+1	1.15185	+ 8	0.95896	- 9
0.49	1.07154	+3	0.97356	+1	1.04334	+1	0.94573	+1	1.15212	+ 8	0.96277	- 9
0.50	1.07161	+3	0.97549	+1	1.04337	+1	0.94763	+1	1.15237	+ 8	0.96643	- 9

TABLE 1-Continued

μ	$\tau = 0.05$; $\varpi_\lambda = 0.80$				$\tau = 0.05$; $\varpi_\lambda = 0.50$				$\tau = 0.10$; $\varpi_\lambda = 1.00$			
	X	δ	Y	δ	X	δ	Y	δ	X	δ	Y	δ
0.51	1.07167	+3	0.97734	+1	1.04341	+1	0.94945	+1	1.15262	+ 8	0.96998	- 8
0.52	1.07172	+3	0.97913	+1	1.04344	+1	0.95121	+1	1.15285	+ 8	0.97340	- 8
0.53	1.07178	+3	0.98085	+1	1.04348	+1	0.95290	+1	1.15308	+ 8	0.97670	- 8
0.54	1.07183	+3	0.98251	+1	1.04351	+1	0.95453	+1	1.15330	+ 8	0.97988	- 8
0.55	1.07188	+3	0.98411	+1	1.04354	+1	0.95611	+1	1.15352	+ 8	0.98296	- 8
0.56	1.07193	+3	0.98566	+1	1.04357	+1	0.95763	+1	1.15371	+ 7	0.98594	- 8
0.57	1.07198	+3	0.98715	+1	1.04360	+1	0.95910	+1	1.15391	+ 7	0.98883	- 8
0.58	1.07203	+3	0.98860	+1	1.04363	+1	0.96053	+1	1.15411	+ 7	0.99162	- 8
0.59	1.07207	+3	0.99000	+1	1.04366	+1	0.96190	+1	1.15429	+ 7	0.99433	- 8
0.60	1.07212	+3	0.99136	+1	1.04368	+1	0.96323	+1	1.15447	+ 7	0.99695	- 8
0.61	1.07216	+3	0.99267	+1	1.04371	+1	0.96453	+1	1.15464	+ 6	0.99950	- 8
0.62	1.07220	+3	0.99394	+1	1.04373	+1	0.96578	+1	1.15481	+ 6	1.00197	- 8
0.63	1.07224	+3	0.99517	+1	1.04376	+1	0.96699	+1	1.15497	+ 6	1.00437	- 8
0.64	1.07228	+3	0.99637	+1	1.04378	+1	0.96817	+1	1.15513	+ 6	1.00669	- 8
0.65	1.07231	+3	0.99753	+1	1.04380	+1	0.96931	+1	1.15529	+ 6	1.00895	- 8
0.66	1.07235	+3	0.99865	+1	1.04382	+1	0.97042	+1	1.15544	+ 6	1.01115	- 8
0.67	1.07239	+3	0.99975	+1	1.04384	+1	0.97149	+1	1.15559	+ 6	1.01329	- 8
0.68	1.07242	+3	1.00081	+1	1.04386	+1	0.97254	+1	1.15573	+ 6	1.01537	- 8
0.69	1.07245	+3	1.00185	+1	1.04388	+1	0.97355	+1	1.15587	+ 6	1.01739	- 8
0.70	1.07249	+3	1.00285	+1	1.04390	+1	0.97454	+1	1.15600	+ 6	1.01936	- 8
0.71	1.07252	+3	1.00383	+1	1.04392	+1	0.97550	+1	1.15614	+ 6	1.02128	- 8
0.72	1.07255	+3	1.00478	+1	1.04394	+1	0.97644	+1	1.15626	+ 6	1.02314	- 8
0.73	1.07258	+3	1.00571	+1	1.04396	+1	0.97735	+1	1.15639	+ 6	1.02496	- 8
0.74	1.07260	+3	1.00661	+1	1.04398	+1	0.97824	+1	1.15651	+ 6	1.02674	- 8
0.75	1.07263	+3	1.00749	+1	1.04399	+1	0.97910	+1	1.15663	+ 6	1.02847	- 8
0.76	1.07266	+3	1.00834	+1	1.04401	+1	0.97995	+1	1.15673	+ 5	1.03015	- 8
0.77	1.07269	+3	1.00918	+1	1.04402	+1	0.98077	+1	1.15685	+ 5	1.03180	- 8
0.78	1.07271	+3	1.00999	+1	1.04404	+1	0.98157	+1	1.15696	+ 5	1.03340	- 8
0.79	1.07274	+3	1.01078	+1	1.04406	+1	0.98235	+1	1.15706	+ 5	1.03497	- 8
0.80	1.07276	+3	1.01156	+1	1.04407	+1	0.98311	+1	1.15717	+ 5	1.03650	- 8
0.81	1.07279	+3	1.01232	+1	1.04409	+1	0.98386	+1	1.15727	+ 5	1.03800	- 8
0.82	1.07281	+3	1.01305	+1	1.04410	+1	0.98458	+1	1.15737	+ 5	1.03946	- 8
0.83	1.07283	+3	1.01378	+1	1.04411	+1	0.98529	+1	1.15747	+ 5	1.04089	- 8
0.84	1.07286	+3	1.01448	+1	1.04413	+1	0.98598	+1	1.15756	+ 5	1.04228	- 8
0.85	1.07288	+3	1.01517	+1	1.04414	+1	0.98666	+1	1.15766	+ 5	1.04365	- 8
0.86	1.07290	+3	1.01584	+1	1.04415	+1	0.98732	+1	1.15775	+ 5	1.04498	- 8
0.87	1.07292	+3	1.01650	+1	1.04417	+1	0.98797	+1	1.15784	+ 5	1.04629	- 8
0.88	1.07294	+3	1.01714	+1	1.04418	+1	0.98860	+1	1.15792	+ 5	1.04757	- 8
0.89	1.07296	+3	1.01777	+1	1.04419	+1	0.98922	+1	1.15801	+ 5	1.04882	- 8
0.90	1.07298	+3	1.01839	+1	1.04420	+1	0.98983	+1	1.15809	+ 5	1.05004	- 8
0.91	1.07300	+3	1.01899	+1	1.04421	+1	0.99042	+1	1.15817	+ 5	1.05124	- 8
0.92	1.07302	+3	1.01958	+1	1.04422	+1	0.99100	+1	1.15825	+ 5	1.05242	- 8
0.93	1.07304	+3	1.02016	+1	1.04424	+1	0.99157	+1	1.15833	+ 5	1.05357	- 8
0.94	1.07305	+3	1.02072	+1	1.04425	+1	0.99213	+1	1.15841	+ 5	1.05469	- 8
0.95	1.07307	+3	1.02128	+1	1.04426	+1	0.99267	+1	1.15848	+ 5	1.05580	- 8
0.96	1.07309	+3	1.02182	+1	1.04427	+1	0.99321	+1	1.15856	+ 5	1.05688	- 8
0.97	1.07311	+3	1.02235	+1	1.04428	+1	0.99373	+1	1.15863	+ 5	1.05794	- 8
0.98	1.07312	+3	1.02287	+1	1.04429	+1	0.99424	+1	1.15870	+ 5	1.05898	- 8
0.99	1.07314	+3	1.02338	+1	1.04430	+1	0.99474	+1	1.15877	+ 5	1.06000	- 8
1.00	1.07315	+3	1.02388	+1	1.04431	+1	0.99524	+1	1.15884	+ 5	1.06101	- 8

TABLE 1-Continued

μ	$\tau = 0.10$; $\varpi = 0.95$				$\tau = 0.10$; $\varpi = 0.90$				$\tau = 0.10$; $\varpi = 0.80$			
	X	δ	Y	δ	X	δ	Y	δ	X	δ	Y	δ
0	1.00000	0	0	0	1.00000	0	0	0	1.00000	0	0	0
0.01	1.02438	+ 6	0.01129	-30	1.02296	+ 6	0.01059	-25	1.02017	+ 6	0.00924	-16
0.02	1.04213	+13	0.03054	-41	1.03963	+11	0.02905	-35	1.03474	+ 9	0.02617	-24
0.03	1.05667	+17	0.07229	-43	1.05326	+14	0.06999	-38	1.04664	+12	0.06554	-28
0.04	1.06848	+21	0.13043	-42	1.06433	+16	0.12740	-38	1.05629	+14	0.12151	-30
0.05	1.07805	+23	0.19390	-39	1.07329	+17	0.19021	-37	1.06410	+15	0.18312	-28
0.06	1.08586	+24	0.25616	-37	1.08063	+19	0.25193	-36	1.07049	+16	0.24380	-27
0.07	1.09232	+24	0.31139	-34	1.08669	+20	0.30971	-33	1.07577	+17	0.30069	-25
0.08	1.09773	+24	0.36768	-32	1.09177	+20	0.36256	-30	1.08019	+17	0.35276	-24
0.09	1.10232	+23	0.41582	-30	1.09607	+20	0.41042	-28	1.08392	+16	0.39996	-23
0.10	1.10624	+22	0.45929	-28	1.09975	+19	0.45360	-27	1.08714	+16	0.44258	-21
0.11	1.10964	+21	0.49849	-27	1.10295	+19	0.49255	-24	1.08991	+15	0.48103	-19
0.12	1.11261	+20	0.53389	-25	1.10573	+18	0.52773	-23	1.09233	+14	0.51577	-18
0.13	1.11522	+18	0.56598	-24	1.10818	+17	0.55957	-22	1.09446	+13	0.54723	-17
0.14	1.11754	+18	0.59508	-23	1.11036	+17	0.58850	-20	1.09635	+12	0.57580	-16
0.15	1.11961	+17	0.62153	-22	1.11230	+16	0.61485	-18	1.09808	+11	0.60182	-16
0.16	1.12147	+16	0.64575	-20	1.11404	+15	0.63892	-17	1.09954	+10	0.62561	-15
0.17	1.12316	+16	0.66794	-19	1.11561	+14	0.66097	-17	1.10092	+10	0.64741	-15
0.18	1.12468	+15	0.68835	-18	1.11703	+13	0.68126	-16	1.10217	+10	0.66747	-14
0.19	1.12606	+14	0.70716	-17	1.11833	+12	0.69996	-15	1.10330	+10	0.68595	-14
0.20	1.12734	+14	0.72455	-17	1.11952	+12	0.71725	-15	1.10434	+10	0.70305	-14
0.21	1.12850	+13	0.74066	-17	1.12061	+11	0.73330	-13	1.10528	+ 8	0.71891	-12
0.22	1.12958	+13	0.75565	-16	1.12162	+11	0.74819	-13	1.10616	+ 8	0.73365	-12
0.23	1.13057	+13	0.76961	-16	1.12255	+10	0.76207	-13	1.10697	+ 8	0.74737	-12
0.24	1.13149	+12	0.78265	-15	1.12342	+10	0.77503	-13	1.10772	+ 8	0.76019	-12
0.25	1.13235	+12	0.79484	-15	1.12422	+10	0.78715	-13	1.10843	+ 8	0.77218	-12
0.26	1.13314	+11	0.80628	-14	1.12497	+10	0.79853	-12	1.10907	+ 7	0.78345	-10
0.27	1.13389	+11	0.81702	-14	1.12568	+10	0.80921	-12	1.10968	+ 7	0.79401	-10
0.28	1.13458	+10	0.82714	-13	1.12633	+10	0.81926	-12	1.11025	+ 7	0.80395	-10
0.29	1.13524	+10	0.83666	-13	1.12695	+10	0.82873	-12	1.11079	+ 7	0.81333	-10
0.30	1.13585	+ 9	0.84566	-13	1.12753	+10	0.83768	-12	1.11129	+ 7	0.82218	-10
0.31	1.13643	+ 9	0.85416	-13	1.12806	+ 8	0.84616	-10	1.11176	+ 6	0.83057	- 8
0.32	1.13698	+ 9	0.86223	-12	1.12857	+ 8	0.85417	-10	1.11221	+ 6	0.83850	- 8
0.33	1.13750	+ 9	0.86987	-12	1.12906	+ 8	0.86177	-10	1.11263	+ 6	0.84601	- 8
0.34	1.13798	+ 8	0.87712	-12	1.12952	+ 8	0.86899	-10	1.11303	+ 6	0.85315	- 8
0.35	1.13845	+ 8	0.88402	-12	1.12996	+ 8	0.87585	-10	1.11341	+ 6	0.85994	- 8
0.36	1.13889	+ 8	0.89060	-11	1.13036	+ 7	0.88238	-10	1.11376	+ 5	0.86641	- 8
0.37	1.13930	+ 7	0.89686	-11	1.13075	+ 7	0.88861	-10	1.11410	+ 5	0.87257	- 8
0.38	1.13970	+ 7	0.90283	-11	1.13113	+ 7	0.89455	-10	1.11443	+ 5	0.87845	- 8
0.39	1.14008	+ 7	0.90854	-11	1.13149	+ 7	0.90022	-10	1.11474	+ 5	0.88406	- 8
0.40	1.14045	+ 7	0.91399	-11	1.13183	+ 7	0.90565	-10	1.11504	+ 5	0.88943	- 8
0.41	1.14080	+ 7	0.91922	-10	1.13214	+ 6	0.91086	- 8	1.11531	+ 4	0.89458	- 7
0.42	1.14113	+ 7	0.92422	-10	1.13245	+ 6	0.91583	- 8	1.11558	+ 4	0.89950	- 7
0.43	1.14144	+ 7	0.92901	-10	1.13275	+ 6	0.92060	- 8	1.11584	+ 4	0.90422	- 7
0.44	1.14175	+ 7	0.93361	-10	1.13304	+ 6	0.92518	- 8	1.11609	+ 4	0.90875	- 7
0.45	1.14204	+ 7	0.93803	-10	1.13331	+ 6	0.92957	- 8	1.11632	+ 4	0.91310	- 7
0.46	1.14232	+ 7	0.94229	- 9	1.13356	+ 5	0.93380	- 8	1.11655	+ 4	0.91728	- 7
0.47	1.14259	+ 7	0.94637	- 9	1.13381	+ 5	0.93786	- 8	1.11677	+ 4	0.92130	- 7
0.48	1.14285	+ 7	0.95030	- 9	1.13405	+ 5	0.94177	- 8	1.11698	+ 4	0.92517	- 7
0.49	1.14309	+ 7	0.95409	- 9	1.13429	+ 5	0.94554	- 8	1.11718	+ 4	0.92890	- 7
0.50	1.14333	+ 7	0.95774	- 9	1.13451	+ 5	0.94917	- 8	1.11738	+ 4	0.93249	- 7

TABLE 1-Continued

μ	τ = 0.10 ; ϖ = 0.95				τ = 0.10 ; ϖ = 0.90				τ = 0.10 ; ϖ = 0.80			
	X	δ	Y	δ	X	δ	Y	δ	X	δ	Y	δ
0.51	1.14355	+ 6	0.96127	- 8	1.13473	+ 5	0.95267	- 8	1.11756	+ 3	0.93596	- 7
0.52	1.14378	+ 6	0.96467	- 8	1.13493	+ 5	0.95605	- 8	1.11774	+ 3	0.93931	- 7
0.53	1.14399	+ 6	0.96795	- 8	1.13513	+ 5	0.95932	- 8	1.11791	+ 3	0.94254	- 7
0.54	1.14420	+ 6	0.97112	- 8	1.13533	+ 5	0.96247	- 8	1.11808	+ 3	0.94566	- 7
0.55	1.14440	+ 6	0.97419	- 8	1.13552	+ 5	0.96552	- 8	1.11824	+ 3	0.94868	- 7
0.56	1.14459	+ 6	0.97716	- 8	1.13569	+ 4	0.96847	- 8	1.11840	+ 3	0.95160	- 7
0.57	1.14477	+ 6	0.98003	- 8	1.13586	+ 4	0.97133	- 8	1.11855	+ 3	0.95443	- 7
0.58	1.14495	+ 6	0.98281	- 8	1.13603	+ 4	0.97409	- 8	1.11870	+ 3	0.95716	- 7
0.59	1.14513	+ 6	0.98550	- 8	1.13619	+ 4	0.97677	- 8	1.11884	+ 3	0.95982	- 7
0.60	1.14530	+ 6	0.98811	- 8	1.13635	+ 4	0.97937	- 8	1.11898	+ 3	0.96239	- 7
0.61	1.14545	+ 5	0.99065	- 8	1.13650	+ 4	0.98189	- 8	1.11910	+ 2	0.96488	- 7
0.62	1.14561	+ 5	0.99310	- 8	1.13665	+ 4	0.98434	- 8	1.11923	+ 2	0.96730	- 7
0.63	1.14576	+ 5	0.99549	- 8	1.13680	+ 4	0.98671	- 8	1.11935	+ 2	0.96965	- 7
0.64	1.14591	+ 5	0.99781	- 8	1.13694	+ 4	0.98901	- 8	1.11948	+ 2	0.97193	- 7
0.65	1.14606	+ 5	1.00006	- 8	1.13707	+ 4	0.99125	- 8	1.11959	+ 2	0.97415	- 7
0.66	1.14620	+ 5	1.00224	- 8	1.13720	+ 4	0.99343	- 8	1.11971	+ 2	0.97630	- 7
0.67	1.14634	+ 5	1.00437	- 8	1.13733	+ 4	0.99555	- 8	1.11982	+ 2	0.97840	- 7
0.68	1.14647	+ 5	1.00644	- 8	1.13746	+ 4	0.99760	- 8	1.11993	+ 2	0.98044	- 7
0.69	1.14660	+ 5	1.00845	- 8	1.13758	+ 4	0.99961	- 8	1.12003	+ 2	0.98242	- 7
0.70	1.14672	+ 5	1.01041	- 8	1.13770	+ 4	1.00156	- 8	1.12014	+ 2	0.98435	- 7
0.71	1.14685	+ 5	1.01232	- 8	1.13781	+ 4	1.00345	- 8	1.12024	+ 2	0.98623	- 7
0.72	1.14696	+ 5	1.01418	- 8	1.13792	+ 4	1.00530	- 8	1.12033	+ 2	0.98806	- 7
0.73	1.14708	+ 5	1.01599	- 8	1.13803	+ 4	1.00711	- 8	1.12043	+ 2	0.98984	- 7
0.74	1.14719	+ 5	1.01776	- 8	1.13814	+ 4	1.00886	- 8	1.12052	+ 2	0.99158	- 7
0.75	1.14730	+ 5	1.01948	- 8	1.13824	+ 4	1.01058	- 8	1.12061	+ 2	0.99328	- 7
0.76	1.14741	+ 5	1.02116	- 8	1.13833	+ 3	1.01225	- 8	1.12070	+ 2	0.99493	- 7
0.77	1.14751	+ 5	1.02280	- 8	1.13843	+ 3	1.01388	- 8	1.12078	+ 2	0.99654	- 7
0.78	1.14762	+ 5	1.02440	- 8	1.13852	+ 3	1.01547	- 8	1.12086	+ 2	0.99812	- 7
0.79	1.14772	+ 5	1.02596	- 8	1.13862	+ 3	1.01702	- 8	1.12094	+ 2	0.99966	- 7
0.80	1.14781	+ 5	1.02748	- 8	1.13871	+ 3	1.01854	- 8	1.12102	+ 2	1.00116	- 7
0.81	1.14791	+ 5	1.02897	- 8	1.13880	+ 3	1.02002	- 8	1.12110	+ 2	1.00262	- 7
0.82	1.14800	+ 5	1.03042	- 8	1.13888	+ 3	1.02146	- 8	1.12118	+ 2	1.00406	- 7
0.83	1.14809	+ 5	1.03185	- 8	1.13897	+ 3	1.02288	- 8	1.12125	+ 2	1.00546	- 7
0.84	1.14818	+ 5	1.03324	- 8	1.13905	+ 3	1.02426	- 8	1.12132	+ 2	1.00683	- 7
0.85	1.14827	+ 5	1.03460	- 8	1.13913	+ 3	1.02562	- 8	1.12139	+ 2	1.00817	- 7
0.86	1.14835	+ 5	1.03593	- 8	1.13921	+ 3	1.02694	- 8	1.12146	+ 2	1.00947	- 7
0.87	1.14843	+ 5	1.03722	- 8	1.13929	+ 3	1.02823	- 8	1.12153	+ 2	1.01075	- 7
0.88	1.14851	+ 5	1.03850	- 8	1.13936	+ 3	1.02950	- 8	1.12159	+ 2	1.01201	- 7
0.89	1.14859	+ 5	1.03975	- 8	1.13944	+ 3	1.03074	- 8	1.12166	+ 2	1.01324	- 7
0.90	1.14867	+ 5	1.04096	- 8	1.13951	+ 3	1.03195	- 8	1.12172	+ 2	1.01444	- 7
0.91	1.14875	+ 5	1.04216	- 8	1.13958	+ 3	1.03314	- 8	1.12178	+ 2	1.01561	- 7
0.92	1.14882	+ 5	1.04333	- 8	1.13965	+ 3	1.03430	- 8	1.12184	+ 2	1.01676	- 7
0.93	1.14889	+ 5	1.04447	- 8	1.13972	+ 3	1.03544	- 8	1.12190	+ 2	1.01789	- 7
0.94	1.14896	+ 5	1.04560	- 8	1.13978	+ 3	1.03656	- 8	1.12196	+ 2	1.01900	- 7
0.95	1.14903	+ 5	1.04669	- 8	1.13985	+ 3	1.03765	- 8	1.12202	+ 2	1.02008	- 7
0.96	1.14910	+ 5	1.04777	- 8	1.13991	+ 3	1.03873	- 8	1.12207	+ 2	1.02114	- 7
0.97	1.14917	+ 5	1.04883	- 8	1.13998	+ 3	1.03978	- 8	1.12213	+ 2	1.02219	- 7
0.98	1.14923	+ 5	1.04987	- 8	1.14004	+ 3	1.04081	- 8	1.12218	+ 2	1.02321	- 7
0.99	1.14930	+ 5	1.05088	- 8	1.14010	+ 3	1.04182	- 8	1.12223	+ 2	1.02421	- 7
1.00	1.14936	+ 5	1.05188	- 8	1.14016	+ 3	1.04281	- 8	1.12228	+ 2	1.02519	- 7

TABLE 1-Continued

μ	$\tau = 0.10$; $\varpi = 0.50$				$\tau = 0.15$; $\varpi = 1.00$				$\tau = 0.15$; $\varpi = 0.95$			
	X	δ	Y	δ	X	δ	Y	δ	X	δ	Y	δ
0	1.00000	0	0	0	1.00000	0	0	0	1.00000	0	0	0
0.01	1.01218	+8	0.00540	- 7	1.02648	+15	0.01034	- 54	1.02496	+14	0.00964	-51
0.02	1.02087	+5	0.01810	-10	1.04609	+28	0.02227	- 80	1.04339	+26	0.02082	-75
0.03	1.02793	+7	0.05318	-12	1.06800	+41	0.04070	- 96	1.05924	+36	0.03848	-87
0.04	1.03368	+8	0.10524	-13	1.07776	+51	0.06998	-102	1.07308	+45	0.06696	-92
0.05	1.03823	+8	0.16843	-13	1.09057	+57	0.10851	-102	1.08510	+52	0.10453	-92
0.06	1.04199	+8	0.22120	-13	1.10169	+63	0.15182	- 99	1.09549	+56	0.14734	-89
0.07	1.04509	+8	0.27559	-12	1.11130	+64	0.19730	- 94	1.10451	+59	0.19217	-85
0.08	1.04768	+7	0.32556	-11	1.11968	+65	0.24259	- 89	1.11235	+59	0.23687	-82
0.09	1.04987	+6	0.37092	-11	1.12701	+65	0.28648	- 85	1.11920	+58	0.28021	-77
0.10	1.05175	+5	0.41194	-10	1.13346	+64	0.32817	- 82	1.12524	+57	0.32148	-75
0.11	1.05338	+4	0.44900	- 9	1.13918	+63	0.36754	- 77	1.13058	+56	0.36041	-72
0.12	1.05480	+4	0.48251	- 8	1.14427	+62	0.40442	- 74	1.13535	+55	0.39693	-68
0.13	1.05605	+3	0.51287	- 8	1.14882	+60	0.43886	- 72	1.13960	+53	0.43103	-66
0.14	1.05717	+3	0.54047	- 8	1.15292	+58	0.47100	- 68	1.14343	+51	0.46285	-64
0.15	1.05815	+2	0.56562	- 8	1.15668	+57	0.50096	- 64	1.14689	+49	0.49252	-61
0.16	1.05904	+2	0.58862	- 8	1.16001	+56	0.52888	- 62	1.15004	+48	0.52020	-58
0.17	1.05984	+1	0.60971	- 8	1.16307	+54	0.55495	- 59	1.15291	+47	0.54602	-56
0.18	1.06057	+1	0.62910	- 8	1.16588	+52	0.57929	- 57	1.15555	+46	0.57014	-55
0.19	1.06123	0	0.64700	- 8	1.16846	+50	0.60206	- 55	1.15795	+44	0.59271	-53
0.20	1.06184	0	0.66855	- 8	1.17088	+48	0.62338	- 53	1.16018	+43	0.61385	-51
0.21	1.06240	0	0.67891	- 7	1.17304	+47	0.64338	- 51	1.16224	+42	0.63369	-48
0.22	1.06292	0	0.69318	- 7	1.17508	+46	0.66216	- 49	1.16414	+41	0.65231	-47
0.23	1.06340	0	0.70648	- 7	1.17698	+45	0.67982	- 48	1.16591	+39	0.66982	-46
0.24	1.06384	0	0.71890	- 7	1.17875	+44	0.69646	- 46	1.16756	+38	0.68632	-44
0.25	1.06425	0	0.73052	- 7	1.18040	+43	0.71215	- 45	1.16910	+37	0.70189	-43
0.26	1.06463	0	0.74142	- 7	1.18195	+42	0.72697	- 44	1.17055	+37	0.71659	-42
0.27	1.06499	0	0.75166	- 7	1.18340	+41	0.74100	- 42	1.17191	+36	0.73051	-40
0.28	1.06533	0	0.76130	- 7	1.18476	+40	0.75428	- 41	1.17318	+35	0.74369	-38
0.29	1.06564	0	0.77039	- 7	1.18605	+39	0.76687	- 40	1.17437	+34	0.75617	-38
0.30	1.06594	0	0.77898	- 7	1.18726	+38	0.77883	- 39	1.17550	+33	0.76804	-37
0.31	1.06622	0	0.78711	- 5	1.18840	+37	0.79019	- 38	1.17657	+32	0.77931	-36
0.32	1.06648	0	0.79480	- 5	1.18949	+37	0.80101	- 37	1.17757	+31	0.79004	-36
0.33	1.06673	0	0.80210	- 5	1.19052	+36	0.81131	- 36	1.17853	+30	0.80026	-35
0.34	1.06696	0	0.80902	- 5	1.19150	+36	0.82114	- 35	1.17943	+29	0.81002	-34
0.35	1.06719	0	0.81561	- 5	1.19242	+35	0.83052	- 35	1.18030	+29	0.81933	-33
0.36	1.06740	0	0.82189	- 4	1.19330	+34	0.83948	- 34	1.18112	+28	0.82822	-33
0.37	1.06760	0	0.82787	- 4	1.19414	+33	0.84806	- 33	1.18190	+27	0.83674	-32
0.38	1.06779	0	0.83357	- 4	1.19495	+33	0.85628	- 32	1.18265	+27	0.84489	-31
0.39	1.06797	0	0.83902	- 4	1.19571	+32	0.86414	- 32	1.18337	+27	0.85270	-30
0.40	1.06814	0	0.84423	- 4	1.19644	+32	0.87170	- 30	1.18404	+26	0.86019	-30
0.41	1.06831	0	0.84922	- 4	1.19714	+31	0.87895	- 30	1.18470	+26	0.86737	-30
0.42	1.06847	0	0.85400	- 4	1.19780	+30	0.88588	- 30	1.18531	+25	0.87427	-30
0.43	1.06862	0	0.85858	- 4	1.19845	+30	0.89256	- 30	1.18592	+25	0.88091	-30
0.44	1.06877	0	0.86297	- 4	1.19906	+29	0.89899	- 30	1.18648	+24	0.88729	-30
0.45	1.06891	0	0.86720	- 4	1.19965	+28	0.90518	- 30	1.18704	+24	0.89343	-30
0.46	1.06903	-1	0.87125	- 4	1.20022	+28	0.91116	- 28	1.18757	+24	0.89938	-27
0.47	1.06916	-1	0.87516	- 4	1.20077	+28	0.91691	- 28	1.18807	+23	0.90509	-27
0.48	1.06928	-1	0.87891	- 4	1.20130	+27	0.92245	- 28	1.18856	+23	0.91059	-27
0.49	1.06940	-1	0.88253	- 4	1.20181	+27	0.92780	- 28	1.18903	+22	0.91591	-27
0.50	1.06951	-1	0.88602	- 4	1.20230	+27	0.93297	- 28	1.18949	+22	0.92104	-27

TABLE 1-Continued

μ	τ = 0.10 ; ϖ = 0.50				τ = 0.15 ; ϖ = 1.00				τ = 0.15 ; ϖ = 0.95			
	X	δ	Y	δ	X	δ	Y	δ	X	δ	Y	δ
0.51	1.06962	-1	0.88939	- 4	1.20276	+26	0.98798	- 26	1.18993	+22	0.92602	-25
0.52	1.06973	-1	0.89264	- 4	1.20322	+26	0.94281	- 26	1.19035	+22	0.93081	-25
0.53	1.06983	-1	0.89578	- 4	1.20367	+26	0.94748	- 26	1.19076	+22	0.93545	-25
0.54	1.06993	-1	0.89881	- 4	1.20409	+25	0.95200	- 26	1.19116	+22	0.93994	-25
0.55	1.07003	-1	0.90174	- 4	1.20450	+25	0.95638	- 26	1.19154	+22	0.94429	-25
0.56	1.07012	-1	0.90458	- 4	1.20490	+25	0.96062	- 26	1.19189	+20	0.94850	-25
0.57	1.07021	-1	0.90732	- 4	1.20529	+25	0.96474	- 25	1.19225	+20	0.95259	-25
0.58	1.07029	-1	0.90998	- 4	1.20566	+25	0.96873	- 25	1.19260	+20	0.95655	-25
0.59	1.07038	-1	0.91256	- 4	1.20603	+25	0.97260	- 25	1.19294	+20	0.96039	-25
0.60	1.07046	-1	0.91505	- 4	1.20637	+24	0.97635	- 25	1.19326	+20	0.96412	-25
0.61	1.07054	-1	0.91748	- 4	1.20671	+24	0.98000	- 25	1.19357	+19	0.96775	-24
0.62	1.07061	-1	0.91985	- 4	1.20705	+24	0.98354	- 25	1.19388	+19	0.97127	-24
0.63	1.07068	-1	0.92211	- 4	1.20737	+24	0.98699	- 25	1.19418	+19	0.97469	-24
0.64	1.07076	-1	0.92432	- 4	1.20768	+24	0.99033	- 25	1.19446	+19	0.97802	-24
0.65	1.07083	-1	0.92648	- 4	1.20798	+23	0.99359	- 25	1.19475	+19	0.98126	-24
0.66	1.07089	-1	0.92857	- 4	1.20827	+23	0.99676	- 25	1.19501	+18	0.98440	-24
0.67	1.07096	-1	0.93060	- 4	1.20856	+23	0.99985	- 24	1.19527	+18	0.98747	-24
0.68	1.07102	-1	0.93258	- 4	1.20884	+23	1.00285	- 24	1.19553	+18	0.99045	-24
0.69	1.07108	-1	0.93451	- 4	1.20911	+23	1.00578	- 24	1.19578	+18	0.99336	-24
0.70	1.07114	-1	0.93638	- 4	1.20936	+21	1.00862	- 24	1.19603	+18	0.99619	-24
0.71	1.07120	-1	0.93821	- 4	1.20962	+21	1.01140	- 24	1.19626	+17	0.99895	-24
0.72	1.07126	-1	0.93998	- 4	1.20987	+21	1.01411	- 24	1.19649	+17	1.00164	-24
0.73	1.07131	-1	0.94172	- 4	1.21012	+21	1.01675	- 24	1.19671	+17	1.00427	-24
0.74	1.07137	-1	0.94341	- 4	1.21036	+21	1.01933	- 24	1.19693	+17	1.00683	-24
0.75	1.07142	-1	0.94505	- 4	1.21059	+21	1.02184	- 24	1.19715	+17	1.00933	-24
0.76	1.07147	-1	0.94666	- 4	1.21082	+21	1.02429	- 24	1.19735	+16	1.01177	-24
0.77	1.07152	-1	0.94823	- 4	1.21104	+21	1.02669	- 24	1.19755	+16	1.01415	-24
0.78	1.07157	-1	0.94976	- 4	1.21126	+21	1.02903	- 24	1.19775	+16	1.01648	-24
0.79	1.07162	-1	0.95125	- 4	1.21147	+21	1.03132	- 24	1.19795	+16	1.01875	-24
0.80	1.07166	-1	0.95271	- 4	1.21167	+20	1.03355	- 24	1.19814	+16	1.02097	-24
0.81	1.07171	-1	0.95413	- 4	1.21187	+20	1.03574	- 24	1.19832	+16	1.02314	-24
0.82	1.07175	-1	0.95553	- 4	1.21207	+20	1.03787	- 24	1.19850	+16	1.02527	-24
0.83	1.07180	-1	0.95689	- 4	1.21226	+20	1.03996	- 24	1.19868	+16	1.02734	-24
0.84	1.07184	-1	0.95822	- 4	1.21245	+20	1.04200	- 24	1.19885	+16	1.02938	-24
0.85	1.07188	-1	0.95952	- 4	1.21263	+20	1.04400	- 24	1.19902	+16	1.03136	-24
0.86	1.07192	-1	0.96079	- 4	1.21282	+20	1.04596	- 24	1.19919	+16	1.03331	-24
0.87	1.07196	-1	0.96203	- 4	1.21299	+20	1.04787	- 24	1.19935	+16	1.03521	-24
0.88	1.07200	-1	0.96325	- 4	1.21317	+20	1.04975	- 24	1.19951	+16	1.03708	-24
0.89	1.07204	-1	0.96444	- 4	1.21334	+20	1.05158	- 24	1.19966	+16	1.03891	-24
0.90	1.07207	-1	0.96561	- 4	1.21350	+20	1.05338	- 24	1.19982	+16	1.04070	-24
0.91	1.07211	-1	0.96675	- 4	1.21367	+20	1.05515	- 24	1.19997	+16	1.04245	-24
0.92	1.07214	-1	0.96787	- 4	1.21383	+20	1.05687	- 24	1.20011	+16	1.04417	-24
0.93	1.07218	-1	0.96897	- 4	1.21398	+20	1.05856	- 24	1.20025	+16	1.04585	-24
0.94	1.07221	-1	0.97004	- 4	1.21414	+20	1.06022	- 24	1.20039	+16	1.04750	-24
0.95	1.07225	-1	0.97110	- 4	1.21429	+20	1.06185	- 24	1.20053	+16	1.04912	-24
0.96	1.07228	-1	0.97213	- 4	1.21444	+20	1.06344	- 24	1.20066	+16	1.05071	-24
0.97	1.07231	-1	0.97314	- 4	1.21458	+20	1.06501	- 24	1.20080	+16	1.05226	-24
0.98	1.07234	-1	0.97413	- 4	1.21472	+20	1.06654	- 24	1.20093	+16	1.05379	-24
0.99	1.07237	-1	0.97510	- 4	1.21486	+20	1.06805	- 24	1.20105	+16	1.05529	-24
1.00	1.07240	-1	0.97606	- 4	1.21500	+20	1.06953	- 24	1.20118	+16	1.05676	-24

TABLE 1-Continued

μ	τ = 0.15 ; ϖ = 0.90				τ = 0.15 ; ϖ = 0.80				τ = 0.15 ; ϖ = 0.50			
	X	δ	Y	δ	X	δ	Y	δ	X	δ	Y	δ
0	1.00000	0	0	0	1.00000	0	0	0	1.00000	0	0	0
0.01	1.02845	+12	0.00900	-44	1.02051	+ 7	0.00775	-33	1.01231	+ 5	0.00444	-10
0.02	1.04072	+22	0.01943	-67	1.03554	+14	0.01661	-52	1.02116	+ 7	0.00983	-17
0.03	1.05558	+32	0.03632	-78	1.04841	+20	0.03223	-60	1.02869	+10	0.02128	-22
0.04	1.06851	+39	0.06408	-83	1.05961	+25	0.05843	-65	1.03520	+12	0.04347	-25
0.05	1.07973	+45	0.10085	-83	1.06931	+28	0.09381	-66	1.04082	+13	0.07500	-26
0.06	1.08948	+47	0.14298	-79	1.07771	+31	0.13459	-66	1.04566	+13	0.11220	-27
0.07	1.09785	+49	0.18718	-76	1.08499	+33	0.17758	-64	1.04985	+13	0.15192	-27
0.08	1.10518	+50	0.23131	-74	1.09133	+34	0.22068	-62	1.05350	+13	0.19202	-27
0.09	1.11158	+50	0.27413	-71	1.09686	+34	0.26248	-59	1.05669	+13	0.23122	-26
0.10	1.11722	+49	0.31496	-67	1.10175	+35	0.30243	-57	1.05948	+12	0.26878	-25
0.11	1.12220	+47	0.35348	-65	1.10606	+34	0.34016	-55	1.06196	+12	0.30438	-24
0.12	1.12664	+46	0.38961	-63	1.10990	+34	0.37558	-53	1.06416	+11	0.33786	-23
0.13	1.13062	+45	0.42340	-59	1.11333	+33	0.40873	-50	1.06613	+10	0.36922	-23
0.14	1.13420	+44	0.45492	-57	1.11643	+33	0.43966	-48	1.06790	+ 9	0.39856	-22
0.15	1.13744	+43	0.48430	-56	1.11923	+32	0.46851	-47	1.06951	+ 9	0.42596	-21
0.16	1.14038	+42	0.51171	-54	1.12176	+31	0.49544	-45	1.07096	+ 8	0.45155	-21
0.17	1.14304	+39	0.53731	-52	1.12407	+29	0.52058	-44	1.07229	+ 8	0.47547	-20
0.18	1.14551	+39	0.56122	-50	1.12618	+28	0.54408	-43	1.07350	+ 7	0.49784	-19
0.19	1.14775	+37	0.58360	-48	1.12813	+27	0.56607	-41	1.07462	+ 7	0.51879	-19
0.20	1.14984	+37	0.60455	-46	1.12991	+25	0.58668	-39	1.07565	+ 7	0.53843	-18
0.21	1.15176	+36	0.62420	-45	1.13156	+24	0.60601	-38	1.07660	+ 6	0.55685	-18
0.22	1.15354	+35	0.64267	-43	1.13309	+23	0.62415	-36	1.07746	+ 6	0.57417	-18
0.23	1.15519	+34	0.66005	-41	1.13452	+22	0.64124	-37	1.07829	+ 5	0.59046	-18
0.24	1.15673	+33	0.67641	-40	1.13584	+21	0.65734	-36	1.07906	+ 5	0.60584	-18
0.25	1.15818	+33	0.69185	-39	1.13708	+20	0.67253	-35	1.07977	+ 4	0.62034	-18
0.26	1.15952	+32	0.70644	-37	1.13824	+19	0.68688	-34	1.08044	+ 4	0.63406	-17
0.27	1.16078	+30	0.72022	-37	1.13933	+18	0.70045	-33	1.08106	+ 4	0.64708	-17
0.28	1.16196	+29	0.73329	-36	1.14036	+18	0.71330	-33	1.08164	+ 3	0.65932	-17
0.29	1.16309	+29	0.74568	-35	1.14132	+17	0.72550	-32	1.08220	+ 3	0.67098	-17
0.30	1.16414	+28	0.75745	-34	1.14224	+17	0.73708	-32	1.08272	+ 3	0.68206	-17
0.31	1.16513	+27	0.76863	-34	1.14309	+16	0.74810	-31	1.08321	+ 2	0.69259	-17
0.32	1.16608	+27	0.77928	-33	1.14390	+15	0.75858	-30	1.08368	+ 2	0.70261	-17
0.33	1.16697	+26	0.78941	-33	1.14466	+15	0.76857	-29	1.08412	+ 2	0.71217	-17
0.34	1.16782	+26	0.79909	-32	1.14540	+14	0.77810	-28	1.08453	+ 1	0.72128	-17
0.35	1.16862	+25	0.80833	-31	1.14610	+14	0.78719	-28	1.08493	+ 1	0.72999	-17
0.36	1.16938	+24	0.81716	-30	1.14676	+13	0.79589	-27	1.08530	0	0.73832	-16
0.37	1.17012	+24	0.82560	-30	1.14739	+13	0.80420	-27	1.08567	0	0.74628	-16
0.38	1.17081	+23	0.83369	-29	1.14798	+12	0.81216	-27	1.08601	0	0.75390	-16
0.39	1.17148	+23	0.84144	-29	1.14856	+12	0.81979	-26	1.08634	0	0.76121	-16
0.40	1.17211	+22	0.84887	-28	1.14910	+11	0.82711	-26	1.08666	0	0.76822	-16
0.41	1.17272	+22	0.85601	-27	1.14963	+11	0.83413	-26	1.08695	- 1	0.77496	-15
0.42	1.17331	+22	0.86286	-27	1.15013	+11	0.84088	-26	1.08724	- 1	0.78142	-15
0.43	1.17386	+21	0.86944	-27	1.15062	+11	0.84737	-25	1.08752	- 1	0.78764	-15
0.44	1.17440	+21	0.87577	-27	1.15108	+11	0.85361	-25	1.08778	- 1	0.79362	-15
0.45	1.17490	+20	0.88187	-27	1.15153	+11	0.85962	-25	1.08804	- 1	0.79938	-15
0.46	1.17540	+20	0.88776	-26	1.15195	+10	0.86541	-24	1.08827	- 2	0.80493	-15
0.47	1.17587	+19	0.89342	-26	1.15236	+10	0.87099	-24	1.08851	- 2	0.81028	-15
0.48	1.17633	+19	0.89888	-26	1.15275	+10	0.87638	-24	1.08873	- 2	0.81544	-15
0.49	1.17676	+18	0.90416	-26	1.15313	+10	0.88158	-23	1.08895	- 2	0.82042	-15
0.50	1.17719	+18	0.90925	-26	1.15350	+10	0.88660	-23	1.08916	- 2	0.82523	-15

TABLE 1-Continued

μ	$\tau = 0.15$; $\varpi_\lambda = 0.90$				$\tau = 0.15$; $\varpi_\lambda = 0.80$				$\tau = 0.15$; $\varpi_\lambda = 0.50$			
	X	δ	Y	δ	X	δ	Y	δ	X	δ	Y	δ
0.51	1.17759	+17	0.91418	-25	1.15384	+ 8	0.89145	-23	1.08937	- 2	0.82990	-13
0.52	1.17798	+17	0.91894	-25	1.15418	+ 8	0.89614	-23	1.08956	- 2	0.83440	-13
0.53	1.17837	+17	0.92354	-25	1.15451	+ 8	0.90068	-22	1.08975	- 2	0.83875	-13
0.54	1.17874	+17	0.92800	-25	1.15483	+ 8	0.90508	-22	1.08993	- 2	0.84296	-13
0.55	1.17909	+17	0.93231	-25	1.15514	+ 8	0.90933	-22	1.09011	- 2	0.84704	-13
0.56	1.17942	+15	0.93651	-24	1.15543	+ 7	0.91345	-22	1.09027	- 3	0.85100	-13
0.57	1.17975	+15	0.94056	-24	1.15571	+ 7	0.91744	-22	1.09043	- 3	0.85483	-13
0.58	1.18008	+15	0.94449	-24	1.15599	+ 7	0.92132	-22	1.09059	- 3	0.85855	-13
0.59	1.18039	+15	0.94831	-24	1.15626	+ 7	0.92508	-22	1.09075	- 3	0.86215	-13
0.60	1.18070	+15	0.95201	-24	1.15653	+ 7	0.92873	-22	1.09090	- 3	0.86566	-13
0.61	1.18099	+15	0.95560	-24	1.15677	+ 6	0.93228	-21	1.09105	- 3	0.86906	-13
0.62	1.18128	+15	0.95910	-24	1.15702	+ 6	0.93572	-21	1.09119	- 3	0.87236	-13
0.63	1.18156	+15	0.96249	-24	1.15726	+ 6	0.93907	-21	1.09132	- 3	0.87557	-13
0.64	1.18183	+15	0.96580	-24	1.15749	+ 6	0.94232	-21	1.09146	- 3	0.87870	-13
0.65	1.18209	+15	0.96901	-24	1.15772	+ 6	0.94549	-21	1.09159	- 3	0.88173	-13
0.66	1.18233	+14	0.97213	-24	1.15793	+ 5	0.94857	-21	1.09171	- 3	0.88469	-13
0.67	1.18258	+14	0.97517	-24	1.15814	+ 5	0.95157	-21	1.09183	- 3	0.88757	-13
0.68	1.18282	+14	0.97813	-24	1.15835	+ 5	0.95448	-21	1.09195	- 3	0.89037	-13
0.69	1.18306	+14	0.98102	-24	1.15855	+ 5	0.95733	-21	1.09207	- 3	0.89310	-13
0.70	1.18328	+14	0.98383	-24	1.15875	+ 5	0.96010	-21	1.09218	- 3	0.89576	-13
0.71	1.18350	+13	0.98657	-24	1.15893	+ 4	0.96280	-21	1.09228	- 4	0.89835	-13
0.72	1.18371	+13	0.98924	-24	1.15911	+ 4	0.96543	-21	1.09239	- 4	0.90088	-13
0.73	1.18392	+13	0.99185	-24	1.15929	+ 4	0.96800	-21	1.09249	- 4	0.90334	-13
0.74	1.18413	+13	0.99439	-24	1.15947	+ 4	0.97051	-21	1.09259	- 4	0.90575	-13
0.75	1.18433	+13	0.99687	-24	1.15964	+ 4	0.97295	-21	1.09269	- 4	0.90810	-13
0.76	1.18451	+12	0.99929	-24	1.15981	+ 4	0.97534	-21	1.09279	- 4	0.91039	-13
0.77	1.18471	+12	1.00166	-24	1.15998	+ 4	0.97767	-21	1.09288	- 4	0.91263	-13
0.78	1.18489	+12	1.00397	-24	1.16014	+ 4	0.97995	-21	1.09297	- 4	0.91481	-13
0.79	1.18507	+12	1.00622	-24	1.16029	+ 4	0.98217	-21	1.09306	- 4	0.91695	-13
0.80	1.18525	+12	1.00843	-24	1.16045	+ 4	0.98435	-21	1.09315	- 4	0.91904	-13
0.81	1.18542	+12	1.01059	-24	1.16059	+ 3	0.98647	-21	1.09323	- 4	0.92108	-13
0.82	1.18559	+12	1.01269	-24	1.16073	+ 3	0.98855	-21	1.09332	- 4	0.92307	-13
0.83	1.18576	+12	1.01476	-24	1.16087	+ 3	0.99058	-21	1.09340	- 4	0.92503	-13
0.84	1.18592	+12	1.01677	-24	1.16101	+ 3	0.99257	-21	1.09348	- 4	0.92694	-13
0.85	1.18608	+12	1.01875	-24	1.16115	+ 3	0.99452	-21	1.09356	- 4	0.92880	-13
0.86	1.18623	+12	1.02068	-24	1.16128	+ 3	0.99642	-21	1.09363	- 4	0.93063	-13
0.87	1.18638	+12	1.02257	-24	1.16141	+ 3	0.99828	-21	1.09371	- 4	0.93242	-13
0.88	1.18653	+12	1.02442	-24	1.16154	+ 3	1.00011	-21	1.09378	- 4	0.93418	-13
0.89	1.18668	+12	1.02623	-24	1.16166	+ 3	1.00190	-21	1.09385	- 4	0.93589	-13
0.90	1.18682	+12	1.02801	-24	1.16179	+ 3	1.00365	-21	1.09392	- 4	0.93757	-13
0.91	1.18696	+12	1.02975	-24	1.16191	+ 3	1.00536	-21	1.09399	- 4	0.93922	-13
0.92	1.18709	+12	1.03146	-24	1.16202	+ 3	1.00704	-21	1.09406	- 4	0.94084	-13
0.93	1.18722	+12	1.03313	-24	1.16214	+ 3	1.00869	-21	1.09412	- 4	0.94242	-13
0.94	1.18735	+12	1.03477	-24	1.16225	+ 3	1.01031	-21	1.09419	- 4	0.94397	-13
0.95	1.18748	+12	1.03637	-24	1.16236	+ 3	1.01189	-21	1.09425	- 4	0.94549	-13
0.96	1.18761	+12	1.03795	-24	1.16247	+ 3	1.01344	-21	1.09431	- 4	0.94699	-13
0.97	1.18773	+12	1.03949	-24	1.16257	+ 3	1.01497	-21	1.09437	- 4	0.94845	-13
0.98	1.18785	+12	1.04101	-24	1.16268	+ 3	1.01646	-21	1.09443	- 4	0.94989	-13
0.99	1.18797	+12	1.04250	-24	1.16278	+ 3	1.01793	-21	1.09449	- 4	0.95130	-13
1.00	1.18808	+12	1.04396	-24	1.16288	+ 3	1.01937	-21	1.09455	- 4	0.95268	-13

TABLE 1-Continued

μ	$\tau = 0.20$; $\varpi_1 = 1.00$				$\tau = 0.20$; $\varpi_1 = 0.95$				$\tau = 0.20$; $\varpi_1 = 0.90$			
	X	δ	Y	δ	X	δ	Y	δ	X	δ	Y	δ
0	1.00000	0	0	0	1.00000	0	0	0	1.00000	0	0	0
0.01	1.02698	+ 21	0.00927	- 75	1.02542	+ 22	0.00849	- 80	1.02384	+18	0.00800	- 59
0.02	1.04711	+ 41	0.01986	-123	1.04430	+ 40	0.01800	-111	1.04151	+34	0.01671	- 97
0.03	1.06469	+ 60	0.03146	-150	1.06074	+ 56	0.02985	-135	1.05686	+48	0.02751	-121
0.04	1.08045	+ 76	0.04342	-166	1.07549	+ 71	0.04554	-148	1.07068	+62	0.04275	-133
0.05	1.09466	+ 90	0.07172	-173	1.08875	+ 83	0.06802	-157	1.08299	+73	0.06445	-140
0.06	1.10743	+101	0.10062	-174	1.10066	+ 92	0.09614	-158	1.09407	+80	0.09182	-142
0.07	1.11888	+110	0.13014	-173	1.11133	+ 98	0.12823	-157	1.10400	+85	0.12317	-143
0.08	1.12918	+114	0.16054	-169	1.12088	+101	0.16263	-155	1.11289	+88	0.15691	-140
0.09	1.13834	+117	0.20158	-165	1.12945	+103	0.19803	-151	1.12089	+91	0.19169	-136
0.10	1.14661	+118	0.24062	-159	1.13716	+103	0.23847	-146	1.12806	+92	0.22655	-132
0.11	1.15409	+119	0.27599	-154	1.14412	+103	0.26829	-142	1.13453	+92	0.26085	-127
0.12	1.16085	+116	0.31080	-149	1.15040	+101	0.30211	-136	1.14038	+90	0.29415	-124
0.13	1.16698	+116	0.34330	-145	1.15612	+100	0.33465	-132	1.14569	+88	0.32623	-121
0.14	1.17258	+114	0.37489	-139	1.16134	+ 99	0.36581	-127	1.15053	+86	0.35696	-117
0.15	1.17771	+113	0.40497	-135	1.16610	+ 97	0.39549	-124	1.15495	+84	0.38627	-113
0.16	1.18239	+110	0.43358	-131	1.17048	+ 96	0.42374	-120	1.15902	+83	0.41416	-109
0.17	1.18671	+107	0.46074	-126	1.17451	+ 95	0.45055	-117	1.16275	+80	0.44064	-106
0.18	1.19070	+105	0.48650	-122	1.17822	+ 93	0.47600	-113	1.16618	+77	0.46578	-102
0.19	1.19439	+103	0.51093	-118	1.18164	+ 90	0.50013	-110	1.16938	+76	0.48961	-100
0.20	1.19781	+100	0.53409	-114	1.18482	+ 88	0.52301	-107	1.17234	+74	0.51223	- 97
0.21	1.20100	+ 98	0.55606	-110	1.18777	+ 84	0.54473	-103	1.17509	+72	0.53369	- 94
0.22	1.20397	+ 96	0.57690	-106	1.19054	+ 83	0.56533	-100	1.17766	+70	0.55404	- 92
0.23	1.20674	+ 93	0.59668	-104	1.19312	+ 81	0.58488	- 98	1.18005	+68	0.57339	- 89
0.24	1.20934	+ 91	0.61547	-101	1.19553	+ 79	0.60346	- 96	1.18230	+67	0.59176	- 87
0.25	1.21178	+ 89	0.63334	- 98	1.19780	+ 77	0.62114	- 93	1.18441	+65	0.60925	- 85
0.26	1.21408	+ 87	0.65034	- 95	1.19993	+ 76	0.63795	- 91	1.18639	+64	0.62587	- 82
0.27	1.21624	+ 85	0.66652	- 93	1.20193	+ 73	0.65397	- 88	1.18825	+62	0.64170	- 81
0.28	1.21829	+ 84	0.68196	- 90	1.20382	+ 72	0.66924	- 86	1.19002	+61	0.65680	- 78
0.29	1.22021	+ 82	0.69668	- 87	1.20560	+ 69	0.68378	- 85	1.19167	+59	0.67120	- 77
0.30	1.22203	+ 80	0.71072	- 85	1.20729	+ 68	0.69769	- 83	1.19324	+57	0.68494	- 76
0.31	1.22376	+ 78	0.72413	- 84	1.20889	+ 66	0.71097	- 81	1.19474	+57	0.69808	- 74
0.32	1.22540	+ 77	0.73696	- 82	1.21041	+ 65	0.72367	- 79	1.19615	+56	0.71064	- 73
0.33	1.22697	+ 76	0.74924	- 80	1.21186	+ 64	0.73583	- 77	1.19749	+54	0.72266	- 72
0.34	1.22845	+ 75	0.76101	- 78	1.21324	+ 63	0.74747	- 76	1.19877	+53	0.73419	- 70
0.35	1.22987	+ 74	0.77227	- 77	1.21454	+ 61	0.75863	- 74	1.19998	+52	0.74524	- 68
0.36	1.23122	+ 73	0.78309	- 75	1.21578	+ 59	0.76933	- 73	1.20113	+50	0.75583	- 67
0.37	1.23250	+ 71	0.79346	- 74	1.21697	+ 58	0.77960	- 72	1.20224	+49	0.76599	- 67
0.38	1.23374	+ 70	0.80342	- 73	1.21812	+ 58	0.78948	- 70	1.20330	+48	0.77576	- 65
0.39	1.23491	+ 69	0.81300	- 72	1.21921	+ 57	0.79898	- 68	1.20431	+47	0.78515	- 65
0.40	1.23604	+ 68	0.82222	- 70	1.22025	+ 56	0.80811	- 67	1.20528	+46	0.79418	- 64
0.41	1.23713	+ 67	0.83110	- 68	1.22125	+ 55	0.81690	- 66	1.20620	+45	0.80288	- 63
0.42	1.23816	+ 66	0.83965	- 67	1.22221	+ 54	0.82537	- 64	1.20709	+44	0.81126	- 62
0.43	1.23916	+ 65	0.84788	- 66	1.22313	+ 53	0.83353	- 63	1.20794	+43	0.81934	- 61
0.44	1.24012	+ 64	0.85582	- 66	1.22402	+ 53	0.84140	- 62	1.20877	+43	0.82713	- 60
0.45	1.24105	+ 64	0.86348	- 65	1.22487	+ 52	0.84900	- 61	1.20956	+42	0.83465	- 59
0.46	1.24193	+ 63	0.87088	- 64	1.22568	+ 51	0.85633	- 60	1.21031	+41	0.84191	- 58
0.47	1.24278	+ 62	0.87803	- 63	1.22646	+ 50	0.86342	- 59	1.21104	+40	0.84892	- 57
0.48	1.24360	+ 61	0.88494	- 62	1.22722	+ 49	0.87027	- 58	1.21174	+39	0.85571	- 56
0.49	1.24440	+ 60	0.89162	- 62	1.22795	+ 48	0.87689	- 57	1.21243	+39	0.86227	- 55
0.50	1.24516	+ 59	0.89810	- 60	1.22865	+ 47	0.88330	- 57	1.21308	+38	0.86862	- 54

TABLE 1-Continued

μ	τ = 0.20 ; ϖ = 1.00				τ = 0.20 ; ϖ = 0.95				τ = 0.20 ; ϖ = 0.90			
	X	δ	Y	δ	X	δ	Y	δ	X	δ	Y	δ
0.51	1.24590	+ 58	0.90435	- 60	1.22934	+ 47	0.88950	- 56	1.21371	+37	0.87475	- 54
0.52	1.24661	+ 57	0.91041	- 59	1.23000	+ 47	0.89552	- 55	1.21432	+37	0.88071	- 53
0.53	1.24730	+ 56	0.91628	- 59	1.23068	+ 46	0.90134	- 55	1.21491	+36	0.88647	- 53
0.54	1.24797	+ 56	0.92198	- 58	1.23124	+ 45	0.90699	- 54	1.21549	+36	0.89207	- 52
0.55	1.24862	+ 55	0.92750	- 58	1.23185	+ 44	0.91247	- 53	1.21603	+35	0.89749	- 51
0.56	1.24925	+ 55	0.93286	- 57	1.23242	+ 44	0.91778	- 53	1.21657	+35	0.90275	- 51
0.57	1.24985	+ 54	0.93806	- 57	1.23297	+ 43	0.92295	- 52	1.21709	+34	0.90787	- 50
0.58	1.25045	+ 54	0.94312	- 56	1.23351	+ 43	0.92796	- 51	1.21759	+34	0.91288	- 50
0.59	1.25102	+ 53	0.94802	- 56	1.23403	+ 42	0.93283	- 51	1.21808	+33	0.91764	- 50
0.60	1.25157	+ 52	0.95280	- 55	1.23454	+ 41	0.93757	- 50	1.21854	+32	0.92233	- 50
0.61	1.25210	+ 51	0.95744	- 55	1.23503	+ 41	0.94216	- 50	1.21901	+32	0.92688	- 50
0.62	1.25262	+ 50	0.96194	- 55	1.23551	+ 40	0.94664	- 50	1.21944	+31	0.93131	- 50
0.63	1.25314	+ 50	0.96634	- 54	1.23598	+ 40	0.95099	- 50	1.21987	+30	0.93562	- 50
0.64	1.25362	+ 49	0.97061	- 54	1.23642	+ 39	0.95524	- 49	1.22029	+30	0.93982	- 49
0.65	1.25410	+ 48	0.97478	- 53	1.23686	+ 38	0.95936	- 49	1.22071	+30	0.94391	- 49
0.66	1.25457	+ 48	0.97883	- 53	1.23729	+ 38	0.96339	- 48	1.22110	+29	0.94789	- 49
0.67	1.25502	+ 47	0.98277	- 53	1.23770	+ 37	0.96731	- 48	1.22148	+28	0.95177	- 49
0.68	1.25547	+ 47	0.98663	- 52	1.23811	+ 37	0.97112	- 48	1.22186	+28	0.95555	- 49
0.69	1.25590	+ 46	0.99038	- 52	1.23850	+ 36	0.97485	- 48	1.22222	+27	0.95924	- 49
0.70	1.25632	+ 46	0.99403	- 52	1.23888	+ 36	0.97848	- 48	1.22256	+27	0.96284	- 48
0.71	1.25674	+ 46	0.99761	- 51	1.23926	+ 36	0.98202	- 48	1.22293	+27	0.96635	- 48
0.72	1.25713	+ 45	1.00109	- 51	1.23962	+ 35	0.98548	- 48	1.22327	+27	0.96977	- 48
0.73	1.25753	+ 45	1.00450	- 50	1.23998	+ 35	0.98885	- 48	1.22360	+27	0.97311	- 48
0.74	1.25791	+ 45	1.00782	- 50	1.24032	+ 34	0.99214	- 48	1.22392	+26	0.97638	- 48
0.75	1.25828	+ 44	1.01106	- 50	1.24066	+ 34	0.99537	- 47	1.22423	+26	0.97957	- 48
0.76	1.25864	+ 44	1.01424	- 49	1.24099	+ 34	0.99852	- 47	1.22454	+26	0.98268	- 48
0.77	1.25900	+ 44	1.01738	- 49	1.24131	+ 34	1.00159	- 47	1.22484	+26	0.98572	- 48
0.78	1.25934	+ 43	1.02045	- 49	1.24163	+ 34	1.00459	- 47	1.22513	+25	0.98871	- 47
0.79	1.25968	+ 43	1.02332	- 48	1.24193	+ 33	1.00753	- 47	1.22541	+25	0.99162	- 47
0.80	1.26002	+ 43	1.02621	- 48	1.24223	+ 33	1.01040	- 47	1.22570	+25	0.99446	- 47
0.81	1.26035	+ 43	1.02904	- 48	1.24253	+ 33	1.01321	- 47	1.22597	+25	0.99725	- 47
0.82	1.26066	+ 43	1.03181	- 48	1.24282	+ 33	1.01596	- 47	1.22623	+24	0.99997	- 47
0.83	1.26098	+ 43	1.03451	- 48	1.24310	+ 33	1.01865	- 47	1.22649	+24	1.00263	- 47
0.84	1.26128	+ 43	1.03717	- 47	1.24337	+ 32	1.02129	- 47	1.22675	+24	1.00524	- 47
0.85	1.26158	+ 43	1.03977	- 47	1.24364	+ 32	1.02387	- 47	1.22700	+24	1.00780	- 47
0.86	1.26188	+ 43	1.04231	- 47	1.24390	+ 32	1.02640	- 46	1.22724	+24	1.01030	- 47
0.87	1.26216	+ 43	1.04480	- 47	1.24415	+ 31	1.02888	- 46	1.22747	+23	1.01276	- 46
0.88	1.26245	+ 43	1.04724	- 47	1.24440	+ 31	1.03130	- 46	1.22771	+23	1.01516	- 46
0.89	1.26271	+ 42	1.04963	- 47	1.24465	+ 31	1.03368	- 46	1.22794	+23	1.01751	- 46
0.90	1.26298	+ 42	1.05198	- 46	1.24489	+ 30	1.03600	- 46	1.22817	+23	1.01982	- 46
0.91	1.26325	+ 42	1.05427	- 46	1.24512	+ 30	1.03829	- 46	1.22838	+22	1.02208	- 46
0.92	1.26351	+ 42	1.05652	- 46	1.24536	+ 30	1.04052	- 46	1.22859	+22	1.02431	- 45
0.93	1.26375	+ 41	1.05873	- 46	1.24557	+ 29	1.04272	- 46	1.22881	+22	1.02648	- 45
0.94	1.26400	+ 41	1.06090	- 46	1.24580	+ 29	1.04487	- 46	1.22901	+22	1.02862	- 45
0.95	1.26425	+ 41	1.06302	- 46	1.24602	+ 29	1.04699	- 45	1.22922	+22	1.03071	- 45
0.96	1.26449	+ 41	1.06511	- 45	1.24623	+ 29	1.04907	- 45	1.22942	+22	1.03276	- 45
0.97	1.26472	+ 41	1.06716	- 45	1.24643	+ 28	1.05110	- 45	1.22961	+22	1.03479	- 44
0.98	1.26495	+ 41	1.06916	- 45	1.24664	+ 28	1.05310	- 45	1.22980	+22	1.03677	- 44
0.99	1.26518	+ 41	1.07113	- 45	1.24684	+ 28	1.05506	- 45	1.22998	+21	1.03871	- 44
1.00	1.26539	+ 40	1.07307	- 45	1.24703	+ 27	1.05698	- 45	1.23017	+21	1.04061	- 44

TABLE 1-Continued

μ	$\tau = 0.20$; $\varpi_* = 0.80$				$\tau = 0.20$; $\varpi_* = 0.50$				$\tau = 0.25$; $\varpi_* = 1.00$			
	X	δ	Y	δ	X	δ	Y	δ	X	δ	Y	δ
0	1.00000	0	0	0	1.00000	0	0	0	1.00000	0	0	0
0.01	1.02082	+15	0.00682	- 46	1.01241	+ 8	0.00379	-17	1.02744	+ 31	0.00850	- 93
0.02	1.03615	+27	0.01425	- 76	1.02137	+13	0.00792	-29	1.04805	+ 62	0.01764	-159
0.03	1.04944	+39	0.02148	- 94	1.02905	+17	0.01361	-36	1.06613	+ 92	0.02768	-204
0.04	1.06130	+49	0.02746	-104	1.03584	+19	0.02382	-41	1.08251	+118	0.03982	-233
0.05	1.07194	+57	0.03273	-109	1.04191	+21	0.04028	-44	1.09740	+136	0.05556	-250
0.06	1.08148	+63	0.03866	-112	1.04732	+22	0.06248	-45	1.11120	+149	0.07545	-260
0.07	1.09000	+66	0.11366	-112	1.05215	+23	0.08891	-46	1.12380	+161	0.09914	-262
0.08	1.09762	+67	0.14611	-111	1.05647	+23	0.11798	-46	1.13536	+172	0.12576	-261
0.09	1.10446	+68	0.17970	-108	1.06034	+23	0.14842	-45	1.14595	+178	0.15439	-259
0.10	1.11061	+68	0.21344	-106	1.06380	+22	0.17925	-44	1.15562	+184	0.18420	-255
0.11	1.11615	+67	0.24671	-103	1.06692	+21	0.20982	-43	1.16449	+187	0.21454	-249
0.12	1.12118	+67	0.27908	-100	1.06976	+21	0.23969	-42	1.17263	+189	0.24489	-243
0.13	1.12573	+66	0.31030	- 97	1.07232	+20	0.26860	-41	1.18013	+190	0.27488	-236
0.14	1.12988	+64	0.34022	- 94	1.07465	+19	0.29639	-40	1.18703	+189	0.30424	-230
0.15	1.13369	+64	0.36878	- 92	1.07680	+19	0.32297	-39	1.19340	+188	0.33280	-224
0.16	1.13716	+62	0.39599	- 88	1.07875	+18	0.34833	-38	1.19930	+186	0.36045	-218
0.17	1.14037	+61	0.42183	- 86	1.08055	+17	0.37248	-37	1.20478	+184	0.38712	-213
0.18	1.14331	+58	0.44635	- 85	1.08222	+17	0.39542	-37	1.20986	+181	0.41281	-206
0.19	1.14603	+56	0.46964	- 83	1.08375	+16	0.41723	-36	1.21460	+178	0.43748	-200
0.20	1.14857	+55	0.49173	- 81	1.08517	+15	0.43794	-36	1.21903	+175	0.46113	-195
0.21	1.15093	+53	0.51270	- 79	1.08650	+15	0.45762	-35	1.22317	+172	0.48382	-190
0.22	1.15313	+52	0.53261	- 77	1.08778	+14	0.47632	-34	1.22706	+169	0.50556	-184
0.23	1.15517	+50	0.55152	- 75	1.08888	+13	0.49408	-34	1.23070	+166	0.52637	-180
0.24	1.15709	+48	0.56949	- 74	1.08996	+12	0.51099	-33	1.23415	+164	0.54632	-174
0.25	1.15890	+47	0.58658	- 73	1.09098	+12	0.52708	-32	1.23738	+161	0.56542	-170
0.26	1.16059	+46	0.60285	- 71	1.09192	+11	0.54240	-32	1.24043	+158	0.58372	-166
0.27	1.16218	+44	0.61835	- 70	1.09281	+10	0.55701	-31	1.24332	+156	0.60126	-162
0.28	1.16369	+43	0.63313	- 68	1.09366	+10	0.57093	-31	1.24606	+154	0.61808	-158
0.29	1.16511	+42	0.64723	- 67	1.09447	+10	0.58423	-30	1.24865	+151	0.63420	-155
0.30	1.16646	+41	0.66070	- 65	1.09522	+ 9	0.59692	-30	1.25110	+148	0.64968	-152
0.31	1.16772	+39	0.67355	- 65	1.09594	+ 9	0.60906	-30	1.25345	+146	0.66454	-148
0.32	1.16892	+37	0.68587	- 63	1.09661	+ 8	0.62068	-29	1.25568	+144	0.67882	-145
0.33	1.17007	+36	0.69765	- 62	1.09726	+ 8	0.63180	-29	1.25780	+142	0.69254	-142
0.34	1.17116	+35	0.70893	- 61	1.09788	+ 8	0.64245	-29	1.25982	+140	0.70573	-139
0.35	1.17220	+34	0.71975	- 60	1.09846	+ 8	0.65268	-28	1.26176	+138	0.71843	-136
0.36	1.17320	+34	0.73013	- 59	1.09901	+ 7	0.66248	-28	1.26360	+136	0.73064	-134
0.37	1.17415	+33	0.74009	- 58	1.09955	+ 7	0.67189	-28	1.26537	+134	0.74242	-131
0.38	1.17505	+32	0.74967	- 57	1.10006	+ 7	0.68095	-27	1.26706	+132	0.75377	-128
0.39	1.17592	+31	0.75887	- 56	1.10055	+ 7	0.68965	-27	1.26868	+130	0.76470	-126
0.40	1.17674	+30	0.76773	- 55	1.10101	+ 6	0.69803	-27	1.27024	+128	0.77525	-124
0.41	1.17753	+29	0.77626	- 54	1.10145	+ 6	0.70610	-26	1.27173	+126	0.78544	-122
0.42	1.17829	+28	0.78448	- 53	1.10188	+ 6	0.71387	-26	1.27317	+125	0.79528	-120
0.43	1.17902	+27	0.79239	- 53	1.10229	+ 5	0.72136	-26	1.27455	+123	0.80478	-118
0.44	1.17973	+27	0.80003	- 52	1.10268	+ 5	0.72858	-26	1.27588	+121	0.81397	-116
0.45	1.18040	+26	0.80740	- 51	1.10306	+ 5	0.73556	-26	1.27716	+120	0.82286	-114
0.46	1.18105	+26	0.81451	- 51	1.10342	+ 4	0.74229	-26	1.27839	+118	0.83146	-112
0.47	1.18167	+25	0.82140	- 50	1.10377	+ 4	0.74880	-26	1.27959	+117	0.83978	-111
0.48	1.18227	+24	0.82805	- 49	1.10410	+ 3	0.75509	-26	1.28074	+116	0.84784	-110
0.49	1.18286	+24	0.83448	- 48	1.10443	+ 3	0.76118	-26	1.28185	+114	0.85566	-108
0.50	1.18341	+23	0.84070	- 48	1.10475	+ 3	0.76708	-26	1.28292	+113	0.86323	-107

TABLE 1-Continued

μ	τ = 0.20 ; ϖ = 0.80				τ = 0.20 ; ϖ = 0.50				τ = 0.25 ; ϖ = 1.00			
	X	δ	Y	δ	X	δ	Y	δ	X	δ	Y	δ
0.51	1.18596	+23	0.84672	- 48	1.10503	+ 1	0.77280	-24	1.28396	+112	0.87058	-105
0.52	1.18648	+22	0.85256	- 47	1.10535	+ 1	0.77833	-24	1.28496	+110	0.87770	-104
0.53	1.18699	+22	0.85821	- 47	1.10561	+ 1	0.78369	-24	1.28592	+108	0.88462	-103
0.54	1.18748	+22	0.86370	- 46	1.10589	+ 1	0.78888	-24	1.28688	+108	0.89133	-102
0.55	1.18795	+21	0.86902	- 46	1.10616	+ 1	0.79392	-24	1.28778	+106	0.89787	-100
0.56	1.18840	+20	0.87418	- 46	1.10641	+ 1	0.79882	-24	1.28867	+105	0.90420	-100
0.57	1.18885	+20	0.87919	- 46	1.10666	+ 1	0.80357	-24	1.28953	+104	0.91036	- 99
0.58	1.18728	+20	0.88406	- 45	1.10691	+ 1	0.80818	-24	1.29036	+103	0.91635	- 98
0.59	1.18769	+19	0.88879	- 45	1.10714	+ 1	0.81266	-24	1.29117	+102	0.92218	- 97
0.60	1.18810	+19	0.89338	- 45	1.10737	+ 1	0.81702	-24	1.29195	+101	0.92786	- 96
0.61	1.18848	+18	0.89785	- 45	1.10758	0	0.82127	-23	1.29272	+100	0.93338	- 95
0.62	1.18887	+18	0.90221	- 44	1.10779	0	0.82540	-23	1.29347	+100	0.93876	- 94
0.63	1.18924	+18	0.90644	- 44	1.10800	0	0.82941	-23	1.29419	+ 99	0.94400	- 94
0.64	1.18960	+18	0.91056	- 44	1.10821	0	0.83332	-23	1.29489	+ 98	0.94910	- 93
0.65	1.18994	+17	0.91457	- 44	1.10840	0	0.83712	-23	1.29557	+ 97	0.95408	- 92
0.66	1.19029	+17	0.91847	- 44	1.10858	- 1	0.84083	-23	1.29624	+ 96	0.95893	- 92
0.67	1.19061	+16	0.92228	- 44	1.10877	- 1	0.84444	-23	1.29690	+ 96	0.96367	- 91
0.68	1.19093	+16	0.92599	- 44	1.10895	- 1	0.84796	-23	1.29753	+ 95	0.96829	- 90
0.69	1.19125	+16	0.92961	- 44	1.10913	- 1	0.85140	-23	1.29814	+ 94	0.97279	- 90
0.70	1.19155	+15	0.93313	- 44	1.10930	- 1	0.85475	-23	1.29874	+ 93	0.97719	- 89
0.71	1.19185	+15	0.93658	- 44	1.10946	- 2	0.85801	-23	1.29932	+ 92	0.98148	- 89
0.72	1.19214	+15	0.93994	- 44	1.10962	- 2	0.86120	-23	1.29990	+ 92	0.98568	- 88
0.73	1.19242	+15	0.94322	- 44	1.10978	- 2	0.86432	-23	1.30047	+ 92	0.98977	- 88
0.74	1.19270	+15	0.94643	- 43	1.10993	- 2	0.86736	-23	1.30101	+ 91	0.99378	- 87
0.75	1.19296	+14	0.94956	- 43	1.11009	- 2	0.87033	-23	1.30154	+ 90	0.99769	- 87
0.76	1.19323	+14	0.95262	- 43	1.11022	- 3	0.87323	-23	1.30207	+ 90	1.00152	- 86
0.77	1.19348	+14	0.95560	- 43	1.11037	- 3	0.87607	-23	1.30258	+ 89	1.00526	- 86
0.78	1.19373	+13	0.95852	- 43	1.11051	- 3	0.87884	-23	1.30308	+ 89	1.00892	- 86
0.79	1.19397	+13	0.96138	- 43	1.11065	- 3	0.88155	-23	1.30356	+ 88	1.01250	- 85
0.80	1.19421	+13	0.96417	- 43	1.11078	- 3	0.88421	-23	1.30404	+ 88	1.01601	- 85
0.81	1.19445	+13	0.96691	- 43	1.11091	- 3	0.88681	-22	1.30451	+ 87	1.01944	- 84
0.82	1.19468	+13	0.96958	- 43	1.11104	- 3	0.88935	-22	1.30497	+ 87	1.02280	- 84
0.83	1.19489	+12	0.97220	- 43	1.11117	- 3	0.89184	-22	1.30541	+ 86	1.02608	- 84
0.84	1.19511	+12	0.97476	- 43	1.11129	- 3	0.89427	-22	1.30585	+ 86	1.02930	- 84
0.85	1.19532	+12	0.97726	- 43	1.11141	- 3	0.89665	-22	1.30629	+ 86	1.03246	- 83
0.86	1.19553	+12	0.97972	- 43	1.11152	- 3	0.89898	-22	1.30670	+ 85	1.03555	- 83
0.87	1.19574	+12	0.98214	- 42	1.11164	- 3	0.90127	-22	1.30712	+ 85	1.03859	- 82
0.88	1.19594	+12	0.98449	- 42	1.11175	- 3	0.90351	-22	1.30751	+ 84	1.04155	- 82
0.89	1.19613	+11	0.98680	- 42	1.11186	- 3	0.90570	-22	1.30791	+ 84	1.04446	- 82
0.90	1.19632	+11	0.98907	- 42	1.11197	- 3	0.90785	-22	1.30831	+ 84	1.04732	- 82
0.91	1.19651	+11	0.99129	- 42	1.11208	- 3	0.90996	-22	1.30869	+ 84	1.05011	- 82
0.92	1.19669	+11	0.99346	- 42	1.11218	- 3	0.91203	-22	1.30906	+ 83	1.05287	- 81
0.93	1.19688	+11	0.99560	- 42	1.11228	- 3	0.91406	-22	1.30943	+ 83	1.05556	- 81
0.94	1.19705	+11	0.99769	- 42	1.11238	- 3	0.91605	-22	1.30979	+ 83	1.05820	- 81
0.95	1.19723	+11	0.99975	- 42	1.11248	- 3	0.91800	-22	1.31014	+ 82	1.06081	- 80
0.96	1.19739	+10	1.00176	- 42	1.11257	- 3	0.91992	-22	1.31049	+ 82	1.06335	- 80
0.97	1.19756	+10	1.00374	- 42	1.11267	- 3	0.92180	-22	1.31083	+ 82	1.06585	- 80
0.98	1.19772	+10	1.00568	- 42	1.11276	- 3	0.92364	-22	1.31117	+ 82	1.06830	- 80
0.99	1.19788	+10	1.00759	- 42	1.11285	- 3	0.92546	-22	1.31150	+ 82	1.07071	- 80
1.00	1.19804	+10	1.00946	- 42	1.11294	- 3	0.92725	-22	1.31183	+ 82	1.07308	- 80

TABLE 1-Continued

μ	τ = 0.25 ; ϖ = 0.95				τ = 0.25 ; ϖ = 0.90				τ = 0.25 ; ϖ = 0.80			
	X	δ	Y	δ	X	δ	Y	δ	X	δ	Y	δ
0	1.00000	0	0	0	1.00000	0	0	0	1.00000	0	0	0
0.01	1.02574	+ 22	0.00800	- 70	1.02411	+ 19	0.00740	- 60	1.02099	+ 13	0.00621	- 50
0.02	1.04498	+ 46	0.01634	-142	1.04210	+ 40	0.01507	-127	1.03654	+ 28	0.01274	- 98
0.03	1.06188	+ 69	0.02564	-184	1.05780	+ 60	0.02366	-166	1.05006	+ 43	0.02005	-128
0.04	1.07708	+ 90	0.03701	-211	1.07201	+ 80	0.03483	-187	1.06226	+ 58	0.02930	-148
0.05	1.09112	+116	0.05196	-226	1.08506	+103	0.04851	-202	1.07344	+ 75	0.04205	-161
0.06	1.10392	+130	0.07105	-236	1.09698	+118	0.06684	-210	1.08368	+ 86	0.05895	-167
0.07	1.11564	+141	0.09396	-238	1.10784	+126	0.08897	-214	1.09295	+ 95	0.07965	-171
0.08	1.12639	+151	0.11983	-237	1.11779	+132	0.11409	-215	1.10144	+100	0.10340	-172
0.09	1.13621	+157	0.14773	-235	1.12688	+136	0.14129	-214	1.10920	+103	0.12927	-172
0.10	1.14520	+162	0.17686	-232	1.13522	+140	0.16975	-211	1.11629	+105	0.15647	-171
0.11	1.15342	+163	0.20655	-228	1.14285	+142	0.19882	-207	1.12278	+105	0.18434	-169
0.12	1.16096	+164	0.23629	-222	1.14984	+142	0.22796	-203	1.12873	+105	0.21237	-166
0.13	1.16790	+164	0.26570	-218	1.15627	+142	0.25680	-200	1.13420	+104	0.24017	-163
0.14	1.17430	+162	0.29453	-212	1.16220	+142	0.28511	-195	1.13924	+103	0.26749	-160
0.15	1.18020	+161	0.32259	-207	1.16767	+140	0.31269	-190	1.14389	+101	0.29415	-156
0.16	1.18567	+159	0.34978	-202	1.17273	+138	0.33942	-186	1.14819	+ 99	0.32001	-153
0.17	1.19074	+157	0.37602	-197	1.17742	+136	0.36524	-181	1.15218	+ 97	0.34501	-150
0.18	1.19544	+154	0.40130	-191	1.18178	+133	0.39010	-177	1.15589	+ 95	0.36912	-146
0.19	1.19983	+152	0.42558	-187	1.18584	+130	0.41400	-173	1.15934	+ 92	0.39230	-143
0.20	1.20393	+149	0.44888	-182	1.18968	+128	0.43694	-169	1.16256	+ 90	0.41457	-140
0.21	1.20777	+147	0.47122	-178	1.19318	+125	0.45896	-164	1.16558	+ 88	0.43594	-137
0.22	1.21135	+144	0.49265	-173	1.19651	+123	0.48006	-160	1.16840	+ 85	0.45644	-134
0.23	1.21472	+141	0.51318	-168	1.19962	+120	0.50027	-157	1.17105	+ 83	0.47609	-131
0.24	1.21790	+139	0.53284	-164	1.20256	+118	0.51965	-153	1.17355	+ 81	0.49492	-129
0.25	1.22089	+137	0.55166	-161	1.20532	+116	0.53822	-150	1.17590	+ 79	0.51299	-126
0.26	1.22371	+134	0.56973	-156	1.20793	+113	0.55602	-146	1.17811	+ 77	0.53029	-124
0.27	1.22638	+132	0.58703	-153	1.21040	+111	0.57307	-144	1.18021	+ 75	0.54689	-122
0.28	1.22889	+129	0.60362	-150	1.21274	+108	0.58944	-141	1.18219	+ 73	0.56282	-120
0.29	1.23128	+127	0.61954	-146	1.21494	+106	0.60514	-138	1.18406	+ 71	0.57811	-118
0.30	1.23355	+125	0.63482	-143	1.21704	+104	0.62020	-136	1.18584	+ 69	0.59278	-116
0.31	1.23570	+122	0.64949	-140	1.21903	+102	0.63468	-133	1.18753	+ 67	0.60686	-114
0.32	1.23775	+120	0.66359	-137	1.22093	+100	0.64859	-130	1.18915	+ 66	0.62042	-113
0.33	1.23971	+118	0.67714	-134	1.22274	+ 98	0.66195	-128	1.19068	+ 64	0.63344	-111
0.34	1.24157	+116	0.69017	-132	1.22446	+ 96	0.67481	-126	1.19214	+ 62	0.64598	-109
0.35	1.24334	+114	0.70270	-130	1.22610	+ 94	0.68718	-124	1.19354	+ 61	0.65803	-108
0.36	1.24504	+112	0.71478	-127	1.22768	+ 92	0.69909	-122	1.19487	+ 59	0.66965	-106
0.37	1.24667	+111	0.72641	-125	1.22918	+ 91	0.71057	-120	1.19615	+ 58	0.68084	-105
0.38	1.24822	+109	0.73762	-123	1.23061	+ 89	0.72164	-118	1.19736	+ 56	0.69162	-104
0.39	1.24971	+107	0.74843	-121	1.23200	+ 88	0.73231	-116	1.19854	+ 55	0.70203	-102
0.40	1.25114	+106	0.75885	-120	1.23331	+ 86	0.74261	-114	1.19966	+ 54	0.71207	-101
0.41	1.25251	+104	0.76892	-118	1.23458	+ 84	0.75254	-113	1.20073	+ 52	0.72176	-100
0.42	1.25382	+102	0.77865	-116	1.23580	+ 83	0.76215	-111	1.20177	+ 51	0.73114	- 98
0.43	1.25508	+100	0.78805	-114	1.23696	+ 81	0.77142	-110	1.20276	+ 50	0.74019	- 97
0.44	1.25681	+ 99	0.79714	-112	1.23809	+ 80	0.78040	-108	1.20372	+ 49	0.74894	- 96
0.45	1.25748	+ 98	0.80592	-111	1.23918	+ 78	0.78907	-107	1.20464	+ 48	0.75740	- 95
0.46	1.25861	+ 96	0.81442	-110	1.24022	+ 77	0.79748	-105	1.20553	+ 47	0.76560	- 94
0.47	1.25970	+ 95	0.82266	-108	1.24123	+ 76	0.80560	-104	1.20637	+ 45	0.77354	- 93
0.48	1.26074	+ 94	0.83063	-107	1.24220	+ 74	0.81348	-103	1.20720	+ 44	0.78122	- 92
0.49	1.26176	+ 92	0.83836	-106	1.24313	+ 73	0.82111	-102	1.20799	+ 43	0.78868	- 91
0.50	1.26274	+ 91	0.84585	-105	1.24404	+ 72	0.82852	-100	1.20876	+ 42	0.79590	- 90

TABLE 1-Continued

μ	τ = 0.25 ; ϖ = 0.95				τ = 0.25 ; ϖ = 0.90				τ = 0.25 ; ϖ = 0.60			
	X	δ	Y	δ	X	δ	Y	δ	X	δ	Y	δ
0.51	1.26369	+ 90	0.85312	-104	1.24492	+ 71	0.85569	-100	1.20950	+ 41	0.80291	- 89
0.52	1.26460	+ 89	0.86016	-104	1.24576	+ 70	0.84266	- 99	1.21028	+ 41	0.80972	- 88
0.53	1.26548	+ 88	0.86701	-103	1.24658	+ 69	0.84982	- 98	1.21093	+ 40	0.81632	- 87
0.54	1.26634	+ 86	0.87365	-102	1.24738	+ 68	0.85599	- 97	1.21160	+ 39	0.82273	- 87
0.55	1.26717	+ 85	0.88011	-101	1.24814	+ 67	0.86237	- 96	1.21225	+ 38	0.82896	- 86
0.56	1.26797	+ 84	0.88639	-100	1.24889	+ 66	0.86857	- 95	1.21288	+ 37	0.83502	- 85
0.57	1.26875	+ 83	0.89249	-100	1.24961	+ 65	0.87460	- 94	1.21349	+ 36	0.84091	- 84
0.58	1.26951	+ 82	0.89842	- 99	1.25031	+ 64	0.88046	- 94	1.21408	+ 35	0.84663	- 84
0.59	1.27024	+ 82	0.90420	- 98	1.25098	+ 63	0.88616	- 93	1.21465	+ 34	0.85220	- 83
0.60	1.27095	+ 80	0.90982	- 97	1.25164	+ 62	0.89171	- 93	1.21522	+ 34	0.85768	- 82
0.61	1.27166	+ 80	0.91529	- 97	1.25228	+ 62	0.89712	- 92	1.21576	+ 33	0.86291	- 82
0.62	1.27233	+ 79	0.92062	- 96	1.25291	+ 61	0.90238	- 92	1.21628	+ 32	0.86805	- 81
0.63	1.27298	+ 78	0.92580	- 96	1.25351	+ 60	0.90751	- 91	1.21679	+ 31	0.87307	- 80
0.64	1.27361	+ 77	0.93087	- 95	1.25410	+ 59	0.91250	- 91	1.21730	+ 31	0.87795	- 80
0.65	1.27423	+ 76	0.93580	- 94	1.25468	+ 58	0.91738	- 90	1.21778	+ 30	0.88272	- 79
0.66	1.27484	+ 76	0.94061	- 94	1.25523	+ 58	0.92213	- 90	1.21824	+ 29	0.88735	- 79
0.67	1.27542	+ 75	0.94530	- 93	1.25577	+ 57	0.92676	- 90	1.21871	+ 29	0.89189	- 78
0.68	1.27599	+ 74	0.94988	- 93	1.25630	+ 56	0.93127	- 90	1.21915	+ 28	0.89630	- 78
0.69	1.27654	+ 74	0.95435	- 92	1.25681	+ 56	0.93569	- 89	1.21958	+ 27	0.90062	- 77
0.70	1.27709	+ 73	0.95871	- 92	1.25731	+ 56	0.94000	- 89	1.22001	+ 27	0.90483	- 77
0.71	1.27762	+ 72	0.96296	- 92	1.25780	+ 55	0.94420	- 89	1.22042	+ 26	0.90895	- 76
0.72	1.27812	+ 72	0.96713	- 91	1.25828	+ 54	0.94831	- 89	1.22083	+ 26	0.91297	- 76
0.73	1.27863	+ 71	0.97119	- 91	1.25875	+ 54	0.95234	- 88	1.22122	+ 25	0.91690	- 75
0.74	1.27912	+ 70	0.97517	- 90	1.25920	+ 54	0.95626	- 88	1.22161	+ 25	0.92073	- 75
0.75	1.27960	+ 70	0.97905	- 90	1.25964	+ 53	0.96009	- 88	1.22198	+ 24	0.92446	- 75
0.76	1.28007	+ 69	0.98284	- 90	1.26008	+ 52	0.96384	- 88	1.22235	+ 24	0.92815	- 74
0.77	1.28052	+ 68	0.98656	- 89	1.26050	+ 52	0.96751	- 88	1.22270	+ 23	0.93174	- 74
0.78	1.28097	+ 68	0.99019	- 89	1.26090	+ 52	0.97109	- 88	1.22306	+ 23	0.93526	- 73
0.79	1.28140	+ 68	0.99374	- 89	1.26132	+ 52	0.97461	- 88	1.22339	+ 22	0.93869	- 73
0.80	1.28183	+ 67	0.99723	- 88	1.26171	+ 51	0.97805	- 87	1.22373	+ 22	0.94205	- 73
0.81	1.28224	+ 66	1.00065	- 88	1.26210	+ 50	0.98141	- 87	1.22405	+ 21	0.94534	- 72
0.82	1.28265	+ 66	1.00396	- 88	1.26247	+ 50	0.98471	- 87	1.22437	+ 21	0.94856	- 72
0.83	1.28304	+ 65	1.00723	- 88	1.26284	+ 50	0.98795	- 87	1.22468	+ 20	0.95172	- 72
0.84	1.28344	+ 65	1.01043	- 87	1.26320	+ 50	0.99109	- 87	1.22499	+ 20	0.95482	- 71
0.85	1.28381	+ 64	1.01357	- 87	1.26355	+ 49	0.99419	- 87	1.22528	+ 19	0.95784	- 71
0.86	1.28419	+ 64	1.01664	- 87	1.26390	+ 49	0.99723	- 86	1.22558	+ 19	0.96091	- 71
0.87	1.28456	+ 64	1.01964	- 87	1.26424	+ 48	1.00021	- 86	1.22586	+ 18	0.96373	- 70
0.88	1.28491	+ 63	1.02260	- 86	1.26457	+ 48	1.00312	- 86	1.22614	+ 18	0.96658	- 70
0.89	1.28526	+ 62	1.02550	- 86	1.26490	+ 48	1.00598	- 86	1.22641	+ 17	0.96937	- 70
0.90	1.28560	+ 62	1.02833	- 86	1.26521	+ 48	1.00878	- 86	1.22668	+ 17	0.97211	- 70
0.91	1.28594	+ 62	1.03111	- 86	1.26552	+ 48	1.01153	- 86	1.22694	+ 16	0.97480	- 70
0.92	1.28627	+ 61	1.03384	- 86	1.26583	+ 47	1.01423	- 86	1.22720	+ 16	0.97745	- 69
0.93	1.28658	+ 60	1.03652	- 86	1.26612	+ 46	1.01688	- 86	1.22746	+ 16	0.98004	- 69
0.94	1.28690	+ 60	1.03916	- 85	1.26642	+ 46	1.01947	- 86	1.22770	+ 15	0.98258	- 69
0.95	1.28722	+ 60	1.04174	- 85	1.26671	+ 46	1.02203	- 86	1.22794	+ 15	0.98508	- 68
0.96	1.28752	+ 60	1.04427	- 85	1.26699	+ 46	1.02453	- 86	1.22817	+ 14	0.98753	- 68
0.97	1.28782	+ 59	1.04676	- 85	1.26726	+ 46	1.02699	- 86	1.22841	+ 14	0.98994	- 68
0.98	1.28810	+ 58	1.04920	- 85	1.26754	+ 46	1.02940	- 86	1.22864	+ 14	0.99229	- 68
0.99	1.28840	+ 58	1.05159	- 85	1.26781	+ 45	1.03177	- 86	1.22886	+ 13	0.99461	- 68
1.00	1.28868	+ 58	1.05396	- 85	1.26807	+ 45	1.03410	- 86	1.22909	+ 13	0.99690	- 67

TABLE 1-Continued

μ	$\tau = 0.25$; $\varpi_\lambda = 0.50$				$\tau = 0.50$; $\varpi_\lambda = 1.00$				$\tau = 0.50$; $\varpi_\lambda = 0.95$			
	X	δ	Y	δ	X	δ	Y	δ	X	δ	Y	δ
0	1.00000	0	0	0	1.0000	0	0	0	1.0000	0	0	0
0.01	1.01247	+ 9	0.00828	-26	1.0288	+ 4	0.0063	-17	1.0268	+ 3	0.0057	-16
0.02	1.02152	+17	0.00687	-39	1.0508	+ 9	0.0130	-32	1.0472	+ 7	0.0118	-29
0.03	1.02928	+23	0.01097	-48	1.0702	+14	0.0201	-45	1.0652	+11	0.0182	-40
0.04	1.03620	+27	0.01678	-56	1.0882	+20	0.0275	-56	1.0818	+17	0.0250	-50
0.05	1.04247	+30	0.02594	-61	1.1051	+26	0.0352	-66	1.0974	+23	0.0321	-58
0.06	1.04817	+32	0.03916	-66	1.1210	+32	0.0436	-78	1.1120	+28	0.0397	-64
0.07	1.05337	+34	0.05625	-68	1.1362	+38	0.0527	-78	1.1259	+34	0.0480	-70
0.08	1.05811	+35	0.07647	-69	1.1506	+44	0.0627	-82	1.1391	+39	0.0572	-74
0.09	1.06243	+36	0.09895	-70	1.1643	+48	0.0737	-86	1.1516	+42	0.0674	-78
0.10	1.06636	+36	0.12292	-70	1.1775	+54	0.0859	-89	1.1637	+47	0.0787	-81
0.11	1.06997	+36	0.14773	-70	1.1900	+57	0.0992	-91	1.1751	+50	0.0912	-83
0.12	1.07327	+36	0.17288	-69	1.2020	+61	0.1136	-92	1.1860	+52	0.1048	-84
0.13	1.07629	+35	0.19797	-68	1.2134	+63	0.1290	-93	1.1963	+54	0.1194	-86
0.14	1.07908	+34	0.22275	-67	1.2244	+66	0.1452	-94	1.2063	+56	0.1348	-86
0.15	1.08165	+33	0.24700	-66	1.2348	+68	0.1621	-94	1.2158	+58	0.1510	-87
0.16	1.08402	+32	0.27062	-65	1.2448	+70	0.1796	-94	1.2248	+60	0.1677	-87
0.17	1.08623	+31	0.29351	-64	1.2543	+71	0.1976	-94	1.2334	+60	0.1849	-86
0.18	1.08826	+29	0.31562	-63	1.2634	+72	0.2159	-93	1.2416	+61	0.2025	-86
0.19	1.09017	+28	0.33694	-62	1.2721	+73	0.2343	-92	1.2495	+62	0.2203	-86
0.20	1.09195	+27	0.35744	-62	1.2804	+74	0.2530	-91	1.2570	+62	0.2382	-85
0.21	1.09361	+26	0.37715	-61	1.2884	+74	0.2716	-91	1.2642	+63	0.2562	-85
0.22	1.09517	+25	0.39608	-60	1.2959	+74	0.2902	-90	1.2710	+63	0.2742	-84
0.23	1.09663	+24	0.41425	-59	1.3032	+74	0.3087	-88	1.2776	+63	0.2922	-83
0.24	1.09800	+23	0.43169	-58	1.3102	+75	0.3271	-87	1.2838	+63	0.3099	-82
0.25	1.09929	+22	0.44841	-58	1.3169	+75	0.3453	-86	1.2898	+62	0.3276	-81
0.26	1.10051	+21	0.46447	-57	1.3233	+75	0.3633	-85	1.2956	+62	0.3450	-80
0.27	1.10166	+20	0.47988	-56	1.3294	+74	0.3810	-84	1.3011	+62	0.3622	-80
0.28	1.10275	+19	0.49467	-55	1.3354	+74	0.3985	-83	1.3064	+62	0.3792	-78
0.29	1.10378	+18	0.50887	-55	1.3411	+74	0.4156	-82	1.3115	+61	0.3959	-78
0.30	1.10476	+17	0.52252	-54	1.3466	+74	0.4325	-80	1.3164	+61	0.4123	-77
0.31	1.10569	+16	0.53564	-53	1.3518	+73	0.4490	-79	1.3211	+60	0.4284	-76
0.32	1.10657	+15	0.54824	-53	1.3569	+73	0.4653	-78	1.3256	+60	0.4442	-75
0.33	1.10742	+15	0.56038	-52	1.3617	+72	0.4812	-77	1.3300	+59	0.4598	-74
0.34	1.10823	+14	0.57204	-52	1.3665	+72	0.4968	-76	1.3342	+59	0.4749	-74
0.35	1.10899	+13	0.58329	-51	1.3710	+71	0.5120	-75	1.3382	+58	0.4898	-72
0.36	1.10972	+12	0.59412	-51	1.3754	+71	0.5270	-74	1.3421	+58	0.5044	-71
0.37	1.11043	+12	0.60456	-50	1.3796	+70	0.5416	-72	1.3458	+57	0.5187	-70
0.38	1.11109	+11	0.61462	-50	1.3837	+70	0.5559	-71	1.3495	+57	0.5327	-70
0.39	1.11173	+10	0.62434	-49	1.3877	+69	0.5699	-70	1.3530	+56	0.5464	-69
0.40	1.11235	+10	0.63371	-49	1.3915	+69	0.5836	-69	1.3564	+56	0.5598	-68
0.41	1.11294	+ 9	0.64277	-48	1.3952	+68	0.5969	-68	1.3596	+55	0.5728	-67
0.42	1.11350	+ 8	0.65152	-48	1.3988	+68	0.6100	-67	1.3628	+55	0.5856	-67
0.43	1.11405	+ 8	0.65998	-47	1.4022	+67	0.6228	-66	1.3658	+54	0.5982	-66
0.44	1.11457	+ 7	0.66816	-47	1.4056	+67	0.6353	-65	1.3689	+54	0.6104	-65
0.45	1.11509	+ 7	0.67607	-47	1.4089	+66	0.6475	-65	1.3717	+53	0.6224	-64
0.46	1.11557	+ 6	0.68374	-46	1.4121	+66	0.6595	-63	1.3745	+53	0.6342	-63
0.47	1.11604	+ 6	0.69116	-46	1.4151	+65	0.6712	-62	1.3772	+52	0.6456	-62
0.48	1.11649	+ 5	0.69836	-45	1.4182	+65	0.6826	-62	1.3798	+51	0.6568	-61
0.49	1.11693	+ 5	0.70535	-45	1.4210	+64	0.6937	-61	1.3823	+51	0.6678	-61
0.50	1.11735	+ 4	0.71209	-45	1.4239	+64	0.7046	-60	1.3848	+50	0.6785	-60

TABLE 1-Continued

μ	τ = 0.25 ; ϖ = 0.50				τ = 0.50 ; ϖ = 1.00				τ = 0.50 ; ϖ = 0.95			
	X	δ	Y	δ	X	δ	Y	δ	X	δ	Y	δ
0.51	1.11776	+ 4	0.71865	-45	1.4266	+63	0.7153	-59	1.3872	+50	0.6890	-60
0.52	1.11816	+ 4	0.72502	-44	1.4293	+63	0.7258	-58	1.3896	+50	0.6998	-59
0.53	1.11853	+ 3	0.73120	-44	1.4319	+62	0.7360	-58	1.3918	+49	0.7098	-58
0.54	1.11890	+ 3	0.73721	-44	1.4344	+62	0.7460	-57	1.3940	+48	0.7192	-58
0.55	1.11926	+ 2	0.74305	-43	1.4369	+61	0.7557	-56	1.3961	+48	0.7288	-57
0.56	1.11961	+ 2	0.74872	-43	1.4393	+61	0.7653	-55	1.3982	+48	0.7382	-56
0.57	1.11994	+ 2	0.75424	-43	1.4416	+60	0.7746	-55	1.4003	+47	0.7475	-55
0.58	1.12026	+ 1	0.75961	-42	1.4439	+60	0.7838	-54	1.4022	+47	0.7565	-55
0.59	1.12058	+ 1	0.76485	-42	1.4461	+59	0.7928	-53	1.4041	+46	0.7654	-54
0.60	1.12088	0	0.76991	-42	1.4483	+59	0.8016	-52	1.4060	+46	0.7740	-54
0.61	1.12118	0	0.77486	-42	1.4504	+58	0.8102	-52	1.4078	+45	0.7825	-53
0.62	1.12148	0	0.77968	-42	1.4525	+58	0.8186	-51	1.4096	+45	0.7908	-53
0.63	1.12175	- 1	0.78439	-41	1.4545	+58	0.8269	-50	1.4113	+44	0.7989	-52
0.64	1.12203	- 1	0.78897	-41	1.4565	+58	0.8349	-50	1.4130	+44	0.8069	-51
0.65	1.12230	- 1	0.79343	-41	1.4584	+57	0.8428	-49	1.4147	+43	0.8147	-51
0.66	1.12256	- 1	0.79778	-41	1.4603	+56	0.8506	-48	1.4163	+43	0.8224	-50
0.67	1.12280	- 2	0.80203	-41	1.4622	+56	0.8582	-48	1.4178	+42	0.8299	-50
0.68	1.12305	- 2	0.80618	-41	1.4640	+56	0.8656	-47	1.4194	+42	0.8373	-49
0.69	1.12329	- 2	0.81023	-40	1.4657	+55	0.8730	-47	1.4209	+42	0.8446	-49
0.70	1.12352	- 3	0.81418	-40	1.4675	+55	0.8801	-46	1.4224	+42	0.8516	-48
0.71	1.12375	- 3	0.81804	-40	1.4692	+54	0.8872	-46	1.4238	+41	0.8586	-48
0.72	1.12397	- 3	0.82181	-40	1.4708	+54	0.8940	-45	1.4252	+40	0.8654	-47
0.73	1.12418	- 4	0.82550	-40	1.4725	+54	0.9008	-44	1.4266	+40	0.8721	-47
0.74	1.12439	- 4	0.82910	-40	1.4740	+53	0.9074	-44	1.4279	+40	0.8787	-46
0.75	1.12460	- 4	0.83262	-40	1.4756	+53	0.9139	-43	1.4292	+39	0.8851	-46
0.76	1.12480	- 4	0.83606	-40	1.4772	+53	0.9203	-43	1.4305	+39	0.8915	-45
0.77	1.12500	- 4	0.83943	-40	1.4786	+52	0.9265	-42	1.4318	+39	0.8977	-45
0.78	1.12518	- 5	0.84272	-40	1.4801	+52	0.9327	-42	1.4330	+39	0.9038	-45
0.79	1.12537	- 5	0.84595	-40	1.4816	+52	0.9387	-41	1.4342	+38	0.9098	-44
0.80	1.12556	- 5	0.84910	-40	1.4830	+52	0.9446	-41	1.4354	+38	0.9157	-44
0.81	1.12574	- 5	0.85220	-39	1.4844	+52	0.9505	-40	1.4365	+37	0.9215	-43
0.82	1.12590	- 6	0.85523	-39	1.4858	+51	0.9562	-40	1.4376	+37	0.9271	-43
0.83	1.12608	- 6	0.85819	-39	1.4871	+51	0.9618	-40	1.4388	+37	0.9327	-43
0.84	1.12625	- 6	0.86109	-39	1.4884	+51	0.9673	-39	1.4398	+36	0.9382	-42
0.85	1.12641	- 6	0.86394	-39	1.4897	+51	0.9727	-39	1.4409	+36	0.9436	-42
0.86	1.12657	- 6	0.86673	-39	1.4910	+50	0.9780	-38	1.4420	+36	0.9489	-42
0.87	1.12673	- 6	0.86946	-39	1.4922	+50	0.9832	-38	1.4430	+36	0.9541	-41
0.88	1.12688	- 7	0.87214	-39	1.4935	+50	0.9884	-37	1.4440	+35	0.9592	-41
0.89	1.12703	- 7	0.87477	-39	1.4947	+50	0.9934	-37	1.4450	+35	0.9642	-41
0.90	1.12718	- 7	0.87734	-39	1.4959	+50	0.9984	-37	1.4459	+35	0.9692	-40
0.91	1.12732	- 7	0.87987	-39	1.4971	+50	1.0033	-36	1.4469	+34	0.9741	-40
0.92	1.12747	- 7	0.88235	-39	1.4982	+49	1.0080	-36	1.4478	+34	0.9788	-40
0.93	1.12761	- 7	0.88479	-39	1.4994	+49	1.0128	-35	1.4487	+34	0.9835	-40
0.94	1.12774	- 7	0.88718	-39	1.5005	+49	1.0174	-35	1.4496	+34	0.9882	-40
0.95	1.12787	- 8	0.88952	-39	1.5016	+49	1.0220	-35	1.4505	+33	0.9928	-39
0.96	1.12800	- 8	0.89182	-39	1.5027	+49	1.0264	-34	1.4514	+33	0.9972	-39
0.97	1.12813	- 8	0.89409	-39	1.5038	+49	1.0309	-34	1.4522	+33	1.0016	-39
0.98	1.12826	- 8	0.89630	-39	1.5048	+49	1.0352	-34	1.4531	+33	1.0060	-39
0.99	1.12838	- 8	0.89848	-39	1.5059	+48	1.0395	-33	1.4539	+32	1.0103	-38
1.00	1.12850	- 8	0.90063	-39	1.5069	+48	1.0437	-33	1.4547	+32	1.0145	-38

TABLE 1-Continued

μ	$\tau = 0.50$; $\varpi = 0.90$				$\tau = 0.50$; $\varpi = 0.80$				$\tau = 0.50$; $\varpi = 0.50$			
	X	δ	Y	δ	X	δ	Y	δ	X	δ	Y	δ
0	1.0000	0	0	0	1.00000	0	0	0	1.00000	0	0	0
0.01	1.0252	+ 5	0.0052	-14	1.02163	+ 24	0.00418	-104	1.01266	+ 15	0.00204	- 36
0.02	1.0443	+10	0.0106	-25	1.03790	+ 58	0.00860	-195	1.02186	+ 27	0.00416	- 70
0.03	1.0610	+14	0.0164	-36	1.05213	+ 90	0.01328	-272	1.02980	+ 38	0.00640	-100
0.04	1.0763	+18	0.0225	-44	1.06503	+117	0.01818	-341	1.03693	+ 46	0.00880	-123
0.05	1.0905	+22	0.0289	-51	1.07715	+159	0.02335	-401	1.04348	+ 59	0.01132	-147
0.06	1.1038	+25	0.0358	-58	1.08843	+192	0.02898	-448	1.04957	+ 69	0.01412	-169
0.07	1.1165	+30	0.0433	-63	1.09910	+224	0.03518	-492	1.05527	+ 79	0.01744	-186
0.08	1.1286	+34	0.0517	-67	1.10920	+252	0.04223	-526	1.06064	+ 88	0.02152	-197
0.09	1.1401	+37	0.0612	-70	1.11875	+273	0.05028	-554	1.06568	+ 93	0.02644	-214
0.10	1.1511	+41	0.0718	-78	1.12793	+300	0.05943	-577	1.07048	+100	0.03244	-224
0.11	1.1615	+43	0.0834	-75	1.13660	+318	0.06968	-598	1.07502	+105	0.03952	-233
0.12	1.1715	+45	0.0962	-76	1.14485	+332	0.08105	-610	1.07932	+109	0.04766	-238
0.13	1.1810	+47	0.1100	-78	1.15278	+346	0.09341	-620	1.08340	+112	0.05680	-246
0.14	1.1900	+49	0.1246	-78	1.16020	+354	0.10668	-629	1.08728	+114	0.06684	-250
0.15	1.1986	+50	0.1400	-79	1.16733	+361	0.12060	-638	1.09095	+114	0.07768	-254
0.16	1.2069	+51	0.1560	-79	1.17412	+366	0.13523	-641	1.09444	+114	0.08916	-260
0.17	1.2147	+51	0.1724	-79	1.18058	+368	0.15035	-645	1.09776	+113	0.10124	-262
0.18	1.2222	+52	0.1893	-79	1.18675	+369	0.16585	-648	1.10092	+112	0.11376	-265
0.19	1.2294	+52	0.2064	-79	1.19263	+369	0.18168	-647	1.10392	+110	0.12666	-266
0.20	1.2362	+53	0.2236	-78	1.19824	+368	0.19768	-647	1.10679	+108	0.13980	-268
0.21	1.2427	+53	0.2409	-78	1.20361	+367	0.21380	-646	1.10952	+105	0.15316	-268
0.22	1.2489	+53	0.2583	-78	1.20874	+365	0.22998	-643	1.11212	+102	0.16661	-270
0.23	1.2549	+53	0.2756	-77	1.21365	+363	0.24613	-640	1.11462	+100	0.18014	-270
0.24	1.2606	+53	0.2927	-76	1.21834	+360	0.26220	-639	1.11700	+ 97	0.19367	-270
0.25	1.2661	+52	0.3098	-76	1.22283	+356	0.27818	-635	1.11927	+ 94	0.20717	-270
0.26	1.2713	+52	0.3266	-75	1.22713	+352	0.29400	-632	1.12145	+ 91	0.22060	-270
0.27	1.2763	+51	0.3433	-74	1.23125	+347	0.30965	-629	1.12354	+ 88	0.23391	-270
0.28	1.2811	+51	0.3597	-74	1.23521	+343	0.32510	-625	1.12555	+ 86	0.24710	-270
0.29	1.2857	+50	0.3759	-73	1.23900	+338	0.34033	-621	1.12747	+ 83	0.26015	-270
0.30	1.2902	+50	0.3918	-72	1.24265	+333	0.35533	-616	1.12931	+ 80	0.27300	-270
0.31	1.2945	+50	0.4074	-72	1.24616	+328	0.37008	-611	1.13108	+ 77	0.28568	-270
0.32	1.2986	+49	0.4228	-71	1.24953	+323	0.38455	-609	1.13278	+ 74	0.29818	-268
0.33	1.3025	+48	0.4378	-70	1.25275	+316	0.39878	-604	1.13441	+ 70	0.31046	-268
0.34	1.3064	+48	0.4526	-69	1.25590	+313	0.41275	-600	1.13599	+ 68	0.32253	-268
0.35	1.3100	+47	0.4670	-69	1.25888	+305	0.42643	-595	1.13751	+ 65	0.33439	-268
0.36	1.3136	+47	0.4812	-68	1.26180	+302	0.43985	-590	1.13897	+ 62	0.34605	-266
0.37	1.3169	+46	0.4951	-67	1.26458	+295	0.45298	-587	1.14038	+ 59	0.35747	-266
0.38	1.3203	+46	0.5087	-66	1.26730	+291	0.46585	-583	1.14173	+ 56	0.36867	-266
0.39	1.3234	+45	0.5220	-66	1.26990	+285	0.47845	-579	1.14304	+ 53	0.37967	-264
0.40	1.3265	+45	0.5350	-65	1.27242	+280	0.49078	-576	1.14431	+ 50	0.39044	-264
0.41	1.3295	+44	0.5477	-65	1.27483	+273	0.50288	-570	1.14553	+ 47	0.40100	-262
0.42	1.3324	+44	0.5602	-64	1.27720	+269	0.51475	-564	1.14672	+ 45	0.41134	-262
0.43	1.3351	+43	0.5724	-63	1.27948	+264	0.52628	-562	1.14786	+ 42	0.42148	-260
0.44	1.3378	+42	0.5843	-63	1.28168	+259	0.53760	-558	1.14896	+ 39	0.43140	-260
0.45	1.3404	+42	0.5959	-62	1.28381	+253	0.54865	-557	1.15004	+ 37	0.44111	-260
0.46	1.3430	+42	0.6074	-61	1.28588	+249	0.55953	-549	1.15107	+ 34	0.45064	-258
0.47	1.3454	+41	0.6185	-61	1.28788	+243	0.57013	-546	1.15208	+ 32	0.45995	-258
0.48	1.3478	+40	0.6294	-60	1.28983	+239	0.58052	-542	1.15305	+ 29	0.46907	-258
0.49	1.3501	+40	0.6401	-60	1.29170	+233	0.59067	-539	1.15400	+ 27	0.47802	-256
0.50	1.3523	+40	0.6506	-59	1.29355	+230	0.60060	-536	1.15493	+ 25	0.48677	-256

TABLE 1-Continued

μ	τ = 0.50 ; ϖ = 0.90				τ = 0.50 ; ϖ = 0.80				τ = 0.50 ; ϖ = 0.50			
	X	δ	Y	δ	X	δ	Y	δ	X	δ	Y	δ
0.51	1.3545	+39	0.6608	-58	1.29532	+224	0.61033	-533	1.15581	+ 22	0.49535	-254
0.52	1.3566	+38	0.6708	-58	1.29705	+220	0.61985	-530	1.15668	+ 20	0.50374	-254
0.53	1.3586	+38	0.6806	-57	1.29873	+216	0.62918	-526	1.15752	+ 18	0.51198	-252
0.54	1.3606	+37	0.6901	-57	1.30036	+211	0.63830	-523	1.15834	+ 16	0.52002	-252
0.55	1.3626	+37	0.6996	-56	1.30195	+207	0.64723	-520	1.15913	+ 13	0.52791	-252
0.56	1.3645	+37	0.7087	-56	1.30349	+203	0.65598	-517	1.15990	+ 11	0.53565	-250
0.57	1.3663	+36	0.7177	-55	1.30500	+199	0.66453	-515	1.16065	+ 9	0.54322	-250
0.58	1.3681	+36	0.7265	-55	1.30645	+194	0.67295	-510	1.16139	+ 7	0.55065	-248
0.59	1.3698	+35	0.7351	-54	1.30788	+190	0.68115	-508	1.16210	+ 5	0.55792	-248
0.60	1.3715	+35	0.7436	-54	1.30925	+185	0.68920	-506	1.16280	+ 4	0.56504	-248
0.61	1.3732	+34	0.7518	-54	1.31060	+181	0.69712	-500	1.16348	+ 2	0.57204	-246
0.62	1.3748	+34	0.7599	-53	1.31193	+176	0.70485	-499	1.16414	0	0.57888	-246
0.63	1.3764	+33	0.7679	-53	1.31321	+174	0.71241	-496	1.16478	- 2	0.58559	-246
0.64	1.3779	+33	0.7757	-52	1.31446	+170	0.71982	-494	1.16540	- 4	0.59219	-244
0.65	1.3794	+33	0.7833	-52	1.31568	+166	0.72710	-492	1.16601	- 6	0.59864	-244
0.66	1.3809	+32	0.7908	-52	1.31688	+163	0.73425	-488	1.16662	- 7	0.60497	-244
0.67	1.3823	+32	0.7981	-51	1.31805	+160	0.74124	-486	1.16720	- 9	0.61120	-242
0.68	1.3837	+32	0.8053	-51	1.31919	+156	0.74810	-484	1.16776	- 11	0.61728	-242
0.69	1.3851	+31	0.8123	-50	1.32029	+152	0.75483	-482	1.16833	- 12	0.62326	-242
0.70	1.3864	+31	0.8192	-50	1.32138	+149	0.76143	-480	1.16886	- 14	0.62912	-242
0.71	1.3877	+30	0.8260	-50	1.32245	+146	0.76790	-478	1.16940	- 15	0.63489	-240
0.72	1.3890	+30	0.8327	-49	1.32348	+142	0.77424	-477	1.16992	- 17	0.64054	-240
0.73	1.3902	+30	0.8392	-49	1.32449	+139	0.78047	-476	1.17043	- 18	0.64608	-240
0.74	1.3914	+29	0.8456	-49	1.32549	+136	0.78659	-474	1.17092	- 20	0.65153	-240
0.75	1.3926	+29	0.8519	-48	1.32645	+132	0.79260	-472	1.17141	- 21	0.65689	-238
0.76	1.3938	+29	0.8581	-48	1.32740	+129	0.79850	-470	1.17188	- 23	0.66214	-238
0.77	1.3949	+28	0.8641	-48	1.32833	+126	0.80429	-469	1.17235	- 24	0.66729	-238
0.78	1.3960	+28	0.8701	-47	1.32925	+124	0.80997	-468	1.17279	- 26	0.67236	-238
0.79	1.3971	+28	0.8760	-47	1.33013	+120	0.81555	-467	1.17324	- 27	0.67733	-238
0.80	1.3982	+27	0.8817	-47	1.33101	+118	0.82103	-466	1.17366	- 28	0.68222	-238
0.81	1.3992	+27	0.8873	-46	1.33187	+116	0.82641	-465	1.17410	- 30	0.68704	-236
0.82	1.4002	+27	0.8929	-46	1.33271	+113	0.83171	-464	1.17452	- 31	0.69176	-236
0.83	1.4012	+26	0.8983	-46	1.33352	+110	0.83691	-463	1.17494	- 32	0.69640	-236
0.84	1.4023	+26	0.9037	-46	1.33433	+108	0.84202	-462	1.17534	- 33	0.70096	-236
0.85	1.4032	+26	0.9090	-45	1.33512	+105	0.84704	-461	1.17573	- 35	0.70544	-236
0.86	1.4042	+26	0.9141	-45	1.33589	+102	0.85198	-460	1.17611	- 36	0.70987	-234
0.87	1.4051	+26	0.9192	-45	1.33665	+100	0.85683	-460	1.17649	- 37	0.71421	-234
0.88	1.4060	+26	0.9242	-45	1.33740	+ 98	0.86159	-460	1.17687	- 38	0.71847	-234
0.89	1.4069	+25	0.9291	-44	1.33813	+ 95	0.86629	-459	1.17723	- 39	0.72267	-234
0.90	1.4078	+25	0.9340	-44	1.33885	+ 93	0.87091	-458	1.17759	- 40	0.72679	-234
0.91	1.4087	+25	0.9387	-44	1.33954	+ 90	0.87546	-457	1.17794	- 41	0.73085	-234
0.92	1.4096	+25	0.9434	-44	1.34023	+ 88	0.87993	-456	1.17829	- 42	0.73485	-234
0.93	1.4104	+25	0.9480	-43	1.34092	+ 86	0.88432	-456	1.17862	- 44	0.73880	-232
0.94	1.4112	+24	0.9525	-43	1.34158	+ 84	0.88864	-456	1.17895	- 45	0.74267	-232
0.95	1.4120	+24	0.9570	-43	1.34223	+ 81	0.89290	-455	1.17928	- 46	0.74648	-232
0.96	1.4128	+24	0.9614	-43	1.34287	+ 79	0.89708	-455	1.17961	- 46	0.75023	-232
0.97	1.4136	+24	0.9657	-42	1.34350	+ 77	0.90121	-454	1.17992	- 47	0.75392	-232
0.98	1.4144	+24	0.9700	-42	1.34412	+ 75	0.90527	-454	1.18023	- 48	0.75755	-232
0.99	1.4151	+24	0.9741	-42	1.34473	+ 73	0.90927	-453	1.18053	- 49	0.76113	-232
1.00	1.4159	+24	0.9782	-42	1.34588	+ 71	0.91320	-453	1.18083	- 50	0.76465	-232

TABLE 1-Continued

μ	$\tau = 1.00$; $\varpi = 1.00$				$\tau = 1.00$; $\varpi = 0.95$				$\tau = 1.00$; $\varpi = 0.90$			
	X	δ	Y	δ	X	δ	Y	δ	X	δ	Y	δ
0	1.0000	0	0	0	1.0000	0	0	0	1.0000	0	0	0
0.01	1.0302	+ 6	0.0052	- 26	1.0279	+ 6	0.0046	- 24	1.0258	+ 4	0.0042	- 20
0.02	1.0537	+ 13	0.0093	- 53	1.0498	+ 12	0.0080	- 50	1.0456	+ 10	0.0071	- 41
0.03	1.0749	+ 22	0.0138	- 81	1.0687	+ 21	0.0122	- 72	1.0633	+ 18	0.0105	- 64
0.04	1.0946	+ 33	0.0189	-104	1.0865	+ 30	0.0167	- 98	1.0796	+ 26	0.0144	- 82
0.05	1.1134	+ 46	0.0241	-126	1.1033	+ 40	0.0214	-113	1.0950	+ 35	0.0188	-100
0.06	1.1312	+ 58	0.0296	-144	1.1192	+ 50	0.0262	-132	1.1094	+ 44	0.0225	-116
0.07	1.1484	+ 70	0.0352	-164	1.1346	+ 61	0.0312	-149	1.1233	+ 53	0.0268	-132
0.08	1.1648	+ 82	0.0412	-180	1.1493	+ 72	0.0362	-167	1.1366	+ 62	0.0312	-147
0.09	1.1808	+ 95	0.0472	-196	1.1634	+ 82	0.0418	-180	1.1493	+ 70	0.0358	-160
0.10	1.1962	+106	0.0534	-211	1.1770	+ 91	0.0474	-193	1.1616	+ 78	0.0406	-178
0.11	1.2113	+118	0.0599	-224	1.1904	+102	0.0532	-206	1.1736	+ 87	0.0456	-184
0.12	1.2259	+130	0.0667	-235	1.2034	+113	0.0592	-217	1.1851	+ 94	0.0508	-196
0.13	1.2403	+143	0.0737	-246	1.2159	+122	0.0655	-228	1.1963	+102	0.0563	-205
0.14	1.2542	+153	0.0811	-255	1.2280	+130	0.0721	-238	1.2072	+109	0.0621	-214
0.15	1.2679	+165	0.0887	-264	1.2398	+138	0.0790	-246	1.2177	+115	0.0681	-223
0.16	1.2811	+174	0.0967	-271	1.2514	+146	0.0862	-254	1.2281	+122	0.0744	-230
0.17	1.2940	+188	0.1051	-278	1.2626	+153	0.0938	-262	1.2380	+127	0.0811	-238
0.18	1.3066	+191	0.1138	-284	1.2735	+160	0.1017	-268	1.2478	+133	0.0881	-244
0.19	1.3189	+199	0.1229	-288	1.2842	+166	0.1100	-274	1.2572	+137	0.0955	-250
0.20	1.3310	+206	0.1322	-293	1.2946	+172	0.1186	-279	1.2665	+142	0.1032	-255
0.21	1.3427	+213	0.1420	-296	1.3046	+177	0.1275	-284	1.2754	+145	0.1112	-260
0.22	1.3542	+219	0.1520	-299	1.3146	+182	0.1368	-288	1.2842	+149	0.1196	-264
0.23	1.3655	+226	0.1623	-302	1.3241	+186	0.1464	-291	1.2927	+152	0.1282	-268
0.24	1.3764	+231	0.1730	-303	1.3335	+190	0.1562	-294	1.3010	+155	0.1371	-272
0.25	1.3872	+236	0.1839	-305	1.3426	+194	0.1664	-297	1.3090	+157	0.1463	-275
0.26	1.3976	+241	0.1950	-306	1.3516	+197	0.1767	-300	1.3169	+159	0.1558	-277
0.27	1.4079	+245	0.2063	-306	1.3603	+200	0.1874	-301	1.3246	+161	0.1655	-280
0.28	1.4179	+249	0.2178	-306	1.3687	+202	0.1982	-303	1.3320	+162	0.1754	-282
0.29	1.4277	+252	0.2295	-306	1.3770	+204	0.2091	-304	1.3393	+163	0.1855	-284
0.30	1.4373	+255	0.2413	-306	1.3850	+207	0.2203	-306	1.3464	+165	0.1957	-286
0.31	1.4466	+258	0.2533	-305	1.3929	+208	0.2316	-306	1.3533	+165	0.2061	-287
0.32	1.4557	+260	0.2653	-304	1.4006	+210	0.2430	-307	1.3601	+166	0.2167	-288
0.33	1.4646	+262	0.2775	-303	1.4080	+211	0.2545	-307	1.3667	+166	0.2273	-289
0.34	1.4734	+264	0.2898	-301	1.4154	+212	0.2661	-308	1.3731	+167	0.2381	-290
0.35	1.4819	+266	0.3020	-300	1.4224	+213	0.2778	-308	1.3794	+167	0.2489	-291
0.36	1.4903	+267	0.3143	-298	1.4294	+214	0.2895	-308	1.3855	+167	0.2598	-291
0.37	1.4984	+268	0.3267	-295	1.4362	+214	0.3012	-308	1.3914	+166	0.2707	-292
0.38	1.5064	+269	0.3390	-293	1.4428	+214	0.3130	-307	1.3973	+166	0.2816	-292
0.39	1.5142	+270	0.3513	-291	1.4493	+214	0.3248	-307	1.4030	+166	0.2926	-292
0.40	1.5219	+271	0.3636	-289	1.4556	+215	0.3366	-306	1.4085	+165	0.3036	-292
0.41	1.5294	+271	0.3759	-286	1.4618	+215	0.3485	-306	1.4139	+165	0.3146	-292
0.42	1.5367	+272	0.3881	-283	1.4678	+215	0.3601	-304	1.4192	+164	0.3256	-292
0.43	1.5440	+272	0.4003	-281	1.4737	+214	0.3718	-304	1.4244	+163	0.3365	-292
0.44	1.5510	+272	0.4124	-278	1.4795	+214	0.3835	-302	1.4294	+162	0.3474	-291
0.45	1.5579	+272	0.4245	-275	1.4851	+213	0.3951	-302	1.4344	+162	0.3583	-291
0.46	1.5647	+272	0.4365	-272	1.4906	+213	0.4067	-300	1.4392	+161	0.3692	-290
0.47	1.5713	+272	0.4484	-268	1.4959	+212	0.4182	-299	1.4439	+160	0.3800	-290
0.48	1.5778	+272	0.4602	-265	1.5012	+212	0.4296	-298	1.4485	+158	0.3907	-289
0.49	1.5842	+271	0.4719	-262	1.5063	+211	0.4410	-296	1.4530	+157	0.4013	-289
0.50	1.5905	+271	0.4836	-258	1.5114	+210	0.4522	-295	1.4574	+156	0.4120	-288

TABLE 1-Continued

μ	τ = 1.00 ; ϖ = 1.00				τ = 1.00 ; ϖ = 0.95				τ = 1.00 ; ϖ = 0.90			
	X	δ	Y	δ	X	δ	Y	δ	X	δ	Y	δ
0.51	1.5966	+270	0.4952	-255	1.5168	+209	0.4684	-294	1.4617	+155	0.4225	-288
0.52	1.6026	+270	0.5066	-251	1.5211	+208	0.4746	-292	1.4659	+154	0.4330	-286
0.53	1.6086	+269	0.5180	-247	1.5258	+207	0.4857	-290	1.4701	+152	0.4433	-286
0.54	1.6144	+268	0.5293	-244	1.5305	+207	0.4966	-289	1.4741	+151	0.4536	-285
0.55	1.6200	+267	0.5404	-240	1.5350	+206	0.5074	-287	1.4781	+150	0.4638	-284
0.56	1.6257	+267	0.5515	-236	1.5394	+204	0.5182	-286	1.4819	+149	0.4740	-283
0.57	1.6311	+266	0.5624	-232	1.5437	+203	0.5288	-284	1.4857	+147	0.4840	-282
0.58	1.6366	+265	0.5733	-227	1.5479	+202	0.5394	-282	1.4894	+146	0.4940	-281
0.59	1.6418	+264	0.5840	-223	1.5521	+201	0.5499	-280	1.4931	+144	0.5038	-280
0.60	1.6470	+263	0.5946	-219	1.5562	+200	0.5602	-280	1.4966	+143	0.5136	-279
0.61	1.6522	+262	0.6051	-215	1.5602	+199	0.5705	-277	1.5001	+142	0.5233	-278
0.62	1.6572	+261	0.6155	-211	1.5641	+198	0.5806	-275	1.5036	+140	0.5329	-276
0.63	1.6622	+260	0.6258	-206	1.5679	+197	0.5907	-273	1.5069	+139	0.5423	-275
0.64	1.6670	+259	0.6360	-202	1.5717	+196	0.6006	-272	1.5102	+138	0.5517	-274
0.65	1.6718	+257	0.6460	-197	1.5754	+194	0.6104	-270	1.5134	+136	0.5611	-272
0.66	1.6765	+256	0.656	-19	1.5790	+193	0.6202	-268	1.5166	+135	0.5702	-272
0.67	1.6811	+255	0.666	-19	1.5826	+192	0.6298	-266	1.5197	+133	0.5794	-270
0.68	1.6857	+254	0.676	-18	1.5860	+190	0.6394	-264	1.5228	+132	0.5884	-268
0.69	1.6902	+252	0.685	-18	1.5894	+189	0.6488	-262	1.5257	+130	0.5973	-267
0.70	1.6946	+251	0.695	-18	1.5928	+188	0.6581	-260	1.5287	+129	0.6061	-266
0.71	1.6989	+250	0.704	-17	1.5961	+187	0.6673	-258	1.5315	+128	0.6149	-264
0.72	1.7032	+248	0.713	-17	1.5993	+186	0.6765	-256	1.5344	+126	0.6235	-263
0.73	1.7074	+247	0.722	-16	1.6025	+184	0.6855	-254	1.5371	+125	0.6321	-261
0.74	1.7115	+246	0.731	-16	1.6056	+183	0.6944	-252	1.5399	+124	0.6405	-260
0.75	1.7156	+244	0.740	-15	1.6087	+182	0.7032	-250	1.5425	+122	0.6489	-258
0.76	1.7196	+243	0.749	-15	1.6117	+181	0.7119	-249	1.5452	+121	0.6572	-257
0.77	1.7236	+241	0.758	-14	1.6146	+179	0.7205	-247	1.5477	+119	0.6653	-255
0.78	1.7275	+240	0.766	-14	1.6176	+178	0.7290	-245	1.5503	+118	0.6734	-254
0.79	1.7313	+238	0.775	-13	1.6204	+177	0.7375	-243	1.5528	+116	0.6814	-252
0.80	1.7352	+237	0.783	-13	1.6232	+176	0.7458	-241	1.5552	+115	0.6894	-250
0.81	1.7389	+235	0.792	-12	1.6260	+175	0.7540	-239	1.5576	+114	0.6972	-249
0.82	1.7426	+233	0.800	-12	1.6287	+173	0.7622	-237	1.5600	+112	0.7049	-247
0.83	1.7462	+232	0.808	-12	1.6313	+172	0.7702	-235	1.5623	+111	0.7126	-246
0.84	1.7498	+231	0.816	-11	1.6340	+171	0.7782	-233	1.5646	+110	0.7201	-244
0.85	1.7534	+229	0.824	-11	1.6366	+170	0.7860	-232	1.5668	+108	0.7276	-242
0.86	1.7568	+227	0.831	-10	1.6391	+169	0.7938	-230	1.5691	+107	0.7350	-241
0.87	1.7603	+226	0.839	-10	1.6416	+168	0.8015	-228	1.5712	+106	0.7423	-240
0.88	1.7637	+224	0.847	- 9	1.6441	+167	0.8091	-226	1.5734	+105	0.7496	-238
0.89	1.7670	+223	0.854	- 9	1.6465	+165	0.8166	-224	1.5755	+103	0.7567	-236
0.90	1.7703	+221	0.862	- 8	1.6489	+164	0.8240	-222	1.5776	+102	0.7638	-234
0.91	1.7736	+219	0.869	- 8	1.6512	+163	0.8314	-220	1.5796	+101	0.7708	-232
0.92	1.7769	+218	0.876	- 8	1.6536	+163	0.8386	-218	1.5816	+100	0.7778	-230
0.93	1.7801	+216	0.883	- 7	1.6559	+162	0.8458	-216	1.5836	+ 98	0.7846	-229
0.94	1.7832	+215	0.890	- 7	1.6581	+160	0.8530	-214	1.5855	+ 97	0.7914	-227
0.95	1.7863	+213	0.897	- 6	1.6603	+160	0.8600	-212	1.5875	+ 96	0.7980	-226
0.96	1.7894	+211	0.904	- 6	1.6626	+159	0.8669	-210	1.5894	+ 95	0.8047	-224
0.97	1.7924	+210	0.911	- 5	1.6647	+158	0.8738	-209	1.5912	+ 94	0.8113	-222
0.98	1.7954	+208	0.918	- 5	1.6668	+157	0.8806	-207	1.5930	+ 92	0.8178	-220
0.99	1.7984	+207	0.924	- 4	1.6689	+156	0.8873	-205	1.5948	+ 91	0.8241	-219
1.00	1.8013	+205	0.931	- 4	1.6710	+156	0.8939	-203	1.5966	+ 90	0.8305	-217

TABLE 1-Continued

μ	τ = 1.00 ; ϖ = 0.80				μ	τ = 1.00 ; ϖ = 0.80				μ	τ = 1.00 ; ϖ = 0.90				μ	τ = 1.00 ; ϖ = 0.90			
	X	δ	Y	δ		X	δ	Y	δ		X	δ	Y	δ		X	δ	Y	δ
0	1.0000	0	0	0	0.50	1.3668	+86	0.3469	-253	0	1.0000	0	0	0	0.50	1.1795	+12	0.2272	-107
0.01	1.0222	+ 5	0.0080	- 17	0.51	1.3700	+85	0.3563	-254	0.01	1.0127	+ 2	0.0010	- 6	0.51	1.1810	+11	0.2344	-108
0.02	1.0390	+ 10	0.0050	- 35	0.52	1.3733	+83	0.3656	-254	0.02	1.0221	+ 4	0.0020	- 11	0.52	1.1824	+10	0.2417	-108
0.03	1.0536	+ 15	0.0079	- 47	0.53	1.3765	+82	0.3750	-253	0.03	1.0301	+ 6	0.0030	- 17	0.53	1.1838	+10	0.2489	-108
0.04	1.0673	+ 20	0.0106	- 68	0.54	1.3796	+81	0.3842	-253	0.04	1.0374	+ 8	0.0042	- 22	0.54	1.1852	+ 9	0.2560	-108
0.05	1.0800	+ 27	0.0136	- 76	0.55	1.3826	+79	0.3934	-253	0.05	1.0440	+10	0.0058	- 27	0.55	1.1865	+ 8	0.2632	-109
0.06	1.0919	+ 33	0.0166	- 89	0.56	1.3856	+77	0.4024	-253	0.06	1.0508	+12	0.0065	- 31	0.56	1.1878	+ 7	0.2703	-109
0.07	1.1033	+ 40	0.0198	-102	0.57	1.3885	+76	0.4115	-253	0.07	1.0561	+14	0.0078	- 35	0.57	1.1891	+ 6	0.2773	-109
0.08	1.1141	+ 46	0.0231	-118	0.58	1.3914	+74	0.4204	-253	0.08	1.0616	+16	0.0091	- 40	0.58	1.1904	+ 6	0.2843	-109
0.09	1.1246	+ 51	0.0265	-134	0.59	1.3942	+73	0.4293	-253	0.09	1.0669	+18	0.0104	- 44	0.59	1.1916	+ 5	0.2912	-110
0.10	1.1348	+ 58	0.0301	-154	0.60	1.3969	+72	0.4380	-253	0.10	1.0719	+20	0.0119	- 47	0.60	1.1928	+ 4	0.2982	-110
0.11	1.1441	+ 68	0.0338	-144	0.61	1.3996	+70	0.4468	-252	0.11	1.0767	+21	0.0134	- 51	0.61	1.1940	+ 3	0.3050	-110
0.12	1.1534	+ 69	0.0377	-152	0.62	1.4022	+69	0.4554	-252	0.12	1.0812	+23	0.0151	- 55	0.62	1.1951	+ 3	0.3118	-110
0.13	1.1628	+ 78	0.0418	-161	0.63	1.4048	+67	0.4640	-252	0.13	1.0856	+24	0.0169	- 58	0.63	1.1962	+ 2	0.3186	-111
0.14	1.1711	+ 78	0.0462	-169	0.64	1.4074	+66	0.4725	-251	0.14	1.0899	+25	0.0188	- 62	0.64	1.1974	+ 1	0.3252	-111
0.15	1.1795	+ 82	0.0509	-176	0.65	1.4098	+64	0.4808	-251	0.15	1.0939	+26	0.0210	- 65	0.65	1.1984	0	0.3319	-111
0.16	1.1877	+ 86	0.0558	-188	0.66	1.4122	+63	0.4891	-251	0.16	1.0978	+27	0.0235	- 67	0.66	1.1995	- 1	0.3384	-111
0.17	1.1956	+ 89	0.0611	-189	0.67	1.4146	+61	0.4974	-250	0.17	1.1016	+28	0.0262	- 70	0.67	1.2005	- 1	0.3450	-112
0.18	1.2033	+ 92	0.0666	-194	0.68	1.4170	+60	0.5055	-250	0.18	1.1053	+28	0.0292	- 72	0.68	1.2015	- 2	0.3514	-112
0.19	1.2108	+ 95	0.0725	-200	0.69	1.4192	+58	0.5136	-249	0.19	1.1088	+29	0.0324	- 75	0.69	1.2026	- 3	0.3578	-112
0.20	1.2181	+ 97	0.0788	-205	0.70	1.4215	+57	0.5215	-249	0.20	1.1122	+29	0.0359	- 77	0.70	1.2035	- 4	0.3642	-112
0.21	1.2251	+ 99	0.0853	-209	0.71	1.4237	+55	0.5294	-248	0.21	1.1155	+29	0.0398	- 79	0.71	1.2045	- 4	0.3704	-112
0.22	1.2320	+101	0.0921	-214	0.72	1.4259	+54	0.5372	-248	0.22	1.1187	+29	0.0439	- 81	0.72	1.2054	- 5	0.3767	-112
0.23	1.2387	+102	0.0993	-217	0.73	1.4280	+52	0.5450	-247	0.23	1.1218	+29	0.0483	- 83	0.73	1.2064	- 6	0.3828	-112
0.24	1.2452	+103	0.1068	-220	0.74	1.4301	+51	0.5526	-247	0.24	1.1248	+29	0.0530	- 85	0.74	1.2072	- 6	0.3889	-112
0.25	1.2515	+104	0.1145	-224	0.75	1.4322	+50	0.5602	-246	0.25	1.1277	+29	0.0580	- 86	0.75	1.2081	- 7	0.3950	-112
0.26	1.2577	+105	0.1225	-227	0.76	1.4342	+48	0.5677	-246	0.26	1.1306	+29	0.0632	- 88	0.76	1.2090	- 8	0.4010	-113
0.27	1.2637	+106	0.1306	-230	0.77	1.4361	+47	0.5751	-245	0.27	1.1333	+28	0.0686	- 89	0.77	1.2099	- 8	0.4069	-113
0.28	1.2695	+106	0.1391	-232	0.78	1.4381	+46	0.5824	-244	0.28	1.1360	+28	0.0743	- 91	0.78	1.2107	- 9	0.4127	-113
0.29	1.2752	+106	0.1477	-234	0.79	1.4400	+44	0.5897	-244	0.29	1.1386	+27	0.0802	- 92	0.79	1.2115	-10	0.4185	-113
0.30	1.2808	+106	0.1565	-237	0.80	1.4419	+43	0.5968	-243	0.30	1.1411	+27	0.0862	- 93	0.80	1.2124	-10	0.4243	-113
0.31	1.2862	+106	0.1654	-239	0.81	1.4437	+41	0.6039	-243	0.31	1.1435	+26	0.0924	- 94	0.81	1.2132	-11	0.4300	-113
0.32	1.2914	+106	0.1746	-240	0.82	1.4455	+40	0.6110	-242	0.32	1.1459	+26	0.0988	- 96	0.82	1.2139	-12	0.4356	-113
0.33	1.2965	+105	0.1838	-242	0.83	1.4473	+39	0.6179	-241	0.33	1.1482	+25	0.1054	- 96	0.83	1.2147	-12	0.4412	-113
0.34	1.3015	+105	0.1931	-243	0.84	1.4491	+38	0.6248	-240	0.34	1.1505	+25	0.1121	- 97	0.84	1.2155	-13	0.4467	-113
0.35	1.3064	+104	0.2026	-245	0.85	1.4508	+36	0.6315	-240	0.35	1.1526	+24	0.1189	- 98	0.85	1.2162	-14	0.4521	-113
0.36	1.3111	+103	0.2121	-246	0.86	1.4525	+35	0.6383	-239	0.36	1.1548	+23	0.1258	- 99	0.86	1.2170	-14	0.4575	-113
0.37	1.3157	+102	0.2216	-247	0.87	1.4542	+34	0.6449	-238	0.37	1.1569	+22	0.1328	-100	0.87	1.2177	-15	0.4628	-113
0.38	1.3203	+102	0.2312	-248	0.88	1.4558	+33	0.6515	-237	0.38	1.1589	+22	0.1398	-101	0.88	1.2184	-15	0.4681	-113
0.39	1.3246	+100	0.2409	-249	0.89	1.4574	+32	0.6580	-237	0.39	1.1608	+21	0.1470	-101	0.89	1.2191	-16	0.4734	-114
0.40	1.3290	+100	0.2506	-250	0.90	1.4590	+30	0.6644	-236	0.40	1.1628	+20	0.1542	-102	0.90	1.2198	-17	0.4785	-114
0.41	1.3331	+ 98	0.2608	-250	0.91	1.4606	+29	0.6708	-235	0.41	1.1646	+20	0.1614	-103	0.91	1.2204	-17	0.4837	-114
0.42	1.3372	+ 97	0.2700	-251	0.92	1.4621	+28	0.6771	-234	0.42	1.1664	+19	0.1686	-103	0.92	1.2211	-18	0.4887	-114
0.43	1.3412	+ 96	0.2797	-251	0.93	1.4636	+27	0.6833	-233	0.43	1.1682	+18	0.1759	-104	0.93	1.2216	-18	0.4937	-114
0.44	1.3452	+ 95	0.2894	-252	0.94	1.4652	+26	0.6894	-233	0.44	1.1700	+17	0.1832	-105	0.94	1.2224	-19	0.4987	-114
0.45	1.3489	+ 93	0.2991	-252	0.95	1.4666	+25	0.6955	-232	0.45	1.1716	+16	0.1906	-105	0.95	1.2230	-20	0.5036	-114
0.46	1.3527	+ 92	0.3087	-252	0.96	1.4681	+24	0.7016	-231	0.46	1.1733	+15	0.1979	-105	0.96	1.2237	-20	0.5085	-114
0.47	1.3563	+ 90	0.3185	-253	0.97	1.4695	+23	0.7075	-230	0.47	1.1749	+15	0.2052	-106	0.97	1.2243	-21	0.5133	-114
0.48	1.3598	+ 89	0.3279	-253	0.98	1.4709	+22	0.7134	-229	0.48	1.1765	+14	0.2126	-106	0.98	1.2249	-21	0.5180	-114
0.49	1.3633	+ 88	0.3374	-253	0.99	1.4723	+20	0.7192	-228	0.49	1.1780	+13	0.2199	-107	0.99	1.2255	-22	0.5227	-114
0.50	1.3668	+ 86	0.3469	-253	1.00	1.4737	+20	0.7250	-227	0.50	1.1795	+12	0.2272	-107	1.00	1.2260	-22	0.5274	-114

THE X- AND Y-FUNCTIONS FOR ISOTROPIC SCATTERING. II

S. CHANDRASEKHAR AND DONNA ELBERT
Yerkes Observatory
Received November 7, 1951

ABSTRACT

The moments of order zero and one of the X- and Y-functions tabulated in the preceding paper are evaluated, and certain relations which these moments should satisfy are verified. In the conservative case ($\varpi_0 = 1$) the standard solutions and the solutions appropriate to the problem of diffuse reflection and transmission are tabulated. Finally, a table is provided for calculating the exact values of the residual intensity on Schuster's model of line formation.

1. *The moments of the X- and Y-functions.*—The solutions for transfer problems involving X- and Y-functions generally involve also their moments. Thus in the theory of diffuse reflection and transmission with a ground surface reflecting according to Lambert's law, the value of the constant (*R.T.*, p. 275, eq. [212])[1]

$$\bar{s} = 1 - \{ (2 - \varpi_0 \alpha_0) \alpha_1 + \varpi_0 \beta_0 \beta_1 \}, \tag{1}$$

where α_n and β_n are the moments of order n of the X- and Y-functions, respectively, is needed. We have therefore evaluated the moments of order zero and one of the solutions tabulated in the preceding paper (p. 244). They are listed in Table 1*a* for $\varpi_0 < 1$. (The case $\varpi_0 = 1$ has to be distinguished for reasons explained in § 2 below.)

With the values of α_0 and β_0 given in Table 1*a*, we can verify the relation (*R.T.*, p. 187, eq. [27])

$$\alpha_0 = \frac{2}{\varpi_0} [1 - (1 - \varpi_0 + \tfrac{1}{4} \varpi_0^2 \beta_0^2)^{1/2}], \tag{2}$$

which must obtain between them. The values of α_0 (denoted by α_0^*) computed from the known β_0's in accordance with the foregoing formula are also given in Table 1*a*; it will be seen that these values agree satisfactorily with the moments evaluated from the tabulated solutions by direct numerical integrations.

2. *The solutions and moments for the conservative case* ($\varpi_0 = 1$).—When $\varpi_0 = 1$, the equations governing X and Y allow a one-parameter family of solutions (*R.T.*, chap. viii, § 58). Thus if X and Y are solutions, then so are

$$\begin{aligned} &X(\mu) + Q\mu [X(\mu) + Y(\mu)] \\ \text{and} \quad &Y(\mu) - Q\mu [X(\mu) + Y(\mu)], \end{aligned} \tag{3}$$

where Q is an arbitrary constant. Since $X + Y$ is invariant to this transformation, the sum of the moments α_n and β_n is also invariant. The values of $\alpha_0 + \beta_0$, $\alpha_1 + \beta_1$, and $\alpha_2 + \beta_2$ were evaluated from the solutions tabulated in Paper I by numerical integration. They are listed in Table 1*b*. It will be noticed that the relation $\alpha_0 + \beta_0 = 2$ (cf. eq. [2]) is satisfied quite well by the computed moments.

In view of the ambiguity in the solutions of the X- and Y-equations in the conservative case, certain solutions, called "standard solutions," are defined. In the present case ($\varpi_0 = 1$) they are defined by the conditions

$$\int_0^1 X(\mu)\, d\mu = 2 \quad \text{and} \quad \int_0^1 Y(\mu)\, d\mu = 0. \tag{4}$$

[1] This refers to S. Chandrasekhar, *Radiative Transfer* (Oxford: Clarendon Press, 1950).

TABLE 1a

MOMENTS OF THE X AND Y FUNCTIONS

(NON-CONSERVATIVE CASE)

τ	ω_*	α_0	β_0	α_0^*	α_1	β_1	$\bar{s}$
0.05	0.95	1.08234	0.90819	1.08282	0.54327	0.49765	0.04270
	0.90	1.07760	0.90354	1.07757	0.54078	0.49519	0.04023
	0.80	1.06825	0.89441	1.06823	0.53586	0.49033	0.03538
	0.50	1.04134	0.86814	1.04134	0.52172	0.47637	0.02142
0.10	0.95	1.13364	0.84994	1.13367	0.57202	0.48632	0.07932
	0.90	1.12543	0.84207	1.12545	0.56759	0.48200	0.07143
	0.80	1.10947	0.82678	1.10947	0.55898	0.47360	0.06493
	0.50	1.06487	0.78418	1.06488	0.53493	0.45019	0.03844
0.15	0.95	1.17423	0.80320	1.17428	0.59561	0.47367	0.11176
	0.90	1.16294	0.79257	1.16298	0.58939	0.46769	0.10450
	0.80	1.14119	0.77217	1.14123	0.57743	0.45621	0.09049
	0.50	1.08209	0.71694	1.08212	0.54498	0.42511	0.05251
0.20	0.95	1.20822	0.76349	1.20831	0.61589	0.46081	0.14091
	0.90	1.19408	0.75042	1.19414	0.60799	0.45331	0.13126
	0.80	1.16713	0.72558	1.16716	0.59295	0.43905	0.11288
	0.50	1.09555	0.66012	1.09556	0.55306	0.40144	0.06434
0.25	0.95	1.23763	0.72871	1.23773	0.63381	0.44808	0.16738
	0.90	1.22079	0.71339	1.22085	0.62428	0.43915	0.15539
	0.80	1.18896	0.68463	1.18900	0.60628	0.42259	0.13277
	0.50	1.10638	0.61069	1.10640	0.55971	0.37918	0.07642
0.50	0.95	1.3436	0.5987	1.3437	0.7010	0.3903	0.2708
	0.90	1.3147	0.5742	1.3148	0.6839	0.3752	0.2476
	0.80	1.26243	0.53036	1.26255	0.65807	0.34816	0.20570
	0.50	1.13887	0.43072	1.13897	0.58058	0.28651	0.10774
1.00	0.95	1.4600	0.4408	1.4604	0.7790	0.3024	0.3959
	0.90	1.4116	0.4041	1.4116	0.7490	0.2785	0.3523
	0.80	1.33015	0.34435	1.33014	0.69879	0.23944	0.28004
	0.50	1.16184	0.23411	1.16190	0.59634	0.16688	0.13421

TABLE 1b

MOMENTS OF THE X AND Y FUNCTIONS AND RELATED CONSTANTS

(CONSERVATIVE CASE)

τ	$\alpha_0 + \beta_0$	$\alpha_1 + \beta_1$	$\alpha_2 + \beta_2$	α_1^s	β_1^s	$(\alpha_1^s)^2 - (\beta_1^s)^2$	Q	$\bar{s}$
0.05	2.00002	1.04595	0.70416	1.1604	-0.1144	1.3334	-0.87279	0.04516
0.10	1.99998	1.06726	0.72364	1.1583	-0.0910	1.3333	-0.80389	0.08434
0.15	1.99993	1.08179	0.73766	1.1571	-0.0758	1.3332	-0.75259	0.11927
0.20	1.99987	1.09262	0.74852	1.1564	-0.0638	1.3331	-0.71121	0.15094
0.25	1.99988	1.10114	0.75732	1.1559	-0.0548	1.3331	-0.67639	0.17987
0.50	1.9998	1.1259	0.7845	1.1549	-0.0290	1.3330	-0.5553	0.2960
1.00	2.0018	1.1457	0.8076	1.156	-0.010	1.337	-0.4226	0.4453

TABLE 2

X AND Y FUNCTIONS FOR THE CONSERVATIVE CASE

$\tau = 0.05$

μ	X^*	Y^*	X_s	Y_s	μ	X^*	Y^*	X_s	Y_s
0	1.00000	0	1.00000	0	0.50	1.09144	0.99509	2.00199	+0.08454
0.01	1.02487	0.02202	1.03401	+0.01288	0.51	1.09151	0.99696	2.02114	+0.06733
0.02	1.04099	0.11254	1.06113	+0.09240	0.52	1.09159	0.99877	2.04030	+0.05006
0.03	1.05173	0.23090	1.08531	+0.19732	0.53	1.09166	1.00051	2.05945	+0.03272
0.04	1.05911	0.33694	1.10785	+0.28820	0.54	1.09173	1.00219	2.07861	+0.01531
0.05	1.06442	0.42455	1.12940	+0.35957	0.55	1.09179	1.00381	2.09775	-0.00215
0.06	1.06841	0.49605	1.15034	+0.41112	0.56	1.09186	1.00537	2.11691	-0.01968
0.07	1.07150	0.55474	1.17086	+0.45538	0.57	1.09192	1.00689	2.13605	-0.03724
0.08	1.07396	0.60347	1.19108	+0.48635	0.58	1.09198	1.00835	2.15520	-0.05487
0.09	1.07597	0.64443	1.21111	+0.50929	0.59	1.09204	1.00976	2.17435	-0.07255
0.10	1.07763	0.67927	1.23097	+0.52593	0.60	1.09209	1.01113	2.19349	-0.09027
0.11	1.07903	0.70924	1.25071	+0.53756	0.61	1.09215	1.01246	2.21264	-0.10803
0.12	1.08023	0.73524	1.27037	+0.54510	0.62	1.09220	1.01375	2.23179	-0.12584
0.13	1.08127	0.75801	1.28996	+0.54932	0.63	1.09225	1.01499	2.25093	-0.14369
0.14	1.08218	0.77811	1.30949	+0.55080	0.64	1.09230	1.01620	2.27007	-0.16157
0.15	1.08298	0.79597	1.32896	+0.54999	0.65	1.09235	1.01738	2.28922	-0.17949
0.16	1.08368	0.81195	1.34839	+0.54724	0.66	1.09239	1.01852	2.30836	-0.19745
0.17	1.08432	0.82632	1.36781	+0.54283	0.67	1.09244	1.01962	2.32750	-0.21544
0.18	1.08488	0.83932	1.38718	+0.53702	0.68	1.09248	1.02070	2.34664	-0.23346
0.19	1.08540	0.85112	1.40653	+0.52999	0.69	1.09252	1.02174	2.36578	-0.25152
0.20	1.08586	0.86189	1.42585	+0.52190	0.70	1.09256	1.02276	2.38491	-0.26959
0.21	1.08629	0.87177	1.44517	+0.51289	0.71	1.09260	1.02375	2.40406	-0.28771
0.22	1.08668	0.88084	1.46446	+0.50306	0.72	1.09264	1.02471	2.42319	-0.30584
0.23	1.08703	0.88920	1.48373	+0.49250	0.73	1.09268	1.02565	2.44234	-0.32401
0.24	1.08736	0.89694	1.50300	+0.48130	0.74	1.09272	1.02656	2.46148	-0.34220
0.25	1.08767	0.90413	1.52227	+0.46953	0.75	1.09275	1.02745	2.48061	-0.36041
0.26	1.08795	0.91081	1.54152	+0.45724	0.76	1.09279	1.02831	2.49976	-0.37866
0.27	1.08822	0.91704	1.56076	+0.44450	0.77	1.09282	1.02916	2.51888	-0.39690
0.28	1.08846	0.92287	1.57998	+0.43135	0.78	1.09286	1.02998	2.53804	-0.41520
0.29	1.08869	0.92833	1.59921	+0.41781	0.79	1.09289	1.03078	2.55716	-0.43349
0.30	1.08890	0.93345	1.61842	+0.40393	0.80	1.09292	1.03156	2.57629	-0.45181
0.31	1.08910	0.93828	1.63763	+0.38975	0.81	1.09295	1.03233	2.59543	-0.47015
0.32	1.08928	0.94283	1.65684	+0.37527	0.82	1.09298	1.03308	2.61457	-0.48851
0.33	1.08945	0.94712	1.67603	+0.36054	0.83	1.09301	1.03381	2.63370	-0.50688
0.34	1.08962	0.95118	1.69523	+0.34557	0.84	1.09304	1.03452	2.65284	-0.52528
0.35	1.08978	0.95501	1.71442	+0.33037	0.85	1.09307	1.03521	2.67197	-0.54369
0.36	1.08993	0.95865	1.73361	+0.31497	0.86	1.09310	1.03589	2.69111	-0.56212
0.37	1.09008	0.96211	1.75280	+0.29939	0.87	1.09312	1.03656	2.71023	-0.58055
0.38	1.09021	0.96540	1.77197	+0.28364	0.88	1.09315	1.03721	2.72938	-0.59902
0.39	1.09034	0.96853	1.79116	+0.26771	0.89	1.09317	1.03786	2.74852	-0.61749
0.40	1.09047	0.97151	1.81034	+0.25164	0.90	1.09319	1.03848	2.76764	-0.63597
0.41	1.09058	0.97435	1.82950	+0.23543	0.91	1.09322	1.03909	2.78678	-0.65447
0.42	1.09070	0.97707	1.84868	+0.21909	0.92	1.09324	1.03968	2.80591	-0.67299
0.43	1.09080	0.97967	1.86785	+0.20262	0.93	1.09326	1.04027	2.82503	-0.69150
0.44	1.09091	0.98215	1.88703	+0.18603	0.94	1.09329	1.04084	2.84418	-0.71005
0.45	1.09100	0.98454	1.90618	+0.16936	0.95	1.09331	1.04140	2.86330	-0.72859
0.46	1.09110	0.98682	1.92535	+0.15257	0.96	1.09333	1.04195	2.88244	-0.74716
0.47	1.09119	0.98901	1.94451	+0.13569	0.97	1.09335	1.04248	2.90156	-0.76573
0.48	1.09127	0.99112	1.96367	+0.11872	0.98	1.09338	1.04301	2.92070	-0.78431
0.49	1.09136	0.99314	1.98283	+0.10167	0.99	1.09340	1.04353	2.93984	-0.80291
0.50	1.09144	0.99509	2.00199	+0.08454	1.00	1.09342	1.04403	2.95896	-0.82151

TABLE 2-Continued

$\tau = 0.10$

μ	X^*	Y^*	X_s	Y_s	μ	X^*	Y^*	X_s	Y_s
0	1.00000	0	1.00000	0	0.50	1.15230	0.96650	2.00396	+0.11484
0.01	1.02583	0.01208	1.03417	+0.00574	0.51	1.15255	0.97005	2.02280	+0.09980
0.02	1.04466	0.03215	1.06199	+0.01484	0.52	1.15278	0.97347	2.04162	+0.08463
0.03	1.06013	0.07469	1.08750	+0.01732	0.53	1.15301	0.97677	2.06044	+0.06934
0.04	1.07268	0.13555	1.11146	+0.09477	0.54	1.15323	0.97995	2.07926	+0.05392
0.05	1.08286	0.19764	1.13433	+0.14617	0.55	1.15345	0.98303	2.09808	+0.03840
0.06	1.09117	0.26045	1.15636	+0.19526	0.56	1.15364	0.98601	2.11687	+0.02276
0.07	1.09803	0.31916	1.17778	+0.23941	0.57	1.15383	0.98891	2.13569	+0.00705
0.08	1.10379	0.37280	1.19876	+0.27783	0.58	1.15403	0.99170	2.15450	-0.00877
0.09	1.10867	0.42133	1.21937	+0.31063	0.59	1.15421	0.99441	2.17331	-0.02469
0.10	1.11285	0.46510	1.23971	+0.33824	0.60	1.15439	0.99703	2.19211	-0.04069
0.11	1.11647	0.50457	1.25981	+0.36123	0.61	1.15456	0.99958	2.21091	-0.05677
0.12	1.11968	0.54019	1.27975	+0.38007	0.62	1.15473	1.00205	2.22970	-0.07292
0.13	1.12242	0.57244	1.29954	+0.39532	0.63	1.15489	1.00445	2.24850	-0.08916
0.14	1.12489	0.60172	1.31921	+0.40740	0.64	1.15504	1.00678	2.26729	-0.10547
0.15	1.12708	0.62838	1.33877	+0.41669	0.65	1.15520	1.00904	2.28610	-0.12186
0.16	1.12906	0.65275	1.35825	+0.42356	0.66	1.15535	1.01124	2.30489	-0.13830
0.17	1.13085	0.67508	1.37766	+0.42827	0.67	1.15550	1.01338	2.32369	-0.15481
0.18	1.13247	0.69560	1.39699	+0.43108	0.68	1.15564	1.01546	2.34248	-0.17138
0.19	1.13394	0.71452	1.41628	+0.43218	0.69	1.15578	1.01748	2.36127	-0.18801
0.20	1.13530	0.73201	1.43552	+0.43179	0.70	1.15591	1.01945	2.38005	-0.20469
0.21	1.13654	0.74823	1.45472	+0.43005	0.71	1.15604	1.02138	2.39885	-0.22143
0.22	1.13768	0.76330	1.47389	+0.42709	0.72	1.15616	1.02324	2.41762	-0.23822
0.23	1.13873	0.77734	1.49301	+0.42306	0.73	1.15629	1.02506	2.43642	-0.25507
0.24	1.13972	0.79045	1.51212	+0.41805	0.74	1.15641	1.02684	2.45519	-0.27194
0.25	1.14063	0.80271	1.53120	+0.41214	0.75	1.15653	1.02857	2.47398	-0.28888
0.26	1.14147	0.81421	1.55024	+0.40544	0.76	1.15663	1.03025	2.49274	-0.30586
0.27	1.14227	0.82501	1.56928	+0.39800	0.77	1.15675	1.03190	2.51153	-0.32288
0.28	1.14301	0.83517	1.58828	+0.38990	0.78	1.15685	1.03351	2.53030	-0.33994
0.29	1.14370	0.84476	1.60727	+0.38119	0.79	1.15695	1.03508	2.54907	-0.35704
0.30	1.14436	0.85380	1.62626	+0.37190	0.80	1.15706	1.03661	2.56786	-0.37419
0.31	1.14497	0.86236	1.64522	+0.36211	0.81	1.15716	1.03811	2.58663	-0.39136
0.32	1.14556	0.87046	1.66418	+0.35184	0.82	1.15726	1.03957	2.60541	-0.40858
0.33	1.14611	0.87814	1.68312	+0.34113	0.83	1.15736	1.04100	2.62419	-0.42583
0.34	1.14664	0.88544	1.70206	+0.33002	0.84	1.15745	1.04239	2.64295	-0.44311
0.35	1.14713	0.89238	1.72098	+0.31853	0.85	1.15754	1.04377	2.66173	-0.46042
0.36	1.14758	0.89900	1.73988	+0.30670	0.86	1.15763	1.04510	2.68050	-0.47777
0.37	1.14802	0.90529	1.75876	+0.29455	0.87	1.15772	1.04641	2.69928	-0.49515
0.38	1.14845	0.91130	1.77767	+0.28208	0.88	1.15780	1.04769	2.71804	-0.51255
0.39	1.14886	0.91703	1.79656	+0.26933	0.89	1.15789	1.04894	2.73682	-0.52999
0.40	1.14925	0.92251	1.81544	+0.25632	0.90	1.15797	1.05016	2.75558	-0.54745
0.41	1.14962	0.92778	1.83432	+0.24308	0.91	1.15805	1.05136	2.77434	-0.56493
0.42	1.14997	0.93280	1.85319	+0.22958	0.92	1.15812	1.05255	2.79312	-0.58245
0.43	1.15030	0.93763	1.87206	+0.21587	0.93	1.15820	1.05370	2.81189	-0.59999
0.44	1.15063	0.94226	1.89092	+0.20197	0.94	1.15828	1.05482	2.83065	-0.61755
0.45	1.15094	0.94670	1.90978	+0.18786	0.95	1.15835	1.05593	2.84941	-0.63513
0.46	1.15123	0.95096	1.92861	+0.17358	0.96	1.15843	1.05701	2.86818	-0.65274
0.47	1.15151	0.95507	1.94744	+0.15914	0.97	1.15850	1.05807	2.88694	-0.67037
0.48	1.15179	0.95902	1.96629	+0.14452	0.98	1.15857	1.05911	2.90571	-0.68803
0.49	1.15206	0.96283	1.98514	+0.12975	0.99	1.15863	1.06014	2.92447	-0.70570
0.50	1.15230	0.96650	2.00396	+0.11484	1.00	1.15870	1.06115	2.94324	-0.72339

TABLE 2-Continued

$\tau = 0.15$

μ	X^*	Y^*	X_s	Y_s	μ	X^*	Y^*	X_s	Y_s
0	1.00000	0	1.00000	0	0.50	1.20209	0.93818	2.00558	+0.12969
0.01	1.02648	0.01034	1.03428	+0.00254	0.51	1.20254	0.93820	2.02420	+0.11654
0.02	1.04609	0.02227	1.06217	+0.00619	0.52	1.20300	0.94303	2.04284	+0.10319
0.03	1.06299	0.04071	1.08791	+0.01579	0.53	1.20344	0.94771	2.06148	+0.08967
0.04	1.07775	0.06999	1.11230	+0.03544	0.54	1.20386	0.95223	2.08009	+0.07600
0.05	1.09056	0.10882	1.13567	+0.06321	0.55	1.20426	0.95662	2.09870	+0.06218
0.06	1.10167	0.15184	1.15828	+0.09523	0.56	1.20466	0.96086	2.11732	+0.04820
0.07	1.11128	0.19732	1.18022	+0.12838	0.57	1.20504	0.96499	2.13594	+0.03409
0.08	1.11966	0.24261	1.20168	+0.16059	0.58	1.20541	0.96898	2.15454	+0.01985
0.09	1.12698	0.28646	1.22272	+0.19072	0.59	1.20577	0.97286	2.17314	+0.00549
0.10	1.13343	0.32820	1.24343	+0.21820	0.60	1.20611	0.97661	2.19172	-0.00900
0.11	1.13915	0.36757	1.26388	+0.24284	0.61	1.20644	0.98027	2.21032	-0.02361
0.12	1.14423	0.40446	1.28409	+0.26460	0.62	1.20676	0.98381	2.22892	-0.03833
0.13	1.14878	0.43890	1.30411	+0.28357	0.63	1.20709	0.98727	2.24751	-0.05315
0.14	1.15287	0.47105	1.32398	+0.29994	0.64	1.20740	0.99061	2.26609	-0.06808
0.15	1.15658	0.50101	1.34370	+0.31389	0.65	1.20769	0.99388	2.28467	-0.08310
0.16	1.15996	0.52893	1.36332	+0.32557	0.66	1.20798	0.99705	2.30324	-0.09821
0.17	1.16301	0.55501	1.38281	+0.33521	0.67	1.20826	1.00015	2.32182	-0.11341
0.18	1.16582	0.57935	1.40223	+0.34294	0.68	1.20854	1.00315	2.34040	-0.12871
0.19	1.16839	0.60213	1.42156	+0.34896	0.69	1.20880	1.00609	2.35897	-0.14406
0.20	1.17076	0.62345	1.44082	+0.35339	0.70	1.20905	1.00893	2.37751	-0.15953
0.21	1.17296	0.64346	1.46004	+0.35638	0.71	1.20930	1.01172	2.39608	-0.17506
0.22	1.17500	0.66224	1.47919	+0.35805	0.72	1.20955	1.01443	2.41465	-0.19067
0.23	1.17689	0.67991	1.49830	+0.35850	0.73	1.20979	1.01708	2.43322	-0.20635
0.24	1.17866	0.69655	1.51736	+0.35785	0.74	1.21003	1.01966	2.45178	-0.22209
0.25	1.18031	0.71224	1.53639	+0.35616	0.75	1.21026	1.02217	2.47033	-0.23790
0.26	1.18185	0.72707	1.55538	+0.35354	0.76	1.21048	1.02463	2.48889	-0.25378
0.27	1.18330	0.74110	1.57433	+0.35007	0.77	1.21070	1.02703	2.50745	-0.26972
0.28	1.18465	0.75439	1.59326	+0.34578	0.78	1.21091	1.02938	2.52601	-0.28572
0.29	1.18594	0.76698	1.61217	+0.34075	0.79	1.21112	1.03167	2.54455	-0.30176
0.30	1.18714	0.77895	1.63104	+0.33505	0.80	1.21131	1.03391	2.56310	-0.31788
0.31	1.18828	0.79031	1.64989	+0.32870	0.81	1.21151	1.03610	2.58164	-0.33408
0.32	1.18936	0.80114	1.66873	+0.32177	0.82	1.21170	1.03824	2.60019	-0.35025
0.33	1.19039	0.81144	1.68755	+0.31428	0.83	1.21189	1.04033	2.61873	-0.36651
0.34	1.19136	0.82128	1.70636	+0.30628	0.84	1.21207	1.04238	2.63728	-0.38283
0.35	1.19228	0.83066	1.72518	+0.29781	0.85	1.21225	1.04438	2.65582	-0.39919
0.36	1.19315	0.83963	1.74390	+0.28888	0.86	1.21243	1.04635	2.67438	-0.41560
0.37	1.19399	0.84821	1.76265	+0.27955	0.87	1.21260	1.04826	2.69290	-0.43204
0.38	1.19479	0.85644	1.78142	+0.26981	0.88	1.21277	1.05015	2.71146	-0.44854
0.39	1.19555	0.86430	1.80018	+0.25972	0.89	1.21294	1.05198	2.72999	-0.46507
0.40	1.19627	0.87187	1.81886	+0.24928	0.90	1.21309	1.05379	2.74852	-0.48164
0.41	1.19697	0.87910	1.83757	+0.23850	0.91	1.21326	1.05556	2.76708	-0.49826
0.42	1.19762	0.88606	1.85625	+0.22743	0.92	1.21341	1.05729	2.78560	-0.51490
0.43	1.19827	0.89274	1.87495	+0.21606	0.93	1.21356	1.05898	2.80413	-0.53159
0.44	1.19888	0.89917	1.89362	+0.20443	0.94	1.21371	1.06065	2.82267	-0.54831
0.45	1.19946	0.90537	1.91229	+0.19254	0.95	1.21386	1.06228	2.84121	-0.56507
0.46	1.20003	0.91135	1.93096	+0.18042	0.96	1.21400	1.06388	2.85974	-0.58186
0.47	1.20057	0.91711	1.94963	+0.16805	0.97	1.21414	1.06545	2.87826	-0.59867
0.48	1.20110	0.92265	1.96829	+0.15546	0.98	1.21427	1.06699	2.89679	-0.61553
0.49	1.20160	0.92801	1.98694	+0.14267	0.99	1.21441	1.06850	2.91532	-0.63241
0.50	1.20209	0.93318	2.00558	+0.12969	1.00	1.21454	1.06999	2.93386	-0.64933

TABLE 2-Continued

$\tau = 0.20$

μ	X^*	Y^*	X_s	Y_s	μ	X^*	Y^*	X_s	Y_s
0	1.00000	0	1.00000	0	0.50	1.24471	0.89855	2.00686	+0.13640
0.01	1.02698	0.00927	1.03435	+0.00190	0.51	1.24544	0.90481	2.02537	+0.12488
0.02	1.04710	0.01937	1.06227	+0.00420	0.52	1.24614	0.91088	2.04387	+0.11315
0.03	1.06468	0.03147	1.08806	+0.00809	0.53	1.24682	0.91676	2.06236	+0.10122
0.04	1.08043	0.04844	1.11255	+0.01632	0.54	1.24748	0.92247	2.08085	+0.08910
0.05	1.09464	0.07174	1.13611	+0.03027	0.55	1.24812	0.92800	2.09934	+0.07678
0.06	1.10740	0.10065	1.15895	+0.04910	0.56	1.24874	0.93337	2.11782	+0.06429
0.07	1.11884	0.13348	1.18119	+0.07118	0.57	1.24933	0.93858	2.13628	+0.05163
0.08	1.12909	0.16858	1.20292	+0.09475	0.58	1.24992	0.94365	2.15477	+0.03880
0.09	1.13829	0.20463	1.22425	+0.11867	0.59	1.25048	0.94856	2.17322	+0.02582
0.10	1.14655	0.24068	1.24521	+0.14202	0.60	1.25101	0.95336	2.19167	+0.01270
0.11	1.15402	0.27606	1.26590	+0.16418	0.61	1.25153	0.95801	2.21012	-0.00058
0.12	1.16078	0.31037	1.28633	+0.18482	0.62	1.25204	0.96252	2.22856	-0.01400
0.13	1.16690	0.34338	1.30654	+0.20374	0.63	1.25255	0.96693	2.24702	-0.02754
0.14	1.17249	0.37498	1.32657	+0.22090	0.64	1.25302	0.97121	2.26544	-0.04121
0.15	1.17761	0.40507	1.34645	+0.23623	0.65	1.25349	0.97539	2.28387	-0.05499
0.16	1.18228	0.43369	1.36617	+0.24980	0.66	1.25395	0.97945	2.30230	-0.06890
0.17	1.18659	0.46086	1.38578	+0.26167	0.67	1.25439	0.98340	2.32072	-0.08293
0.18	1.19057	0.48663	1.40529	+0.27191	0.68	1.25483	0.98727	2.33916	-0.09706
0.19	1.19425	0.51107	1.42469	+0.28063	0.69	1.25525	0.99103	2.35757	-0.11129
0.20	1.19766	0.53424	1.44401	+0.28789	0.70	1.25566	0.99469	2.37598	-0.12563
0.21	1.20085	0.55621	1.46327	+0.29379	0.71	1.25607	0.99828	2.39442	-0.14007
0.22	1.20381	0.57706	1.48245	+0.29842	0.72	1.25645	1.00177	2.41282	-0.15460
0.23	1.20657	0.59685	1.50157	+0.30185	0.73	1.25684	1.00519	2.43124	-0.16921
0.24	1.20916	0.61565	1.52063	+0.30418	0.74	1.25721	1.00852	2.44965	-0.18392
0.25	1.21159	0.63353	1.53965	+0.30547	0.75	1.25757	1.01177	2.46804	-0.19870
0.26	1.21388	0.65054	1.55864	+0.30578	0.76	1.25791	1.01497	2.48645	-0.21357
0.27	1.21603	0.66673	1.57757	+0.30519	0.77	1.25826	1.01807	2.50485	-0.22852
0.28	1.21807	0.68218	1.59648	+0.30377	0.78	1.25859	1.02110	2.52324	-0.24355
0.29	1.21998	0.69691	1.61534	+0.30155	0.79	1.25892	1.02408	2.54164	-0.25864
0.30	1.22179	0.71096	1.63416	+0.29859	0.80	1.25925	1.02698	2.56004	-0.27381
0.31	1.22351	0.72438	1.65297	+0.29492	0.81	1.25957	1.02982	2.57845	-0.28906
0.32	1.22514	0.73722	1.67175	+0.29061	0.82	1.25987	1.03260	2.59682	-0.30435
0.33	1.22670	0.74951	1.69051	+0.28570	0.83	1.26018	1.03531	2.61522	-0.31973
0.34	1.22817	0.76129	1.70924	+0.28022	0.84	1.26047	1.03798	2.63360	-0.33515
0.35	1.22958	0.77256	1.72796	+0.27418	0.85	1.26076	1.04059	2.65199	-0.35064
0.36	1.23092	0.78339	1.74665	+0.26766	0.86	1.26105	1.04314	2.67038	-0.36619
0.37	1.23219	0.79377	1.76532	+0.26064	0.87	1.26132	1.04564	2.68876	-0.38180
0.38	1.23341	0.80375	1.78398	+0.25318	0.88	1.26160	1.04809	2.70715	-0.39746
0.39	1.23457	0.81334	1.80260	+0.24531	0.89	1.26185	1.05049	2.72550	-0.41316
0.40	1.23569	0.82257	1.82123	+0.23703	0.90	1.26210	1.05286	2.74388	-0.42892
0.41	1.23677	0.83146	1.83986	+0.22837	0.91	1.26236	1.05516	2.76226	-0.44474
0.42	1.23779	0.84002	1.85845	+0.21936	0.92	1.26261	1.05742	2.78064	-0.46061
0.43	1.23878	0.84826	1.87704	+0.21000	0.93	1.26284	1.05964	2.79899	-0.47651
0.44	1.23973	0.85621	1.89562	+0.20032	0.94	1.26308	1.06182	2.81737	-0.49247
0.45	1.24065	0.86388	1.91420	+0.19033	0.95	1.26332	1.06395	2.83574	-0.50847
0.46	1.24152	0.87129	1.93274	+0.18007	0.96	1.26355	1.06605	2.85411	-0.52451
0.47	1.24236	0.87845	1.95128	+0.16953	0.97	1.26377	1.06811	2.87247	-0.54059
0.48	1.24317	0.88537	1.96981	+0.15878	0.98	1.26399	1.07012	2.89083	-0.55672
0.49	1.24396	0.89206	1.98835	+0.14767	0.99	1.26421	1.07210	2.90920	-0.57289
0.50	1.24471	0.89855	2.00686	+0.13640	1.00	1.26441	1.07405	2.92754	-0.58908

TABLE 2-Continued

$\tau = 0.25$

μ	X^*	Y^*	X_s	Y_s	μ	X^*	Y^*	X_s	Y_s
0	1.00000	0	1.00000	0	0.50	1.28210	0.86405	2.00792	+0.13823
0.01	1.02743	0.00851	1.03444	+0.00150	0.51	1.28512	0.87142	2.02636	+0.12818
0.02	1.04803	0.01766	1.06245	+0.00324	0.52	1.28411	0.87855	2.04476	+0.11790
0.03	1.06611	0.02770	1.08830	+0.00551	0.53	1.28505	0.88549	2.06316	+0.10738
0.04	1.08248	0.03985	1.11284	+0.00949	0.54	1.28599	0.89222	2.08158	+0.09665
0.05	1.09736	0.05560	1.13635	+0.01661	0.55	1.28687	0.89878	2.09996	+0.08569
0.06	1.11115	0.07550	1.15930	+0.02735	0.56	1.28774	0.90513	2.11835	+0.07452
0.07	1.12374	0.09920	1.18164	+0.04130	0.57	1.28858	0.91131	2.13673	+0.06316
0.08	1.13528	0.12584	1.20352	+0.05760	0.58	1.28939	0.91732	2.15509	+0.05162
0.09	1.14584	0.15448	1.22500	+0.07532	0.59	1.29018	0.92317	2.17346	+0.03989
0.10	1.15552	0.18430	1.24614	+0.09368	0.60	1.29094	0.92887	2.19181	+0.02800
0.11	1.16437	0.21466	1.26698	+0.11205	0.61	1.29169	0.93441	2.21017	+0.01593
0.12	1.17250	0.24502	1.28755	+0.12997	0.62	1.29242	0.93981	2.22853	+0.00370
0.13	1.17999	0.27502	1.30793	+0.14708	0.63	1.29312	0.94507	2.24687	-0.00868
0.14	1.18687	0.30440	1.32809	+0.16318	0.64	1.29380	0.95019	2.26520	-0.02121
0.15	1.19323	0.33297	1.34807	+0.17813	0.65	1.29446	0.95519	2.28352	-0.03387
0.16	1.19911	0.36064	1.36791	+0.19184	0.66	1.29511	0.96006	2.30185	-0.04668
0.17	1.20457	0.38733	1.38762	+0.20428	0.67	1.29575	0.96482	2.32020	-0.05963
0.18	1.20964	0.41308	1.40720	+0.21547	0.68	1.29636	0.96946	2.33851	-0.07269
0.19	1.21436	0.43772	1.42668	+0.22540	0.69	1.29695	0.97398	2.35681	-0.08588
0.20	1.21877	0.46139	1.44606	+0.23410	0.70	1.29753	0.97840	2.37512	-0.09919
0.21	1.22290	0.48409	1.46536	+0.24163	0.71	1.29809	0.98271	2.39341	-0.11261
0.22	1.22677	0.50585	1.48460	+0.24802	0.72	1.29865	0.98693	2.41173	-0.12615
0.23	1.23039	0.52668	1.50374	+0.25333	0.73	1.29920	0.99104	2.43004	-0.13980
0.24	1.23383	0.54664	1.52285	+0.25762	0.74	1.29972	0.99507	2.44832	-0.15355
0.25	1.23704	0.56576	1.54189	+0.26091	0.75	1.30023	0.99900	2.46661	-0.16738
0.26	1.24007	0.58408	1.56087	+0.26328	0.76	1.30074	1.00285	2.48492	-0.18133
0.27	1.24294	0.60164	1.57981	+0.26477	0.77	1.30123	1.00661	2.50320	-0.19536
0.28	1.24566	0.61848	1.59871	+0.26543	0.78	1.30171	1.01029	2.52148	-0.20948
0.29	1.24824	0.63461	1.61756	+0.26529	0.79	1.30217	1.01389	2.53975	-0.22369
0.30	1.25067	0.65011	1.63636	+0.26442	0.80	1.30263	1.01742	2.55804	-0.23799
0.31	1.25300	0.66499	1.65517	+0.26282	0.81	1.30308	1.02087	2.57632	-0.25237
0.32	1.25521	0.67929	1.67392	+0.26058	0.82	1.30352	1.02425	2.59459	-0.26682
0.33	1.25731	0.69303	1.69264	+0.25770	0.83	1.30394	1.02755	2.61285	-0.28136
0.34	1.25931	0.70624	1.71134	+0.25421	0.84	1.30436	1.03079	2.63112	-0.29597
0.35	1.26123	0.71896	1.73002	+0.25017	0.85	1.30478	1.03397	2.64940	-0.31065
0.36	1.26305	0.73119	1.74866	+0.24558	0.86	1.30517	1.03708	2.66765	-0.32540
0.37	1.26481	0.74298	1.76728	+0.24051	0.87	1.30557	1.04014	2.68593	-0.34022
0.38	1.26648	0.75435	1.78589	+0.23494	0.88	1.30594	1.04312	2.70415	-0.35509
0.39	1.26808	0.76530	1.80447	+0.22891	0.89	1.30632	1.04605	2.72242	-0.37005
0.40	1.26962	0.77587	1.82304	+0.22245	0.90	1.30670	1.04893	2.74069	-0.38506
0.41	1.27109	0.78608	1.84158	+0.21559	0.91	1.30706	1.05174	2.75894	-0.40014
0.42	1.27251	0.79594	1.86012	+0.20833	0.92	1.30741	1.05452	2.77719	-0.41526
0.43	1.27387	0.80546	1.87864	+0.20069	0.93	1.30776	1.05723	2.79544	-0.43045
0.44	1.27518	0.81467	1.89714	+0.19271	0.94	1.30810	1.05989	2.81368	-0.44569
0.45	1.27644	0.82358	1.91564	+0.18438	0.95	1.30843	1.06252	2.83193	-0.46098
0.46	1.27765	0.83220	1.93411	+0.17574	0.96	1.30876	1.06508	2.85018	-0.47634
0.47	1.27883	0.84054	1.95259	+0.16678	0.97	1.30908	1.06760	2.86841	-0.49173
0.48	1.27996	0.84862	1.97104	+0.15754	0.98	1.30940	1.07007	2.88666	-0.50719
0.49	1.28105	0.85646	1.98949	+0.14802	0.99	1.30971	1.07250	2.90490	-0.52269
0.50	1.28210	0.86405	2.00792	+0.13823	1.00	1.31002	1.07489	2.92315	-0.53824

TABLE 2-Continued

$\tau = 0.50$

μ	X^*	Y^*	X_s	Y_s	μ	X^*	Y^*	X_s	Y_s
0	1.0000	0	1.0000	0	0.50	1.4197	0.7088	2.0107	+0.1178
0.01	1.0288	0.0063	1.0345	+0.0006	0.51	1.4223	0.7196	2.0289	+0.1150
0.02	1.0507	0.0131	1.0625	+0.0013	0.52	1.4249	0.7302	2.0472	+0.1079
0.03	1.0701	0.0202	1.0882	+0.0021	0.53	1.4274	0.7405	2.0654	+0.1025
0.04	1.0880	0.0277	1.1128	+0.0029	0.54	1.4298	0.7506	2.0836	+0.0968
0.05	1.1049	0.0354	1.1365	+0.0038	0.55	1.4321	0.7605	2.1018	+0.0908
0.06	1.1207	0.0439	1.1595	+0.0051	0.56	1.4344	0.7702	2.1200	+0.0846
0.07	1.1359	0.0530	1.1821	+0.0068	0.57	1.4366	0.7796	2.1381	+0.0781
0.08	1.1502	0.0631	1.2041	+0.0092	0.58	1.4388	0.7889	2.1563	+0.0714
0.09	1.1639	0.0741	1.2257	+0.0123	0.59	1.4409	0.7980	2.1745	+0.0644
0.10	1.1770	0.0864	1.2471	+0.0163	0.60	1.4430	0.8069	2.1926	+0.0573
0.11	1.1894	0.0998	1.2682	+0.0210	0.61	1.4450	0.8156	2.2108	+0.0498
0.12	1.2014	0.1142	1.2891	+0.0265	0.62	1.4470	0.8241	2.2289	+0.0422
0.13	1.2127	0.1297	1.3096	+0.0328	0.63	1.4488	0.8326	2.2470	+0.0344
0.14	1.2236	0.1460	1.3301	+0.0395	0.64	1.4507	0.8407	2.2651	+0.0265
0.15	1.2340	0.1629	1.3503	+0.0466	0.65	1.4525	0.8487	2.2832	+0.0180
0.16	1.2439	0.1805	1.3705	+0.0539	0.66	1.4543	0.8566	2.3013	+0.0096
0.17	1.2533	0.1986	1.3904	+0.0615	0.67	1.4561	0.8643	2.3194	+0.0010
0.18	1.2624	0.2169	1.4102	+0.0691	0.68	1.4578	0.8718	2.3374	-0.0078
0.19	1.2710	0.2354	1.4299	+0.0765	0.69	1.4593	0.8794	2.3555	-0.0168
0.20	1.2792	0.2542	1.4495	+0.0839	0.70	1.4610	0.8866	2.3736	-0.0260
0.21	1.2871	0.2729	1.4690	+0.0910	0.71	1.4626	0.8938	2.3917	-0.0353
0.22	1.2945	0.2916	1.4883	+0.0978	0.72	1.4641	0.9007	2.4096	-0.0446
0.23	1.3017	0.3102	1.5076	+0.1043	0.73	1.4657	0.9076	2.4278	-0.0545
0.24	1.3087	0.3286	1.5269	+0.1104	0.74	1.4671	0.9143	2.4456	-0.0642
0.25	1.3153	0.3469	1.5461	+0.1161	0.75	1.4685	0.9210	2.4637	-0.0742
0.26	1.3216	0.3650	1.5651	+0.1215	0.76	1.4700	0.9275	2.4819	-0.0844
0.27	1.3276	0.3828	1.5840	+0.1264	0.77	1.4713	0.9338	2.4997	-0.0946
0.28	1.3335	0.4004	1.6031	+0.1308	0.78	1.4727	0.9401	2.5178	-0.1050
0.29	1.3391	0.4176	1.6220	+0.1347	0.79	1.4741	0.9462	2.5358	-0.1155
0.30	1.3445	0.4346	1.6409	+0.1382	0.80	1.4753	0.9523	2.5538	-0.1262
0.31	1.3496	0.4512	1.6596	+0.1412	0.81	1.4766	0.9583	2.5719	-0.1370
0.32	1.3546	0.4676	1.6784	+0.1438	0.82	1.4779	0.9641	2.5899	-0.1479
0.33	1.3593	0.4836	1.6970	+0.1459	0.83	1.4791	0.9698	2.6078	-0.1589
0.34	1.3640	0.4993	1.7158	+0.1475	0.84	1.4803	0.9754	2.6258	-0.1701
0.35	1.3684	0.5146	1.7344	+0.1486	0.85	1.4815	0.9809	2.6437	-0.1813
0.36	1.3727	0.5297	1.7530	+0.1494	0.86	1.4826	0.9864	2.6617	-0.1927
0.37	1.3768	0.5444	1.7715	+0.1497	0.87	1.4837	0.9917	2.6797	-0.2043
0.38	1.3808	0.5588	1.7901	+0.1495	0.88	1.4849	0.9970	2.6978	-0.2159
0.39	1.3847	0.5729	1.8087	+0.1489	0.89	1.4860	1.0021	2.7157	-0.2276
0.40	1.3884	0.5867	1.8271	+0.1480	0.90	1.4871	1.0072	2.7337	-0.2394
0.41	1.3920	0.6001	1.8456	+0.1465	0.91	1.4881	1.0123	2.7517	-0.2513
0.42	1.3955	0.6133	1.8640	+0.1448	0.92	1.4891	1.0171	2.7695	-0.2633
0.43	1.3988	0.6262	1.8823	+0.1427	0.93	1.4902	1.0220	2.7876	-0.2754
0.44	1.4021	0.6388	1.9007	+0.1402	0.94	1.4912	1.0267	2.8055	-0.2876
0.45	1.4053	0.6511	1.9191	+0.1373	0.95	1.4922	1.0314	2.8235	-0.2999
0.46	1.4083	0.6633	1.9375	+0.1341	0.96	1.4931	1.0360	2.8414	-0.3123
0.47	1.4112	0.6751	1.9558	+0.1305	0.97	1.4941	1.0406	2.8595	-0.3248
0.48	1.4142	0.6866	1.9742	+0.1266	0.98	1.4950	1.0450	2.8773	-0.3373
0.49	1.4169	0.6978	1.9923	+0.1224	0.99	1.4960	1.0494	2.8953	-0.3499
0.50	1.4197	0.7088	2.0107	+0.1178	1.00	1.4969	1.0537	2.9132	-0.3626

TABLE 2-Continued

$\tau = 1.00$

μ	X^*	Y^*	X_s	Y_s	μ	X^*	Y^*	X_s	Y_s
0	1.0000	0	1.0000	0	0.50	1.5752	0.4989	2.0134	+0.061
0.01	1.0300	0.0054	1.0344	+0.001	0.51	1.5806	0.5110	2.0316	+0.060
0.02	1.0534	0.0096	1.0624	+0.001	0.52	1.5864	0.5228	2.0498	+0.059
0.03	1.0744	0.0143	1.0882	+0.001	0.53	1.5919	0.5347	2.0682	+0.058
0.04	1.0939	0.0196	1.1128	+0.001	0.54	1.5973	0.5464	2.0864	+0.057
0.05	1.1126	0.0249	1.1366	+0.001	0.55	1.6024	0.5580	2.1045	+0.056
0.06	1.1302	0.0306	1.1596	+0.001	0.56	1.6077	0.5695	2.1229	+0.054
0.07	1.1472	0.0364	1.1822	+0.001	0.57	1.6126	0.5809	2.1409	+0.053
0.08	1.1634	0.0426	1.2041	+0.002	0.58	1.6177	0.5922	2.1592	+0.051
0.09	1.1792	0.0488	1.2259	+0.002	0.59	1.6224	0.6034	2.1773	+0.048
0.10	1.1944	0.0552	1.2472	+0.002	0.60	1.6271	0.6145	2.1954	+0.046
0.11	1.2092	0.0620	1.2683	+0.003	0.61	1.6316	0.6255	2.2137	+0.044
0.12	1.2236	0.0690	1.2891	+0.004	0.62	1.6364	0.6363	2.2316	+0.041
0.13	1.2378	0.0762	1.3099	+0.004	0.63	1.6409	0.6471	2.2500	+0.038
0.14	1.2514	0.0839	1.3304	+0.005	0.64	1.6452	0.6578	2.2680	+0.035
0.15	1.2649	0.0917	1.3509	+0.006	0.65	1.6495	0.6683	2.2861	+0.032
0.16	1.2778	0.1000	1.3710	+0.007	0.66	1.6537	0.6788	2.3042	+0.028
0.17	1.2905	0.1086	1.3910	+0.008	0.67	1.6579	0.6890	2.3223	+0.025
0.18	1.3028	0.1176	1.4109	+0.010	0.68	1.6620	0.6992	2.3404	+0.021
0.19	1.3149	0.1269	1.4306	+0.011	0.69	1.6660	0.7093	2.3585	+0.017
0.20	1.3267	0.1365	1.4503	+0.013	0.70	1.6699	0.7193	2.3766	+0.013
0.21	1.3381	0.1466	1.4698	+0.015	0.71	1.6737	0.7291	2.3946	+0.008
0.22	1.3493	0.1569	1.4893	+0.017	0.72	1.6775	0.7389	2.4126	+0.004
0.23	1.3603	0.1675	1.5088	+0.019	0.73	1.6812	0.7485	2.4307	-0.001
0.24	1.3709	0.1785	1.5280	+0.021	0.74	1.6848	0.7580	2.4486	-0.006
0.25	1.3814	0.1897	1.5474	+0.024	0.75	1.6884	0.7674	2.4666	-0.011
0.26	1.3915	0.2011	1.5665	+0.026	0.76	1.6919	0.7767	2.4846	-0.016
0.27	1.4015	0.2127	1.5856	+0.029	0.77	1.6954	0.7859	2.5027	-0.021
0.28	1.4111	0.2246	1.6047	+0.031	0.78	1.6987	0.7951	2.5207	-0.027
0.29	1.4206	0.2366	1.6237	+0.034	0.79	1.7020	0.8041	2.5386	-0.032
0.30	1.4299	0.2487	1.6427	+0.036	0.80	1.7054	0.8130	2.5567	-0.038
0.31	1.4388	0.2611	1.6615	+0.038	0.81	1.7086	0.8218	2.5747	-0.044
0.32	1.4476	0.2734	1.6803	+0.041	0.82	1.7118	0.8305	2.5927	-0.050
0.33	1.4561	0.2860	1.6990	+0.043	0.83	1.7149	0.8391	2.6106	-0.057
0.34	1.4645	0.2987	1.7179	+0.045	0.84	1.7180	0.8475	2.6285	-0.063
0.35	1.4727	0.3112	1.7365	+0.047	0.85	1.7210	0.8560	2.6466	-0.070
0.36	1.4807	0.3239	1.7552	+0.049	0.86	1.7239	0.8643	2.6645	-0.076
0.37	1.4884	0.3367	1.7738	+0.051	0.87	1.7269	0.8725	2.6825	-0.083
0.38	1.4960	0.3494	1.7924	+0.053	0.88	1.7297	0.8807	2.7004	-0.090
0.39	1.5034	0.3621	1.8109	+0.055	0.89	1.7325	0.8887	2.7183	-0.097
0.40	1.5108	0.3747	1.8294	+0.056	0.90	1.7353	0.8966	2.7362	-0.104
0.41	1.5179	0.3874	1.8479	+0.057	0.91	1.7381	0.9044	2.7542	-0.112
0.42	1.5248	0.4000	1.8663	+0.058	0.92	1.7408	0.9122	2.7722	-0.119
0.43	1.5316	0.4127	1.8849	+0.059	0.93	1.7435	0.9199	2.7901	-0.127
0.44	1.5382	0.4252	1.9033	+0.060	0.94	1.7461	0.9274	2.8080	-0.134
0.45	1.5447	0.4377	1.9217	+0.061	0.95	1.7486	0.9350	2.8259	-0.142
0.46	1.5511	0.4501	1.9401	+0.061	0.96	1.7512	0.9424	2.8439	-0.150
0.47	1.5573	0.4624	1.9584	+0.061	0.97	1.7536	0.9498	2.8617	-0.158
0.48	1.5633	0.4747	1.9767	+0.061	0.98	1.7561	0.9570	2.8796	-0.166
0.49	1.5693	0.4868	1.9950	+0.061	0.99	1.7586	0.9642	2.8976	-0.175
0.50	1.5752	0.4989	2.0134	+0.061	1.00	1.7609	0.9713	2.9154	-0.183

Given any pair of solutions X and Y, the construction of the standard solutions is a straightforward matter. The standard solutions (denoted by X_s and Y_s) derived from the solutions for $\varpi_0 = 1$ tabulated in the preceding paper are given in Table 2. The moments α_1^s and β_1^s of these standard solutions are given in Table 1*b*; they must satisfy the relation (*R.T.*, p. 194, eq. [68]; p. 215, eq. [46])

$$[\alpha_1^s]^2 - [\beta_1^s]^2 = \tfrac{4}{3}. \tag{5}$$

In Table 1*b* we have verified this relation.

The laws of diffuse reflection and transmission for the case $\varpi_0 = 1$ are expressed in terms of the functions (*R.T.*, pp. 212–214)

$$X^*(\mu) = X_s(\mu) + Q\mu[X_s(\mu) + Y_s(\mu)] \tag{6}$$

and

$$Y^*(\mu) = Y_s(\mu) - Q\mu[X_s(\mu) + Y_s(\mu)],$$

where

$$Q = -\frac{\alpha_1^s - \beta_1^s}{(\alpha_1 + \beta_1)\tau + 2(\alpha_2 + \beta_2)}. \tag{7}$$

The functions X^* and Y^* derived in accordance with these equations are given in Table 2; the values of Q are given in Table 1*b*.

3. *The exact solution of Schuster's problem in the theory of line formation.*—One of the classical problems in the theory of stellar atmospheres is that of Schuster in the theory of line formation. In *Radiative Transfer* (chap. xii, § 83) the exact solution for this problem is given in terms of the X- and Y-functions for $\varpi_0 = 1$. In particular, it is shown that the residual intensity is given by (p. 320, eq. [13])

$$\frac{F(0)}{F^{(\text{Cont.})}(0)} = \frac{I^{(0)} + I^{(1)}(\alpha_2 + \beta_2)/(\alpha_1 + \beta_1)}{(I^{(0)} + \frac{2}{3}I^{(1)})[\frac{3}{4}\tau + \frac{3}{2}(\alpha_2 + \beta_2)/(\alpha_1 + \beta_1)]}; \tag{8}$$

it thus depends only on the single constant $(\alpha_2 + \beta_2)/(\alpha_1 + \beta_1)$. It is known that this constant tends to $\frac{2}{3}$ as $\tau \to 0$ and to 0.710447 . . . as $\tau \to \infty$ (cf. *R.T.*, p. 320). We can now give the "exact" values of this constant for the values of τ in Table 1*b*. In Table 3

TABLE 3

THE CONSTANT $(\alpha_2 + \beta_2)/(\alpha_1 + \beta_1)$ IN THE FORMULA FOR THE RESIDUAL INTENSITY IN SCHUSTER'S PROBLEM

τ	$(\alpha_2+\beta_2)/(\alpha_1+\beta_1)$	$(\alpha_2+\beta_2)/(\alpha_1+\beta_1) - \frac{2}{3}$	$e^{-\tau}$
0	0.66667	0	1.00000
0.05	.67322	0.00655	0.95123
0.10	.67804	.01137	0.90484
0.15	.68188	.01521	0.86071
0.20	.68507	.01840	0.81873
0.25	.68776	.02109	0.77880
0.50	.69675	.03008	0.60653
1.00	.70491	.03824	0.36788
∞	0.71045	0.04378	0

we give these values with $e^{-\tau}$ as the argument; from this table it appears that the run of $(\alpha_2 + \beta_2)/(\alpha_1 + \beta_1) - \frac{2}{3}$ with $e^{-\tau}$ is sufficiently smooth for accurate interpolation for all intermediate values of τ.

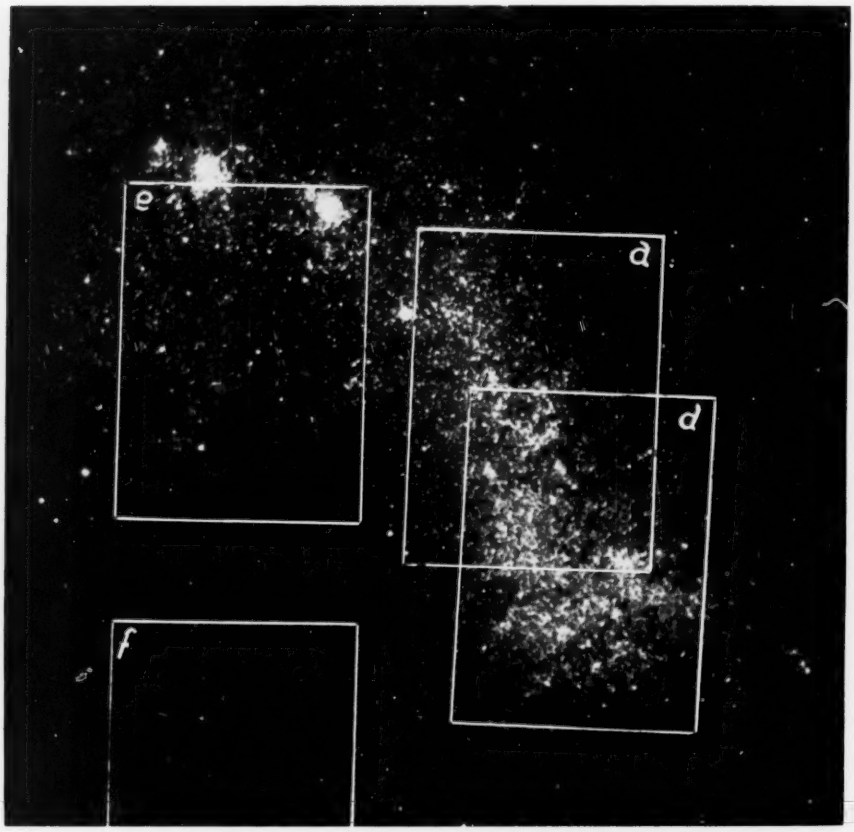

FIG. 1.—The four selected regions in the Small Cloud. Region *f* extends beyond the plate margin

STUDIES OF VARIABLES IN THE MAGELLANIC CLOUDS

I. TWENTY NEW FAINT VARIABLES IN A REGION IN THE SMALL CLOUD

MARTIN DARTAYET AND JORGE LANDI DESSY
Observatorio Astronómico, Córdoba, Argentina
Received November 26, 1951

ABSTRACT

In the Magellanic Clouds several regions were selected for the study of faint variables. Data on 20 new variables of a region in the Small Cloud are given. Among the new variables are cluster-type cepheids, classical cepheids, β Lyrae-type, and long-period variables. Discussion of the material shows that the new variables are members of the cloud; the cluster-type and cepheid variables can be considered as members of the same family, with maximum period frequency of about 1 or 2 days.

INTRODUCTION

This work was originated on suggestions by Dr. Walter Adams, made on the occasion of the dedication of our Astrophysical Station at Bosque Alegre, in July, 1942. Serious difficulties delayed the execution of the program considerably, among others the impossibility of obtaining, during the war, fast plates for the reflector, only old commercial plates of low sensitivity being available. However, a few pairs of these plates have served for the preliminary "blinking."

In the clouds, several regions were selected: four in the Small Cloud and three in the large one. The location of the four regions in the Small Cloud is shown in Figure 1.

Up to the present, nearly one thousand 30-minute exposure plates have been taken, and 724 new suspected variables found. In view of the large number, it was decided to study, in each region, all the variables within $18' \times 18'$ around the center of the field. To facilitate the search and study of long-period variables, a new series of 60-minute-exposure, red-sensitive plates is being taken.

REGION *a* IN THE SMALL CLOUD

Material and reduction.—For this region, 79 Ilford HP2 panchromatic plates and 137 103*a*-O Eastman Kodak plates have been taken at the Newtonian focus of the 154-cm reflector at Bosque Alegre. Except for a few plates whose exposure was interrupted by weather conditions, all the plates were exposed for 30 minutes. Fourteen pairs of plates were examined with our Zeiss blink microscope. The time intervals of the plate pairs are given in Table 1.

In this way 93 variables were detected in our field of $18' \times 18'$, 12 of them being Harvard variables. However, this blinking cannot be considered exhaustive, as there are, for example, 3 more Harvard variables which have not been found in our search. The 60-minute-exposure, red-sensitive plates which have not been blinked may also increase the number of variables.

The brightness of each variable was determined according to the Argelander Stufen method referred to near-by stars (local sequence).

Magnitudes.—In order to determine the magnitudes, a preliminary south polar sequence of 23 stars was established by intercomparison with 76 stars in Selected Area 71. The magnitudes of these 76 stars have been determined by Dr. W. Baade (private communication). The numbers of plates used for intercomparisons were three pairs of 5 minutes' exposure, two pairs of 20 minutes', and three pairs of 60 minutes'. All the

76 stars of Selected Area 71 were present on our 60-minute plates. The plates were measured with a photoelectric photometer constructed at the Observatory by Dr. Ricardo Platzeck. The method applied was the usual star-minus-background measurement. The sequence was tested and smoothed by means of sixteen different south pole plates, the residuals showing good inner agreement. During the exposures, no protection against air-humidity was applied. Our south polar sequence ranges from magnitude 14.97 to 19.06. The 9 stars brighter than magnitude 17.0 are the same as those of the Harvard south polar region. The comparison between the new magnitudes and the Harvard magnitudes is plotted in Figure 2. The Harvard magnitudes were corrected with the values given in *Harvard Bulletin*, No. 781, 1923, and *Harvard Annals*, Volume **89**, No. 11, 1937. A master-sequence in region *a* of the Small Cloud was established by intercomparison with our polar sequence, for which purpose seven pairs of 5-minute, six pairs of 20-minute, and three pairs of 60-minute exposure plates were available. Here a difficulty had to be overcome, since the dense stellar field of the cloud did not furnish a good background for the "clear" measures, although the sequence stars had been

TABLE 1

TIME INTERVALS FOR PAIRS OF PLATES

No. of Pairs	Time Interval	No. of Pairs	Time Interval
1	1½ hours	1	20 days
1	3 hours	1	33 days
3	4 hours	1	56 days
2	6 hours	1	60 days
1	7 hours	1	67 days
1	1 day		

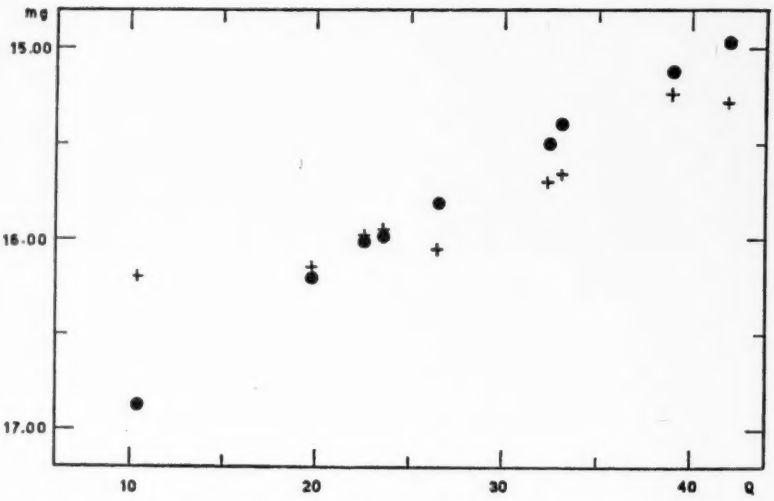

FIG. 2.—Comparison between the Córdoba and Harvard magnitudes in the South Polar Sequence. *Ordinate*, magnitudes; *abscissa*, average galvanometer deflection for three plates of 20-minute exposure; *dots*, Córdoba magnitudes; *crosses*, Harvard magnitudes.

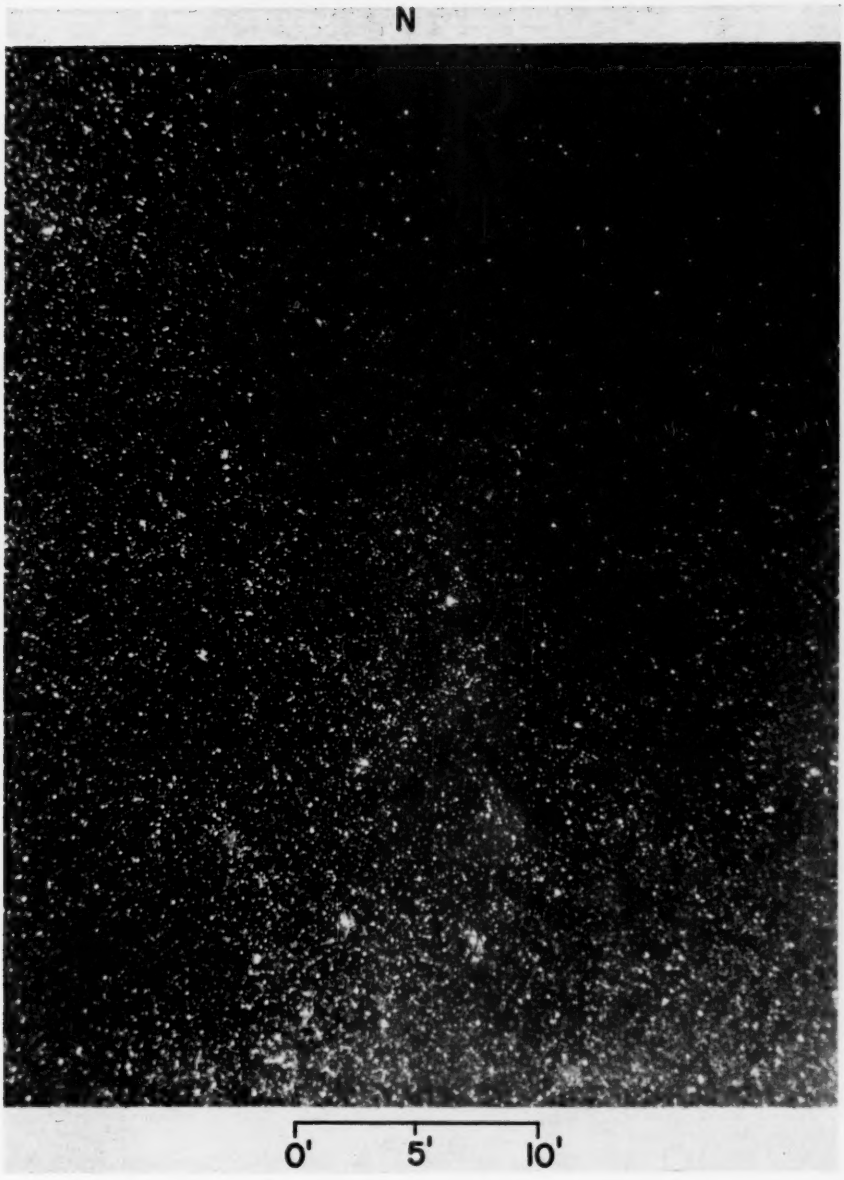

FIG. 3.—Standard 30-minute exposure plate (103*a*–O emulsion), showing the saturated stellar background. Centered on the star CGA 796 ($X = 11{,}956''$; $Y = 10{,}024''$).

chosen in the poorest region of the plate. Since allowance for the background resulted in systematically different magnitudes from the plates with 5-, 20-, and 60-minute exposures, we decided to omit the reference to the background and to use directly the galvanometer readings of the star images. Thus we succeeded in improving the agreement considerably, but it became clear to us that, in order to obtain a good agreement of magnitudes, the smallest diaphragm compatible with the plates had to be used, with the purpose of eliminating the background as far as possible. Figure 3 shows a background saturated with stars, in spite of an exposure of only 30 minutes.

The magnitudes at maximum and minimum were obtained by connecting the local sequence of each variable with the master-sequence. The same precaution was taken with the background as mentioned above. Taking into account all the facts mentioned, our magnitudes have to be considered as preliminary; however, the period-luminosity-curve of the region does not show an appreciable systematic difference between our

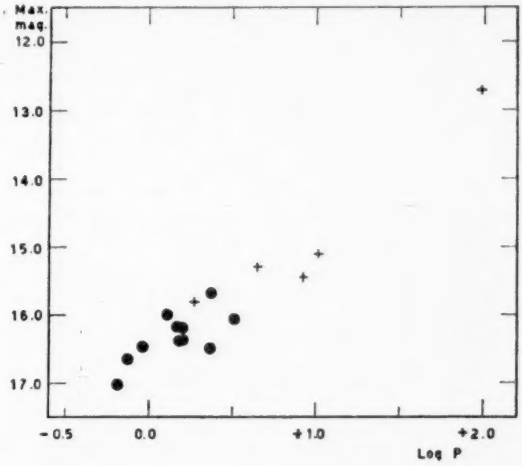

FIG. 4.—Period-luminosity diagram (photographic magnitudes at maximum). *Dots*, Córdoba values; *crosses*, Harvard values.

cepheids and those previously observed at Harvard (Fig. 4). Because of the inadequate distribution of the material for the long-period variables, their magnitudes are less accurate.

The new variables in region a.—Figure 1 shows that region *a* is an intermediate one, being situated neither in the densest nor in the poorest part of the cloud. Our first 20 variables are of four different kinds: cluster-type cepheids, cepheids with periods >1 day, eclipsing binaries, and long-period variables (Table 2).

As already mentioned, there are, altogether, 96 variables—15 Harvard variables and 81 Córdoba variables—in our field of $18' \times 18'$ (40×40 mm on the plate), data being available for 6 Harvard variables and 18 Córdoba variables (2 of our variables are beyond the field of $18' \times 18'$). These 24 variables represent roughly one-quarter of the total and provide sufficient material for a preliminary discussion. More data will become available in the near future after the investigation of the remaining variables has been finished.

From the period-luminosity relation (Fig. 4) it is evident that the cepheids of our field are members of the cloud. Their periods—with two exceptions—are less than 10

days, with the most frequent period between 1 and 2 days. Of course, the position of the maximum frequency cannot be given with accuracy, but there is good reason to believe that the remaining variables of the field are likely to increase rather than to decrease the percentage of the short-period cepheids. On the other hand, cluster-type cepheids with very short periods seem to be infrequent. The amplitudes of our cepheids are everywhere larger than 0.5 mag.; and this fact, together with the discovery of variables with periods less than 1 day, makes the assumption quite plausible that the majority of our cepheids are closely related to the cluster-type variables.[1] The period-amplitude diagram (Fig. 5) shows a breakup at 1.6 days, which, of course, may be accidental, more material with accurate measures being necessary before anything concerning this fact can be concluded.

The 5 eclipsing binaries are of the β Lyrae type and doubtless belong to the cloud.

TABLE 2*

VARIABLES FOUND IN REGION *a* OF SMALL CLOUD

CÓRDOBA VARIABLES	*X*	*Y*	*x*	*y*	PERIOD (DAYS)	MAGNITUDE			AMPLITUDE
						Max.	Min. I	Min. II	
	Cepheids								
270	11,934	10,255	− 0.8	+ 8.3	0.64732	17.02	17.55	.....	0.53
233	11,773	10,005	− 6.6	− 0.7	0.74689	16.65	17.15	.....	0.50
106	11,614	9741	−12.3	−10.2	0.91285	16.46	17.00	.....	0.54
158	12,159	10,396	+ 7.3	+13.4	1.28163	16.00	16.74	.....	0.74
109	12,545	10,457	+21.2	+15.6	1.40359	15.80	16.86	.....	1.06
95	12,106	10,310	+ 5.4	+10.3	1.49554	16.19	17.07	.....	0.88
127	12,070	10,327	+ 4.1	+10.9	1.49606	16.38	17.52	.....	1.14
274	11,787	10,113	− 6.1	+ 3.2	1.5716	16.38	17.02	.....	0.64
3	12,087	9905	+ 4.7	− 4.3	1.58115	16.20	17.63	.....	1.43
92	12,281	9918	+11.7	− 3.8	2.36526	16.50	17.08	.....	0.58
214	11,975	9768	+ 0.7	− 9.2	2.3690	15.68	16.22	.....	0.54
70	11,600	10,168	−12.8	+ 5.2	3.24414	16.07	17.03	.....	0.96
	Eclipsing Binaries								
5	11,628	9774	−11.8	− 9.0	0.768890	16.62	17.20	17.17	0.58
18	12,920	9505	+34.7	−18.7	0.496686	15.98	17.00	16.91	1.02
229	12,373	10,363	+15.0	+12.2	1.04318	15.70	16.38	16.19	0.68
9	12,173	9546	+ 7.8	−17.2	0.83629	15.73	16.63	16.16	0.90
108	12,028	10,466	+ 2.6	+15.9	0.501098	16.28	16.67	16.63	0.39
	Long-Period Variables								
7	12,139	9471	+ 6.6	−19.9	279	17.5	.....	.....	.....
12	11,984	10,116	+ 1.0	+ 3.3	~200	17.5	.....	.....	.....
37	11,859	9693	− 3.5	−11.9	245	17.1	.....	.....	.....

* *X* and *Y* are co-ordinates given in the usual Harvard system; *x* and *y* are co-ordinates of a system for region *a* centered at the star CGA 796 ($x = 0.0$, $y = 0.0$), whose axis is parallel to the axis of the Harvard system. The condition for a star to fall into the field 18′ × 18′ is given when its co-ordinates are less than ± 20.0. The light-curve for Variable 108, considered by us as an eclipsing binary, might suggest the possibility of its being a cluster-type cepheid, in which case it would not belong to the cloud. The image of the star CV 18 is affected by coma, and therefore the magnitudes given are less accurate. The maximum magnitudes of the long-period variables are also less accurate.

[1] Cf. O. J. Eggen, *Ap. J.*, **113**, 367, 1951.

So do the long-period variables, since their luminosity agrees with the one generally attributed to them. Color estimates indicate that they are red. No novae have been found on our plates.

We briefly conclude:

1. There are cluster cepheids, cepheids with periods >1 day, eclipsing binaries, and long-period variables in the Small Cloud.

2. As Shapley and McKibben have already pointed out,[2] the most common periods of the cepheids are the shortest ones.

3. It seems plausible that the cepheids with short periods ($P < 2^d$) and large amplitudes belong to the same group as the cluster-type variables.

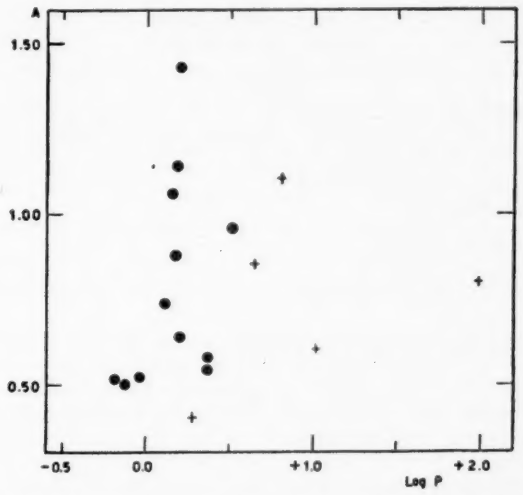

FIG. 5.—Period-amplitude diagram. *Dots*, Córdoba values; *crosses*, Harvard values

4. The variables suggest that the two Baade populations are present in the Small Cloud.

With our new photoelectric plate-photometer we hope to save time and to obtain more accuracy, since each variable can be directly referred to the master-sequence and a large number of variables can be measured at the same time.

After a complete and definite elaboration of the material accumulated, it is intended to publish the light-curves, improved magnitudes, and other data concerning the new variables of each region in the form of a catalogue, in *Resultados del Observatorio Nacional Argentino*.

We are much indebted to Dr. W. Baade for his most valuable suggestions and help and for making accessible to us the unpublished magnitudes of Selected Area 71. Furthermore, we are greatly obliged to Dr. Ricardo Platzeck for the construction of the photoelectric photometer and the continuous control of its performance, in addition to the encouragement and interest shown by him throughout the execution of our program. Finally, we wish to express our sincere thanks to Miss Nélida Keller, who has done most of the blinking, measuring, and computing.

[2] *Proc. Nat. Acad. Sci.*, **28**, 200, 1942.

MAGNITUDES AND COLORS OF 176 EXTRAGALACTIC NEBULAE

JOEL STEBBINS AND ALBERT E. WHITFORD
MOUNT WILSON AND PALOMAR OBSERVATORIES
CARNEGIE INSTITUTION OF WASHINGTON
CALIFORNIA INSTITUTE OF TECHNOLOGY
AND
WASHBURN OBSERVATORY
Received November 6, 1951

ABSTRACT

The magnitudes of 176 extragalactic nebulae from 9.2 to 18.2 mag. have been determined with a photomultiplier; of these, 97 have also been measured for color, and both magnitudes and colors are reduced to the International System. Together with a previous list, published in 1937, the results give magnitudes for 310 and colors for 187 different nebulae. Relations for reducing all results to a common system are derived. The new data indicate a correction of -0.2 mag. to the photographic magnitudes between 10 and 13 of the Harvard Survey.

As before, the nebulae of Hubble's types E, S0, Sa, and Sb average about the same color at $C = +0.85$ mag., International; the Sc's are bluer at $C_p = +0.47$ mag.

Owing to the high latitudes of the objects in the present list, they are not suitable for detection of space reddening in the galaxy. The excess reddening of the distant nebulae has been discussed in a previous paper.

The present extension of the earlier photoelectric photometry of extragalactic nebulae with the reflectors at Mount Wilson[1] was undertaken at the suggestion of Edwin Hubble and Walter Baade to provide additional standards of magnitude and color for faint nebulae. The observations were obtained in the spring of 1947, Whitford going to Mount Wilson for March and April, Stebbins for May and June. The installation and the method of observation have already been described in a paper on some of the fainter nebulae of the present program.[2] The principal improvements on the work of 1937 have been the substitution of a 1P21 photomultiplier for a Kunz photocell; the rebuilding of the photometer to take focal diaphragms up to 19 mm instead of 10 mm in diameter, thus increasing the field from 2'.7 to 5'.1 on the 100-inch; and the reference of the measures to polar standards directly instead of by way of the Harvard visual magnitudes.

At the outset we planned to get the magnitudes of nebulae correct to 0.1, but, after the work was well started, the suggestion was made that we might also measure some stars in Selected Areas to 0.01 or 0.02 mag. for additional standards. This expansion of the program, with another decimal place of accuracy thrown in, added some difficulties, but the enlarged program was carried through. The results for stars in Selected Areas 57, 61, and 68 have since been published.[3] The present report includes the magnitudes of 176 nebulae, with the colors of 97 of them, all reduced to the International scale.

The observations were taken with the series of focal diaphragms listed in Table 1, where the corresponding fields are given for each telescope. When a diaphragm is mentioned in the tables which follow, these field diameters serve to identify the telescope. We prefer to use fixed known openings rather than a variable-iris diaphragm.

The results of the observations are in Table 2. The first column contains the NGC number. In the next two columns the galactic co-ordinates l and b are from the Lund

[1] Stebbins and Whitford, *Mt. W. Contr.*, No. 577; *Ap. J.*, **86**, 247, 1937.

[2] Stebbins and Whitford, *Mt. W. Contr.*, No. 753; *Ap. J.*, **108**, 413, 1948.

[3] Stebbins, Whitford, and Johnson, *Ap. J.*, **112**, 469, 1950.

tables, interpolated from the NGC positions brought up to 1900. The type is by Hubble or Baade. In the next two columns the Harvard photographic magnitude *HPg* and the diameters are from the Shapley and Ames catalogue.[4] The first diameter in the diaphragm column applies to the magnitude measurement; the second applies to the color. In the few cases where a rectangular diaphragm was used, the two dimensions are given, e.g., 6'.8 × 2'.3 for NGC 3556; here there was no change for the color. When a diaphragm includes the whole nebula, the sky often contributes 80 per cent of the total light. Since the color is in most cases rather insensitive to the size of the diaphragm, a smaller hole for this part of the measurement gives a better nebula-to-sky ratio and higher accuracy. In spirals, however, the outer regions are always bluer than the inner

TABLE 1

FOCAL DIAPHRAGMS

Diameter (Mm)	60-Inch	100-Inch	Diameter (Mm)	60-Inch	100-Inch
0.7	0'.3	0'.2	9.1	4'.1	2'.4
1.5	0.7	0.4	12.6	5.7	3.4
2.7	1.2	0.7	19.0	8.6	5.1
5.0	2.3	1.3			

ones;[5] but we could not stop to make a detailed study of every nebula, even if that were possible.

The magnitudes Pg_p and colors C_p on the International scale were derived from the photoelectric measures by the relations

$$\begin{aligned} C_p &= +0^m.96 + 1.00C_{47}\,, \\ Pg_p &= Pe \qquad\quad + 0.29C_p\,, \end{aligned} \tag{1}$$

where C_{47} is the photoelectric color index with blue and yellow filters and Pe is the photoelectric magnitude measured in the clear, both corrected for atmospheric extinction and referred to standards of the North Polar Sequence. Relations (1) differ little from the revised ones later derived for the stars observed in 1947.[6] When the color was not measured, C_p was assumed to be +0.86 mag. for types E, S0, Sa, and Sb, and equal to +0.47 mag. for Sc. The adoption of mean colors seldom leads to an error of 0.1 mag. in Pg_p. When the field of the diaphragm is smaller than the major diameter of the nebula, Pg_p is in parentheses; the difference $Pg_p - HPg$ is given only when Pg_p takes in the whole nebula.

Additional data are in the "Remarks" column. For instance, the first object, NGC 147, was observed on two nights in 1944 with average deviations ±0.15 mag. and ±0.00 mag. for magnitude and color, respectively. When an additional magnitude with a smaller diaphragm was obtained, the difference is, of course, always in the direction of numerically greater magnitudes; e.g., for NGC 2685 the magnitude for 2'.3 was 0.24 fainter than for 4'.1. An interfering near-by star was either excluded ("Star out"), or if it was included with the nebula, its light was determined separately and subtracted from the total ("Star elim."). Other remarks are self-explanatory.

[4] *Harvard Ann.*, **88**, 43, 1932.

[5] F. H. Seares, *Proc. Nat. Acad. Sci.*, **2**, 553, 1916; E. F. Carpenter, *Pub. A.S.P.*, **43**, 294, 1931; C. K. Seyfert, *Ap. J.*, **91**, 529, 1940; also unpublished photoelectric measures by the authors.

[6] Stebbins, Whitford, and Johnson, *op. cit.*, p. 471.

TABLE 2

MAGNITUDES AND COLORS OF NEBULAE

NGC	l	b	Type	HP_g	Diam.		Diaph.		P_{g_p}	C_p	$P_{g_p}-HP_g$	Remarks
147*	87°9	−14°0	Ep	12m1	6′.5	3′.8	8′.6	8′.6	11m2	0m90	−0m9	±0.15, ±0.00 (2), 1944
147*	87.9	−14.0	Ep	12.1	6.5	3.8	2.4	2.4	(12.7)	0.87	.....	1947
185*	88.9	−14.2	Ep	11.8	3.5	2.8	4.1	4.1	11.4	0.96	−0.4	±0.02, ±0.04 (2), 1944
185*	88.9	−14.2	Ep	11.8	3.5	2.8	2.4	2.4	(11.6)	0.86	.....	1947
205	89.0	−20.9	Ep	10.8	8.0	3.6	4.1	4.1	(10.1)	0.77	.....	±0.06, ±0.02 (2), 1944
205	89.0	−20.9	Ep	10.8	8.0	3.0	2.4	2.4	(10.6)	0.67	.....	1947
206	89.0	−21.8	.....	.....	.....	.....	4.1	4.1	11.0	0.66	.....	1944
221	89.4	−21.7	E2	9.5	2.6	2.1	4.1	4.1	9.4	0.90	−0.1	±0.06, ±0.00 (2), 1944
221	89.4	−21.7	E2	9.5	2.6	2.1	0.7	0.7	(10.2)	0.88	.....	1947
224	89.5	−21.3	Sb	(4.5)	160	40	4.1	4.1	(7.2)	1.00	.....	±0.02, ±0.01 (2), 1944
224	89.5	−21.3	Sb	(4.5)	160	40	2.0	2.0	(8.0)	1.01	.....	±0.08, ±0.01 (3), 1944
224	89.5	−21.3	Sb	(4.5)	160	40	0.7	0.7	(9.5)	0.98	.....	1947
598	102.1	−30.7	Sc	7.8	60	40	.....	4.1	.....	0.63	.....	C_p only, 1944
2146	102.7	+25.5	Sap	11.6	5.0	2.5	5.7	...	11.6	.....	0.0	
2300	94.6	+28.2	E1	12.2	1.0	0.7	2.3	2.3	12.5	0.97	+0.3	
2314	106.6	+28.1	E3	12.9	.....	.....	1.2	1.2	13.3	0.93	+0.4	
2379	152.5	+23.2	E1	.....	.....	.....	1.2	...	14.7	.....	.....	
2403	117.6	+30.2	Sc	10.2	16	10	...	2.3	.....	0.50	.....	C_p only
2460	123.7	+32.4	Sb	12.7	.....	.....	2.3	...	12.7	.....	0.0	
2532	155.1	+31.7	Sc	.....	.....	.....	2.3	...	13.0	.....	.....	
2535	164.9	+29.4	Sc	.....	.....	.....	2.3	...	13.4	.....	.....	
2536	165.0	+29.5	Sb	.....	.....	.....	1.2	...	14.7	.....	.....	
2537	141.1	+34.3	Sc	12.2	1.0	0.7	2.3	...	12.3	.....	+0.1	
2549	126.7	+35.4	S0	12.5	1.5	0.7	2.3	...	12.2	.....	0.3	
2639	135.9	+39.5	Sa	12.4	1.0	0.5	4.1	...	12.6	.....	+0.2	
2654	123.0	+38.8	Sa	12.9	2.1	0.7	4.1	...	12.6	.....	−0.3	
2655	101.7	+33.3	S0	11.6	4.0	....	4.1	4.1	11.1	0.79	−0.5	
2681	134.4	+40.9	Sa	11.3	3.0	....	2.3	2.3	(11.4)	0.66	.....	
2685	124.6	+40.0	S0p	12.5	2.0	0.5	4.1	...	12.1	.....	−0.4	2′.3, 0.24
2693	134.2	+41.5	E2	12.9	0.7	0.3	1.2	...	13.2	.....	+0.3	Combined 2.3, 12.8
2694	134.2	+41.5	E0	.....	.....	.....	0.7	...	15.3	.....	.....	
2712	142.8	+42.3	SBb	12.7	1.6	1.0	2.3	...	12.8	.....	+0.1	
2768	122.3	+41.6	S0	12.0	1.5	0.7	4.1	...	11.2	.....	−0.8	
2787	110.8	+38.9	SBa	12.1	2.3	....	2.3	...	12.0	.....	−0.1	
2798	146.8	+45.7	SBa	12.9	0.4	0.4	2.3	...	13.1	.....	+0.2	
2880	118.1	+42.7	SB0	12.9	1.4	0.7	2.3	...	12.6	.....	−0.3	
2950	121.8	+45.7	SB0	12.1	1.4	....	2.3	1.2	11.9	0.86	−0.2	P_{g_p} ± 0.00 (2)
2976	110.5	+41.7	Sc	11.2	3.2	1.1	4.1	2.3	10.9	0.51	−0.3	4′.1, Star elim.; 2′.3, Star out
3031	108.7	+41.7	Sb	8.9	16	10	...	2.3	.....	0.91	.....	Too large for P_{g_p}
3034	108.0	+41.3	Irr	9.4	7.0	1.5	8.6	4.1	9.4	0.72	0.0	Star elim., 5′.7, 0.32
3115	216.3	+37.8	E7	9.8	4.0	1.0	5.7	4.1	10.2	0.89	+0.4	Star elim., 4′.1, 0.15
3147	102.9	+40.1	Sb	11.9	2.0	1.7	4.1	...	11.3	.....	−0.6	
3158	150.2	+56.7	E3	12.7	0.5	0.5	2.3	2.3	13.1	0.90	+0.4	P_{g_p} + 0.01 (2)
3166	206.8	+46.7	Sa	11.6	1.0	....	4.1	1.2	11.6	0.85	0.0	4′.1 C_p 0.85
3184	145.1	+57.0	Sc	11.8	6.0	6.0	8.6	...	10.4	.....	−1.4	Star elim.
3310	122.9	+55.1	Sb	10.9	1.5	0.8	2.3	...	11.3	.....	+0.4	
3448	101.1	+41.9	E0	12.1	0.7	0.7	2.3	...	12.0	.....	−0.1	
3516	99.7	+43.0	SB0	12.2	1.6	1.6	2.3	...	12.5	.....	+0.3	
3556	114.3	+57.2	Sc	11.0	8.0	1.5	6.8×2.3*		(10.7)	0.50	.....	
3610	109.5	+55.3	E5	11.7	1.4	0.8	4.1	...	11.6	.....	−0.1	
3613	110.2	+55.9	E5	12.0	1.8	0.7	5.7	...	11.7	.....	−0.3	
3619	110.3	+56.2	S0	12.8	1.0	1.0	2.3	...	12.7	.....	−0.1	
3623	211.2	+65.3	Sa	10.5	8.0	2.0	8.6	1.2	10.4	0.98	−0.1	Star elim.
3627	211.8	+65.5	Sb	9.9	8.0	2.5	8.6	0.7	9.7	0.87	−0.2	Star elim.
3642	108.5	+55.3	Sc	12.4	5.3	....	5.7	...	11.8	.....	−0.6	
3665	140.7	+69.8	S0	12.3	1.0	0.8	2.3	...	11.9	.....	−0.4	
3675	129.3	+67.4	Sb	11.8	3.0	1.0	4.1	...	11.0	.....	−0.8	Stars out
3726	120.7	+65.9	Sc	11.7	4.6	3.5	5.7	5.7	12.0	0.42	+0.3	Star out
3893	113.2	+66.1	Sc	11.0	4.1	....	4.1	...	11.1	.....	+0.1	
3898	105.3	+59.7	Sa	12.0	2.7	0.7	4.1	4.1	11.7	0.83	−0.3	
3941	135.8	+75.4	SBa	11.4	2.0	1.0	4.1	...	11.3	.....	−0.1	Faint star in
3945	101.1	+55.7	SBa	12.1	1.6	....	2.3	...	11.9	.....	−0.2	
3949	112.6	+67.3	Sc	11.6	2.2	....	4.1	4.1	11.4	0.32	−0.2	
3953	107.4	+63.4	Sb	11.5	6.3	3.2	5.7	...	(11.1)	.....	.....	
3990	103.6	+60.7	S0	.....	.....	.....	1.2	...	13.6	.....	.....	
3992	105.3	+62.7	SBb	11.2	7.0	....	8.6	...	10.6	.....	−0.6	Three stars about compensated
3998	103.5	+60.7	S0	11.6	1.7	1.3	2.3	2.3	11.6	0.84	0.0	
4026	106.9	+65.0	S0	12.0	3.0	0.6	5.7	...	11.7	.....	−0.3	
4036	98.7	+54.8	S0	11.9	4.0	1.0	4.1	4.1	11.7	0.82	−0.2	
4038	256.0	+42.5	Scp	11.0	2.5	2.5	4.1	4.1	10.94	0.52	−0.1	
4038–9	256.0	+42.5	.....	.....	.....	.....	5.7	...	10.90	.....	.....	Combined
4051	113.3	+71.0	Sb	11.7	4.0	2.0	4.1	...	11.2	.....	−0.5	
4102	103.1	+63.7	Sa	12.1	2.3	....	4.1	...	12.3	.....	+0.2	Star elim.
4111	113.6	+72.6	S0	11.6	3.5	1.0	5.7	...	11.6	.....	0.0	4′.1, 0.05
4125	96.1	+51.6	E6	11.3	2.0	1.2	4.1	2.3	11.0	0.82	−0.3	
4138	111.4	+72.3	Sa	12.2	1.6	....	4.1	...	12.3	.....	+0.1	Star out
4143	113.0	+73.3	SB0	12.2	1.3	....	2.3	...	12.1	.....	−0.1	

*The asterisks in the first and seventh columns refer to the notes at end of table.

TABLE 2—*Continued*

NGC	l	b	Type	HPg	Diam.	Diaph.	Pg_p	C_p	$Pg_p - HPg$	Remarks
4151	118°5	+76°1	Sb	11m2	2'5 1'6	4'1 ...	11m3	.....	+0m1	Star elim., 2'3, 0.34, star out
4168	240.1	+73.9	E2	12.8	1.4 1.4	2.3 1'2	12.4	0m79	−0.4	1'2, 0.39
4214	122.9	+79.2	Irr	10.7	8.0 4.0	8.6 4.1	10.2	0.32	−0.5	
4216	243.0	+74.2	Sb	11.3	7.0 1.0	8.6 0.7	11.2	1.01	−0.1	
4220	103.3	+68.8	Sa	12.4	2.5 0.4	4.1 ...	12.2	.....	−0.2	
4244	117.2	+78.1	Sc	11.0	13.0 0.9	4.5×1.4*	(11.2)	0.43	.....	
4245	158.5	+83.6	SBb	12.3	1.5 0.9	2.3 ...	12.4	.....	+0.1	
4251	171.6	+84.1	S0	11.6	1.8 0.8	4.1 ...	11.6	.....	0.0	
4254	243.6	+75.6	Sc	10.5	4.5 4.5	5.7 5.7	10.4	0.44	−0.1	$Pg_p \pm 0.02$ (2)
4258	102.6	+69.5	Sb	10.2	20.0 6.0	8.6 ...	(9.4)	.....	.....	
4261	253.1	+67.5	E3	11.7	1.6 1.3	2.3 ...	11.7	.....	−0.0	
4267	246.8	+74.2	SB0	12.6	2.2 2.2	4.1 ...	12.0	.....	−0.6	
4270	253.6	+67.2	S0	12.8	1.6 0.6	2.3 ...	13.1	.....	+0.3	
4278	159.9	+84.3	E1	11.6	1.0 0.9	2.3 2.3	11.4	0.87	−0.2	
4283	159.5	+84.2	E0	12.8	0.3 0.3	1.2 1.2	13.2	0.82	+0.4	
4291	92.0	+42.0	E2	12.5	0.3 0.3	2.3 ...	12.4	.....	−0.1	
IC 783	244.0	+77.1	S0*	.....	.....	0.7 0.7	15.2	0.78	.....	±0.02, ±0.05 (2), same night
Anon	244.7	+77.1	S0*	.....	.....	0.7 0.4	16.3	0.78	.....	Fol. IC 783, 41sec; 1' south, difficult
4321	245.1	+77.3	Sc	10.8	5.0 5.0	8.6 5.7	9.9	0.57	−0.9	5'7, 0.17
4321	245.1	+77.3	Sc	10.8	5.0 5.0	0.4 0.4	(12.8)	0.53	.....	
4322	245.0	+77.4	S0*	.....	.....	1.3 0.7	15.0	0.74	.....	0'7, 0.62
4328	245.3	+77.3	S0*	.....	.....	0.7 0.7	15.0	0.73	.....	±0.00, ±0.03 (2), same night
4339	255.6	+68.0	E0	12.6	1.5 1.5	2.3 1.2	12.6	0.83	0.0	1'2, 0.28
4365	255.5	+69.3	E2	11.0	4.0 3.0	4.1 2.3	11.1	0.89	+0.1	2'3, 0.31
4374	251.2	+74.7	E1p	10.9	2.9 2.6	5.7 5.7	10.5	0.92	−0.4	
4382	243.0	+79.7	E3p	10.5	4.0 2.5	5.7 5.7	10.2	0.81	−0.3	Star out
4387	251.8	+74.7	E4	.....	0.8 0.6	2.3 1.2	13.1	0.85	.....	1'2, 0.20
4406	252.1	+74.8	E3	10.9	3.8 2.9	5.7 5.7	10.5	0.93	−0.4	
4449	100.3	+73.0	Irr	10.3	4.5 2.5	8.6 5.7	9.8	0.23	−0.5	5'7, 0.04
4450	248.9	+79.0	Sb	11.4	4.4 3.5	3.4 3.4	(11.2)	0.77	.....	
4458	254.4	+75.3	E0	.....	0.7 0.7	2.3 1.2	13.1	0.78	.....	
4464	258.4	+70.4	E3	.....	.....	1.2 1.2	13.6	0.91	.....	
4467	258.5	+70.2	E2	.....	.....	0.7 0.7	15.6	0.86	.....	±0.02, ±0.00 (2), same night
4472	258.8	+70.2	E1	10.1	4.5 4.0	8.6 5.7	9.5	0.89	−0.6	5'7, 0.20
4476	256.1	+74.5	E2	13.2	.....	1.2 1.2	13.4	0.77	+0.2	
4485	100.6	+75.5	Scp	12.9	1.0 0.7	2.3 ...	12.4	.....	−0.5	
4486	256.9	+74.6	E0p	10.7	3.3 3.3	5.7 5.7	9.9	0.89	−0.8	
Anon	256.5	+74.7	E0	.....	.....	0.7 0.7	14.5	0.93	.....	Prec. NGC 4486 18sec; 6' north; ±0.01, ±0.01 (2), same night
4490	100.5	+75.5	Irr	10.5	4.0 1.8	5.7 5.7	10.1	0.27	−0.4	
4494	208	+86.5	E1	10.9	1.6 1.6	4.1 1.2	10.9	0.88	0.0	1'2, 0.69
4501	256.2	+76.6	Sc	10.9	6.0 3.0	0.2 0.2	(14.1)	1.03	.....	Nucleus, $C_p \pm 0.01$ p.e.
4551	261.2	+74.6	E3	.....	0.8 0.6	2.3 1.2	13.0	0.87	.....	1'2, 0.13
4565	217	+87.5	Sb	10.7	15.0 1.1	0.7 0.7	(12.4)	0.99	.....	
4578	264.0	+72.0	E2	12.5	2.5 1.5	2.3 2.3	(12.5)	0.77	.....	
4579	263.4	+74.3	Sb	11.0	3.6 3.2	5.1 5.1	10.6	0.79	−0.4	
4579	263.4	+74.3	Sb	11.0	3.6 3.2	0.7 0.7	(12.1)	0.92	.....	
4589	90.6	+43.3	E1	12.1	0.5 0.5	2.3 ...	12.1	.....	0.0	
4594	268.0	+51.0	Sb	8.1	7.0 1.5	8.6 5.7	9.2	0.92	+1.1	5'7, 0.18
4594	268.0	+51.0	Sb	8.1	7.0 1.5	4.1 4.1	(9.5)	0.92	.....	
4636	268.6	+65.2	E0	10.8	1.2 1.1	4.1 4.1	10.8	0.85	0.0	
4649	268.8	+74.1	E2	10.6	3.9 3.1	4.1 4.1	10.2	0.91	−0.4	
4725	302	+87.7	Sb	10.8	5.0 4.0	8.6 1.2	10.1	0.93	−0.7	
4736	85.1	+76.3	Sb	9.0	5.0 3.5	5.7 5.7	9.0	0.66	0.0	
4800	84.8	+70.8	Sb	12.0	1.3 0.8	2.3 ...	12.3	.....	+0.3	Star elim.
4814	87.2	+59.0	Sb	12.3	3.6 ...	4.1 ...	12.8	.....	+0.5	
4826	295.3	+83.6	Sb	8.0	8.0 4.0	8.6 5.7	9.4	0.77	+1.4	Star out, 5'7, 0.07
4872*	11	+86.6	E0	.....	.....	0.7 0.7	(15.1)	0.96	.....	±0.15, ±0.00 (2), Pg_p discordant
4874*	11	+86.6	S0	.....	1.0 1.0	1.3 0.7	13.5	0.96	.....	±0.00, ±0.01 (2)
Anon*	9	+86.7	E0	.....	.....	0.4 0.4	17.4	0.96	.....	±0.04, ±0.05 (2), 0'2, 0.28
4889*	12	+86.5	E4	12.6	1.3 0.9	1.3 0.7	13.2	1.05	+0.6	±0.03, ±0.03 (2), 0'7, 0.38
5005	61.7	+78.9	Sb	11.3	5.0 1.5	5.7 ...	10.4	.....	−0.9	Sky?
5055	68.5	+74.1	Sbc	10.5	8.0 3.0	8.6 2.3	9.3	0.56	−1.2	Star elim., $Pg_p \pm 0.10$ (2)
5173	68.6	+69.0	E0⁻	.....	.....	2.3 ...	13.7	.....	.....	Sky?
5194	68.8	+68.4	Sc	10.1	12.0 6.0	8.6 8.6	(9.0)	0.47	.....	
5195	68.8	+68.3	Irr	11.1	2.0 1.5	4.1 4.1	10.6	0.77	−0.5	
5198	68.0	+68.8	E1	12.9	0.7 0.6	2.3 ...	12.9	.....	0.0	±0.04 (2)
5273	37.5	+75.3	S0	12.9	1.0 1.0	2.3 ...	12.6	.....	−0.3	
5308	76.8	+54.9	S0	12.8	1.9 0.6	2.3 2.3	12.5	0.89	−0.3	
5322	75.8	+55.5	E4	11.6	1.4 1.0	4.1 4.1	11.1	0.81	−0.5	$Pg_p \pm 0.06$ (2), 2'3, 0.35
5363	310.4	+62.1	Irr	11.1	1.6 ...	2.3 2.3	11.4	0.95	.....	
5448	60.5	+63.6	Sa	12.5	3.0 0.8	5.7 ...	12.1	.....	−0.4	
5485	67.1	+58.7	S0	12.9	0.9 0.9	2.3 ...	12.4	.....	−0.5	Sky?
5533	27.7	+69.1	Sb	12.9	2.0 0.8	4.1 ...	12.6	.....	−0.3	Star out

TABLE 2—*Continued*

NGC	l	b	Type	HPg	Diam.		Diaph.		Pg_p	C_p	$Pg_p - HPg$	Remarks
5548	358°9	+69°0	Sa	12^m.9	0'.5	0'.5	2'.3	...	13^m.3	...	+0^m.4	
5557	30 3	+68 3	E1	12 6	0 7	0 7	2 3	...	12 2	...	−0 4	
5614	25 3	+67 6	Sa	12 9	1 0	0 8	2 3	...	12 6	...	−0 3	
5631	65 0	+55 7	S0	12 5	0 9	0 9	2 3	...	12 5	...	0 0	Sky?
5672	16 6	+66 2	Sb	...	...	...	1 3	1'.3	14 2	0^m.46	...	
Boo1*	16 6	+66 4	E1	...	...	...	0 2	0 2	18 2	1 36	...	±0 02, ±0 07 (3)
5813	327 5	+48 5	E1	12 2	1 4	1 4	2 3	...	12 0	...	−0 2	
5820	53 6	+54 0	S0	12 8	0 7	0 3	2 3	2 3	13 4	1 15	+0 6	Pg_p ±0 17 (2), discordant
5831	327 7	+47 6	E3	12 7	0 5	0 5	2 3	...	12 7	...	0 0	
5838	329 0	+47 9	S0	12 1	1 6	...	4 1	...	11 7	...	−0 4	
5846	328 7	+47 4	E0	11 6	1 0	1 0	4 1	...	11 2	...	−0 3	Companion included
5846	328 7	+47 4	E0	...	...	...	0 7	...	13 7	...	...	Companion alone
5866	57 9	+52 0	S0	11 5	3 0	1 0	4 1	2 3	10 9	0 78	−0 6	Two stars elim., Pg_p ±0 04 (2)
5879	59 2	+50 9	Sb	12 1	3 3	1 3	5 7	...	12 2	...	+0 1	4'.1, 0 00
5899	35 4	+56 2	Sb	12 4	2 3	0 6	4 1	...	12 5	...	+0 1	
5921	336 2	+46 5	SBb	12 5	5 0	5 0	4 1	...	(11 7)	...	...	Star elim.
CrB1*	9 6	+55 3	E0	...	...	...	0 4	0 2	16 8	1 13	...	±0 02 (2), ±0 03 (3) 0'.2, 0 50
CrB2*	9 6	+55 3	E1	...	...	...	0 4	0 2	17 3	1 15	...	±0 04 (2), ±0 07 (3), 0'.2, 0 28
CrB3*	9 6	+55 3	E1	...	...	...	0 4	0 2	17 14	1 13	...	0'.2, 0 60
CrB4*	9 6	+55 3	E3	...	...	...	0 4	0 2	17 09	1 13	...	0'.2, 0 60
5962	358 8	+49 0	Sc	12 5	1 9	1 0	4 1	...	11 9	...	−0 6	
5970	348 1	+46 7	SBb	12 4	3 0	1 0	4 1	...	12 4	...	0 0	
5981	59 4	+46 5	Sab	...	...	...	2 3	...	13 9	...	...	On edge; may be Sb
5982	59 4	+46 5	E4	12 5	1 0	0 7	2 3	2 3	12 3	0 85	−0 2	±0 00, ±0 02 (2)
5985	59 2	+46 4	Sb	12 2	4 0	2 0	5 7	...	11 9	...	−0 3	4'.1, 0 10
6015	62 0	+43 8	Sc	12 1	5 5	2 1	4 1	2 3	(11 7)	0 45	...	Star elim., 2'.3, 0 14
IC 1183	359 1	+43 0	E1	...	...	...	0 7	...	14 9	...	...	
6207	26 4	+39 5	Sc	12 3	2 0	0 7	2 3	...	12 3	...	0 0	Star elim.
6217	78 0	+33 4	Sc	12 6	1 8	1 2	4 1	...	11 8	...	−0 8	
6503	67 4	+30 5	Sc	11 4	5 0	1 0	4 5×1	4*	(11 0)	0 57	...	
6574	9 7	+14 0	Sb	12 7	1 0	0 6	1 3	1 3	12 8	0 76	+0 1	
7177	43 8	−29 8	Sb	12 1	2 5	1 5	2 4	2 4	(12 0)	0 71	...	Sky?
7217	54 7	−20 3	Sb	11 6	3 0	2 5	3 4	3 4	11 0	0 86	−0 6	Sky?
7217	54 7	−20 3	Sb	11 6	3 0	2 5	1 3	1 3	(11 7)	0 92	...	Sky?
7332	55 9	−30 2	S0	12 6	2 0	0 3	2 4	2 4	11 8	0 85	−0 8	Sky?
7339	56 0	−30 3	Sc	...	...	...	2 4	2 4	13 0	0 84	...	Sky?
7448	56 4	−39 7	Sc	11 8	2 0	0 8	2 4	2 4	11 9	0 39	+0 1	Sky?
7457	64 6	−27 3	S0	12 3	2 0	0 5	1 3	1 3	(12 6)	0 84	...	Sky?

NOTES TO TABLE 2

NGC

147, 185 } Diameter probably considerably larger than Shapley-Ames value. See comment in text.

3556 Rectangular diaphragm.

4244 Rectangular diaphragm.

IC 783 to 4328 } These four are called S0; they are probably dwarf members of Virgo cluster similar to NGC 147 and 185 of the local group. All four look alike and lie near NGC 4321 (M 100) (comment by W. Baade).

4872 to 4889 } All are members of the Coma cluster. Only 4872 is listed in Shapley-Ames, but the dimensions and magnitude fit 4889, the brightest member. The catalogue values for 4872 are listed under 4889 in the "HPg" and "Diam." columns of Table 2. The nebula here identified as 4872 is 0'.8 south prec. 4874, the second-brightest member of the cluster. The faint Anon member has the following rectangular co-ordinates relative to 4874: 5'.3 prec., 5'.7 south.

Boo 1 Brightest member of the Bootes cluster (see Stebbins and Whitford, *Mt. W. Contr.*, No. 753; *Ap. J.*, Vol. **108,** 413, Fig. 5, 1948).

CrB 1 to CrB 4 } Four brightest members of Corona Borealis cluster (see *ibid.*, Fig. 4).

6503 Rectangular diaphragm.

At the beginning of Table 2 are results on several members of the local group of nebulae obtained in 1944 with a photocell and filters[7] giving colors C_5 on about double the scale of International C. These measures were also referred to polar standards and reduced to the same system of Pg_p and C_p. After NGC 598 in the list, all observations were made in 1947 and on one night only, unless otherwise noted.

Summarized comparisons of our magnitudes in Table 2 with those of Shapley and Ames and with our previous ones of 1937 are in Table 3. Since the stars included in each

[7] J. Stebbins, *M.N.*, **110,** 422, 1950.

mean difference are not the same ones, the three values under m are not necessarily consistent. The probable error r_1 of a single difference indicates a good enough internal agreement in each of two series of the photoelectric measures. The systematic difference is to be ascribed in part to the decision[3] to base the zero point of photoelectrically determined magnitudes on polar stars between 7.0 and 14.0 mag. rather than on stars near 6.0 mag., which presumably was the basis of the Harvard visual system which we used in 1937. By grouping the differences of 1947 in five means from 10.6 to 12.7 mag., we find

$$Pg_p - HPg = -0^m4 + 0.12\,(HPg - 10^m0)\,; \qquad (2)$$

but four nebulae averaging 9.5 mag. are quite discordant from this relation, giving an observed mean difference of −0.05 mag. instead of the computed −0.46. In 1937 a mean correction of −0.1 mag. to the Harvard magnitudes brought them nearly enough into accord with our values at that time. We now conclude from the 117 stars of Table 3

TABLE 3

SYSTEMATIC DIFFERENCES

	m	r_1	No.
Pg_p (47) − HPg	−0.19	±0.22	117
Pg_p (37) − HPg	− .08	± .17	59
Pg_p (47) − Pg_p (37)	−0.15	±0.08	11

TABLE 4

MEAN COLORS BY TYPES

	E	S0	Sa	Sb	Sc
C_p (37)	+0^{m}90±0.12 (30)		+0^{m}86±0.10 (13)	+0^{m}84±0.12 (12)	+0^{m}59±0.18 (36)
C_p (47)	+0.86±0.06 (32)	+0.83±0.04 (8)	+0.83±0.12(4)	+0.82±0.12 (11)	+0.47±0.08 (11)

that a correction of −0.2 mag. to the Harvard magnitudes from 10 to 13 will bring them into agreement with our present determination of the International scale from magnitude 7 to 14.

From 17 nebulae suitably observed for color in both series we find the relation between C_p of 1947 and C_2 of 1937 to be

$$C_p = +0^m70 + 2.26C_2 \qquad (3)$$
$$\pm 0.01 \pm 0.10 \qquad \text{(p.e.)}.$$

Using equation (3), we compare the colors for different nebular types in Table 4. Following each C_p in the table is the standard deviation for one color and the number of objects in the mean. The differences are scarcely significant except the one for *Sc*, which is probably caused by the larger diaphragms ordinarily used in 1947. Reverting to equations (1), we see that it requires a deviation of about 0.3 mag. from the mean of C_p to cause a change of 0.1 mag. in Pg_p.

Table 2 contains five nebulae of the irregular type, which divide sharply into two color types: +0.74 ± 0.03 (2), and +0.27 ± 0.04 (3). A similar division has been noted by E. Holmberg[8] in his recent study of near-by systems. Although many of the brightest

[8] *Lund Medd.*, Ser. II, No. 128, 1950.

near-by systems are too large to be completely covered by the 8′.6 diaphragm on the 60-inch telescope, the present list of magnitudes has five objects also covered in Whitford's measurements of these objects in 1936. The agreement is satisfactory:

$$Pg_p\,(47) - Pg_p\,(36) = +0^m06 \pm 0.05 \qquad \text{(p.e.)}.$$

For the same reason of large angular diameter, there are not enough objects in common with Holmberg's results on near-by nebulae for a comparison of the magnitude scales. There are, however, ten colors common to the two lists and for these the mean difference comes out:

$$C_p - C_{H_0} = -0^m01 \pm 0.08 \qquad \text{(p.e.)}.$$

Since most of the nebulae in Table 4 are brighter than the thirteenth magnitude, there is little effect of the red shift on the colors. Excluded are the members of the Coma, Corona, and Boötes clusters, for which the effect of the red shift has been discussed separately.[2] Also the variation of csc b in the present list is so small that any latitude effect would be insignificant.

In the two lists of 1937 and 1947, 316 nebulae were observed in one way or another. Of these, there are 222 magnitudes for total light, including 11 nebulae in both series. A correction of -0.1 reduces the $Pg_p\,(37)$ to the system of $Pg_p\,(47)$, which is as near as we can get to International. Similarly, there are colors for 187 different nebulae, including 22 common to the two series. The reduction of $C_2\,(37)$ to $C_p\,(47)$ is given by equation (3). Most of the colors refer to inner regions which, for the spirals, are redder than the outer regions, but for the E nebulae no difference between inner and outer regions has been detected.

Attempts by any method to measure the integrated light of objects like nebulae which fade gradually into the sky background must run the risk of missing the extremely faint outer extensions,[9,10,11,12] which, because of their considerable area, may contribute an appreciable amount to the total. In general, where a magnitude has been given in Table 2 as that of the whole nebula, it represents a measurement of an area whose diameter is at least as large as that estimated by visual inspection of a good original plate. In the majority of the cases, the diameter was checked by Hubble on Mount Wilson plates, using a set of rings which showed the size of the available diaphragms.

The two dwarf elliptical systems NGC 147 and NGC 185 are exceptional cases. W. Baade[13] remarked on the abnormally low density gradient in these systems and found for the latter a major axis of 14′.5, about four times that given by Shapley and Ames. This figure for the diameter has been confirmed in Holmberg's photometry, which finds the total light 1.2 mag. brighter than the result in Table 2 for the Shapley-Ames diameter. On Baade's illustration showing resolved stars,[14] the diaphragm used would be represented by a circle 53 mm in diameter. Even after inspection of this carefully made photograph, one is not prepared for Holmberg's result, which would assign two-thirds of the total light to the area outside the circle.

For nebulae of normal density gradient, however, the light in the outer areas adds a much smaller fraction to the total. Holmberg[8] found an average correction of 0.06 mag. to Whitford's magnitudes in allowing for the area outside diaphragm in the five cases where it was as large as the Shapley-Ames diameter. The difficulty of evaluating these low surface brightnesses against the sky background is shown, however, by the fact that Redman and Shirley[11] found for M 31 a major diameter 1.35 times larger than Holmberg's and a total light 0.7 mag. brighter. A similar discrepancy for the minor diameter

[9] Stebbins and Whitford, *Proc. Nat. Acad. Sci.*, **20**, 93, 1934.

[10] *Harvard Bull.*, No. 895, 1934.

[11] *M.N.*, **97**, 416, 1937.

[12] *Pub. Obs. U. Michigan*, **8**, 103, 1941.

[13] *Mt. W. Contr.*, No. 696; *Ap. J.*, **100**, 147, 1944.

[14] *Ibid.*, Pl. VI.

of M 31 exists in the widely different values found by Shapley[10] and by Williams and Hiltner.[12]

The diaphragms chosen in the present measurements represent a slight concession to the practical observational considerations of dodging field stars and of avoiding too unfavorable a nebula-to-sky ratio. Complete coverage of the outer fringes must remain as the ideal. Until this rather elusive ideal is attained, however, working magnitudes based on stated criteria for the apparent diameter should prove useful. In discussions of nebular distance using total magnitudes, the most important question is not the complete coverage of the faint outer fringe, but the homogeneous treatment of all nebulae of a given type, whether large and bright, or small and faint.

The present paper completes the report on photoelectric observations of nebulae at Mount Wilson extending over the years from 1931 to 1947. We are indebted to Messrs. Hubble and Baade for many suggestions in the planning of this last program, also to them and to Mr. Edison Pettit for co-operation in the work at the telescopes. We also thank Mr. Halton C. Arp for furnishing the galactic co-ordinates in Table 2.

SIX-COLOR PHOTOMETRY OF STARS. VII. LIGHT-CURVES OF ETA AQUILAE*

JOEL STEBBINS, GERALD E. KRON, AND J. LYNN SMITH†
Lick Observatory, University of California
Received October 22, 1951

ABSTRACT

Light-curves of the variable star η Aquilae have been obtained in six colors from the ultraviolet at 3530 A to the infrared at 10,300 A. The variations in all colors show the well-known hump in the light-curve about halfway down in the decreasing phase, with indications of other secondary fluctuations. The *amplitudes* of variation range from 1.45 mag. in the ultraviolet to 0.37 in the infrared. The *times of maximum and minimum* come progressively later in the longer wave lengths, the displacement of phase being 0.05 period between 3530 A and 10,300 A, the same retardation that was found in δ Cephei.

The *colors* of η Aquilae at maximum nearly match those of supergiant stars of spectrum cF7; at minimum they approximate cG3; but the variable is not quite a typical star at either phase.

The *mean radius* is found from the light- and color-curves, combined with an integrated velocity-curve, to be $R = 4.7 \times 10^7$ km $= 68R_\odot$, a value somewhat larger than previous determinations.

The *period* of this variable is shown to be lengthening at the present time.

The variable star η Aquilae is well known as the prototype of the cepheid stars with "humps" in their light-curves. Although many reported secondary fluctuations in the variations of similar stars have been shown to be spurious, the reality of the hump in the curve of η Aquilae has not been questioned since the photoelectric determination of C. C. Wylie[1] in 1920. A short unpublished series of measures of this star was taken with the 60-inch telescope by Stebbins and Whitford on eight nights in the summer of 1946, the last season available at Mount Wilson. When the Crossley reflector of the Lick Observatory had been adapted to photoelectric photometry in 1949, one of the first items on the program was to obtain complete light-curves of η Aquilae in six colors.

The installation on the Crossley is similar to the former one on the 60-inch, but differs in details. A second Western Electric D97087 photocell of about the same over-all color-sensitivity is used, but the primary amplifier is a Victoreen-type 5800 electrometer tube mounted in the refrigerated container with the cell, and the current is further amplified to drive a Brown recorder instead of the former galvanometer, read by eye. The use of such a recorder is now practically universal among photoelectric observers in this country. Under good conditions the new six-color photometer may reach about the same faint limit formerly attainable with the 60-inch—say, the eighth magnitude for solar-type stars—but for a fourth-magnitude star like η Aquilae there is little to choose between the two installations. Actually, the agreement on the same night of measures of this star was slightly better with the Crossley than with the 60-inch—internal probable error ± 0.0062 against ± 0.0067 mag. for one of the magnitudes of the present Table 1; but the residuals depend probably not so much on the instrument as on the number of times that observations happen to be taken with a variable sky.

The observing procedure was practically the same as that for δ Cephei.[2] The variable was measured forward and backward through the series of six filters; then the same was

* *Contributions from the Lick Observatory*, Ser. II, No. 39. This work was supported in part by the Office of Naval Research, under a contract with the University of California.

† Now at United States Bureau of Standards.

[1] *Ap. J.*, **56**, 222, 1922.

[2] J. Stebbins, *Mt. W. Contr.*, No. 704; *Ap. J.*, **101**, 47, 1945.

done for the comparison star. Such a double run is called a "set," and ordinarily two sets were taken on a night. The comparison star was β Aquilae, Harvard vis. mag. 3.90, spectrum dG8, controlled by measures of δ Aquilae, vis. mag. 3.44, spectrum A5. Although Wylie in his photoelectric study of η found a small variation in the light of β, no such change was detected in the present series. The deviations from the means of 13 nights give a probable error of one difference, $\beta - \delta$, of ± 0.008 mag. for all colors, ranging from ± 0.011 mag. for the ultraviolet to ± 0.005 for the infrared. Also, in regular routine, β was compared with two or more polar stars on each of the 23 nights that η was observed.

The results of the observations are in Table 1. The measures in the first section, taken

TABLE 1

SIX-COLOR OBSERVATIONS OF η AQUILAE

JD 2430000+	Phase	U 3530 A	V 4220 A	B 4880 A	G 5700 A	R 7190 A	I 10,300 A	Remarks
1998.947	0.722	+1.07	+0.73	+0.64	+0.56	+0.49	+0.40	1946
1999.945	.861	+0.28	+ .14	+ .23	+ .25	+ .26	+ .26	
2000.946	.001	−0.42	− .57	− .35	− .22	− .08	.00	
2001.936	.139	−0.11	− .25	− .12	− .06	+ .02	+ .04	
2031.908	.315	+0.16	− .30	+ .05	+ .05	+ .08	+ .08	
2032.912	.455	+0.60	+ .41	+ .36	+ .32	+ .28	+ .22	
2054.799	.505	+0.74	.....	+ .43	+ .34	+ .30	+ .21	Violet defective
2055.784	0.642	+1.00	+0.72	+0.61	+0.51	+0.44	+0.35	
3070.947	0.095	−0.20	−0.40	−0.23	−0.10	−0.03	+0.02	1 set, 1949
3074.916	.648	+1.05	+ .72	+ .60	+ .50	+ .44	+ .34	1 set
3076.914	.926	−0.05	− .24	− .08	+ .02	+ .09	+ .15	1 set
3082.841	.752	+0.96	+ .68	+ .62	+ .54	+ .48	+ .38	
3083.894	.898	+0.09	− .06	+ .08	+ .14	+ .18	+ .21	
3084.880	.036	−0.34	− .53	− .32	− .17	− .06	+ .02	
3090.869	.871	+0.24	+ .09	+ .19	+ .21	+ .24	+ .25	
3098.859	.984	−0.36	− .55	− .32	− .17	− .05	+ .03	
3104.876	.823	+0.66	+ .43	+ .45	+ .42	+ .39	+ .35	
3117.783	.621	+1.02	+ .67	+ .57	+ .48	+ .42	+ .31	
3123.741	.451	+0.63	+ .40	+ .35	+ .29	+ .28	+ .19	
.871	.469	+0.64	+ .40	+ .37	+ .32	+ .29	+ .22	
3131.791	.573	+0.88	+ .57	+ .47	+ .43	+ .36	+ .28	
3140.829	.832	+0.52	+ .35	+ .37	+ .38	+ .38	+ .36	
3144.859	.394	+0.40	+ .16	+ .20	+ .17	+ .16	+ .12	
3151.823	.364	+0.26	+ .04	+ .10	+ .10	+ .12	+ .09	
3158.822	.339	+0.22	+ .01	+ .06	+ .08	+ .09	+ .09	
3172.801	.287	+0.22	− .01	+ .05	+ .08	+ .09	+ .10	
3177.709	.971	−0.34	− .52	− .30	− .15	− .03	+ .05	
.804	.984	−0.39	− .55	− .32	− .19	− .06	+ .04	
.842	.990	−0.41	− .55	− .32	− .18	− .05	+ .04	Low altitude
3179.685	.247	+0.16	− .04	+ .03	+ .08	+ .08	+ .09	
3192.690	.059	−0.31	− .47	− .28	− .15	− .05	+ .02	
.756	.068	−0.30	− .45	− .27	− .14	− .04	+ .03	
3193.679	.196	+0.09	− .11	.00	+ .04	+ .07	+ .07	
.719	.202	+0.10	− .08	+ .01	+ .05	+ .08	+ .08	
3200.689	.173	+0.03	− .17	− .05	+ .01	+ .05	+ .08	
.722	.178	+0.02	− .15	− .04	+ .01	+ .06	+ .09	
3206.684	.009	−0.39	− .57	− .34	− .20	− .07	+ .02	
.718	.013	−0.38	− .56	− .33	− .19	− .07	+ .02	
3207.682	.148	−0.07	− .24	− .10	− .03	+ .02	+ .05	
3217.644	.536	+0.78	+ .50	+ .44	+ .40	+ .34	+ .25	
3221.644	.093	−0.24	− .40	− .22	− .12	− .04	+ .02	
3225.640	.650	+1.04	+ .73	+ .61	+ .53	+ .45	+ .35	
.704	0.659	(+1.02)	+0.72	+0.63	+0.53	+0.46	+0.36	Low altitude

with the 60-inch in 1946, are on the regular system of six colors. The measures at Lick in 1949 have been made homogeneous with the previous ones by applying small systematic corrections derived from other stars common to the two series of 1946 and 1949; these corrections will be discussed in a later paper. The first column of the table gives the Julian date in heliocentric Greenwich mean time. The second column gives the phase in fractions of the period from the elements of J. Hellerich:[3]

$$\text{Max.} = \text{JD } 2414827.15 + 7^{d}.176678E\,. \tag{1}$$

The epoch and period will be discussed later. In the next six columns the wave lengths are indicated by the headings and the Δm's are given for each color, a plus sign meaning that η was fainter than β. For example, in the first observation η was 1.07 mag. fainter than β in the ultraviolet and likewise fainter in the other colors; in the fourth observation η was 0.11 mag. brighter in the ultraviolet, but 0.04 fainter in the infrared. The last column gives the years and the remarks. On JD 2432054, through an accident, these two stars and some others were observed with one of the two glasses missing in the violet filter. On the important night of JD 2433225 the observations were pushed to a low altitude, air mass 2.4, and the ultraviolet measure was discarded as doubtful.

The observations in Table 1 are shown graphically in Figure 1, where the average deviations from the freehand curves are less than ± 0.01 mag. Because some of the measures of 1946 came at the critical points of maximum and minimum without enough other measures to establish possible systematic differences, this series was not used in the graph, and it is included in the table only for the record. The curves are tabulated in Table 2, first with η referred to β and then referred to the median magnitude of η itself. The mentioned corrections, 1949 to 1946, average ± 0.01 mag. and may reach ± 0.03 mag. in U and V. They were applied to the tabular values after the curves were drawn; hence the numbers in Table 2 represent the definitive results of the present study.

The amplitudes at the bottom of Table 2 range from 1.45 mag. in the ultraviolet to 0.37 in the infrared; their ratio is $1.45/0.37 = 3.9$. The corresponding figures for δ Cephei are $1.48/0.43 = 3.4$. As in the case of δ Cephei, the retardation of phase in the longer wave lengths is shown in Figure 1 for η Aquilae. While it is scarcely possible to derive unprejudiced figures for this effect, a progressive increase of the retardation is evident along the colors as recorded at the bottom of Table 2. The total effect between 3530 A and 10,300 A is about $0^{p}05$, the same as found for δ Cephei. As pointed out by others,[4] the retardation is readily explained on the theory of a star pulsating with changing diameter and surface brightness. For any color, let L be the total light, A the area of the disk, and s the surface intensity; then, in proper units,

$$L = A\,s\,,$$

$$\frac{dL}{L} = \frac{dA}{A} + \frac{ds}{s}\,. \tag{2}$$

From the radial-velocity measures it is known that at maximum light the diameter is increasing and hence that dA/A is positive and of the same value for all colors; but near this phase ds/s changes sign from positive to negative and in the cooling star becomes numerically equal to dA/A progressively later in the longer wave lengths. A similar retardation occurs at minimum when the diameter is decreasing and the star begins to get hotter.

The variations of η Aquilae during the four months of 1949 were repeated accurately in each cycle of 7.18 days. No disturbance or outburst was detected like that recorded

[3] *A.N.*, **222**, 28, 1924.

[4] A. J. Wesselink, *B.A.N.*, **10**, 256, 1947.

by W. E. Bernheimer[5] in 1930, when the star brightened by 0.15 mag. in 40 minutes. The average form of the present light-curves can be compared with the one of Wylie by interpolating between our violet and blue for a curve of the same amplitude as his. In Table 2 we use the values in the second column, each under V and B, and derive

$$\text{Wylie's mag.} = V - \tfrac{11}{16}(V - B) + 0^{m}06 . \qquad (3)$$

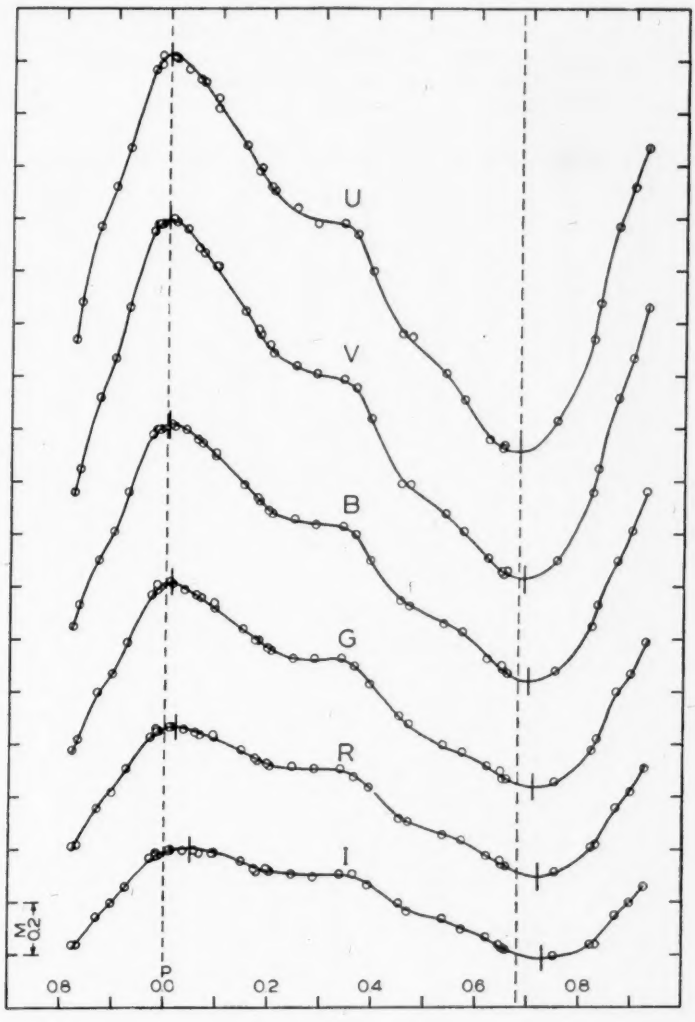

FIG. 1.—Light-curves of η Aquilae

[5] *Lund Medd.*, Ser. II, No. 61, p. 11, 1931.

Then, if we shift our 1949 phase 0^{p}007 earlier, we get the comparison of curves in Table 3. From the differences in the last column we see that the interpolated curve of 1949, with only the amplitude forced, agrees within an average of $\pm 0^m01$ mag. over the entire range with Wylie's curve obtained 29 years earlier. For this reason and for several others, we are rather pessimistic about reported changes in the hump in the light-curve. At first we were doubtful about another secondary wave in our curves, with maxima at about phase 0^{p}55; but, since this wave is also present in Wylie's curve, it is probably real. The six colors also give evidence of another common wave on the ascending branches of the

TABLE 2

SIX-COLOR LIGHT-CURVES OF η AQUILAE

Phase	U	V	B	G	R	I
0^{p}00	−0^{m}39 −0^{m}725	−0^{m}57 −0^{m}66	−0^{m}34 −0^{m}50	−0^{m}20 −0^{m}38	−0^{m}06 −0^{m}275	+0^{m}02 −0^{m}185
0.05	−0.33 − .665	− .50 − .59	− .30 − .46	− .16 − .34	− .06 − .275	+ .02 − .185
0.10	−0.20 − .535	− .37 − .46	− .21 − .37	− .11 − .29	− .03 − .245	+ .02 − .185
0.15	−0.06 − .395	− .23 − .32	− .10 − .26	− .03 − .21	+ .02 − .195	+ .06 − .145
0.20	+0.10 − .235	− .09 − .18	.00 − .16	+ .05 − .13	+ .07 − .145	+ .08 − .125
0.25	+0.18 − .155	− .04 − .13	+ .04 − .12	+ .08 − .10	+ .08 − .135	+ .09 − .115
0.30	+0.21 − .125	.00 − .09	+ .05 − .11	+ .08 − .10	+ .09 − .125	+ .09 − .115
0.35	+0.23 − .105	+ .02 − .07	+ .07 − .09	+ .09 − .09	+ .10 − .115	+ .09 − .115
0.40	+0.43 + .095	+ .20 + .11	+ .21 + .05	+ .18 .00	+ .17 − .045	+ .12 − .085
0.45	+0.63 + .295	+ .38 + .29	+ .35 + .19	+ .29 + .11	+ .28 + .065	+ .20 − .005
0.50	+0.71 + .375	+ .46 + .37	+ .41 + .25	+ .36 + .18	+ .31 + .095	+ .24 + .035
0.55	+0.82 + .485	+ .53 + .44	+ .45 + .29	+ .41 + .23	+ .35 + .135	+ .27 + .065
0.60	+0.96 + .625	+ .62 + .53	+ .52 + .36	+ .45 + .27	+ .40 + .185	+ .30 + .095
0.65	+1.05 + .715	+ .72 + .63	+ .61 + .45	+ .52 + .34	+ .45 + .235	+ .35 + .145
0.70	+1.05 + .715	+ .75 + .66	+ .66 + .50	+ .56 + .38	+ .49 + .275	+ .38 + .175
0.75	+0.96 + .625	+ .69 + .60	+ .62 + .46	+ .54 + .36	+ .49 + .275	+ .38 + .175
0.80	+0.78 + .445	+ .52 + .43	+ .52 + .36	+ .47 + .29	+ .43 + .215	+ .37 + .165
0.85	+0.43 + .095	+ .24 + .15	+ .28 + .12	+ .30 + .12	+ .30 + .085	+ .30 + .095
0.90	+0.08 − .255	− .07 − .16	+ .07 − .09	+ .13 − .05	+ .17 − .045	+ .20 − .005
0.95	−0.22 − .555	− .42 − .51	− .20 − .36	− .08 − .26	+ .02 − .195	+ .10 − .105
1.00	−0.39 −0.725	−0.57 −0.66	−0.34 −0.50	−0.20 −0.38	−0.06 −0.275	+0.02 −0.185
Max.	−0^{m}39 −0^{m}725	−0^{m}57 −0^{m}66	−0^{m}34 −0^{m}50	−0^{m}20 −0^{m}38	−0^{m}07 −0^{m}285	+0^{m}02 −0^{m}185
Min.	+1.06 +0.725	+0.75 +0.66	+0.66 +0.50	+0.56 +0.38	+0.50 +0.285	+0.39 +0.185
Amp.	1.45	1.32	1.00	0.76	0.57	0.37
Phase (Max.)	0^{p}000	0^{p}000	0^{p}005	0^{p}010	0^{p}020	0^{p}040
Phase (Min.)	0.680	0.690	0.700	0.710	0.720	0.730
Min. − Max.	0.680	0.690	0.695	0.700	0.700	0.690

TABLE 3

COMPARISON OF LIGHT-CURVES

	Phase	Wylie	Comp.	W−C*
0^{d}0	0^{p}000	−0^{m}50	−0^{m}49	−0^{m}01
0.5	.070	− .42	− .41	− .01
1.0	.139	− .25	− .25	.00
1.5	.209	− .10	− .11	+ .01
2.0	.279	− .05	− .05	.00
2.5	.348	− .04	− .02	− .02
3.0	.418	+ .17	+ .16	+ .01
3.5	.488	+ .31	+ .32	− .01
4.0	.557	+ .38	+ .40	− .02
4.5	.627	+ .53	+ .52	+ .01
5.0	.697	+ .59	+ .61	− .02
5.18	.721	+ .60	+ .60	.00
5.68	.791	+ .51	+ .48	+ .03
6.18	.861	+ .17	+ .17	.00
6.68	.930	− .20	− .20	0.00
7.18	0.000	−0.50	−0.49	.....

* Average difference = $\pm 0^m010$.

curves with maxima at 0^p85, but we leave to the future the demonstration of this possibility. The maxima of the main hump seem to come at phase 0^p35 in all colors, without the retardation effect present in the main maxima and minima; a displacement of as much as 0^p05 between short and long wave lengths would be conspicuous. The probable wave at 0^p55 is too subtle for detection of difference in phase. If we assume maxima at 0^p35, 0^p55, and 0^p85, a harmonic with period equal to a simple fraction of the main period is out of the question.

The colors of η Aquilae at different phases are reduced to the colors of the six-color system in Table 4. Each first Δm in Table 2 was added to the corresponding value of β Aquilae at the bottom of Table 4; the sum was then referred to the mean of blue, green,

TABLE 4

COLORS OF η AQUILAE

Phase	U	V	B	G	R	I	V − I
0.00	+0m28	−0m14	−0m03	−0m01	+0m04	+0m03	−0m17
0.05	+ .33	− .10	− .02	.00	+ .01	.00	− .10
0.10	+ .41	− .02	+ .02	.00	− .01	− .05	+ .03
0.15	+ .46	+ .04	+ .05	.00	− .04	− .09	+ .13
0.20	+ .53	+ .10	+ .07	.00	− .07	− .14	+ .24
0.25	+ .58	+ .13	+ .08	.00	− .08	− .16	+ .29
0.30	+ .61	+ .16	+ .09	.00	− .08	− .17	+ .33
0.35	+ .61	+ .16	+ .09	− .01	− .09	− .19	+ .35
0.40	+ .71	+ .24	+ .13	− .01	− .12	− .26	+ .50
0.45	+ .79	+ .30	+ .14	− .01	− .13	− .29	+ .59
0.50	+ .82	+ .33	+ .16	− .01	− .15	− .31	+ .64
0.55	+ .89	+ .34	+ .16	− .01	− .15	− .32	+ .66
0.60	+ .97	+ .39	+ .17	− .02	− .16	− .35	+ .74
0.65	+ .99	+ .42	+ .19	− .02	− .18	− .37	+ .79
0.70	+ .95	+ .41	+ .20	− .02	− .18	− .38	+ .79
0.75	+ .88	+ .37	+ .18	− .02	− .16	− .36	+ .73
0.80	+ .78	+ .29	+ .15	− .01	− .14	− .29	+ .58
0.85	+ .61	+ .18	+ .11	− .01	− .10	− .19	+ .37
0.90	+ .45	+ .02	+ .06	.00	− .05	− .10	+ .12
0.95	+ .34	− .10	.00	.00	+ .01	− .01	− .09
1.00	+0.28	−0.14	−0.03	−0.01	+0.04	+0.03	−0.17
0.05	+0.33	−0.10	−0.02	0.00	+0.01	0.00	−0.10
.95	+ .34	− .10	.00	.00	+ .01	− .01	− .09
.15	+ .46	+ .04	+ .05	.00	− .04	− .09	+ .13
.90	+ .45	+ .02	+ .06	.00	− .05	− .10	+ .12
.25	+ .58	+ .13	+ .08	.00	− .08	− .16	+ .29
.866	+ .56	+ .13	+ .09	− .01	− .08	− .16	+ .29
.35	+ .61	+ .16	+ .09	− .01	− .09	− .19	+ .35
.85	+ .61	+ .18	+ .11	− .01	− .10	− .19	+ .37
.40	+ .71	+ .24	+ .13	− .01	− .12	− .26	+ .50
.82	+ .71	+ .25	+ .13	− .01	− .12	− .25	+ .50
.45	+ .79	+ .30	+ .14	− .01	− .13	− .29	+ .59
.80	+ .78	+ .29	+ .15	− .01	− .14	− .29	+ .58
.50	+ .82	+ .33	+ .16	− .01	− .15	− .31	+ .64
0.78	+0.82	+0.32	+0.16	−0.01	−0.15	−0.32	+0.64
β Aql	+0.47	+0.23	+0.11	−0.01	−0.10	−0.19	+0.42

and red for the same phase. For example, the first U in Table 2 is -0^m39, which, added to $+0^m47$ for β, gives $+0^m08$. The corresponding mean of B, G, and R for η is -0^m20; hence, $+0^m08 - (-0^m20) = +0^m28$, the first figure under U in Table 4. The colors of β cancel, and we have η on the six-color system. Some of the values in Table 4 have been smoothed by 0.01 mag., and 5 out of the 120 by 0.02 mag. The pairs of colors in the second part of Table 4 will be discussed presently.

In Table 5 the colors of η Aquilae at maximum and minimum are compared with

TABLE 5

COLOR CLASS OF η AQUILAE AT MAXIMUM AND MINIMUM

HD	Star	Spectrum or Color Class	Abs. Mag.	U	V	B	G	R	I	V−I
171635	45 Dra	cF8	-2^M0	$+0^m28$	-0^m09	-0^m04	-0^m01	$+0^m06$	$+0^m12$	-0^m21
194093	γ Cyg	cF7	−2.1	+0.39	−0.05	−0.02	−0.02	+0.04	+0.09	−0.14
	Mean	cF7	−2.0	+0.34	−0.07	−0.03	−0.02	+0.05	+0.10	−0.17
(Max.)	η Aql	cf7	.....	+ .28	− .14	− .03	− .01	+ .04	+ .03	− .17
	η − Mean	.....	.....	−0.06	−0.07	0.00	+0.01	−0.01	−0.07	0.00
159181	β Dra	cG2	−1.7	+0.78	+0.33	+0.16	−0.01	−0.15	−0.25	+0.58
209750	α Aqr	cG1	−2.2	+0.94	+ .39	+ .16	− .01	− .15	− .23	+0.62
192876	α^1 Cap	cG5	−2.7	+1.03	+ .50	+ .21	− .01	− .20	− .40	+0.90
206859	9 Peg	cG3	−1.3	+1.32	+0.62	+0.24	−0.01	−0.23	−0.46	+1.08
	Mean	cG3	−2.0	+1.02	+0.46	+0.19	−0.01	−0.18	−0.33	+0.79
(Min.)	η Aql	cg3	.....	+0.97	+ .42	+ .20	− .02	− .18	− .37	+0.79
	η − Mean	.....	.....	−0.05	−0.04	+0.01	−0.01	0.00	−0.04	0.00

those of supergiant stars available in our list of six colors.[6] Although for δ Cephei it was possible to find pairs of stars at cF4 and cG2 whose average colors matched those of the variable at maximum and minimum within less than 0.01 mag., for η Aquilae the agreement is not nearly so good. The stars for comparison were all observed with the 60-inch in 1944 or earlier, and we naturally suspect that systematic errors between years may have crept in, but the colors of 1949 agree within 0.01 mag. with those found with the 60-inch in 1946. Apparently there are excesses in U, V, and I for η when B, G, and R match the averages of other stars. The comparison with δ Cephei, if the temperature from V−I is taken as 5500° for dG6, is given in the accompanying tabulation.

	δ CEPHEI, $P = 5^d37$			η AQUILAE, $P = 7^d18$		
	Color Class	V−I	Temp.	Color Class	V−I	Temp.
Maximum	cf4	-0^m57	6500°	cf7	-0^m17	5770°
Minimum	cg2	+0.43	4950	cg3	+0.79	4550

It is well known that the variations of the spectral class in cepheids are much larger when estimated from the hydrogen lines than from the other lines in the spectrum. For

[6] J. Stebbins, *Mt. W. Contr.*, No. 712, p. 9; *Ap. J.*, **102**, 326, 1945.

instance, Shapley[7] gave F0–G2 for δ Cephei and A8–G5 for η Aquilae, presumably from the hydrogen lines in objective-prism spectra. We have quoted the Mount Wilson types for supergiant stars; the colors for ordinary giants of the same types are quite different; η could be gg8 at minimum, but we assume that it is a supergiant at all phases.

Pulsations in the atmosphere of η Aquilae have been studied from spectroscopic radial-velocity measures by W. C. Rufus,[8] D. W. Lee,[9] T. S. Jacobsen,[10] and especially by M. Schwarzschild, B. Schwarzschild, and W. S. Adams[11] from coudé spectrograms taken at Mount Wilson with the 100-inch reflector. Although all these workers agree that pulsations or waves repeat themselves at different levels in the period of the light-cycle, the relations between these differential velocities and the main hump and other waves in the light-curves have not been clarified. In fact, although η Aquilae has been studied about as much as any other star of its class, the phenomenon of the hump remains a riddle. Neglecting the complications of these secondary effects, we proceed to determine the absolute size of this star by a simple method similar to that of Wesselink.[4] We adopt what he calls the "basic assumption," namely, that, at two separate phases of a pulsating star when the relative colors are of the same intensity, the difference in over-all luminosity is caused simply by the variation in the size of the apparent disk. For a black body this assumption would hold without question; for an actual star measured in two colors there might be some doubt; but with six colors in agreement the case is much stronger for the simple geometric picture. Any complication such as variable darkening of the limb throughout the cycle will resist evaluation in the present case.

In the second part of Table 4 the colors in the selected pairs on the descending and ascending branches of the light-curves are practically the same. The over-all differences of magnitude in each pair, combined with the displacement-curve or integrated velocity-curve, give the absolute size of the pulsating disk. Let R be the mean radius in regard to time, Δr_1 and Δr_2 the differences from R at phases 1 and 2, and Δm the difference $m_2 - m_1$; then

$$\frac{(R+\Delta r_1)^2}{(R+\Delta r_2)^2} = \log^{-1}(0.4\,\Delta m)\,.$$

Or, if $n = \log^{-1}(0.2\,\Delta m)$, then

$$R = \frac{\Delta r_1 - n\Delta r_2}{n-1}\,. \tag{4}$$

The Δr's are given by the Schwarzschilds and Adams as $r - R$,[12] the displacements integrated from the radial velocity-curve with intermediate darkening of the limb. In averaging our Δm's for each pair, the ultraviolet has been omitted as of less weight because of greater extinction. The average deviation of a Δm for one color from the mean of five is ± 0.007 mag.; for the ultraviolet it is ± 0.011 mag. We solve equation (4) for R in each pair, with the results in Table 6. The weights assigned are only rough, and, since the number of pairs is arbitrary and the Δm's are taken from curves and not from observations, the probable error of R does not follow readily. Nevertheless, we treat the seven values of R in the table as though they were independent, increase the computed probable error by 50 per cent for safety, and obtain

$$\text{Mean } R = (4.7 \pm 0.2) \times 10^7 \text{ km} = (68 \pm 3)\,R_\odot\,.$$

In contrast with this value, the Schwarzschilds and Adams, using the effective temperature from the spectral type and Shapley's period-luminosity relation of 1930, found $R = 2.55 \times 10^7$ km. Since the present method is more direct, we might consider turning the problem around and using our result to improve the constants in the other

[7] *Ap. J.*, **44**, 287, 1916.
[8] *Pub. Obs. U. Michigan*, **4**, 101, 1932.
[9] *Pub. Obs. U. Michigan*, **4**, 109, 1932.
[10] *J.R.A.S. Canada*, **43**, 104, 1950.
[11] *Ap. J.*, **108**, 207, 1948.
[12] *Op. cit.*, Table 1.

relations, but such a procedure is scarcely warranted for a single star. We note also that W. Becker,[13] by combining another displacement-curve with the total light and the surface brightness from the radiation temperature at any phase, obtained the equivalent of $R = 3.9 \times 10^7$ km $= 57R_\odot$. From Becker's three-color light-curves for η Aquilae at 5570 A, 4800 A, and 4100 A and from the displacement-curve of the Schwarzschilds and Adams, we find, in the same manner as in our Table 6, $R = (5.2 \pm 0.5) \times 10^7$ km. This larger value of R is caused in part by the smaller amplitude of Becker's light-curves. If we interpolate between the different six-color curves for his wave lengths, we find that our amplitudes average about 0.15 mag. larger than his. The photoelectric scale has been checked in several ways, and the reasons for the discordance are not evident. In any event the solution from the six-color curves gives a larger value for the mean radius of η Aquilae than those previously found.

The period of 7.176678 days from Hellerich in our elements (1) seems to have been

TABLE 6

CALCULATION OF MEAN RADIUS R

Phase 1	0^p05	0^p15	0^p25	0^p35	0^p40	0^p45	0^p50
Phase 2	0.95	0.90	0.866	0.85	0.82	0.80	0.78
Δ mag.	0^m084	0^m156	0^m176	0^m210	0^m214	0^m162	0^m138
Δr_1, 10^5 km	−8.6	+3.9	+11.9	+15.8	+16.6	+16.8	+16.8
Δr_2, 10^5 km	−23.7	−28.8	−29.0	−28.1	−24.4	−20.9	−17.0
R, 10^7 km	4.1	4.7	5.1	4.6	4.2	5.1	5.3
Weight	1	2	2	3	3	2	1

used in most of the recent investigations of η Aquilae. Hellerich was undecided whether the period changed gradually or jumped suddenly about 1890. Likewise, A. V. Nielsen[14] found that the period started to lengthen near 1891. If we take the time of our maximum for the mean of violet and blue, call it at 4500 A, and the period from the comparison with Wylie's photoelectric curve, we have the elements

$$\text{Max.} = \text{JD } 2433156.404 + 7^d.176724E\,, \qquad (5)$$

which give the comparison in the accompanying tabulation. Thus the evidence is strong

Years	Period (Days)	Authority
1787–1889	7.176401	Hellerich
1890–1920	7.176678	Hellerich
1891–1928	7.176625	Nielsen
1920–1949	7.176724	Present paper

enough that the period is still growing longer. Nielsen noted rightly that the photographic and photoelectric maxima come earlier than the visual ones, but he was not quite convinced that the effect was real. In any future study of this or other cepheid variables this dependence of the phase upon the wave length should be considered.

In addition to our obligation to the Office of Naval Research, we are indebted to the American Philosophical Society for two grants from the Penrose Fund in support of this and other works in photometry.

[13] *Zs. f. Ap.*, **19**, 296, 1940.

[14] *A.N.*, **243**, 409, 1931.

A PHOTOELECTRIC STUDY OF THE DWARF M ECLIPSING VARIABLE YY GEMINORUM*

GERALD E. KRON
Lick Observatory, University of California
Received November 15, 1951

ABSTRACT

Photoelectric light-curves have been obtained in the visual and in the infrared spectral regions for the eclipsing variable YY Geminorum. Relative and absolute elements, with their probable errors, derived from the light-curves and available spectrographic data, are in good agreement with elements derived by other investigators. Absolute limb-darkening coefficients could not be derived, but it was found that the darkening coefficient in the visual region is greater than that in the infrared by 0.3. Secondary light-variations of considerable amplitude were found during the course of the observing. A study of the photometric and spectrographic data leads to the conclusion that the secondary variations probably are caused by the effects of rotation and eclipse of stellar components with a patchy, nonuniform surface illumination. This conclusion is supported by evidence, discussed in some detail, from three other eclipsing variables.

INTRODUCTION

The star YY Geminorum (Castor C) is a double-lined spectroscopic binary and an eclipsing variable with partial eclipses, with a period of 0.8142 day. Its spectral type has been given by Joy and Sanford,[1] the discoverers of the star's binary nature, as dM1e. As the only known late-type main-sequence eclipsing variable, it is an important source of information about the properties of such objects. Moreover, a very accurate trigonometric parallax enhances its significance.

The purpose of the present study, based upon new two-color photoelectric light-curves, was to improve our understanding of the physical nature of the stars constituting the system of YY Geminorum, with the components considered as typical M-type main-sequence stars. The observational work included a photoelectric determination of the apparent magnitude.

There are two velocity-curves for YY Geminorum: the original one by Joy and Sanford based upon spectrograms having a dispersion of 75 A/mm, and a recent curve by Struve, Herbig, and Horak[2] based upon spectrograms having dispersions of 26, 40, and 50 A/mm. Photographic light-curves have been obtained by H. van Gent,[3, 4] the discoverer of the eclipsing nature of YY Geminorum, while a photovisual light-curve has been published recently by L. Binnendijk.[5]

THE OBSERVATIONS

The original intention was to obtain light-curves in the blue and visual spectral regions with the 12-inch refractor. For two-color photometry with this achromatic doublet, it is necessary to employ a focal-plane aperture at least 30 seconds of arc in diameter, in order to give clearance to the color aberrations of the lens. Though YY Geminorum is well separated (by 73 seconds of arc) from the bright A-type star α Geminorum, it was found that 30 per cent of the measured light in the blue spectral region came from the bright star, and only 70 per cent from YY Geminorum itself. However, owing to the strong

* *Contributions from the Lick Observatory*, Series II, No. 40.

[1] *Ap. J.*, **64**, 250, 1926.
[2] *Ap. J.*, **112**, 216, 1950.
[3] *A.N.*, **228**, 353, 1926.
[4] *B.A.N.*, **6**, 99, 1931.
[5] *B.A.N.*, **11**, 203, 1950.

wave-length dependence of atmospheric scattering and to the relatively greater brightness of YY Geminorum in the longer-wave-length regions of the spectrum, photometry in the visual region involved scattered light of only 4 per cent, while in the infrared region there is no appreciable scattered light. These considerations led to the adoption of the visual and infrared spectral regions for the present study.

Observations in the visual region were made from February 11, 1948, to April 17, 1948, with the 12-inch refractor and a 1P21 multiplier phototube (Table 1, upper part). The output from the multiplier was amplified by a d.c. amplifier and was fed to a Weston Model 430 milliammeter. Observations were made through a piece of Corning 3385 filter

TABLE 1

SCHEDULE OF OBSERVATIONS

Date	JD 2430000+	No.	Type
12-inch refractor (1948):			
11 February	2593	8	Vis.
12 February	2594	32	Vis.
14 February	2596	8	Vis.
19 February	2601	27	Vis.
23 February	2605	36	Vis.
24 February	2606	42	Vis.
25 February	2607	8	Vis.
26 February	2608	33	Vis.
4 March	2615	32	IR
10 March	2621	33	Vis.
12 April	2654	20	Vis.
17 April	2659	13	Vis.
36-inch refractor (1949):			
25 January	2952	74	IR
26 January	2953	68	IR
16 February	2964	17	IR
17 February	2965	60	IR
18 February	2966	51	IR
24 February	2972	15	IR
31 March	3007	45	IR
30 April	3037	10	Vis.
2 May	3039	12	Vis.
3 May	3040	20	Vis.
12 May	3049	7	Vis.

glass of standard thickness, in sets of five 10-second deflections each on comparison and variable stars. A one-deflection determination of the scattered light, made by moving the telescope to an area adjacent to YY Geminorum and equally distant from α Geminorum, preceded and followed each set on the variable star. The observations were timed at the middle deflection to an accuracy of ±10 seconds, by means of a watch compared before and after the observing session with an accurate clock. The infrared observations were made from January 25, 1949, until March 31, 1949, through a cemented Wratten 88 filter, with an unrefrigerated CE-25 photocell in a feedback circuit[6] attached to the 36-inch refractor (Table 1, lower part). A new photometer permitted sampling the sky and scattered light once for each deflection by sliding the focal plane of the photometer to one side of the star. Experimental observations in the infrared had been made on March 4, 1948. Observations in the visual were made with the new photometer on the 36-inch refractor from April 30 to May 12, 1949, to check certain properties of the light-curve

[6] G. E. Kron, *Pub. A.S.P.*, **59**, 190, 1947.

described later, but they were not used to add weight to the 1948 light-curve. The two comparison stars were observed alternately in the visual, and the magnitude difference was based upon the mean deflection of the two stars. Only one comparison star was used in the infrared, because a second near-by star of proper brightness in the infrared could not be found. The approximate wave lengths of the two series of observations were 5200 A and 8100 A, estimated from the manufacturer's data on the filters and monochromator measures on the photocell. A more precise knowledge of the effective wave lengths is not required for interpretation of the observations. Data on the variable and comparison stars are given in Table 2.

TABLE 2

VARIABLE AND COMPARISON STARS

Name	R.A. 1900	Dec. 1900	B.D. Mag.	Spectrum	Remarks
YY Geminorum	$7^h28^m15^s$	+32°05'.4	8.6	dM1e	Variable
BD+31°1627	7 30 02	+31 53.3	8.5	.....	Comparison in visual region
BD+31°1611	7 27 08	+31 54.5	8.7	.....	Comparison in visual region
BD+32°1577	7 27 05	+32 50.3	8.0	K0	Comparison in infrared region

The precision of the observations made with the 12-inch refractor in 1948 was less than expected, chiefly because of the inefficient method of observing the scattered-light level but also because of the inadequate aperture of the telescope. Observations made in the visual with the 36-inch refractor and the translating photometer in 1949 were of satisfactory precision, as were the 1949 observations in the infrared.

The observations in the visual, numbering 315, are given in Table 3. The first column contains the heliocentric Julian Date of the observation, the second the heliocentric phase computed from the formula t_1 = JD 2424989.1169 + $0^d.8142822E$,[4] and the third the difference in magnitude between the variable and comparison stars in the sense Δm = (comp. − var.). The heliocentric corrections, which are of significant size for this star, were computed to four decimals. These corrections were found to agree with those derived from Binnendijk's equation[5] to within one part in the last decimal. The large systematic displacement between the 1948 and the 1949 observations in the visual was caused by the use of only a single comparison star (BD+31°1627) for the 1949 observations. The individual 1949 infrared observations, numbering 362, are not tabulated here, but they are available to interested persons on IBM punched cards at the Lick Observatory.

TIMES OF MINIMA

Times of minima were determined by plotting the observations on two separate pieces of transparent paper. Estimated center lines were drawn identically on each of the two plots, and then one plot was superimposed as a mirror image upon the other and was adjusted so that the plotted points were in phase agreement. Any error in drawing the original estimated center phase was clearly revealed. The plots were useful later for studying the distortions found in the individual records of minima compared with the computed and normal curves. Mean times of minima are given in the accompanying table. Since $P/2$ = 0.4071 day, the secondary minimum seems more nearly centrally

TIMES OF MINIMA

Epoch	Primary	(t_2-t_1)
1948	JD 2432605.9146	$0^d.4076$
1949	2432965.8275	0.4078

TABLE 3

OBSERVATIONS AT λ 5200

Helio. JD 2430000+	Helio. Phase	Δ Mag.	Helio. JD 2430000+	Helio. Phase	Δ Mag.
2594.6616	+0^{d}1490	−0^{m}156	2601.8589	+0^{d}8320	−0^{m}488
.6644	+ .1518	− .164	.8615	+ .8346	− .394
.6686	+ .1560	− .164	.8643	+ .8374	− .369
.6713	+ .1587	− .166	.8672	+ .8403	− .318
.6741	+ .1615	− .167	.8705	+ .8436	− .272
.6776	+ .1650	− .162	.8733	+ .8464	− .213
.6811	+ .1685	− .170	.8763	+ .8494	− .203
.6845	+ .1719	− .165	.8792	+ .8523	− .168
.6880	+ .1754	− .152	.8826	+ .8557	− .170
.6908	+ .1782	− .170	.8856	+ .8587	− .152
.6936	+ .1810	− .165	.8886	+ .8617	− .186
.6963	+ .1837	− .173	.8930	+ .8661	− .160
.7304	+ .2178	− .164	.8962	+ .8693	− .139
.7338	+ .2212	− .160	.8990	+ .8721	− .151
.7373	+ .2247	− .164	.9018	+ .8749	− .153
.7401	+ .2275	− .166	.9032	+ .8763	− .161
.7436	+ .2310	− .164	.9080	+ .8811	− .150
.7470	+ .2344	− .179	2605.7037	+ .6054	− .259
.7505	+ .2379	− .190	.7074	+ .6091	− .248
.7533	+ .2407	− .182	.7103	+ .6120	− .270
.7561	+ .2435	− .165	.7152	+ .6169	− .248
.7908	+ .2782	− .169	.7187	+ .6204	− .229
.7949	+ .2823	− .175	.7222	+ .6239	− .266
.7984	+ .2858	− .189	.7266	+ .6283	− .233
.8019	+ .2893	− .187	.7311	+ .6328	− .250
.8061	+ .2935	− .175	.7409	+ .6426	− .240
.8095	+ .2969	− .169	.7441	+ .6458	− .224
.8123	+ .2997	− .170	.7473	+ .6490	− .199
.8470	+ .3344	− .182	.7504	+ .6521	− .218
.8498	+ .3372	− .198	.8304	+ .7321	− .230
.8540	+ .3414	− .181	.8352	+ .7369	− .204
.8568	+ .3442	− .170	.8383	+ .7400	− .250
2596.7948	+ .6536	− .196	.8426	+ .7443	− .222
.7976	+ .6564	− .266	.8457	+ .7474	− .260
.8004	+ .6592	− .218	.8492	+ .7509	− .265
.8032	+ .6620	− .244	.8537	+ .7554	− .262
.8060	+ .6648	− .194	.8569	+ .7586	− .257
.8117	+ .6705	− .163	.8601	+ .7618	− .231
.8147	+ .6735	− .212	.8634	+ .7651	− .235
.8174	+ .6762	− .203	.8674	+ .7691	− .226
2601.8303	+ .8034	− .534	.8719	+ .7736	− .246
.8330	+ .8061	− .587	.8752	+ .7769	− .235
.8358	+ .8089	− .650	.8784	+ .7801	− .217
.8386	+ .8117	− .698	.8820	+ .7837	− .250
.8410	+ .8141	− .726	.8858	+ .7875	− .277
.8442	+ .8173	− .725	.8892	+ .7909	− .355
.8469	+ .8200	− .714	.8926	+ .7943	− .384
.8497	+ .8228	− .661	.8959	+ .7976	− .465
.8532	+ .8263	− .614	.9003	+ .8020	− .540
.8558	+0.8289	−0.546	.9043	+0.8060	−0.638

TABLE 3—*Continued*

Helio. JD 2430000+	Helio. Phase	Δ Mag.	Helio. JD 2430000+	Helio. Phase	Δ Mag.
2605.9075	+0^{d}8092	−0^{m}653	2607.7642	+0^{d}2230	−0^{m}174
.9111	+ .8128	− .748	.7677	+ .2265	− .158
2606.6715	+ .7589	− .266	2608.6760	+ .3206	− .194
.6757	+ .7631	− .222	.6795	+ .3241	− .186
.6797	+ .7671	− .235	.7100	+ .3546	− .202
.6832	+ .7706	− .232	.7140	+ .3586	− .232
.6861	+ .7735	− .236	.7176	+ .3622	− .200
.6895	+ .7769	− .217	.7228	+ .3674	− .224
.6926	+ .7800	− .230	.7267	+ .3713	− .209
.6960	+ .7834	− .277	.7350	+ .3796	− .265
.6992	+ .7866	− .297	.7396	+ .3842	− .364
.7025	+ .7899	− .301	.7439	+ .3885	− .425
.7070	+ .7944	− .386	.7476	+ .3922	− .502
.7100	+ .7974	− .454	.7512	+ .3958	− .528
.7134	+ .8008	− .516	.7546	+ .3992	− .600
.7168	+ .8042	− .608	.7590	+ .4036	− .733
.7203	+ .8077	− .649	.7637	+ .4083	− .763
.7237	+ .8111	− .737	.7686	+ .4132	− .708
.7262	+ .8136	− .799	.7724	+ .4170	− .685
.7348	+ .0079	− .761	.7768	+ .4214	− .578
.7378	+ .0109	− .661	.7819	+ .4265	− .477
.7410	+ .0141	− .581	.7856	+ .4302	− .413
.7450	+ .0181	− .541	.7892	+ .4338	− .349
.7678	+ .0409	− .134	.7927	+ .4373	− .242
.7707	+ .0438	− .188	.7968	+ .4414	− .235
.7736	+ .0467	− .184	.8002	+ .4448	− .216
.7772	+ .0503	− .175	.8130	+ .4576	− .180
.7804	+ .0535	− .165	.8164	+ .4610	− .219
.8132	+ .0863	− .164	.8199	+ .4645	− .204
.8166	+ .0897	− .168	.8234	+ .4680	− .198
.8197	+ .0928	− .139	.8272	+ .4718	− .188
.8228	+ .0959	− .150	.8306	+ .4752	− .212
.8261	+ .0992	− .132	.8348	+ .4794	− .194
.8297	+ .1028	− .155	.8384	+ .4830	− .227
.8328	+ .1059	− .132	.8420	+ .4866	− .222
.8371	+ .1102	− .183	2615.6589*	− .0251	+ .275
.8403	+ .1134	− .181	.6635	− .0205	+ .215
.8504	+ .1235	− .143	.6673	− .0167	+ .168
.8540	+ .1271	− .170	.6712	− .0128	+ .086
.8571	+ .1302	− .130	.6756	− .0084	+ .010
.8609	+ .1340	− .140	.6801	− .0039	− .066
.8634	+ .1365	− .148	.6848	+ .0008	− .122
.8676	+ .1407	− .092	.6887	+ .0047	− .139
.8707	+ .1438	− .131	.6927	+ .0087	− .089
2607.7420	+ .2008	− .158	.6982	+ .0142	+ .049
.7454	+ .2042	− .175	.7030	+ .0190	+ .126
.7489	+ .2077	− .181	.7256	+ .0416	+ .411
.7524	+ .2112	− .165	.7299	+ .0459	+ .426
.7559	+ .2147	− .162	.7345	+ .0505	+ .414
.7579	+0.2167	−0.148	.7388	+0.0548	+0.414

* Observations on this night were at λ 8100.

TABLE 3—*Continued*

Helio. JD 2430000+	Helio. Phase	Δ Mag.	Helio. JD 2430000+	Helio. Phase	Δ Mag.
2615.7433	+0^{d}0593	+0^{m}426	2654.6643	+0^{d}7090	−0^{m}205
.7476	+ .0636	+ .428	.6681	+ .7128	− .206
.7528	+ .0688	+ .418	.6718	+ .7165	− .215
.7578	+ .0738	+ .422	.6749	+ .7196	− .226
.7631	+ .0791	+ .426	.6787	+ .7234	− .246
.7670	+ .0830	+ .432	.6827	+ .7274	− .236
.7736	+ .0896	+ .404	.6865	+ .7312	− .243
.7777	+ .0937	+ .450	.6907	+ .7354	− .204
.8303	+ .1463	+ .420	.6942	+ .7389	− .234
.8346	+ .1506	+ .442	.6983	+ .7430	− .216
.8389	+ .1549	+ .390	.7019	+ .7466	− .230
.8429	+ .1589	+ .423	.7056	+ .7503	− .250
.8477	+ .1637	+ .431	.7193	+ .7540	− .252
.8535	+ .1695	+ .427	.7227	+ .7574	− .213
.8577	+ .1737	+ .402	.7267	+ .7614	− .224
.8629	+ .1789	+ .404	.7303	+ .7650	− .235
.8683	+ .1843	+ .415	.7343	+ .7690	− .237
2621.7140	+ .3300	− .196	.7383	+ .7730	− .267
.7189	+ .3349	− .208	.7417	+ .7764	− .274
.7229	+ .3389	− .212	.7450	+ .7797	− .313
.7267	+ .3427	− .204	2659.6718	+ .0166	− .538
.7309	+ .3469	− .210	.6759	+ .0207	− .458
.7356	+ .3516	− .188	.6803	+ .0251	− .397
.7391	+ .3551	− .200	.6840	+ .0288	− .288
.7432	+ .3592	− .206	.6880	+ .0328	− .272
.7463	+ .3623	− .216	.6914	+ .0362	− .208
.7494	+ .3654	− .191	.6951	+ .0399	− .211
.7525	+ .3685	− .215	.6990	+ .0438	− .186
.7557	+ .3717	− .226	.7029	+ .0477	− .162
.7599	+ .3759	− .254	.7071	+ .0519	− .166
.7622	+ .3782	− .257	.7103	+ .0551	− .198
.7783	+ .3943	− .549	.7139	+ .0587	− .183
.7824	+ .3984	− .592	.7178	+ .0626	− .183
.7858	+ .4018	− .695	3037.6715	+ .175	− .272
.7888	+ .4048	− .720	.6777	+ .181	− .285
.7918	+ .4078	− .733	.6819	+ .185	− .271
.7947	+ .4107	− .734	.6854	+ .188	− .276
.7978	+ .4138	− .727	.6896	+ .193	− .278
.8011	+ .4171	− .674	.6944	+ .197	− .284
.8042	+ .4202	− .592	.6979	+ .201	− .278
.8073	+ .4233	− .563	.7000	+ .205	− .274
.8104	+ .4264	− .504	.7076	+ .211	− .286
.8138	+ .4298	− .431	.7111	+ .214	− .279
.8175	+ .4335	− .400	3039.6569	+ .531	− .347
.8210	+ .4370	− .318	.6611	+ .535	− .340
.8259	+ .4419	− .278	.6694	+ .543	− .336
.8293	+ .4453	− .219	.6729	+ .547	− .333
.8329	+ .4489	− .200	.6764	+ .550	− .330
.8363	+ .4523	− .202	.6805	+ .554	− .321
.8394	+0.4554	−0.212	.6840	+0.558	−0.327

TABLE 3—*Continued*

Helio. JD 2430000+	Helio. Phase	Δ Mag.	Helio. JD 2430000+	Helio. Phase	Δ Mag.
3039.6882	+0^{d}562	−0^{m}336	3040.7050	−0^{d}0496	−0^{m}289
.6927	+ .566	− .346	.7095	− .0451	− .302
.6951	+ .569	− .330	.7131	− .0415	− .347
.6990	+ .573	− .332	.7170	− .0376	− .385
3040.6616	− .0930	− .280	.7202	− .0344	− .440
.6673	− .0873	− .284	.7243	− .0303	− .512
.6709	− .0837	− .291	.7278	− .0268	− .584
.6741	− .0805	− .281	.7327	− .0219	− .670
.6774	− .0772	− .288	3049.6643	+ .581	− .301
.6808	− .0738	− .289	.6682	+ .585	− .318
.6842	− .0704	− .295	.6716	+ .589	− .312
.6880	− .0666	− .296	.6752	+ .592	− .311
.6910	− .0636	− .287	.6788	+ .596	− .313
.6945	− .0631	− .280	.6823	+ .599	− .328
.6980	− .0566	− .284	.6858	+0.603	−0.318
.7017	−0.0529	−0.316			

located than it was during the epoch of Binnendijk's observations (Binnendijk gives $t_2 - t_1 = 0^d4084$), and the primary minimum seems to occur later by about 0.0020 day than predicted by Binnendijk's formula for times of minima. The 1949 primary minimum, however, occurs a little earlier than the one in 1948. The difference cannot be a wave-length effect, for the March 4, 1948, infrared observations do not show the shift. It can only be concluded, therefore, that the small shift in the time of minimum between 1948 and 1949, if real, must have been the result of other, unknown causes that operated during the year separating the two sets of observations. The distortions in the minima, described later, undoubtedly produce on the phases of the minima an apparent effect that is not completely distinguishable from a genuine shift in phase. A careful examination of the phase shifts of each observed minimum makes it seem unlikely that the observed irregularities in the times of minima can be caused entirely by amplitude distortion. A definite decision on this point, however, can be made only with the aid of more photometric observations.

NORMAL POINTS

When the original observations were plotted as a function of phase, certain obvious distortions were found in the light-curve. To facilitate their study and to help remove them as much as possible before solving for the elements, the observations were grouped in sets of three, according to phase, to form normal points. These normal points are given in Table 4 for the 1948 observations in the visual, and in Table 5 for the 1949 observations in the infrared. In these tables the first two columns are derived directly from the original observational data and are self-explanatory. The third column contains the rectification quantities that were added to each value in the second column before forming the final rectified normal points. The first two columns of Tables 4 and 5 yield the plots shown in Figures 2, *A*, and 1, *A*, respectively. (The 1948 observations in the infrared and the 1949 observations in the visual have not been tabulated as normal points.) The normals during minima were next subjected to a rectification process described below for removal of the distortion. The rectified normals were then reflected about the centers of the minima. Primary and secondary minima in each color were brought together by superposition, and the observations were re-formed into combined normal

TABLE 4

NORMAL POINTS, 1948 VISUAL OBSERVATIONS

Phase (Days)	Obs. Δ Mag.	Rectification	Phase (Days)	Obs. Δ Mag.	Rectification
0.7517	−0m256	+0m71	0.2186	−0m157	
.7571	− .244	+ .71	.2247	− .165	
.7607	− .240	+ .71	.2310	− .170	
.7644	− .231	+ .71	.2407	− .179	
.7684	− .233	+ .71	.2821	− .178	
.7724	− .245	+ .71	.2932	− .177	
.7756	− .246	+ .71	.3148	− .183	
.7789	− .259	+ .71	.3331	− .195	
.7824	− .248	+ .71	.3392	− .197	
.7880	− .292	+ .71	.3446	− .195	
.7932	− .375	+ .71	.3538	− .197	
.7986	− .478	+ .71	.3600	− .213	0m00
.8032	− .561	+ .71	.3650	− .210	.00
.8066	− .625	+ .71	.3705	− .217	.00
.8097	− .680	+ .71	.3779	− .259	.00
.8127	− .748	+ .71	.3883	− .430	.00
.0028	− .722	.00	.3962	− .556	.00
.0091	− .694	.00	.4015	− .676	.00
.0136	− .580	.00	.4070	− .739	.00
.0175	− .522	.00	.4126	− .723	.00
.0214	− .407	.00	.4181	− .650	.00
.0266	− .334	.00	.4237	− .548	.00
.0314	− .252	.00	.4288	− .440	.00
.0364	− .193	.00	.4348	− .356	.00
.0407	− .172	.00	.4402	− .252	.00
.0440	− .175	.00	.4463	− .212	.00
.0473	− .177	0.00	.4551	− .198	0.00
.0513	− .167		.4645	− .207	
.0545	− .167		.4755	− .198	
.0590	− .162		.4848*	− .224	
.0638	− .165		.6088	− .259	
.0896	− .157		.6204	− .248	
.0993	− .146		.6346	− .241	
.1098	− .165		.6490	− .214	
.1269	− .148		.6564	− .227	
.1371	− .127		.6658	− .200	
.1482	− .150		.6862	− .207	
.1587	− .166		.7163	− .216	
.1685	− .166		.7273	− .242	
.1782	− .162		.7348	− .213	
.1962	− .169		.7406	− .233	
0.2112	−0.169		0.7461	−0.237	

* Two observations only.

TABLE 5

NORMAL POINTS, 1949 INFRARED OBSERVATIONS

Phase (Days)	Obs. Δ Mag.	Rectification	Phase (Days)	Obs. Δ Mag.	Rectification
0.7514	−0^m.294	+0^m.010	0.2673	−0^m.258	
.7568	− .283	+ .009	.2762	− .267	
.7648	− .279	+ .009	.2845	− .262	
.7733	− .321	+ .008	.2965	− .263	
.7790	− .389	+ .006	.3091	− .262	−0^m.022
.7833	− .433	+ .006	.3250	− .265	− .019
.7870	− .499	+ .006	.3375	− .270	− .016
.7909	− .583	+ .005	.3490	− .272	− .012
.7946	− .656	+ .005	.3605	− .289	− .007
.7983	− .700	+ .004	.3722	− .397	− .005
.8025	− .778	+ .004	.3814	− .544	− .004
.8065	− .806	+ .003	.3900	− .711	− .003
.8103	− .789	+ .002	.3969	− .794	− .002
.0000	− .718	.000	.4039	− .771	− .001
.0046	− .630	.000	.4113	− .635	.000
.0088	− .545	− .001	.4159	− .542	.000
.0132	− .451	− .002	.4210	− .463	.000
.0191	− .388	− .003	.4252	− .386	+ .001
.0259	− .312	− .004	.4294	− .341	+ .001
.0328	− .265	− .006	.4337	− .299	+ .001
.0384	− .254	− .008	.4381	− .302	+ .002
.0432	− .271	− .010	.4431	− .287	+0.002
.0471	− .259	− .010	.4460	− .294	
.0518	− .251	−0.012	.4495	− .295	
.0559	− .265		.4535	− .280	
.0603	− .263		.4572	− .297	
.0655	− .253		.4613	− .287	
.0719	− .256		.4670	− .280	
.0777	− .258		.4759	− .291	
.0829	− .242		.4883	− .281	
.0892	− .257		.5003	− .287	
.1002	− .267		.5134	− .289	
.1063	− .253		.5207	− .295	
.1130	− .248		.5281	− .310	
.1217	− .253		.5392	− .299	
.1328	− .261		.5468	− .284	
.1412	− .244		.5540	− .313	
.1477	− .258		.5617	− .295	
.1529	− .247		.5692	− .292	
.1595	− .251		.5760	− .304	
.1656	− .254		.5874	− .293	
.1720	− .252		.5988	− .278	
.1785	− .249		.6067	− .286	
.1887	− .244		.6128	− .285	
.2000	− .241		.6186	− .296	
.2120	− .244		.6231	− .291	
.2237	− .247		.6278	− .288	
.2357	− .246		.6321	− .292	
.2463	− .250		.6362	− .298	
0.2567	−0.248		0.6406	−0.298	

TABLE 5—*Continued*

Phase (Days)	Obs. Δ Mag.	Rectification	Phase (Days)	Obs. Δ Mag.	Rectification
0.6456	−0^{m}289		0.6999	−0^{m}284	
.6514	− .296		.7045	− .294	
.6584	− .294		.7096	− .281	
.6639	− .289		.7139	− .285	
.6689	− .284		.7207	− .276	
.6740	− .289		.7267	− .278	
.6779	− .288		.7316	− .288	
.6824	− .286		.7364	− .291	
.6876	− .298		.7412	− .281	
.6919	− .286		0.7473	−0.278	
0.6958	−0.284				

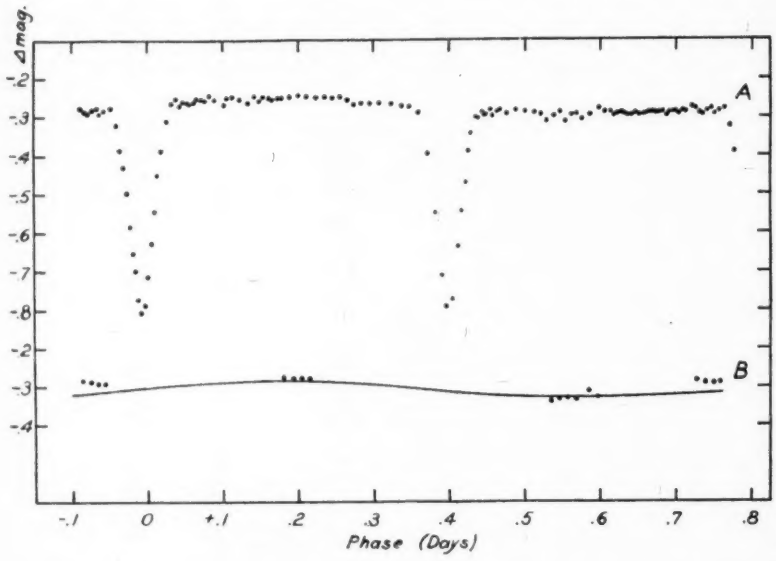

FIG. 1.—Upper diagram (*A*), plot of the subnormal points of 1949 obtained in the infrared spectral region. Lower diagram (*B*), the solid line represents a smoothed transcription of the distortion component of diagram *A*. The plotted points are averages of three observations made in the visual spectral region, approximately contemporaneously with the observations in the infrared.

points of three normals each. Observational weight is divided very nearly equally between the two minima; justification for their combination is given below. The combined normal points are given in Table 6, along with the residuals from the orbital solutions. In Table 6 the phases are given as a function of the mean anomaly, sin θ, and the magnitude differences have been converted into light-units.

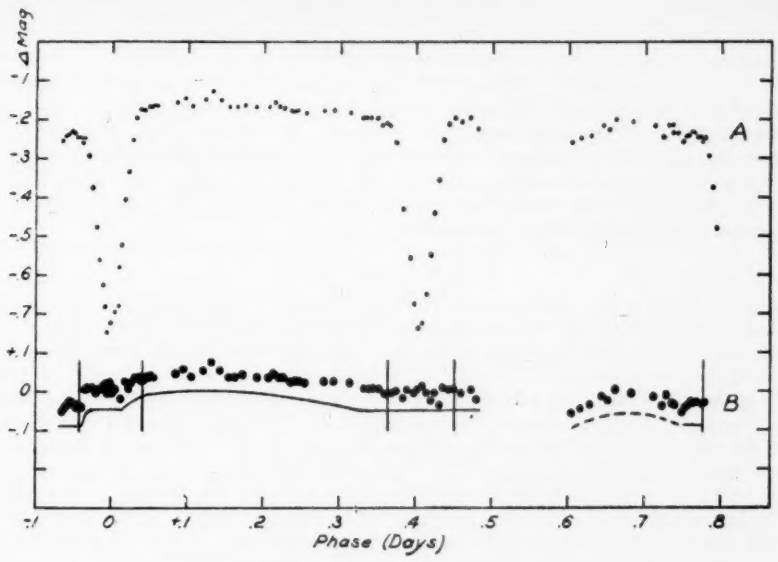

FIG. 2.—Upper diagram (*A*), plot of the normal points of 1948 obtained in the visual spectral region. Lower diagram (*B*), the plotted points represent the distortion components of curve *A* separated from the eclipse component by a process described in the text. In diagram *B* the radius of the points is equal to their probable error. The solid line is a smoothed transcription of the plotted points, displaced in the vertical co-ordinate to reduce confusion. The dashed line represents a portion of the curve that is uncertain, because the departure from a horizontal straight line depends upon only three points just following phase 0^d6.

TABLE 6

COMBINED NORMAL POINTS AND RESIDUALS

Visual				Infrared			
No.	sin θ	l	$(O-C)_l$	No.	sin θ	l	$(O-C)_l$
1	0.368	0.998		1	0.3354	1.005	
2	.342	.997		2	.2999	0.991	−0.008
3	.319	.992		3	.2609	0.970	− .003
4	.291	.986	−0.008	4	.2167	0.922	+ .002
5	.267	.987	+ .010	5	.1934	0.888	+ .002
6	.235	.952	+ .009	6	.1626	0.837	+ .001
7	.199	.891	− .901	7	.1316	0.784	+ .001
8	.162	.824	− .0	8	.1060	0.733	− .006
9	.121	.756	.000	9	.0712	0.686	+ .004
10	.098	.715	+ .001	10	.0460	0.641	− .007
11	.069	.671	+ .005	11	.0131	0.623	+0.003
12	.047	.630	− .005		0.0000	0.617*	
13	.017	.610	+0.002				
	0.000	0.604*					

* Computed.

ROTATIONAL DISTORTION

Although the period of rotation of YY Geminorum is short, the small size of the components and their high densities prevent significant effects on the shape of the light-curve from the perturbations caused by rotational distortion of the components. To within the degree of precision of this investigation, observed distortions of the light-curve will therefore not be attributed to the effects of rotational perturbations. Because the two components are nearly identical in all their physical properties, differential rotational-distortion effects are vanishingly small.

RECTIFICATION

The rectification process used here is entirely empirical, since there is no basis for employing standard methods. The process started with the light-curve in the infrared (Fig. 1), because the distortions present in 1949 not only were fewer than in 1948 but were of a smoothly varying character and because the observations were more accurate. It is evident in the figure that both minima must have an asymmetrical component, because, in both, the light after egress is at a different level from that before ingress. In the rectification the assumption was made that the secondary variation was linear during minima; an estimate of its slope was made, and appropriate quantities as tabulated in Table 5 were added to or subtracted from the three-point normals. The elements were derived from the normal points of these observations. The computed curve thus provided was of nearly the shape to be expected for the undistorted light-curve in the visual region, and this computed curve was therefore compared with the 1948 normal points. The comparison indicated a lack of distortion in the secondary minimum and the presence of a strong peculiar distortion in the primary minimum. In order not to transfer the shape of the computed curve in the infrared to the observed curve in the visual, it was decided to make only the most rudimentary rectification of the latter. This procedure took the form of adding a constant amount of light to all the observations during minimum preceding the normal point at phase $+0^{d}0028$ (see Table 4). The elements in the visual were now determined, and a comparison between the computed curve and the observed normals in the visual made possible an empirical separation of the light-variations caused by the eclipse of one sphere by the other from those due to other causes. The normal points in the visual are plotted in Figure 2, *A*, while the secondary variations separated according to the process just described are shown in Figure 2, *B*.

DEPTHS OF MINIMA

The depths of the minima are, of course, affected by the distortions, and therefore the precision of measurement is not so high as it otherwise would be. Binnendijk found that the primary minimum exceeds the secondary in depth by an appreciable amount, and his treatment of Van Gent's data supports this conclusion. Both the light-curves from the present study give results in qualitative agreement with Binnendijk's conclusions regarding the relative depths of the two minima. Data regarding depths of minima are collected in Table 7, where the values of depths from the present study were measured from smooth curves drawn through the rectified normals. The depths of the computed light-curves are slightly different.

An apparently curious result is that the minima are *both* deeper at the shorter wave length. The secondary minimum is shallower than the primary by less than 2 per cent in the light in 1948–1949, which indicates a difference in surface brightness between the two components of less than 2 per cent. If one accepts the existence of a strict relationship between surface brightness and radius for main-sequence stars, an extrapolation for the relative radii of the two components can be made. Such an estimate, based on the surface brightness and radius of the sun and of the mean component of YY Geminorum, indicates that the radii of the two components probably do not differ by more than 1 per cent.

The ratio of the radii, k, must then be of the order of 0.99. An examination of Irwin's[7] tabulated differential coefficients shows that, for $k > 0.98$, the derived elements of the system will not depend appreciably upon the value of k. We may therefore call the ratio of the radii unity and solve for the characteristics of the mean component by employing the primary and secondary minima combined into a single reflected series of normal points, as described earlier. This process eliminates one unknown from the solution for the elements, and it contributes to simplicity and determinateness in the solution. Nothing about either the photometric or spectrographic observations of YY Geminorum casts doubt upon the validity or the closeness of this approximation.

THE DISTORTIONS

In this discussion the word "distortions" will be used to designate light-variations from causes other than simple eclipse of one stellar component by the other or from tidal distortion and reflection effects. The distortions discussed here may affect at any time any part of the light-curve of a rotating star. They certainly are present in the light-

TABLE 7

DEPTHS OF MINIMA

Authority	Spectral Region	Min. I	Min. II	Epoch
Van Gent*	Photographic	0^{m}56	0^{m}52	1926
Binnendijk	Visual	.59	.49	1929–1942
Kron	Visual	.55	.54	1948
Kron	Infrared	0.527	0.516	1949

* According to Binnendijk.

curves of at least four[8] eclipsing variables: AR Lacertae,[9] RT Andromedae,[10] RS Canum Venaticorum,[11, 12] and YY Geminorum. The distortions referred to here have been found to be transient features of a given light-curve. They may appear or disappear suddenly, as well as remain unchanged, except possibly in detail, for considerable lengths of time. The suddenness with which a noticeable change may take place makes the interpretation and gathering of significant data difficult and sometimes exceedingly exasperating.

As a star rotates, the observed light may vary. When the variation is caused only by the form or spottedness, however, the light-curve cannot contain large-amplitude high harmonics of the rotational period; only an eclipse process taking place during the rotation can result in the generation of such harmonics.[13] The distortions considered here are clearly caused by the rotation process, for they are periodic with the rotation. The light-

[7] *Ap. J.*, **106**, 380, 1947.

[8] Linnell's light-curve of UX Ursae Majoris (*Harvard Circ.*, No. 455, 1950) shows distortions. Owing to the very unusual physical nature of UX Ursae Majoris, however, it probably would be inconsistent to include a discussion of the properties of this star along with those of normal objects. Future work on UX Ursae Majoris may indicate that some of its physical properties may be compared with those of normal objects.

[9] G. E. Kron, *Pub. A.S.P.*, **59**, 261, 1947. Attention has been called to peculiarities in the light-curve of AR Lacertae by Himple (*A.N.*, **261**, 233, 1936) and by Wood (*Contr. Princeton U. Obs.*, No. 21, p. 10, 1941).

[10] Unpublished photoelectric data in two colors by Katherine C. Gordon.

[11] Sitterly, *Contr. Princeton U. Obs.*, No. 11, p. 21, 1930.

[12] Keller and Limber, *Ap. J.*, **113**, 637, 1951.

[13] H. N. Russell, *Ap. J.*, **24**, 1, 1906. I am indebted to Professor Russell for pointing this out to me during his tenure as Morrison Research Associate at the Lick Observatory in 1948.

variation outside eclipse, shown in Figure 1, *A*, does not contain high harmonics of appreciable amplitude, but its asymmetry shows that it is a distortion and not the product of tidal or reflection effects. In the light-curve shown in Figure 2, *A*, there is evidence of high harmonics of the rotation period in the region of primary minimum. Figure 2, *B*, represents the distortion components of the light-variation separated from the eclipse component by the method described earlier. The radii of the plotted points are equal to the probable errors of the points. The gap in the curve at phase 0^d5-0^d6, caused by the interference of persistent bad weather, is large enough to prevent a significant analysis of events taking place during almost one-sixth of the period. The harmonics appear at phase -0^d037 and $+0^d006$. That the difference in distortion between the light-curves of 1948 and 1949 is principally a time effect, and not entirely a wave-length effect, is shown by the plotted points of Figure 1, *B*. The solid curve is a smoothed transcription of the distortion components of the 1949 light-curve in the infrared; the plotted points are observations in the visual made nearly contemporaneously (see observing schedule, Table 1). The 1949 observations in the visual show the same kind of asymmetry as the infrared observations, but with slightly greater amplitude. An exception is the group of observations in the visual at phase 0^d75 just preceding primary minimum (Fig. 2, *A*). These observations indicate an almost total absence of the large distortion present at this phase in 1948; inasmuch as these observations were not exactly contemporaneous with the infrared ones, the lack of agreement with them could indicate that a change, which affected the light at this phase, had taken place in the star.

Figures 1 and 2 give reasonable observational evidence that the light-variation of YY Geminorum contains distortions that are temporary, that have a more or less random phase and amplitude, and that have more amplitude in λ 5200 light than in λ 8100 light. It is evident, furthermore, that a short-lived distortion of the light-curve indicates that, whatever the source of the maldistributed luminosity responsible for the distortion, it probably undergoes eclipse. In that case it may be concluded that the agent responsible for the distortion (Fig. 2, *B*) possibly is on the surface of the star eclipsed or is between the two stars. Material suspended between the two stars would be of very low density, and one would not expect it to emit enough luminous energy to affect broad-band photometry. On the basis of the material available here for study one is forced to conclude, therefore, that the distorting agent lies on the surface of the star. The case may be identical with that of AR Lacertae,[9] where peculiar, secondary light-variations were ascribed to the presence of nonuniform, or patchy, illumination of the eclipsed star.

One interpretation of the light-variations shown in Figure 2, *B*, may be as represented by Figure 3. The system is thought to be normal at phase -0^d12, but a dark patch is beginning to come around the approaching limb of the eclipsed star *A*, as shown in drawing *I* (orbital and stellar rotation periods are assumed to be equal). From phase -0^d12 to -0^d037 the light decreases slowly, a phenomenon that is explained by reduction of the foreshortening of the patch as it approaches the stellar meridian. At phase -0^d037, drawing *II*, the dark patch is covered by the eclipsing star *B*, with an apparent increase in brightness that is actually a reduction in the rate of light-decrease during the growth of the stellar-disk eclipse. Meanwhile, a bright patch follows the dark one around the limb by about 15° in astrocentric longitude, and at phase $+0^d006$, shortly after conjunction, the bright patch (previously not noted either because it was greatly foreshortened or because it was eclipsed) is uncovered, as shown in drawing *III*, with a gain in brightness at this phase. The light of the bright patch more than compensates for the loss due to the uncovering of the dark patch immediately thereafter. Drawing *IV*, phase 0^d15, shows the star at its brightest, with the bright patch fully displayed and the dark patch foreshortened. By phase 0^d32, drawing *V*, the bright patch is so foreshortened that it has negligible effect, the dark patch has disappeared around the limb, and a normal secondary minimum is about to occur. This interpretation is admittedly not unique, for it must be kept in mind that the observed light-curve is a composite of light-variations that took

place over a period of three months. Although small changes in the patch configurations during this time did not affect the variations between minima, nevertheless they could seriously affect the shape of the distortions during the eclipse process, where detail of patch configuration will be of importance. The noncontinuity of the data, therefore, makes difficult a unique and certain interpretation of the distortions in the present light-curve.

SPECTRAL CHARACTERISTICS

It may be significant that all four[14] of the eclipsing stars mentioned above as having distorted light-curves also have bright lines in their spectra. Spectra available at the Lick Observatory, taken by A. B. Wyse[15] in 1934, indicate that the bright lines of the subgiant AR Lacertae undergo variations in intensity that depend upon the orbital revolution.

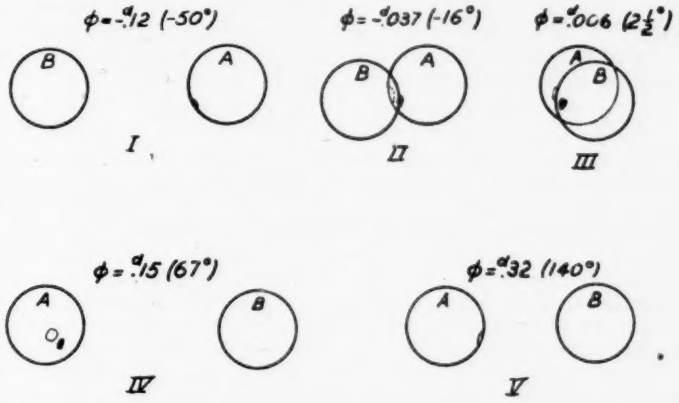

FIG. 3.—Diagram illustrating an interpretation of the distortions shown in Figure 2, *B* in terms of the eclipse of a light and of a dark area on the surface of the star eclipsed. Star *A* is eclipsed, the dark area or patch is shown by a solid patch, and the bright area is indicated by an open patch.

Two spectrograms of YY Geminorum, taken by Herbig on February 26, 1950, at the Lick Observatory (see Fig. 4), show that the brightness of the emission lines for this star may also vary with orbital rotation. In Figure 4 the H and K lines of each component are weaker at phase 0^d62 than at phase 0^d11. The results of Joy and Sanford compared with those of Struve, Herbig, and Horak indicate that there can be long-term changes in the emission-line intensity. Joy and Sanford found strong variability of the lines in 1926, whereas the recent work of Struve, Herbig, and Horak showed that the variability had vanished in 1949, at nearly the mean epoch of the 1949 photometric results, showing low distortion. The similarity in the behavior of the emission lines with the behavior of the photometric distortions lends weight to the conclusion that the two phenomena have a common origin.

The emission-line phenomena of stars that have photometric distortions belong to the second of two types recognized by Struve.[16] In this type the emitting material is so situated in the binary system that its velocity shares the orbital velocity of the components.

[14] RT Andromedae has shown faint H and K emission (Kron, *Pub. A.S.P.*, **62**, 141, 1950).

[15] *Lick Obs. Bull.*, **17**, 37, 1935 (No. 464).

[16] *Ann. d'ap.*, **9**, 1, 1946.

Struve[16] and Hiltner[17, 18] conclude that the emitting material in binaries of this type may be located at the ends of the tidal bulges of one of the two components. Recently, however, Sanford[19] published the results of a very thorough spectrographic study of AR Lacertae, based upon 10 A/mm coudé plates. Even with this high dispersion, Sanford found for each stellar component single emission lines that were broadened enough to suggest that the emitting material for this star probably was distributed, to some extent at least, in the equatorial region of the two components. In some stars, therefore, the emitting material need not necessarily be localized permanently in certain areas, though it still may possibly show a statistical preference for certain areas. Although Sanford's observations showed that the emitting material must have been present all around the components of AR Lacertae, such a result does not rule out a patchy distribution of the emitting material, so long as the patches are well distributed in astrocentric longitude. It is now clear that the interpretation of the YY Geminorum distortions in terms of the variations produced by the presence of one bright and one dark patch must be a great oversimplification. All we are able to observe are unusually large variations in the uniformity of distribution of the patchy material, which may, in many cases, be distributed over much of the surface of the star.

DERIVATION OF ELEMENTS

The derived elements of YY Geminorum are based upon the normal points given in Table 6. Preliminary elements were derived first for the light-curve in the infrared by the simplifying assumption that $k = 1$ for the ratio of the radii. Solutions were made for values of the limb darkening with $u = 0$ and 0.4; the latter value seemed to give slightly better residuals. A least-squares solution with corrections to the four unknowns: darkening coefficient u, mean relative radius r, inclination i, and relative light L, was attempted, but the solution diverged. A derivation of the weights of the unknowns showed that the correction to the darkening coefficient had very low weight. Correction of the remaining three elements was successful, but the solution yielded small corrections and no appreciable decrease in the residuals. These elements, along with their probable errors as computed from the three-unknown least-squares correction, are given in Table 8. The element of most immediate use is the mean radius. The size of this datum depends upon the assumed darkening coefficient, but not to an extent that seriously affects its precision, especially if the derived value is based upon a solution having a reasonable assumed value for the darkening coefficient. The probable error of the mean radius from the three-unknown least-squares solution is less than 1 per cent.

The deeper minima of the λ 5200 light-curve compared with the λ 8100 curve indicates that the component stars have a higher darkening coefficient in the shorter wave length, larger radii, or both. If both, then both will be indeterminate, owing to the indeterminateness of the darkening coefficient. The solution of the light-curve in the visual was therefore based upon the assumption that the radius of the mean component is independent of wave length, as this assumption is more plausible, in view of the present state of our knowledge, than the alternative one of variation with wave length. No attempt was made to derive a separate value for the inclination from the light-curve in the visual. In fitting the normal points in the visual, a series of representations was made for a sequence of darkening coefficients, until a good fit was obtained to the observational data, with a radius reasonably close to that derived from the data in the infrared. In effect, the solution yielded only a darkening coefficient, dependent in size upon the assumed darkening coefficient used in the orbital derivation of the infrared curve. The weight of the visual observations has thus been used effectively to derive a difference between the limb darkening in the infrared and the visual. This difference depends primarily upon the differ-

[17] *Pub. A.S.P.*, **58**, 166, 1946.

[18] *Ap. J.*, **106**, 481, 1947.

[19] *Ap. J.*, **113**, 299, 1951.

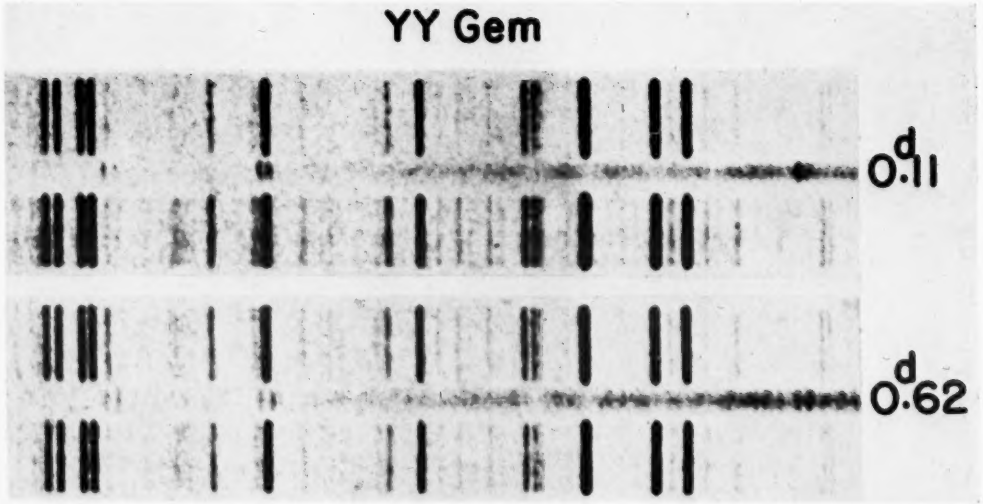

FIG. 4.—The spectrum of YY Geminorum. The two spectrograms were obtained on the same night, separated by a lapse of time equivalent approximately to a half-turn of the binary. Note the changes in the intensity of the emission lines, first pointed out by Joy and Sanford. Spectrograms obtained at the Lick Observatory by G. Herbig.

ence in the depths of equivalent minima in the two colors, and not appreciably upon a difference in the shapes of the minima, as one might expect. If the assumption that the radius of the mean component is independent of wave length is correct, then the probable error of the differential darkening coefficient, as estimated from the behavior of seven trial representations, is about ± 0.05.

The failure to derive a determinate darkening coefficient is caused partly by the inherent indeterminateness of the derivation of elements from partial eclipses and partly by the effects of observations of insufficient accuracy. In view of the increase in determinateness caused by a knowledge of the ratio of the radii, the indeterminateness in the darkening coefficient was not obvious previous to the least-squares correction in four

TABLE 8

ELEMENTS OF THE SYSTEM OF YY GEMINORUM

Element	Infrared Curve	Visual Curve	Van Gent (Photographic)
$\cos^2 i$	0.0040 ± 0.0009	0.0040*	0.0042
r	0.156 ± 0.0010	0.159	0.162
L	0.500 ± 0.016	0.500*	.....
α_0	0.767	0.792	.....
u	0.4*	$u_{IR}+0.3$	.....
p.e. of one normal	$\pm 0^m.0032$	$\pm 0^m.0047$	.....

* Assumed.

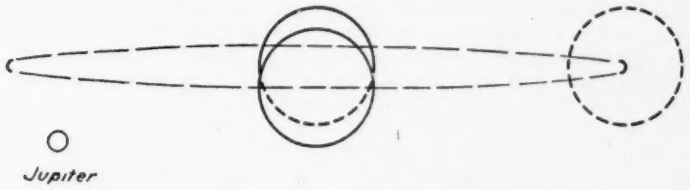

FIG. 5.—Diagram of the system of YY Geminorum

unknowns. The least-squares solution therefore accomplished a useful purpose in making this limitation evident and in yielding probable errors for the remaining elements, even though the improvement in the elements was trivial. It probably will be possible to obtain photoelectric observations of YY Geminorum of sufficient precision to permit a determinate solution for the darkening coefficient, especially if the observer has the good fortune to gather most of his data during a time when the distortions are small. This opinion is supported by the success of Huffer and Eggen[20] in deriving a darkening coefficient for AR Aurigae, a star that has a geometry almost identical with that of YY Geminorum.

A diagram of the system of YY Geminorum is given in Figure 5.

ABSOLUTE ELEMENTS

Joy and Sanford's velocity-curve for YY Geminorum indicates an appreciable difference in mass between the two components; that by Struve, Herbig, and Horak indicates that both components are of the same mass. The latter authors suggest that a genuine

[20] *Ap. J.*, **106**, 106, 1947.

change may have taken place in the star during the twenty-five years between the two sets of observations. This conclusion is supported by the photometric evidence, which indicates (Table 7) that the difference in depth between the two minima was greater years ago than it is now. One would expect, however, that the rotational period would be the best indicator of a change in mass or in distribution of mass. Inasmuch as there is no evidence for even a small change in period, the supposition that a real change took place in the relative masses of the two components is greatly weakened. A simple average of the four available values for the spectrographic semi-amplitude, K, seems, therefore, the most reasonable value to adopt here:

Joy and Sanford: $K_1 = 114.0$ km/sec,
$K_2 = 126.7$.

Struve, Herbig, and Horak: $K_1 = 125.0$,
$K_2 = 125.0$,
Mean $K = 123 \pm 2.9$ (p.e.).

Therefore: $a = (1.38 \pm 0.03) \times 10^6$ km,
$\mathfrak{M} = (0.64 \pm 0.04)\ \odot$,

where a is the radius of the relative orbit and $\mathfrak{M}$ is the mass of the mean component.

The apparent magnitude of YY Geminorum was measured during an extensive photoelectric program of determining red and infrared magnitudes for red-dwarf stars. The values, resulting from measurements on three nights, are $R = 8^m.08 \pm 0^m.02$ and $I = 7^m.31 \pm 0^m.02$, where the symbols R and I have been defined by Kron and Smith.[21] From an unpublished conversion-curve, known to be valid for main-sequence stars, these magnitudes can be converted into derived photographic and photovisual magnitudes on a system very close to International. The values are $P = 10^m.37 \pm 0^m.03$ and $V = 0^m.07 \pm 0^m.03$. The probable errors are estimates formed by arbitrarily increasing the R and I average deviations by 0.01 mag. The visual magnitude of the mean component is thus $V = 9^m.82 \pm 0^m.03$. The parallax is very accurately known, partly because the other members of the α Geminorum system have been measured, as well as YY Geminorum itself. The Yale *Catalogue*[22] gives the parallax as $0''.073 \pm 0''.003$, and a recent Allegheny determination[23] of unusually high precision is $0''.073 \pm 0''.002$, after reduction to the Yale system. The mean, then, is

$$\pi = 0''.073 \pm 0''.0018, \quad \text{and} \quad (M - m) = -0^m.68 \pm 0^m.05.$$

The absolute visual magnitude of the mean component of YY Geminorum, for negligible space absorption, therefore, is

$$M_v = +9^m.14 \pm 0^m.06.$$

One remaining simple computation yields the radius of the mean component, $r = (4.31 \pm 0.13) \times 10^5$ km $= (0.62 \pm 0.02)\ \odot$. The absolute dimensions are collected in Table 9.

The agreement of all elements with those derived by van Gent is very good. On the red-infrared magnitude system, YY Geminorum is redder than 61 Cygni B (dK5) and BD+33°2777 (dK6), the same color as BD+66°717 (dM1), but bluer than BD+15°4733 (dM2) and BD+61°195 (dM1+). The color therefore corresponds to that of a star of about dM0.

[21] *Ap. J.*, **113**, 324, 1951.

[22] *General Catalogue of Stellar Parallaxes* (New Haven: Yale University Press, 1935).

[23] *A.J.*, **53**, 137, 1948.

FUTURE WORK

The system of YY Geminorum could profitably be studied photometrically and spectrographically at the same time, for further investigation of the origin of the bright lines and of the light-curve distortions. Quantitative spectrophotometry of the bright lines would furnish information of great value. The general study of the physical nature of the late-type dwarf stars may be advanced by attention to the many new spectroscopic binary stars of this type announced by Joy.[24] A selected group of these stars, followed spectrographically, would yield rotation periods and velocity-curves. Photometric work would then contribute further to the study of distortions, as previously suggested,[25] and may even result in the discovery of another eclipsing binary.

TABLE 9

ABSOLUTE DIMENSIONS OF THE MEAN COMPONENT OF YY GEMINORUM

Element		Kron	Van Gent
Radius	r (km)	$(4.31 \pm 0.13) \times 10^5$	$(4.32) \times 10^5$
	r ($\odot$)	0.62 ± 0.02	.....
Mass, $\mathfrak{M}$ ($\odot$)		0.64 ± 0.04	0.593
Luminosity ($\odot$)*		0.0017 ± 0.0001	.....
Density ($\odot$)		2.7	2.468

* Absolute visual magnitude of sun = +4.73.

CONCLUSIONS

The eclipsing variable YY Geminorum has secondary fluctuations in light that are periodic with the rotation, but temporary in their duration. These secondary variations can be explained on the hypothesis that the surfaces of the components are nonuniformly illuminated in a patchy fashion. The origin of the emission lines found in the spectrum may be related to the presence of the patches. The coefficient of limb darkening cannot be derived from photometric observations unless they are of greater precision than the present series. However, it was found that the infrared coefficient of limb darkening was less than the visual by 0.3, which indicates a strong wave-length dependence for a dwarf M star.

It is a pleasure to acknowledge the help of Katherine C. Gordon and J. Lynn Smith in making the observations. Valuable help and advice were given by A. Pannekoek, H. N. Russell, L. Binnendijk, and O. J. Eggen before or during the course of the work. I am much indebted to G. H. Herbig for obtaining spectrograms and for general discussion, and to Joel Stebbins for discussion and reading of the manuscript.

[24] *Ap. J.*, **105**, 96, 1947.

[25] G. E. Kron, *Ap. J.*, **103**, 376, 1946.

A SOLAR FLARE AND ASSOCIATED DARK FLOCCULI OF MAY 19, 1951*

HELEN W. DODSON
McMath-Hulbert Observatory, University of Michigan
Received October 2, 1951

ABSTRACT

The dark absorbing material that accompanied the flare of May 19, 1951, 19^h57^m, extended at least 125,000 km from the apparent region of ejection and displayed radial velocities that ranged from −182 to +225 km/sec. The motions indicated are consistent with the interpretation of the dark flocculus as a giant surge seen in projection on the disk. This absorbing material modified the form and intensity of the associated flare.

The large spot group that crossed the central meridian of the sun on May 15–16, 1951, was a center of extensive flare activity. A number of the flares in this region were accompanied by unusually large and active dark hydrogen flocculi. *Hα* spectroheliograms taken at 30-second intervals during the flare of May 19, 1951, 19^h57^m, illustrate the magnitude of the absorption phenomena that occurred concurrently with the brightening of the flare. Furthermore, the spectroheliograms indicate that the actual form and intensity of the flare were greatly modified by the presence of the overlying absorption.

The spectroheliograms here shown were taken with the tower telescope and spectroheliograph of the McMath-Hulbert Observatory. A selective slit transmitting 0.4 A was used throughout the entire study. For the principal record of the flare, *Hα* was centered in this slit; but during two intervals in the course of the flare the portion of the spectrum transmitted through the slit was displaced by known amounts to either side of *Hα*. By this procedure it was possible to record the extent of the absorbing material and to determine the magnitude of the radial velocities represented.

The development of the flare is shown in line *a* of Figure 1 and in Figure 2. The brightening began close to and over the small spot that was relatively far to the south of the principal members of the spot group. The flare extended northward to the edge of the penumbra of the large spot and overlapped it in only one small section. This section, however, included one of the small umbrae within the complex penumbra. When the absorbing material or dark flocculus developed, part of the well-defined flare region was darkened by this overlying absorption. This effect is clearly shown in the last picture of line *a*, Figure 1.

The position and extent of the active dark flocculi are shown in lines *b* and *c* of Figure 1 and in Figure 2. At 20^h08^m, absorbing material extended as far as 125,000 km from the apparent region of ejection (marked *E* in Fig. 2). At this time the radial velocities of the absorbing material were principally negative. Portions of the dark flocculus appeared in negative wave-length displacements as great as −4A, corresponding to a radial velocity of −182 km/sec. The densest absorption appeared when $\Delta\lambda = -2$A, or for a radial velocity of −90 km/sec. Positive velocities were present, but in only two small regions were they as large as 140 km/sec. Eleven minutes later, long streamers for which the radial velocity was of the order of −180 km/sec were still present, but at this later time the principal absorption appeared on the long-wave-length side of *Hα*. Radial velocities were as great as +225 km/sec. The densest absorption occurred at $\Delta\lambda = +2.0$ A, in essentially the same place in which the densest ascending gases had appeared, 11 minutes earlier. This is consistent with the interpretation of the active dark flocculus as a giant surge-type prominence seen in projection on the disk.

* Work supported in part by Contract N6-onr-232-V with the Office of Naval Research.

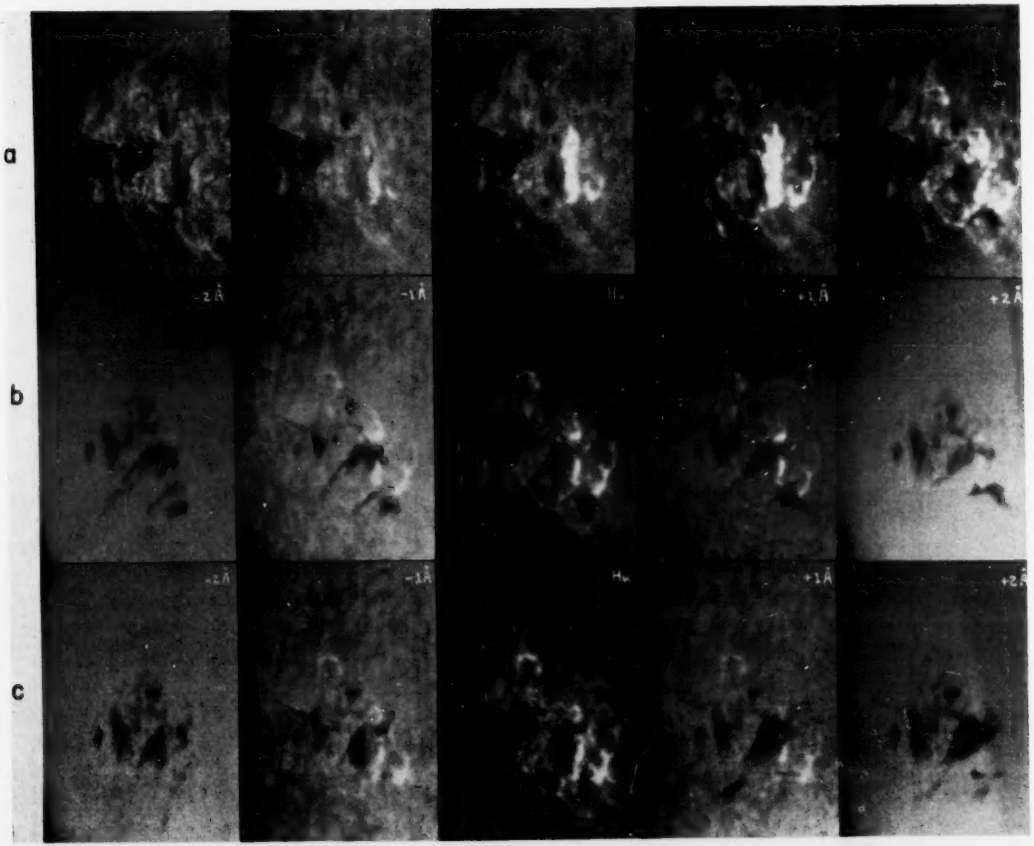

FIG. 1.—Spectroheliograms, showing development of flare and associated active dark flocculi, May 19, 1951. Line *a*, *Hα* spectroheliograms—1337, 1952, 1956, 1957, 2006 U.T. Line *b*, spectroheliograms in neighborhood of *Hα*, 2008 U.T. Line *c*, spectroheliograms in neighborhood of *Hα*, 2019 U.T.

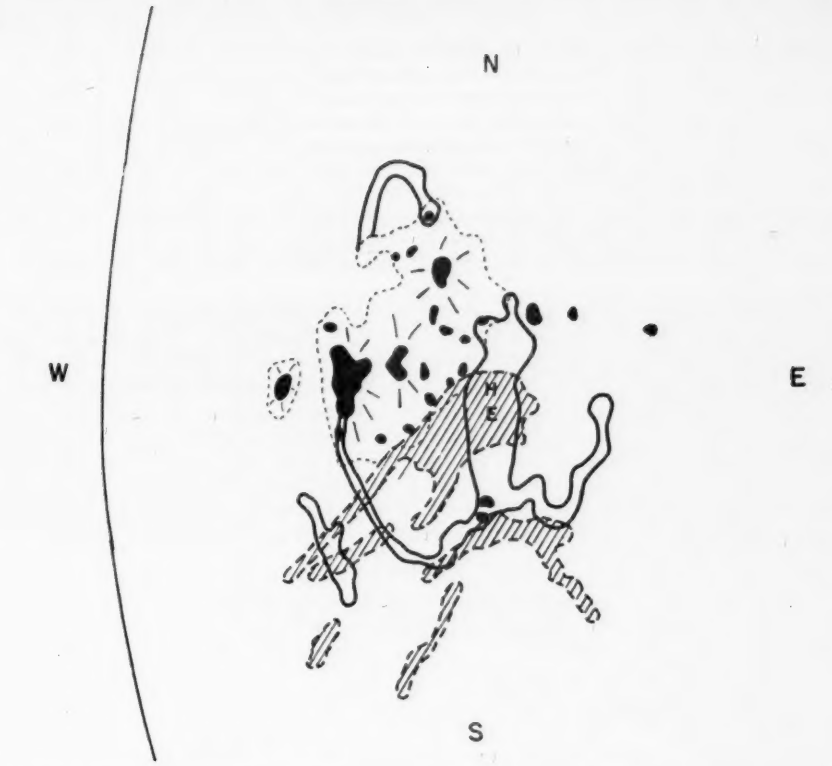

FIG. 2.—Composite diagram, showing spot group, flare (*full outline*), active dark flocculus (*shaded*), May 19, 1951.

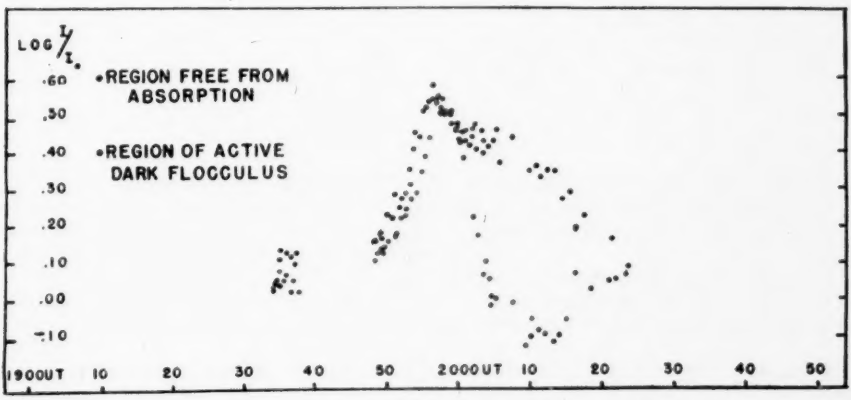

FIG. 3.—Light-curve for two parts of flare, May 19, 1951. Sudden ionospheric disturbance, 1950, 2110 U.T.

Light-curves have been derived for different portions of the flare. At maximum the intensity of the flare was 3.5 times that of the undisturbed *Hα* disk. For the part of the flare free from overlying absorption the decline from maximum was gradual and steady; where the absorption was densest, the decline from maximum was more sudden. The portion of the flare covered by absorbing material not only faded rapidly from flare intensity but, for a short time, became darker than the undisturbed *Hα* disk (see Fig. 3 for 20^h10^m).

It was during the course of this flare of May 19, 1951, that the equivalent width of the infrared helium absorption line λ 10830 was found by Mohler[1] to be extraordinarily great. When the slit of the infrared spectrograph was placed directly over the densest part of the active dark flocculus (position *H* in Fig. 2), intense helium absorption was recorded.

The writer wishes to express her appreciation to all members of the Observatory staff for their co-operation and especially to Mr. Willard Olson and Mr. Clifford Bennett for their part in securing and presenting the above observations. The continued support of the work of the Observatory by McGregor Fund of Detroit is gratefully acknowledged.

[1] *Ap. J.*, 115, 323, 1952.

NOTES

SOME RECENT OBSERVATIONS OF HELIUM LINES IN THE INFRARED SOLAR SPECTRUM*

The lines of helium appear in spectra of solar features in unusual and variable guises. Sometimes they appear in emission, but most often helium reveals its presence by faint absorption lines. Van Dijke[1] has summarized selected portions of the literature on the behavior of helium in the solar atmosphere. With the development of new techniques, additional information is now available and is presented in part in this note. The results that follow have been obtained with the infrared spectrometer of the McMath-Hulbert Observatory by tracing a short section of the solar spectrum centered on the helium lines λλ 10830.34, 10830.25, and 10829.08, $2^3S_1 - 2^3P^0_{2,1,0}$. The lines λ 10830.34 and λ 10830.25 are unresolved on the tracings. The line λ 10829.08 appears at times as a faint line, blended with the stronger combined line at λ 10830. The sum of the equivalent widths of the three components has been measured in a number of solar features. Table 1 lists

TABLE 1

COMBINED EQUIVALENT WIDTHS OF HELIUM
λλ 10830.34, 10830.25, AND 10829.08

	Average	Extreme Values	No. of Measures
Undisturbed disk:			
Center	45 mA*	20– 83 mA	30
Limb:			
North pole	61	32– 90	17
East equator	138	34–195	11
South pole	63	20–100	24
West equator	135	39–312	13
Plages	306	236–417	10
Filaments	113	69–202	5
Flares	260	0–400	4

* "mA" = milliangstroms.

some of the results recently obtained. All measures were made with a circular hole forming the entrance slit of the spectrometer. The area of the sun's surface transmitted by the aperture was 35 millionths of the visible hemisphere (radius of hole = 8 seconds of arc). Some comments on the entries in Table 1 follow.

Center of the undisturbed disk.—Faculae were carefully avoided in making the measures near the center of the disk. It is evident that even in the regions of the sun where there is no conspicuous facula, or plage, there are large variations in the equivalent width of λ 10830.

Undisturbed disk—north and south polar regions.—The most noteworthy feature of the

* Work supported in part by Contract N6-onr-232V with the Office of Naval Research.

[1] *Ap. J.*, 99, 121, 1944.

measures in the polar regions of the sun is the low value of the equivalent width. The first measures in the polar regions were not made at specific distances from the apparent edge of the disk, but, once the abnormally low value of the equivalent width was discovered, all subsequent limb measures, either at the poles or in the equatorial areas, were made 25 seconds of arc from the edge toward the center of the sun.

Undisturbed disk—east and west equatorial regions.—The change in equivalent width of λ 10830 from center to edge of the sun in the equatorial regions is conspicuous and larger than the change from center to edge in the direction of the poles. Figure 1 compares two tracings 25 seconds from the edge of the sun, one near the poles, the other in the equatorial areas.

Plages.—Large equivalent widths are always found in these regions. This result agrees with the fact that the plage areas appear dark on spectroheliograms taken at λ 10830 by the d'Azambujas.[2] Near the center of the sun a plage of average brightness in *Ca* II, λ 3933.7, produces lines of λ 10830 with at least five or six times the equivalent width of the same line in the undisturbed disk.

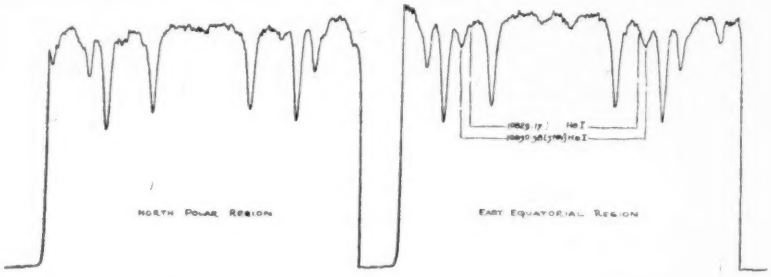

FIG. 1.—Tracing of λ 10830 in the polar and equatorial regions of the sun. The direction of tracing has been reversed midway in each record.

Filaments.—The equivalent width of λ 10830 in the filaments is of the same order as the equivalent width in plages. The widths listed in Table 1 refer to quiescent filaments; those moving with unusually high velocities have much larger equivalent widths.

Flares.—Four flares, or flare regions, are represented in Table 1. In two of these the observations were made very late in the course of the disturbance, when the area had nearly returned to normal. The other two observations were made just before the optical flare began. In general, before the onset of a flare, the equivalent width of λ 10830 is about the same or larger than the equivalent width of an ordinary plage. Immediately, at the start of a flare, the equivalent width drops to an abnormally low value, and it is possible that the line changes from absorption to emission.[3] After the flare subsides, λ 10830 regains the large equivalent width characteristic of a plage area.

One of the flares observed, that of May 19, 1951, was so complex that the significance of the measures is not yet clear. A large, high-speed dark flocculus developed early in the disturbance and, by moving across the site of the flare, produced abnormally large equivalent widths in absorption. These changes in equivalent width, corrected for the effects of neighboring solar and atmospheric lines, are shown in the line profiles in Figure 2. The first six profiles certainly refer to the flare alone, but the two last profiles result from both the flare and the high-speed dark flocculus. It is evident from the figure that the equivalent width at λ 10830 in the high-speed dark flocculus is nearly twenty times

[2] *Bull. astr.*, **11**, 349, 1938.

[3] Richardson and Minkowski, *Ap. J.*, **89**, 347, 1939.

larger than in the flare. The optical phenomena accompanying this flare are described by Dodson.

Two other infrared lines that may possibly arise from helium have been observed. One of these lines at λ 10123.9 has very close coincidence with *He* II, λ 10123.61, $4^2F^0-5^2G$, etc. Babcock and Moore[5] have commented on the weakening of this line from center

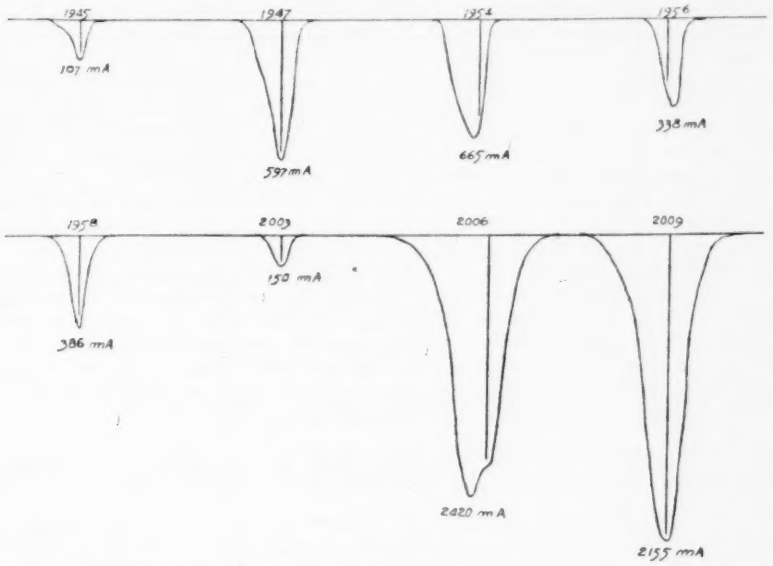

FIG. 2.—Changes in λ 10830 flare of May 19, 1951. The straight line near the center of each profile is the position of the line for zero radial velocity.

to edge of the solar disk and in sunspots. The present observations confirm the results of Babcock and Moore, but the line shows no conspicuous change in plage areas. This behavior makes its identification as *He* II doubtful. Another line of helium, λ 20581.4, $2^1S_0-2^1P_1^0$ might appear in the solar spectrum, and there is a weak line at λ 20583.6. It is more than 2 angstroms displaced from the position predicted for the singlet line of helium and probably cannot be identified with it.

The writer wishes to acknowledge with gratitude the continued support of the work of the Observatory by McGregor Fund of Detroit.

ORREN C. MOHLER

McMATH-HULBERT OBSERVATORY
OF THE UNIVERSITY OF MICHIGAN
October 2, 1951

[4] *Ap. J.*, 115, 320, 1952.

[5] *The Solar Spectrum λ 6600 to λ 13495* ("Carnegie Institution of Washington Publications," No. 579 [Washington, D.C., 1947]), p. 92, n. 55.

HIGH-DISPERSION SOLAR SPECTROGRAMS BETWEEN 15 μ AND 24 μ

In 1941 A. Adel,[1] at Flagstaff, Arizona, found a new atmospheric window by recording the solar spectrum between 15 and 24 μ. However, these observations were made under low dispersion, and the published curves show only sixteen absorption maxima (including four inflexions). To our knowledge, no other observation of the solar spectrum has been carried out in the above region.

In October, 1951, we succeeded in mapping the solar spectrum with high resolution between 15.90 and 23.73 μ; our spectrograms reveal 145 lines in this region. Toward shorter wave lengths, that is, between 14.2 and 15.9 μ, we find a complete absorption due to the 15 μ band (ν_2) of telluric CO_2. Owing to the water-vapor absorption, we have not as yet been able to detect any energy in the region beyond 23.73 μ.

Nearly all the newly observed lines have been identified. They are ascribed to the 16.24 μ band ($2\nu_2-\nu_2$) of CO_2, the 17 μ band (ν_2) of N_2O, and water vapor. New laboratory data are needed for the identification of the few remaining faint lines.

The observations have been made with the prism-grating spectrograph[2] of the University of Liége. This instrument was installed in the Jungfraujoch International Scientific Station, Switzerland, at an elevation of 11,725 feet. The spectrograph was equipped with an original echelette grating from the University of Michigan, having 1200 lines per inch (dimensions of the ruled surface: 7×9 inches). As receiver, we used a Perkin-Elmer thermocouple, which was connected to a Leeds and Northrup Speedomax recorder, through a 13-cycle Perkin-Elmer electronic amplifier.

We are indebted to the Fonds National Belge de la Recherches Scientifique, the Royal Observatory of Belgium, and the University of Liége for their support of this work.

M. MIGEOTTE
L. NEVEN

JUNGFRAUJOCH
October 20, 1951

NUCLEAR REACTIONS IN STARS WITHOUT HYDROGEN*

The more luminous main-sequence stars (O and B) exhaust their hydrogen supply in times of the order of magnitude of 10^9 years or less, the bulk of the hydrogen being converted into helium by means of the carbon-nitrogen cycle. When the energy supply of the carbon-nitrogen cycle has been exhausted, the star undergoes gravitational contraction, and its temperature increases. Various nuclear processes[1, 2, 3] have been suggested for such a contracting star, all of which require temperatures of well over $10^{9\circ}$ K. The main aim of this note is to point out that there is one nuclear process which takes place at a much lower temperature of about $2 \times 10^{8\circ}$ K, namely, the conversion of three helium nuclei into one carbon nucleus.

We take as an example a main-sequence star of mass $5M_\odot$ (B8 star), central density

[1] *Ap. J.*, **96**, 239, 1942.

[2] M. Migeotte, *Mém. Soc. R. Sci. Liége*, 1st ser., Fasc. 3, Vol. 1, 1945.

* This work was carried out during the summer of 1951 at the Kellogg Radiation Laboratory, California Institute of Technology, Pasadena. The author is indebted to several colleagues at the California Institute of Technology and at the Mount Wilson and Palomar Observatories for valuable discussions.

[1] F. Hoyle, *M.N.*, **106**, 343, 1946.

[2] G. Gamow and M. Schoenberg, *Phys. Rev.*, **59**, 539, 1941.

[3] L. Borst, *Phys. Rev.*, **78**, 807, 1950.

$\rho = 25$ gm/cm^3, and central temperature $T = 2 \times 10^{7°}$ K. The average energy radiated by the star, $\bar{\epsilon}$, is about 60 erg/gm sec, and most of the hydrogen is exhausted in about 10^9 years. We assume that in the ensuing gravitational contraction the central temperature and density are given by

$$T \propto R^{-1}, \qquad \rho \propto R^{-3}, \tag{1}$$

where R is the radius of the star. Gravitational energy is the only source of energy during the contraction until temperatures over $10^{8°}$ K are reached in a few million years. At these temperatures the following nuclear reaction sets in:

$$\begin{aligned} He^4 + He^4 + 95 \text{ kev} &\rightarrow Be^8 + \gamma, \\ He^4 + Be^8 &\rightarrow C^{12} + \gamma + 7.4 \text{ mev}. \end{aligned} \tag{2}$$

The nucleus Be^8 is unstable to disintegration into two He^4 nuclei. But, since an energy of only (95 ± 5) kev, comparable with thermal energies at temperatures over $10^{8°}$ K, is required for its formation, a fraction of about 1 in 10^{10} of the material of the star is kept in the form of Be^8 in a state of dynamic equilibrium. The Be^8 present then easily absorbs a helium nucleus. Once carbon has been produced, the following reactions also become possible

$$C^{12} + He^4 \rightarrow O^{16} + \gamma + 7.1 \text{ mev}, \tag{3a}$$

$$O^{16} + He^4 \rightarrow Ne^{20} + \gamma + 4.7 \text{ mev}, \tag{3b}$$

and so on. Owing to the increasing Coulomb barrier, the reaction rates decrease with increasing atomic number. Assuming the absence of γ-ray resonances, the rates for reactions (2) and (3*b*) are of the same order of magnitude. Hence the helium is probably converted mainly into C^{12}, O^{16}, and Ne^{20} and into decreasing amounts of Mg^{24}, Si^{28}, S^{32}, A^{36}, and Ca^{40}.

Energies of 3–4 mev per helium nucleus are produced in these reactions (about one-seventh the production in the carbon-nitrogen cycle). At temperatures T in the neighborhood of $2 \times 10^{8°}$ K, the rate of energy production ϵ is given by

$$\epsilon = 1^{(3} \left(\frac{\rho}{2.5 \times 10^4} \right)^2 \left(\frac{T}{2 \times 10^{8°}\text{K}} \right)^{18} X_\alpha^3 \text{ erg/gm sec}, \tag{4}$$

where ρ is the density in gm/cm^3 and X_α is the concentration by weight of helium. No detailed calculations have as yet been carried out with specific stellar models, but a temperature of slightly more than $2 \times 10^{8°}$ K should be sufficient for the energy generation (4) to supply the radiative-energy loss. In deriving equation (4), the nuclear γ-ray width for the formation of C^{12} (but *not* the one for Be^8) is required. This width has not yet been measured, and the position of resonance levels is not yet known accurately enough, and an estimate of 0.1 e.v. was used for this width. Hence the correct production rate could be smaller than equation (4) by a factor of as much as 10, or larger than equation (4) by as much as 1000. However, even a factor of 100.0 in the production rate alters the temperature necessary by a factor of only 1.33. If we assume an average radiative-energy loss of about 200 erg/gm sec, the energy content of reactions (2) and (3) is sufficient to maintain the star at an almost constant temperature and radius (central density ρ about 2.5×10^4 gm/cm^3) for about 5×10^7 years, after which time the bulk of the helium will have been converted into carbon and heavier nuclei.

We are thus led to the conclusion that *a few per cent of all visible stars of mass $5M_\odot$ or larger are converting helium into heavier nuclei, the central temperature being about ten times larger (and radius ten times smaller) than that of a main-sequence star of the same mass.* It is hoped that some connection will be found between stars undergoing this process, on the one hand, and carbon-rich and high-temperature stars (Wolf-Rayet, nuclei of planetary

nebulae), on the other (and possibly even with some of the variable stars and novae).

The fate of stars which have exhausted their helium supply and consist mainly of carbon, oxygen, and neon is much more controversial, but some tentative qualitative conclusions can be drawn about the various competing nuclear reactions. The star again contracts gravitationally until temperatures of about $10^{9°}$ K are reached. At these temperatures collisions between two C^{12} nuclei, giving Mg^{24} or $(Na^{23} + H^1)$, become possible and at slightly higher temperatures collisions involving O^{16} and Ne^{20}. At temperatures of (2 to 4) $\times$ $10^{9°}$ K the dissociation of the lighter nuclei into helium nuclei and into protons becomes important. These helium nuclei and protons can be absorbed by heavier nuclei, with the result that a significant fraction of the nuclei in the star might be converted into a variety of different nuclei of atomic weight A up to about 40 or 60. The relative concentrations of the various nuclear species might be expected to be similar to that obtained on Hoyle's[1] theory of thermodynamic equilibrium. At (1 to 4) $\times$ $10^{9°}$ K, however, the Urca processes of Gamow and Schoenberg[2] become important, which extract energy from the star in the form of escaping neutrinos. This energy loss results in a very rapid contraction of the star without any increase in temperature, as soon as the energy supply from the conversion into the very stable nuclei (A about 40–60) is exhausted. This contraction continues (unless the star becomes unstable because of its rotational momentum) until densities of more than 10^{10} gm/cm^3 are reached. The electron gas is then highly degenerate, and fairly large concentrations of beta-active nuclei are built up because of the high kinetic energies of the degenerate electron gas. More detailed calculations will be necessary to determine whether enough time is available during this collapse to build up the very heavy nuclei (up to uranium), as was suggested by Hoyle.[1] If the star becomes unstable during the collapse and becomes a supernova, one would expect the various beta-active nuclei to be expelled and to decay in the envelope of the supernova. These considerations lead to difficulties for Borst's[3] hypothesis that the energy generation in envelopes of supernovae of type I is due, to a large extent, to the beta decay of one *single* nucleus, Be^7, obtained from the reaction $He^4 + He^4 \rightarrow Be^7 + n$. It may, however, be possible that this reaction predominates over the others discussed in this note, if in a supernova of type I convection sets in suddenly (with velocities comparable to those of free fall), so that He^4 from the cooler outer layers of the star is *suddenly* brought into the central regions at a temperature of about $4 \times 10^{9°}$ K. It should be emphasized again that the remarks in *this* paragraph are quite tentative and speculative.

A fuller account of the calculations on the various processes discussed in this note will be given elsewhere.

E. E. SALPETER

LABORATORY OF NUCLEAR STUDIES
CORNELL UNIVERSITY
October 2, 1951

A NOTE ON ENERGY GENERATION IN RED DWARF STARS

Recent work by I. Epstein,[1] J. B. Oke,[2] and others[3] has indicated that the proton-proton reaction may be the most important source of energy generation in the cooler stars of the main sequence and even in the sun.

We have attempted to compute a model for the red dwarf star Krueger 60A, taking into account the energy generation throughout the layers where it may occur, on the assumption that the proton-proton reaction alone is responsible for the energy production. We have adopted for the mass, luminosity, and radius of the star the following data: $\log M = -0.60$, $\log L = -1.77$, $\log R = -0.29$.

[1] *Ap. J.*, **112**, 207, 1950.

[2] *J.R.A.S. Canada*, **44**, 135, 1950.

[3] See, e.g., L. H. Aller, *Ap. J.*, **111**, 173, 1950.

In this reconnaissance of the problem we have assumed a Russell mixture and have represented the guillotine factor (g/l) in Kramers' formula

$$\kappa = \kappa_0^1 \left(\frac{g}{l}\right) \rho T^{-3.5} \tag{1}$$

by an expression of the broken-line type,[4]

$$\log \frac{l}{g} = \alpha + \beta \log \rho , \tag{2}$$

where

$$\begin{aligned} \alpha &= \alpha_1 , \qquad \beta = \beta_1 , \qquad \rho < \rho_1 ; \\ \alpha &= \alpha_2 , \qquad \beta = \beta_2 , \qquad \rho \geq \rho_2 . \end{aligned} \tag{3}$$

In order to evaluate the constants over the range of density and temperature likely to be encountered in the red dwarf atmosphere, we must employ some approximate model of the star. For this zero-order approximation we take a modification of Schwarzschild's model for the sun,[5] in which it is assumed that the energy is supplied by the proton-proton reaction. The hydrogen and helium contents are then $X = 0.34$ and $Y = 0.64$, respectively, and the central temperature is 10,700,000° K.[3] The model is homologous to that for the sun, and we find

$$\begin{aligned} \log \rho &= \log \rho_\odot + 0.27 , \\ \log T &= \log T_\odot - 0.26 , \end{aligned} \tag{4}$$

for the same values of $Z = r/R$. We next plot $\log \rho$ against $\log T$ for this zero-order model of Krueger 60A, and for each selected value of $\log \rho$ we interpolate $\log (l/g)$ from Morse's table.[6] The functional dependence of $\log l/g$ on ρ can then be represented by the formulae

$$\begin{aligned} \log \frac{l}{g} &= 0.670 + 0.267 \log \rho \qquad [\log \rho (1+X) < 1.0] , \\ \log \frac{l}{g} &= 0.489 + 0.473 \log \rho \qquad [\log \rho (1+X) > 1.0] . \end{aligned} \tag{5}$$

The Morse tables are only approximate. They should be recomputed, taking into account the fact that the bound electron moves in a field of different effective nuclear charge than does the free electron. Furthermore, the bound-bound (line) transitions are not taken into account. An exact treatment is difficult, but the corrections range from about 10 to 40 per cent at the temperatures and densities likely to be encountered in stellar interiors. Furthermore, if *H* and *He* are extremely abundant, their free-free absorptions have to be taken into account. We have done this in our present calculations. Bound-free absorptions in *H* and *He* are less important, and, at the temperatures and densities of the red dwarfs, electron scattering may be neglected.

For the energy generation we have modified the previously employed formulae[7] to take into account the fact that two deuterons must be formed for each He^4 nucleus, instead of one, as formerly supposed. More recent work indicates a higher rate of energy production, however.[8]

[4] R.E. Williamson and G. F. D. Duff, *M.N.*, **109**, 46, 55, 1949.

[5] *Ap. J.*, **104**, 203, 1946.

[6] *Ap. J.*, **92**, 27, 1940.

[7] Aller, *op. cit.*, p. 176. The factor 1.91 in eq. (7) is replaced by 0.98.

[8] Edwin E. Salpeter, private communication.

The equations of stellar structure have been integrated in a straightforward fashion; our procedure was very similar to that employed by Epstein in his model for the sun.[9] That is, one chooses a series of values of X, i.e., X_1, X_2, X_3, and X_4, and carries out integrations for various values of Y until a pair of values, X_0Y_0, is found for which the luminosity, as well as the mass, comes out right.

Extensive calculations with values of X ranging from 0.60 to 0.90 and various values of Y showed no solution to be possible for the proton-proton reaction. The model star would always be too bright.

It might be possible to construct models composed almost entirely of helium, but for stars with compositions similar to that of the solar atmosphere no solution appears possible. The introduction of further refinements, e.g., improved cross-sections for the proton-proton reaction, degeneracy corrections, and the narrowing of the atomic potential barrier at high densities would make the discrepancies even worse.

We should like to emphasize that there is no difficulty in accounting for the observed luminosities of the red dwarf stars on the assumption that the energy is supplied by the carbon cycle.

L. H. Aller, J. W. Chamberlain,
E. M. Lewis, W. C. Liller, Jean K.
McDonald, W. H. Potter, and Nancy E.
Weber

The Observatory
University of Michigan
November 6, 1951

LABORATORY REPRODUCTION OF AURORAL EMISSIONS BY PROTON BOMBARDMENT

The detection of very energetic protons in certain auroral displays[1] has led to considerable speculation as to the possible contribution of the protons in exciting the auroral emissions. To clarify the situation, the authors made an experiment, using protons from the Kevatron at the Institute for Nuclear Studies, University of Chicago. The spectra that were obtained of the emissions excited by the proton beam in air show a striking similarity to the aurora, more striking than has yet been achieved with other types of laboratory excitation.[2]

The experiment used an absorption tube of approximately 26 cm in length attached to the proton accelerator, in which the pressure of the air could be varied. The protons were permitted to enter this chamber through a thin window of nylon, coated with vacuum-deposited aluminum to prevent damage to the window from heating due to the proton beam. The attenuation of the proton beam by this window amounted to approximately 15 kev at 230 kev. Because of the fragility of the nylon window, the differential pressure between the accelerator and the test chamber was kept below 1 mm *Hg*. No attempt was made to modify the composition of the room air flowing through the chamber, except to protect the chamber from hydrocarbon products from the vacuum-pump system by a liquid-air trap.

The spectrum of the emissions was obtained with the McDonald Observatory nebular grating spectrograph.[3] This spectrograph provided a dispersion of 400 A/mm as used in the first order. Since this spectrograph has a solid-glass Schmidt camera, the ultra-

[9] *Ap. J.*, **114**, 438, 1951. We are grateful to Dr. Epstein for sending us his results prior to publication.

[1] A. B. Meinel, *Ap. J.*, **113**, 50, 1951.

[2] L. Vegard and H. Raastad, *Geophys. Pub. Oslo*, Vol. **17**, No. 7, 1950.

[3] T. Page, *Ap. J.*, **108**, 157, 1948.

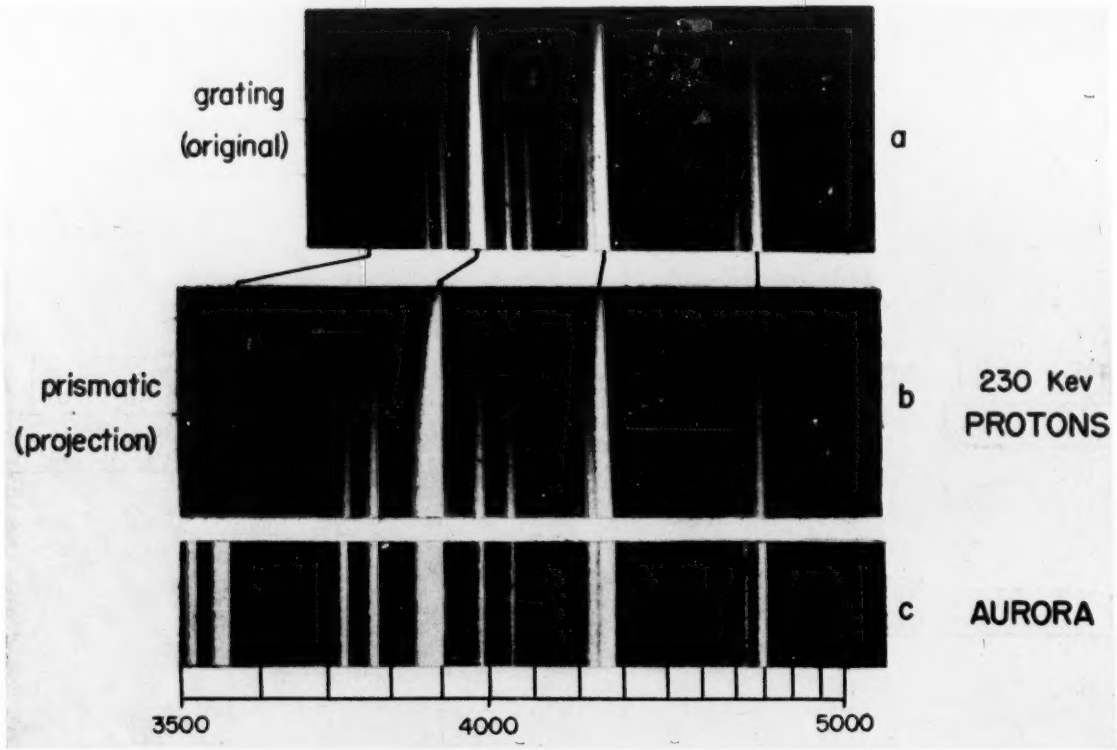

FIG. 1.—*a*, *b*, laboratory spectrum of air under proton bombardment: exposure 4000 microcoulombs protons cm^{-2}, 230 kev, 0.3 mm air, grating spectrograph *f* 0.7; *c*, auroral spectrum, Barbier and Williams: exposure 2 hours, quartz-prism spectrograph *f* 2.

violet spectrum beyond 3700 A was heavily absorbed. Figure 1, *a* and *b*, shows the spectrum emitted by the air under proton bombardment, where spectrum *a* is a reproduction of the original negative with grating dispersion, while spectrum *b* is a projection of spectrum *a* distorted to reproduce approximately prismatic dispersion. Spectrum *c* is of the Aurora Borealis obtained by Barbier and Williams,[4] using a quartz spectrograph at College, Alaska. A comparison between spectra *b* and *c* immediately shows the striking similarity between the laboratory and auroral emissions. It is interesting to note that the molecular bands, particularly the second positive bands near 4000 A, show more strongly developed violet wings in the laboratory spectrum than in the auroral spectrum, indicating that the rotational temperature in the aurora is significantly lower than in the laboratory emission. The relative intensities of the N_2^+ and N_2 bands are very similar in both the auroral and the laboratory spectrum.

The great similarity between the aurora and the emissions excited by the protons, and the lack of close similarity when electronic excitation is used (Vegard *et al.*), would at first seem to indicate that protons offer a more satisfactory explanation of the aurora. This does not necessarily follow, since the mechanism of excitation in a "discharge" is very different from that which exists in the stopping of energetic particles. Since no adequate test using electrons accelerated to a high energy *in vacuo* and then injected into an absorbing gas has been made, the performance of such an experiment will provide a crucial test: either the electrons must give an auroral spectrum under the same conditions as the proton test, or the number of electrons in the primary auroral particle beam must be small. Such a test could establish with certainty whether the auroral particles are merely an enhancement of the low-energy region of the cosmic-ray energy distribution or are a unique phenomenon as has hitherto been believed. It is expected that this test can be performed in the immediate future. Work is continuing on the excitation caused by protons with various energies and over the entire spectroscopic range.

The authors wish to express their thanks to Dr. S. K. Allison for the use of the Kevatron and the facilities of the Institute for Nuclear Studies. This investigation has been supported in part by the Geophysical Research Directorate of the Air Force Cambridge Research Center under Contract 19-122-480.

A. B. Meinel
C. Y. Fan

Yerkes Observatory
University of Chicago
February 1952

THE PLANETARY NEBULAE AS IONIZED HYDROGEN REGIONS

T. Page and J. L. Greenstein[1] conclude in a recent paper that most planetary nebulae are regions of ionized hydrogen in a vaster nebula that is obscure. This conclusion opens important new points of view for the theory of these nebulae and their forms. In this note I ask whether the method employed by Page and Greenstein makes this conclusion indeed more certain or more plausible. I believe the answer must be negative because their computation is, in principle, a check on an identical formula. In order to demonstrate this point, I shall oversimplify the computation by leaving out all known factors. This includes constants of nature and conversion factors from practical to theoretical units. I shall also leave out factors that depend slightly on the star's temperature, T_*. Such a factor is, for instance, the average energy of a quantum beyond the Lyman limit; so the energy beyond the Lyman limit and the number of quanta beyond the Lyman limit will be considered as one unknown quantity. Also the electron temperature is considered as a known factor and left out.

[1] *J. Geophys. Res.*, **55**, 401, 1950. [4] *Ap. J.*, **114**, 98, 1951.

Both Zanstra's method of determining T_e and Strömgren's calculation of the radius of the *H* II region are based on the assumption that all quanta beyond the Lyman limit are consumed in the nebula. A consumption is completed when an electron set free by such a quantum recombines with a proton on a level different from the ground level. Let Q_{uv} be the total number of quanta beyond the Lyman limit emitted by the star per unit time. This supply must equal the total consumption, which is proportional to N^2, where N is the density of electrons and protons, and to r^3, where r is the radius of the *H* II region. The further factors are capture cross-section and velocity, both dependent on T_e and thus known. So Strömgren's formula is written as

$$r^3 = Q_{uv} N^{-2} . \tag{1}$$

The Q_{uv} is R_s^2 times a function of T_e. When the derivation of Strömgren's formula sketched here is worked out with the known factors, it leads in a simple way to a formula identical with Strömgren's.

Each consumption of a quantum gives rise to a quantum in the Balmer or Paschen or further hydrogen continua. Hydrogen lines are emitted in "known" proportions to these continua. The excess energy of the ionizing quanta is largely converted to emission in the forbidden lines. So the light received from the nebula, l_{neb}, by which we may understand hydrogen continua, hydrogen lines, or forbidden lines, gives a direct measure of Q_{uv}, while it is also inversely proportional with the square of the distance, D. Hence

$$Q_{uv} = l_{neb} D^2 . \tag{2}$$

The basic idea of Zanstra's method is to contrast this light with the light of the star and thus to find a color index over the very wide base line from the visual and photographic range to beyond the Lyman limit. This color index gives T_e. Then follow the bolometric correction and, finally, the radius R_s. This part of the computation we can leave out, for in Strömgren's method Q_{uv} is computed from T_e and R_s by the same formulae in the reverse order.

Menzel's method of determining the density of the nebula is based on the measured surface brightness, which is $S = l_{neb}/A^2$, where A is the angular radius of the nebula. From theory, this same S is proportional to N^2R, where R is the depth of the nebula, which may be identified with the linear radius AD. So, together,

$$N^2 = \frac{S}{R} = \frac{l_{neb}}{A^3 D} . \tag{3}$$

The computation in Page and Greenstein's paper is, in broad lines, this: l_{neb} and A are known from observations, and a fair estimate of D is made. Then Q_{uv} and N are computed from equations (2) and (3), respectively, and these values inserted in equation (1). The result is identically $r^3 = (AD)^3$.

The argument in this note is not new. Various authors have emphasized at one time or another that the assumption of a nebula just big enough and dense enough to consume all available quanta is unlikely. So the majority of planetary nebulae must conform to either of two possibilities: (*a*) Not all quanta are consumed; this gives temperatures exceeding the Zanstra temperature. Or (*b*) not enough quanta are available to keep the entire nebula in an ionized state. The computations made by Page and Greenstein demonstrate that the formulae relevant to assumption *b* can be worked out consistently. But it seems quite likely that a paper might be written based on the same data and demonstrating that the formulae relevant to assumption *a* may be worked out consistently. Neither paper would prove or confirm the correctness of the assumption.

Several ways remain open to reach a decision for individual nebulae or groups of nebulae. The first is a critical discussion of the classical question of differences between hydrogen temperatures, "nebulium temperatures," and "helium temperatures," i.e., a

discussion of the minor effects that were considered as known in the simplified treatment above. This approach is reputedly difficult because of observational uncertainties. The other way is by plausibility arguments of a quite different nature, such as the unlikelihood of a higher stellar temperature or the unlikelihood of an actual drop in density at the visible edge of the nebula.

H. C. VAN DE HULST

LEIDEN OBSERVATORY
October 25, 1951

NOTE ON THE ORIGIN OF COMETS

In a recent paper on comets, F. L. Whipple[1] has stated (p. 470 n.) in regard to Lyttleton's theory of the origin of comets: "It can easily be shown that planetary perturbations destroy the precise convergence of particles *and render the process inoperative.*" Now there can be no doubt that the planets will produce small deviations from strictly hyperbolic motion for the particles, but it does not follow that the collisions necessary to start the accretion process will not occur. In the present note it is shown that, in fact, these perturbations do not in any way reduce the efficacy of the collision mechanism.

In the first place, the perturbations will have components both along and perpendicular to the accretion axis, and it is a simple matter to estimate their size. This shows that the order of magnitude, s, say, of the perturbations for particles crossing any part of the axis at distance of order GM/V^2 from the sun will be extremely small compared with the general length of the inward stream itself, which is of order $2GM/V^2$. (G = constant of gravitation, M = mass of the sun, V = relative velocity of sun and cloud.) Let us now consider a small cylinder of length s and radius s situated symmetrically around the axis at such a distance. The amount of material entering it per unit time will be $2\pi\rho_\infty GMs/V$, where ρ_∞ is the undisturbed density of the cloud. Also the time spent by a particle in crossing the cylinder would be of order $2s/V$. Hence the mass in the cylinder in the initial stages of the process would be $4\pi\rho_\infty GMs^2/V^2$. The volume density will be equal to this divided by πs^3, namely, $4\rho_\infty GM/V^2 s$, and the particle density would therefore be $4n_\infty GM/V^2 s$, where n_∞ is the density of the undisturbed cloud. The length of path described within the cylinder by a particle would be of order $2s$, and hence, if A is the collision cross-section of a particle, the probability of its undergoing a collision within the cylinder, calculated in the standard way, depends only on

$$\frac{4n_\infty GM}{V^2 s}\, 2s\, A = 8n_\infty AGM V^{-2},$$

and *is therefore independent of* s, which establishes the result referred to above that perturbations are not of importance. The calculation is approximate to the extent that it relies on the smallness of s compared with the typical length GM/V^2 associated with the accretion process, but there can be no doubt whatever of the validity of this approximation. In the same way, small velocity differences within the cloud will not affect the probability of collisions.

To take the result a little further: If we consider the particles to be equal spheres of radius r cm and density σ gm/cm^3, then we have $n_\infty = 3\rho_\infty/4\pi\sigma r^3$, $A = 4\pi r^2$, and the above expression for the probability of a collision for a single particle in the initial stages of the process becomes $24\rho_\infty GM/\sigma r V^2$. If we also take $\sigma = 3$ gm/cm^3 and write $V = 10^5 v$ cm/sec, this reduces to $10^{17}\, \rho_\infty/rv^2$, which agrees, as it must, with the result given on page 470 of my original paper.[2] As explained therein, even though the initial probability of collisions should be small, there are so many particles involved that some collisions

[1] *Ap. J.*, **113**, 464, 1951.

[2] *M.N.*, **108**, 465, 1948.

would be bound to occur and thereby commence the process of building up the stream. Once this has begun to form, its presence will bring about an increasing probability of collisions for all particles thereafter attempting to cross through it. My own view is that these planetary perturbations may play some part in settling the general width of the stream, and thence possibly in determining the initial sizes and densities of comets; but this part of the problem appears to be very complex.

In developing the accretion hypothesis for the formation of comets, I have considered the least favorable case by ignoring the possibility that the dust clouds are accompanied by interstellar gas at comparable or even higher space density. But, if such gaseous material were also present, the stoppage of small solid particles at and near the axis would be assisted by the presence of a concentrated stream of gas formed there also by accretion. The mathematical difficulties of the general process of accretion are unfortunately well-nigh insuperable, as study of the very simplest case of line accretion shows, and this makes it difficult to establish the nature of the details of the process. We must accordingly be on our guard against summary dismissal of the whole hypothesis merely because early attempts to understand it are not at once entirely perfect.

R. A. LYTTLETON

ST. JOHN'S COLLEGE
CAMBRIDGE, ENGLAND
November 23, 1951

REVIEWS

Photometric Atlas of the Near Infra-red Solar Spectrum λ 8465 to λ 25,242. By ORREN C. MOHLER, A. KEITH PIERCE, ROBERT R. MCMATH, and LEO GOLDBERG. Ann Arbor: University of Michigan Press, 1950. Pp. 7+238 tracings. $4.00.

This is the first photometric atlas covering the near infrared region and therefore will be of considerable value in research on the structure of the solar atmosphere. The resolution (as high as 50,000 under the best conditions) is entirely adequate for the measurement of equivalent widths of the solar lines; it is not sufficient, however, to reveal the true profiles of the narrower solar or telluric lines.

Many interesting band structures originating in the terrestrial atmosphere appear on the tracings. A detailed analysis of these bands should provide valuable information regarding the atmosphere of the earth. The bands are relatively weak and better suited for measurement and analysis than are the strong, saturated, fundamental bands at longer wave lengths.

The use of the lead sulfide cell (developed by R. J. Cashman) in place of the previously necessary thermocouples or bolometers has resulted in a greatly increased sensitivity, which has been used to increase the resolution above that previously possible.

The particular amplifier used in the recording system is not linear for small intensities; this makes necessary a calibration-curve. The correction is constant for intensities larger than about 10 per cent of the maximum and can be made with adequate accuracy for the smaller intensities. Satisfactory corrections can be made for the effects of scattered light.

There are, unfortunately, two defects in the *Atlas*. The centimeter réseau did not have all lines spaced equally; in addition, the paper did not always move smoothly through the recording meter but, instead, seems often to have moved in short jumps. As an example, see tracing No. 38. On the small line at 11403.9 A, the paper seems actually to have jumped backward several times. This effect could be serious in the measurement of the weaker lines.

The *Photometric Atlas of the Near Infra-red Solar Spectrum* is a very valuable contribution to our knowledge.

H. L. JOHNSON

Yerkes Observatory

Grating Spectrum of Iron. By A. GATTERER. Vatican City: Specola Vaticana, 1951. Pp. 16+47 photographic prints, 24×30 cm. $25.00.

During the last sixteen years the scientific world has seen the issurance of two editions of the prismatic spectrum of iron. These atlases were designed for the hundreds of scientific and technical laboratories engaged in spectral research at a time when prismatic instruments were used almost exclusively. In recent years the trend has been more and more toward the use of grating spectrographs of large dispersion. In view of this changing condition, the Vatican Astrophysical Observatory has issued a new atlas of grating spectra of iron.

The present atlas has made use of the progress in the precision of measurement of wave lengths in order to present the most accurate data possible. Moreover, the range has been extended both in the ultraviolet and in the infrared, with a dispersion of 0.7 A/mm throughout. Since some spectral regions are poor in iron lines, a zirconium-arc spectrum is included along with the *Fe*-arc spectra; while the *Zr*-arc spectrum is subject to several limitations as a reference for accurate work, it does provide a spectrum which greatly facilitates orientation and approximate measurement.

The Introduction discusses the technical problems related to the production and presentation of the spectra and gives tables of the impurity lines present in the *Fe* spectrum. For convenience all iron secondary standards of wave length are identified by a distinguishing symbol after the wave lengths given on the spectrum reproduction. The final section of the atlas presents a comparison between the neon spectrum and the *Fe* arc at a dispersion of about 3 A/mm.

The quality of the entire work is up to the high standards that have made the Vatican photographic atlases welcomed throughout the scientific world. As has always been the case, this atlas should perform a highly useful function at all scientific and technical laboratories engaged in any of the fields of spectroscopy.

A. B. MEINEL

Yerkes Observatory

The Aurorae. By LIEV HARANG. New York: John Wiley & Sons, Inc., 1951. Pp. 166+152 figs. $4.50.

This book on the subject of aurorae represents the first volume of the "International Astrophysics Series." According to the editors, "The need for such a series of books has arisen because of the great developments which have taken place in these fields of work during recent years." While the publishers should be commended for recognizing the scarcity of up-to-date books on these subjects, their first attempt has fallen short of the target, since they have indeed achieved nothing more than a historical account—primarily of the Norwegian work on aurorae. While one cannot expect to have a book written on a currently active subject be completely up-to-date, the lack of discussion of other auroral theories, such as have been developed by Chapman, Ferraro, and others, dealing with neutral ionized corpuscular beams, cannot be excused.

As a historical account of the basic Norwegian contributions in auroral physics, the book is very good because a great many of the original publications are difficult to obtain. The thorough presentation of Störmer's monumental studies of the orbits of an electrically charged particle in the terrestrial magnetic field is welcome; however, while Störmer orbits represent a major contribution in explaining cosmic-ray phenomena, their association with auroral phenomena is no longer retained by the majority of auroral theorists.

As far as the book goes, it is well written and has numerous illustrations and should prove interesting to other workers in auroral physics, since it gives a clear impression of the opinion of the Norwegian school concerning the aurora.

A. B. MEINEL

Yerkes Observatory